# PROCEEDINGS

# OF THE

# FIRST INTERNATIONAL CONFERENCE

# ON WOOD FRACTURE

Banff, Alberta

14 – 16 August 1978

ISBN 0-86488-014-6

Forintek Canada Corp.

Western Forest Products Laboratory

Vancouver, British Columbia

V6T 1X2

July 1979

# PREFACE

The First International Conference on Wood Fracture was held in Banff, Alberta, Canada, from August 14 to 16, 1978. The idea for this conference arose from a desire to bring together people working on mechanical properties of wood, with a particular emphasis on fracture mechanics applications, creep and creep-rupture effects. Above all, the central focus was the discussion of new approaches in wood fracture that would aid the rational development of reliability studies for engineering applications of wood.

The invitation to participate in the conference struck a very good response from all parts of the world. A total of 52 researchers met in Banff and this volume contains all the papers presented, including those corresponding to the conference and invited lectures.

The organizing committee wishes to acknowledge the financial support received from Forintek Canada Corp., the valuable help received from the staff of the Banff Centre and the collaboration of the staff of the Wood Mechanics Department of the Western Forest Products Laboratory, Forintek Canada Corp., without which the conference could not have taken place.

We have every intention of continuing the exchange of ideas generated by the conference, and anticipate that the next wood fracture meeting will be as rewarding as the first.

J. David Barrett and Ricardo O. Foschi
Organizing Committee

## CONTENTS

Page

Barrett, J. David, and Ricardo O. Foschi — 1
On the Application of Brittle Fracture Theory, Fracture Mechanics and Creep-Rupture Models for the Prediction of the Reliability of Wood Structural Elements.

Chow, C.L., and C.W. Woo — 39
Orthotropic and Mixed-Mode Fractures in Wood

Goodman, James H., and Jozsef Bodig — 53
Mathematical Model of the Tension Behavior of Wood with Knots and Cross Grain

Ivanov, Yuri M. — 63
Evaluation of Long-Term Bearing Capacity of Wood Structures by Their Performance Under Short-Term Loading

Keenan, F.J., and T.A. Jaeger — 73
Effect of Transverse Stress on the Shear Strength and Failure Mechanism of Douglas-fir

Lei, Young-kong, and James B. Wilson — 89
A Model for Fracture Toughness of Oriented Flakeboard

Madsen, Borg — 101
Size Effects in Lumber for Bending

Madsen, Borg — 111
Time-Strength Relationship for Lumber

Meierhofer, Ulrich A. — 129
Climatic Stresses of Wooden Construction Elements

Mindess, Sidney, Borg Madsen and J.D. Barrett — 143
Rate of Loading and Duration of Load Tests on Douglas-fir in Tension Perpendicular to the Grain

Murphy, Joseph F. — 159
Using Fracture Mechanics to Predict Failure of Notched Wood Beams

Nadeau, J.S. — 175
Fracture Mechanics: An Overview
Invited Lecture

Nielsen, Lauge Fuglsang — 187
Crack Failure of Dead-, Ramp- and Combined-Loaded Viscoelastic Materials

Page

Ruedy, Tom C., and Jay A. Johnson 201
Glueline Fracture of Wood Adhesive Compact-Tension Specimens at Various Grain Orientation Configurations 219

Schniewind, A.P.
A Seven Year Tale: Or How Boards Have Breakdowns from Everyday Pressure – Invited Lecture

Schniewind, A.P., H.J. Bartels and B.W. Gammon 227
Effect of Preloading on Fracture Toughness of Wood

Smith, F.W., and D.T. Penney 239
Fracture Mechanics Analysis of Butt Joints in Laminated Wood Beams

Spencer, Richard 259
Rate of Loading Effect in Bending for Douglas-fir Lumber

Sugiyama, Hideo 281
Theoretical Analysis of the Behavior of Bending Creep in Wooden Beams

Wilson, James B., Robert P. McEvoy Jr. and Richard W. Perkins 289
On Compression Failure in Wood Materials: A Mathematical and Experimental Simulation

List of Participants 303

# ON THE APPLICATION OF BRITTLE FRACTURE THEORY, FRACTURE MECHANICS AND CREEP-RUPTURE MODELS FOR THE PREDICTION OF THE RELIABILITY OF WOOD STRUCTURAL ELEMENTS

By

J. David Barrett and Ricardo O. Foschi

---

Research Scientists, Western Forest Products Laboratory, Forintek Canada Corp., Vancouver, B.C.

## INTRODUCTION

In the terms of reference, the organizing committee has asked that approaches used to solve problems of the mechanical and physical behavior of wood and wood-based materials be discussed in detail. In this session, we are concerned with approaches used to assess strength properties and, before beginning the discussion, some relevant background information will be presented.

Any discussion of approaches for solving strength problems will depend, to a large extent, on the problem itself and, to some extent, on the mechanical behavior of the particular material studied. This makes it necessary to outline, at the outset, the types of problems that will be considered. These develop mainly from a concern for improving our knowledge about the structural reliability of wood structures. In this session, strength properties will be discussed mainly from the point of view of predicting the behavior of individual structural elements, since a refined knowledge about this behavior is an essential prerequisite for the development of reliability models for structural systems, such as walls, roofs and floors. Nearly all of the examples to be discussed are related to structural engineering aspects of wood utilization. We believe, however, that the approaches to be discussed are of such a general nature that they can be used to treat a much wider variety of strength problems.

Our justification for focussing our research effort on the behavior of structural wood products is based on the obvious need to radically redefine our approaches to the characterization of strength properties for materials, such as lumber, plywood, glued-laminated and solid sawn timbers, to optimize the utilization of these materials. While the motivating force for this type of research varies from country to country, it is fair to say that most wood scientists and engineers of timber-engineering problems now recognize that new approaches must be applied to the study of strength properties. In some countries like Canada, the motivating force relates to a decision to change design codes from the current working-stress approach to a reliability based format. In others like the United States, the concern that appropriate technical information be developed to reduce exposure to product-liability-related litigation seems to be the impetus for research.

Design stresses for wood and wood products have traditionally been based on tests of relatively small, clear specimens. Consider, for example, the determination of a bending strength for a particular grade of dimension lumber. The basic strength data would be determined from a series of tests on small, clear, straight-grained specimens. The design stresses for the particular grade would then be obtained by modifying the small, clear specimen strength by a series of factors according to ASTM rules. The grade would have a specified strength ratio determined by the maximum slope of grain, knot sizes and splits specified for the grade. If the small, clear specimens were tested in the green condition, adjustments for the effect of moisture content would be required. Generally, the largest required adjustment to test data is that for effects of loading history. Wood is susceptible to creep-rupture and the test results obtained in the standard "static" configuration are reduced by as much as 50% for certain loading conditions considered to be of a permanent nature. Current ASTM standards tacitly assume the factors applied to the "short-term" static strength value to be cumulative, independent of species, grade, size and service condition.

An alternative approach for determining the strength values for dimension lumber and other structural wood elements is now gaining wide acceptance. The new philosophy incorporates the concept of testing, in-grade, the individual product in full-size configurations consistent with the end use. For example, in the case of dimension lumber bending strength, full-size pieces of material are tested in the various widths, grades and species groups to determine, in a direct manner, the short-term strength of the product. Testing on an in-grade basis can simplify interpretation of results by eliminating the need to make corrections for effects of knots, sloping grain, moisture content and end splits, since the composite effect of these characteristics is evaluated directly. The results of in-grade tests can be compared with the strength predictions based on the small, clear specimen approach, and comparisons in the case of dimension lumber, plywood, glued-laminated and solid sawn timbers have shown that large differences exist between the two approaches. Fortunately, these large differences in strength properties, for a traditional material such as dimension lumber, should not raise undue concern for the structural adequacy of traditional applications, since wood structures have a record of satisfactory service. Design in timber has developed, to a large extent, on the basis of traditional practice and it is not surprising to find that certain structural configurations could not be justified on the basis of the current strength properties and the design procedures of most codes. For example, roof-truss designs have been developed in many countries on the basis of proof-testing standards, allowing smaller member sections than would be justified by engineering-design codes. Some very serious difficulties are created, however, and it is to attempt to address these problems that we will present approaches that we feel can be useful.

Earlier it was stated that the traditional structural applications in wood had served well. While we believe this to be true, if one cannot explain why these systems have performed adequately, it will not be possible to refine or significantly alter construction practice; or to introduce new products without being extremely conservative in design assumptions and having to rely, instead, on the development of extensive in-service performance data. Consider, for example, the problem of designing prefabricated roof trusses for the residential truss market. Designs based initially on the allowable stresses and loads, as recommended by codes, resulted in member sizes which were later shown to be unnecessarily large on the basis of proof tests. In searching for reasons for these differences, many potential sources were identified, including the strength information, the analytical model for the truss, the connections, and the loading assumptions used to transform the short-term strength to long-term performance. Some of the earliest attempts to rationalize the differences involved evaluation of the in-grade strength of dimension lumber in tension parallel to the grain. These studies showed that tension-parallel-to-grain strength was considerably less than the strength predicted from bending tests. Tension strength for dimension lumber was subsequently reduced to nearly half of the corresponding bending-strength value. These studies, which began some five to 10 years ago, can be considered as the first indicator of the problems which face us today in revamping our approach to the treatment of strength problems.

The transformation of design codes from a working stress to a reliability format has required a complete reconsideration of strength aspects in Canada. According to the code philosophy adopted in Canada, it is desired that the treatment of structural reliability and loading models be made independent of materials. Accordingly, common load factors are proposed for steel, concrete, masonry and wood. Timber structures, however, have a much higher proportion of live loading and are subject to much more pronounced effects of creep-rupture, and considerable more attention must be given to the suitability of such a common approach for timber design. The issue of safety in wood structures is complicated by a lack of adequate information on strength and load-history models to be used in the prediction of behavior of full-size structural elements. It is imperative that a more refined knowledge of strength behavior be obtained for all structural wood products, if we are to take advantage of the unique characteristics of wood as a renewable resource which can be produced at very favorable energy-conversion rates.

The strength of wood in structural sizes is influenced by: 1) the size of the member and the stress distribution in it ("size effects"); 2) the presence of cracks and dominant defects, such as splits and notches; 3) the load history to which the member is subjected; and 4) environmental conditions as they affect the three previous strength-influencing factors. We will concentrate our discussion on approaches to solve problems in the first three areas, using mainly research carried out at the Western Forest Products Laboratory during the last few years. Finally, we will discuss briefly some issues in reliability of wood structures as they relate to the need for more research in strength properties and loading models.

## SIZE EFFECTS

It is known that the short-term strength of wood, for a particular type of stress distribution, shows a strong dependence on the volume of the test specimen. For people working on wood mechanical properties, it has always been puzzling that longitudinal shear strength, for example, when measured with the small ASTM block, is much higher than the shear strength of beams. While the ASTM block gives, for example, a mean strength for air-dry Douglas-fir of nearly 1,400 psi, the shear strength of glued-laminated beams is usually observed in the 400 to 700 psi range. Accordingly, the development of allowable stresses in shear, deduced from the ASTM test, has included a "stress-concentration" factor to account for the difference between the two test results. If anything, the stress-concentration factor should work in the reverse: the ASTM block has a dominant 90° notch which enforces the plane of fracture, while an ordinary beam has no such notches or stress raisers. A finite element analysis of the stress distribution in a beam does show a concentration of shear stresses near the point of support, at the base of the beam. These high shear stresses, however, only contribute to crushing over the support, as longitudinal shear failures normally occur within the middle third of the depth.

Another experimental result that has been difficult to quantify is the influence of stress distribution when the volume of the test specimen is kept constant. Thus, a bending test on a 2 x 8-inch dimension-lumber specimen shows a higher bending strength for center-point loading than for third-point loading.

It is apparent that, as in other materials, these effects are controlled by the random distribution of defects in the piece, both natural and man made through machining and conditioning. These defects will all have different local strengths, and it stands to reason that the appearance of "volume" or "volume under stress" as independent variable is due to the fact that, the larger is the volume of the member, the larger is the probability of encountering a weaker defect in the zone of high stresses.

A stochastic model that allows the representation of these volume and stress distribution phenomena is the "weakest-link" model of fracture in brittle materials when there is no dominant or strength-controlling defect. The model, first proposed by Weibull (1939), is discussed in detail by Bolotin (1969). The concept of weakest link permits the development of a probabilistic approach to the problem, but it does not give an insight into the mechanics of fracture, the propagation and coalescence of initially small flaws into larger cracks until failure takes place. We feel, however, that although this is an area of interest, it would be extremely difficult to extrapolate behavior from the cell level to the macroscopic behavior observed in a testing machine.

Briefly, let us examine the concept of weakest link. Consider a volume V under a stress distribution $\tau(x,y,z)$. Assuming that total collapse follows immediately upon failure at a point (weakest link), Weibull's model allows the computation of the probability of failure $p_f$ of the volume V:

$$P_f = 1.0 - e^{-\int_V \left[\frac{\tau - \tau_o}{m}\right]^k dV} \quad (1)$$

where:

m, k and $\tau_o$ are material constants. Eq. (1) thus involves three parameters, with $\tau_o$ being the minimum strength, and the integration in Eq. (1) must be performed only over those portions of the volume V where the stresses $\tau$ exceed the minimum $\tau_o$. If this minimum strength is assumed to be zero, the model becomes a two-parameter Weibull model (m,k). The use of a two-parameter model may be considered unrealistic, but it has two definite advantages: it provides a conservative approach to the problem and it allows a simpler mathematical treatment. Furthermore, for some mechanical properties, such as tension perpendicular to the grain and longitudinal shear, the assumption of zero or near-zero minimum strength is not unrealistic. Let us assume, therefore, $\tau_o = 0$.

Eq. (1) can be used to compare two volumes, V and V*, under corresponding stress distributions $\tau$ and $\tau^*$, when both these volumes have the *same* probability of failure. Under this condition,

$$\int_V \tau^k \, dV = \int_{V^*} \tau^{*k} \, dV^* \quad (2)$$

*Arbitrarily*, let us consider that the volume V* is unity and that it is ***uniformly stressed*** with $\tau^*$. Thus,

$$\int_V \tau^k \, dV = \tau^{*k} \quad (3)$$

Further, let the stress distribution $\tau$ be normalized with respect to a reference stress $\tau_M$. This can be any convenient stress parameter, like the maximum bending stress in a beam or the maximum shear stress computed from elementary beam theory. Thus, let

$$\tau = \tau_M \, \phi \, (x, y, z) \quad (4)$$

Introducing Eq. (4) into Eq. (3),

$$\tau_M^k \int_V \phi^k \, dV = \tau^{*k} \quad (5)$$

As the parameter k is not necessarily an integer, the integration in Eq. (5) is usually too complicated to be carried out in closed form. A numerical integration procedure can be used with stress distributions from elementary theory or from more exact analyses based on, for example, finite element methods. In any case, the integral may be expressed as follows:

$$\int_V \phi^k \, dV = I(k) \; V \quad (6)$$

Eq. (5) may thus be written

$$\tau_M = \beta \, \frac{\tau^*}{V^{1/k}} \quad (7)$$

where

$$\beta = [I(k)]^{-1/k} \quad (8)$$

is a factor solely dependent on the stress distribution. Eq. (7) allows the calculation of the characteristic strength $\tau_M$, at different failure probability levels, if the parameter $\kappa$ is given and $\tau^*$ is known at different levels of probability of failure. Eq. (7) gives the dependence of $\tau_M$ on the volume V: for the same stress distribution, a linear relationship exists between the logarithms of $\tau_M$ and V with a negative slope 1/k. This, in fact, allows a method for determining k by using the mean strengths $\tau_M$ corresponding to different volumes V but having the same stress distribution (i.e., a constant $\beta$). In a two-parameter Weibull model, k is related to the coefficient of variation $C_v$ according to the approximate formula

$$C_v = \frac{1.2}{k} \quad (9)$$

from which, for mechanical properties with coefficient of variation in the range 0.15 to 0.40, the resulting parameter k has a range of approximately 3.0 to 8.0.

The stress-distribution factor $\beta$ of Eq. (8) is shown in Figure 1 for the case of longitudinal shear in a beam under a single concentrated load and for k = 5.0 (Foschi and Barrett, 1976a). The reference stress $\tau_M$ is, in this case, the maximum shear stress

$$\tau_M = 1.5 \, \frac{V_o}{A} \quad (10)$$

where $V_o$ is the maximum shear force and A is the cross section of the beam. The distribution of shear stresses, here determined via finite element analysis, is a function of the aspect ratio L/d and the position of the load, a/L. Figure 2 shows the factor $\beta$ corresponding to the case of shear in a beam under uniformly distributed load, where only the ratio L/d influences the distribution of stresses.

For the same beam (V and L/d constants), Figure 1 shows how the shear strength diminishes as the load moves towards midspan. It is interesting to note that, at the same time, the maximum shear force $V_o$ also diminishes, and the total load carrying capacity of the beam shows a minimum somewhere between the support and midspan. The location of this minimum (around a/L = 0.25 for L/d = 20) gives the "most unfavorable" position for the concentrated load from the point of view of design, Figure 3. A most unfavorable position for a concentrated load has long been recognized in design procedures for bridges, for example. It is interesting to note that the positions that have always been recommended, based mostly on empirical rules, agree quite closely with the ones derived using the weakest-link approach. For bridge design, however, the weakest link goes one step further. To be consistent, one must consider the largest shear stress that each point in the beam sees as the concentrated load travels from one end to the other. That is, the shear-stress distribution that must be considered in the integration of Eq. (6) is that corresponding to the envelope of shear. This "moving load" case results in values about 20% lower than those estimated for a stationary load located at its most unfavorable position. Figure 4 shows the factor β for the case of a single concentrated load. A comprehensive study of β for longitudinal shear, including many combinations of live and dead loading, and moving-load trains for bridges, is given by Foschi and Barrett (1977).

Barrett, Foschi and Fox (1975) show stress-distribution factors β for perpendicular-to-the-grain strength, considering the case of radial stresses in pitched-curved beams and in nailed connections loaded normal to the grain.

How to determine the parameter k and the unit volume strength τ* at different probability-of-failure levels? In the case of longitudinal shear for air-dry Douglas-fir (m.c. ≃ 12%), Foschi and Barrett (1976a) used tests on different specimens in conjunction with a nonlinear regression to fit Eq. (7), in a least-squares sense, to the measured median strength from each test configuration. Thus, it was possible to determine k and τ*(0.5), corresponding to a 0.5 failure-probability level. The tests used were the ASTM block and five series of beams, each with different volume, obtaining k = 5.53 and τ*(0.5) = 2526 psi, Figure 5. Using Eq. (1) with $\tau_o = 0$ and considering the particular case of uniform stresses in an unit volume, the values of τ* at other probability levels can be determined. Eq. (1) gives

$$p_f = 1.0 - e^{-\left[\frac{\tau^*}{m}\right]^k} \tag{11}$$

from which

$$m = \frac{\tau^*(0.5)}{\left\{-\ln(0.5)\right\}^{1/k}} \tag{12}$$

and, in general, for a failure probability $p_f$,

$$\tau^*(p_f) = \tau^*(0.5)\left[\frac{\ln(1 - p_f)}{\ln(0.5)}\right]^{1/k} \tag{13}$$

In the case of tension perendicular to the grain of Douglas-fir, Barrett (1974) determined the parameter k and the unit volume strength τ* by using tension test results on blocks of different volumes, obtaining k = 4.63 and τ*(0.5) = 469 psi.

The usefulness of Eq. (7), and of the weakest-link approach in general, is that once the stress distribution for a particular application is known, the strength of the specimen can be derived at different levels of probability of failure. This *unifying approach* is important, as it allows the treatment of different problems with the same theoretical framework. To verify the predictions made with Eq. (7), tests were conducted with specimen configurations other than those used to obtain the parameter k and the unit-volme strength τ*. In the case of longitudinal shear, Foschi and Barrett (1976a) used test results on torque tubes and on a nailed connection that failed in shear by pulling out a plug of wood with all the nails enclosed. Figures 6 and 7 show how well the model is able to predict the median (and approximately, therefore, the mean) strength in these different situations. Similarly, the tension perpendicular-to-the-grain parameters derived from tensile blocks (Barrett, 1974) allow a good estimation of mean failure strengths of different configurations, including curved-pitched beams and nailed connections loaded normal to the grain, Figure 8 (Barrett, Foschi and Fox, 1975).

## INFLUENCE OF CRACKS AND NOTCHES: FRACTURE MECHANICS

The strength of a piece of wood with a crack or a notch is usually determined by the presence of that crack or notch. The situation of a dominant strength-controlling defect does not have, therefore, the stochastic character of the problem discussed in the previous section. Consider, for example, Figure 9. The shear strength of this beam will be controlled by the propagation of the horizontal cracks along the direction of the grain.

The ideas of Linear-Elastic Fracture Mechanics (LEFM) have been successfully applied to the prediction of loads that will produce the propagation of existing cracks (Barrett and Foschi, 1977a, 1977b; Barrett, 1976). Considering only planar problems, two fundamental modes of crack propagation can be identified: Mode I, where the crack surfaces are separated from each other as in a cleavage test; and Mode II, where the crack advances by shear action, producing sliding of one crack surface on the opposite one. To discuss briefly the concepts of LEFM, consider Figure 10. It shows a beam under uniformly distributed load and with an end crack of length a. An elastic analysis of this beam, including orthotropic properties, will show that the stress field presents a singularity at the crack tip, with the stresses having the form

$$\tau = \frac{K}{(r)^{\frac{1}{2}}} \quad F(\theta) + \; . \; . \; . \quad (14)$$

in which r and θ are polar coordinates centered at the crack tip and with $\theta = 0$ coinciding with the grain direction. The factor K associated with the singularity is called the "stress-intensity factor" and depends on the level of applied stresses and the geometrical configuration. It is usually expressed as

$$K = \tau_o \sqrt{\pi a} \quad H(L/d, a/L) \quad (15)$$

where $\tau_o$ is a nominal stress [for example, the maximum shear stress of Eq. (10)] and H is a nondimensional factor which accounts for the geometry of the configuration. The basic hypothesis of LEFM is that, at the moment of propagation, the stress-intensity factor K equals a critical value $K_{cr}$,

$$K_{cr} = \tau_o \sqrt{\pi a} \quad H \quad (16)$$

which must be determined by experimentation as any other mechanical property and for each propagation mode.

Using Eq. (16) and knowing the value $K_{cr}$, and given the initial crack length and the configuration factor H, it is possible to compute the stress level $\tau_o$ (and therefore the applied loads) that will cause crack growth.

Two problems must, therefore, be considered in this approach: 1) the critical stress-intensity factors $K_{cr}$ and their corresponding statistics must be determined by testing, considering the influence of environmental conditions, species and the effect of specimen width; 2) the configuration factors H must be determined by stress analyses, using theory of elasticity for orthotropic materials and, normally, one of several numerical methods: finite element analysis with a refined mesh, collocation techniques, finite element analysis with singular elements or boundary integral methods. The results of Figure 10 have been obtained with a finite element approach that uses isoparametric singular elements to represent the stress field near the crack tip (Foschi and Barrett, 1976b).

Figure 11 shows factors H for a beam with an end crack under a single concentrated load located at a distance s from the support. This information, together with Eq. (16), was used by Barrett and Foschi (1977a) to determine the critical values $K_{IIcr}$ in Mode II for western hemlock (***Tsuga heterophylla***) at approximately 10% m.c. The dimensions of the test beam were L = 20 in., d = 5 in., width = 1.4 in., and an end-crack length a = 5 in. A natural end crack was simulated by introducing a bandsaw notch which was subsequently extened with a sharpened steel blade. To avoid notch closure during loading, two steel rods were introduced between the faces of the bandsaw cut, as shown in Figure 12. This figure also shows the typical output from a test: plotted against the relative crack displacement, the load increases linearly at the beginning and then reaches a maximum $P_{max}$ for which the crack propagates rapidly forward. A smaller load $P_Q$ can be determined following the procedure in ASTM E399, using the broken line of Figure 12 corresponding to a 5% offset from the initial slope. The critical stress-intensity factor $K_{IIcr}$ was computed on the basis of the $P_Q$ load, obtaining a mean value of 2037 psi $(in)^{1/2}$.

If LEFM can be used to predict the strength of wood in the presence of cracks, the measured value of $K_{IIcr}$ can be applied to other configurations to predict their load-carrying capacity according to Eq. (16). Barrett and Foschi (1977a), using tests on dimension lumber with end splits (2 x 8 in. western hemlock, $L = 66$ in., load at midspan, and three crack lengths: $a = 8.75$ in., 16.5 in., and 24.75 in.) show that the LEFM approach is indeed very useful and accurate. A comparison between predicted mean results and measured means is shown in Figure 13, for Select Structural and No. 2 grades.

A detailed description of an application of LEFM to the study of shear strength of dimension lumber with end splits, under uniformly distributed loads, is shown by Barrett and Foschi (1977b). This study served to evaluate the strength-reducing factors recommended by ASTM for the derivation of allowable shear stresses and to assess the grading rules that specify maximum end splits for the different grades of lumber. The broken line in Figure 14 shows the strength-reducing factor $K_2$ as recommended by ASTM: it is a linear relationship that decreases the strength to zero when the crack length is equal to three times the depth ($a/d = 3$). Figure 14 also shows the factor $K_2$ as obtained from the LEFM application, each curve corresponding to a different ratio $L/d$. Although LEFM predicts infinite strength for a zero crack lenth, the curves of Figure 14 have an upper bound given by the strength of material with small cracks and no dominant defects. Such bound, computed as described in the previous section, is shown in Figure 15, together with an approximation to the reduction factor $K_2$ for $L/d = 20$.

Critical values for $K_I$ (Mode I) have been determined by Barrett (1976) for Douglas-fir and, at the same time, the effect of crack-front width has been studied using a weakest-link approach similar to that described for size effects in general. It was found that there is a dependence of $K_{Icr}$ on specimen width and that this dependence is quantifiable by using the weakest-link model.

Notches can be treated, in general, following the same approaches used for sharp cracks. It must be noted, however, that the $(r)^{-1/2}$ singularity in Eq. (14) must be replaced, in general, by $(r)^{\lambda}$, with the exponent $\lambda$ being dependent on the notch configuration ($-1 < \lambda < 0$) (Leicester, 1971). The calculation of the exponent $\lambda$ corresponding to a given notch follows from an application of Williams' eigenfunction approach to the stress distribution around the notch vertex (Williams, 1952). Usually, two values for $\lambda$ are obtained and to each one correspond a different singular stress field. For sharp cracks, only one such eigenvalue $\lambda$ is obtained ($\lambda = -0.5$), but there are two independent eigenfunctions; when the crack is oriented along the grain, one of the eigenfunctions can be identified with the opening mode (Mode I) and the other with the shear mode (Mode II). When the sharp crack is at an angle to the grain, the two singular solutions corresponding to $\lambda = -0.5$ cannot be separated into pure Mode I and pure Mode II solutions. The crack will propagate along the grain direction, at an angle to the initial crack, in a mixed mode of fracture. For notches, the two singular solutions correspond to two different values for the singularity exponent $\lambda$ and, in most cases, these solutions also correspond, each one, to a mixed mode of fracture. Work on the effect of notches currently hinges on a better understanding of fracture in mixed modes, an area that needs further research. In a sense, we are fortunate that wood, being a highly oriented material, has a very predictable direction of crack propagation (i.e., normally along the grain), Figure 16.

## EFFECT OF LOAD HISTORY ON STRENGTH

Design stresses for materials which exhibit creep-rupture effects must be modified for effects of loading history. Design stresses can be greater for loads of short duration than would be allowed for similar loads continuously applied. Design codes, such as CSA-086, the Code of Recommended Practice for Engineering Design in Wood in Canada, generally separates loads into categories according to their duration: 1-day, 7-days, normal and continuous. No distinction is made between loads applied continuously or intermittently, since it is the cumulative period of loading that is considered important. Design stresses specified for "normal loading" correspond to a cumulative period of full-design load not greater than 10 years. Increases in the allowable stresses are specified for loading periods less than 10 years, and such increases are permitted for snow loading, wind and earthquakes. Continuous loading represents a cumulative period of more than 10 years, and the design stresses given by the code are correspondingly reduced.

The adjustment factors for load duration currently applied have been derived empirically from ramp- and constant-load tests of small, clear, straight-grained Douglas-fir specimens (Wood, 1951). The tests on which these factors are based used a loading condition seldom encountered in service, and the results have not allowed the development of a systematic approach to the assessment of safety in wood structures. A rational discussion of reliability in wood engineering requires that the load-duration effects be considered and that the dependence of strength and time to failure on load history be quantified.

Before beginning the examination of potential approaches to the problem, it is necessary to consider in some detail the experimental results which form the basic data used to characterize creep-rupture effects. The creep-rupture test is carried out by applying a constant load to a specimen and measuring the time to failure as a function of the applied stress level. In studies of creep-rupture in wood, it has been common to express the applied stress in terms of a *stress ratio* obtained by dividing the applied stress by the strength of the specimen in a "standard" short-term ramp-load test. Wood (1951) presented the results of constant-load tests for small, clear specimens loaded at stress ratios ranging from 0.95 to 0.60, Figure 17. In Figure 18, the constant-load trend line has been plotted and also shown is the trend line for ramp-load tests carried out at various displacement rates. The constant- and ramp-load tests were represented by Wood using an empirical hyperbolic curve as shown in Figure 17. This curve is the basis for the development of the duration-of-load factors currently used in nearly every wood-engineering design code in the world. Wood recognized that loads applied for short durations could allow higher design stresses and, for snow loads, recommended an increase of 15% over the design stress for normal loading, corresponding to 10 years of cumulative application. This 15% increase, as shown in Figure 17, corresponds to approximately two months of constant loading. For wind and earthquake loads, Wood recommended an increase of 33%, corresponding to one day of constant loading. Conversely, for loads of a permanent nature, the design stresses should be reduced by 10%. These recommendations have been widely used and the excellent performance of wood structures suggests that the recommendations were effective. A thorough investigation of the duration-of-load phenomenon, however, suggests that the approach to the problem, at least in the case of wood and wood-based materials, has been extremely simplistic. For example, the duration-of-load factors developed on the basis of small, clear specimens in bending tests have been applied to other strength properties, including shear, tension parallel and perpendicular to the grain, and compression, in spite of a considerable body of evidence which suggests that the creep-rupture behavior in these other modes of fracture can differ considerably from the bending response, Figures 19 and 20. The factors developed for solid wood also have been applied to other products, such as plywood and glued-laminated material. Furthermore, no detailed investigation has been undertaken to analyze the effect of loading history on time to fracture in order that the choice of modification factors for loading condition be rationalized. Recent studies by Madsen and Barrett (1976) have shown that the creep-rupture response of dimension lumber differs considerably from that observed for small, clear specimens. Figure 21 shows trend lines through constant and ramp-load test results for 2 x 6-in. Douglas-fir, No. 2 and Better grade dimension lumber in comparison to the small, clear bending-test results. For high stress ratios, the results indicate that the duration-of-load effect is less severe for in-grade material than it would be predicted on the basis of the small, clear tests.

Test results from the limited investigations of the duration-of-load effect in dimension lumber indicate that the behavior of lumber cannot be accurately predicted using the response of the small, clear tests. It is apparent, therefore, that both the experimental and theoretical aspects of the load-duration problem need to be thoroughly investigated. The development of suitable experiments would be simplified if models for the duration-of-load effect were available. In this section of our presentation, two approaches for treating duration-of-load effects will be discussed. The first approach utilizes the concept of material "damage" as a basis for development of phenomenological laws, and the second uses fracture-mechanics concepts to study the process of slow crack growth.

### I. Damage Models: Modelling Creep-Rupture

Creep-rupture can be modelled using a phenomenological approach based on the concept of "damage" $\alpha$. This is defined such that $\alpha = 0$ for virgin material and $\alpha = 1$ at fracure. The rate of damage accumulation is assumed to be a function of the current stress level and the current damage, and a law for the damage rate has been presented by Barrett and Foschi (1978a):

$$\frac{d\alpha}{dt} = a(\sigma - \sigma_0)^b + \lambda\,\alpha\,; \quad (\sigma > \sigma_0) \quad (17)$$

where:

$\alpha$ = current damage;

$\sigma$ = applied stress ratio;

$\sigma_0$ = threshold stress ratio;

a, b, $\lambda$ = material parameters.

Two cases will be considered: A) using the complete Eq. (17) and B) using a simplified model obtained by assuming $\sigma_0 = 0$ and $\lambda = 0$. The suitability of these two models was assessed by studying their predictions for ramp and step-function load tests.

1. Step-function load test. The stress history assumed is given by

$$\sigma(t) = \sigma H(t) \quad (18)$$

where H(t) is the Heaviside-unit step function. Integrating the damage-rate law for this particular load history, the following expressions are obtained for the time to fracture $T_x$ and the applied-stress ratio $\sigma$:

$$\text{Case A:} \quad T_s = \frac{1}{\lambda}\,\ell n\left(1.0 + \frac{\lambda}{a(\sigma - \sigma_0)^b}\right) \quad (19)$$

$$\text{Case B:} \quad T_s = 1 / a\sigma^b \quad (20)$$

2. Ramp-load test. In this test the rate of load application is controlled and assumed to produce a stress history according to

$$\sigma(t) = k\,t \quad (21)$$

where k is the stress rate. The integration of the damage-rate Eq. (17) cannot be achieved in closed form for all assumed load histories. In particular, a closed-form solution cannot be obtained for the general case A (a numerical procedure is required, as described by Barrett and Foschi, 1978a). For case B, however, the time to fracture in a ramp loading can be obtained as follows:

$$T_r = \frac{b+1}{a} \sigma^{-b} \quad (22)$$

Figure 22 shows the fit of case B solutions for ramp- and step-function loading to results of Wood (1951) for small, clear bending specimens. The results are presented on the basis of a "standard" short-term test producing fracture in five minutes and using a ramp-load function. Thus, from Eq. (22), the parameters a and b satisfy (for $\sigma = 1$),

$$\frac{b+1}{a} = 0.0833 \text{ hrs. (5 minutes)} \quad (23)$$

The fit of case B to data shown in Figure 22 was obtained by using Eq. (20) to fit constant-load test results with the constraint given by Eq. (23). Thus, the agreement shown in Figure 22 between predicted and observed response for ramp loading (other than at $\sigma = 1$) can be considered as a measure of the suitability of the damage model to represent the effect of load duration. The result of fitting the models to the small, clear bending data is:

for Case A: $a = 0.110 \times 10^7$ (hour $^{-1}$),

$b = 34.20$

$\lambda = 0.789 \times 10^{-3}$ (hour $^{-1}$),

for Case B: $a = 444.0$ (hour $^{-1}$),

$b = 36.0$

Both models were fitted to the median of the times to fracture corresponding to a given stress ratio and, it was assumed in the fit of case A, that the threshold $\sigma_o$ was 0.20. The fit of the general model of case A is shown in Figure 23.

A comparison of the results in Figures 22 and 23 shows that the general model allows for a change in the sign of the curvature for the relationship between stress ratio and time to fracture. Such flexibility is not present in the simple model of Case B. The selection of a threshold level is, at this point, largely arbitrary, and it requires a refinement of experimental studies for a more rational determination. Comparison of the fit for Case A and Case B for the small, clear bending data indicates that it would be difficult to justify the selection of one model over the other.

Results of ramp- and constant-load shear tests are shown in Figure 24, with a fit of model for Case A. The fit is considerably better than the one that could be achieved by using the model of Case B, due to the rapid downturn in the constant-load data which occurs around 1000 hours. Excellent agreement is shown between the fitted and observed responses for long-term ramp loading.

To this point we have been interested only in the capability of the models for representing the results of the constant and ramp-load tests normally performed in a laboratory. It is apparent that the models are sufficiently flexible to represent experimental data, and can be used to study more realistic loading histories and their effect on time to fracture.

Consider, for example, the case of a cyclic stress-ratio history given by

$$\sigma = \sigma_{max} \left[\frac{2t}{\Delta}\right]^n \quad (24)$$

where t is the time coordinate referred to the beginning of the cycle, $\sigma_{max}$ is the cycle amplitude, $\sigma$ is the cycle duration and n a parameter that controls the shape of the cycle. This shape is shown in Figure 25 as a function of n. The damage accumulated after N cycles of constant amplitude can be computed in closed form for the simplified model of Case B:

$$\alpha = \frac{N \Delta}{(n\,b + 1)\; a\; \sigma_{max}^{b}} \quad (25)$$

The number of cycles to fracture $N_f$ can be determined, therefore, for $\alpha = 1$,

$$1 = \frac{N_f \Delta}{(n\,b + 1)\; a\; \sigma_{max}^{b}} \quad (26)$$

Comparing the results of Eqs. (20) and (26), when the stress ratios $\sigma$ and $\sigma_{max}$ are equal, it is possible to define an effective period of step-function loading, T*, corresponding to the $N_f$ cycles of constant amplitude,

$$T^* = \frac{N_f \Delta}{(n b + 1)} \quad (27)$$

Effective periods of step-function loading are shown in Table 1 for four values of the cycle-shape parameter n. Since the damage per cycle is independent of the previous damage, the results derived using Case B exhibit a linear cumulative behavior. This is not the case for the general model of Case A because the parameter λ introduces a dependence on the prior damage.

## II. Damage Models: Assessing Reliability

The formulation of the damge-rate law as given by Eq. (17) does not account for the effects of variability in time to fracture for a series of nominally identical members subjected to the same load history. A generalization of the damage-rate law, as shown by Barrett and Foschi (1978b), allows for variability by letting the parameters a and λ be random variables. Assuming that these are lognormally distributed, the damage-rate law becomes

$$\frac{d\alpha}{dt} = a\, e^{\omega_1 R_N} (\sigma - \sigma_o)^b + \lambda\, e^{\omega_2 V_N} \quad (28)$$

where $R_N$ and $V_N$ are standard random normal variates. In the median, Eq. (28) coincides with Eq. (17) and, thus, the parameters a and λ of Eq. (28) coincide with those determined by fitting the median results of tests.

Again, let us consider Cases A and B. Integrating Eq. (28) for a step-function load history, the time to fracture $T_c$ is given by:

Case A:

$$T_c = \frac{1}{\lambda\, e^{\omega_2 V_N}} \ln\left(1.0 + \frac{\lambda\, e^{\omega_2 V_N}}{a\, e^{\omega_1 R_N} (\sigma - \sigma_o)^b}\right) \quad (29)$$

Case B:

$$T_c = \frac{1}{a\, e^{\omega_1 R_N}\, \sigma^b} \quad (30)$$

Examining Eq. (29), the time to fracture under constant load is influenced by both parameters $\omega_1$ and $\omega_2$. Only $\omega_1$ controls the time $T_c$ in Case B. For ramp loading, a closed-form solution is possible only in Case B. A numerical procedure is required for the general model, as shown by Barrett and Foschi (1978b). For Case B,

$$T_r = \frac{b + 1}{a\, e^{\omega_1 R_N}}\, \sigma^{-b} \quad (31)$$

While only $\omega_1$ controls the variability in $T_r$ for Case B, both parameters $\omega_1$ and $\omega_2$ affect the time to fracture $T_r$ in the general Case A. It can be shown, however, that the effect of $\omega_2$ is negligible and, thus, the value of the parameter $\omega_1$ can be determined from a known variability in the "standard" short-term ramp-load test. The value of $\omega_2$ can be chosen to reflect the variability in time to fracture at any other stress ratio. A value $\omega_2 = 1.15$ corresponds to a range of time to fracture of two decades at a stress ratio $\sigma = 0.7$ in the data of Wood (1951). The relationship between $\omega_2$ and the range of time to fracture, derived by computer simulation, is given in Barrett and Foschi (1978b).

Given the variability parameters $\omega_1$ and $\omega_2$, varying the standard random normals $R_N$ and $V_N$ allows the determination of the cumulative-distribution function for time to fracture for any specified load history. Consider, for example, the case of a wood member subjected to a constant stress level $\tau_c$. The problem is to determine the distribution of times to fracture and, thereby, predict the reliability at any given time to fracture or, given the desired life, predict the reliability for different stress levels $\tau_c$. Our traditional approach to the development of design stresses assumes that the 5th percentile of the short-term strength distribution is known. This 5th percentile, $\tau_s(0.05)$, is divided by a factor ϕ, to account for duration-of-load effects and to provide a factor of safety. For bending members, the factor $\phi = 2.1$ is commonly used. Thus, the design stress $\tau_c$ can be written

$$\tau_c = \frac{\tau_s(0.05)}{\phi} \quad (32)$$

The stress ratio $\sigma$ applied to the member can be determined by dividing the design stress $\tau_c$ by the short-term strength $\tau_s$. Using Eq. (31) and (32), the stress ratio $\sigma$ can be expressed as follows,

$$\sigma = \frac{e^{\omega_1 R_N}}{e^{1.645\,\omega_1}} \quad (33)$$

Thus, introducing Eq. (33) into Eq. (30), one obtains an expression for the logarithm of the time to fracture $T_c$,

$$\ln T_c = b \ln \phi + 1.645\ \omega_1 - \ln a \quad (34)$$
$$- R_N\, b\, \omega_1\ (1 + 1/b)$$

It is apparent, therefore, that the distribution of $T_c$ is lognormal and of the form

$$\ln T_c = \mu + \beta^* s \quad (35)$$

where:

$$\mu = b \ln\phi + 1.645\ \omega_1 - \ln a \quad (36)$$

$$s = b\ \omega_1\ (1 + 1/b) \quad (37)$$

and $\beta^*$ a standard random-normal variate. The value of $\beta^*$ corresponding, from Eq. (35), to a given value of $\phi$ and a desired life $T_c$, can be directly correlated with the probability of failure at $T_c$ by using normal probability tables. Thus, for the constant-load test, Eq. (35) can be used to determine the relationship between failure probability and time to fracture as a function of the variability in short-term strength and the design factor $\phi$.

Figure 26 shows the relationship between $T_c$ and $\beta^*$ for different levels of $\omega_1$ maintaining constant $\phi = 2.1$. Figure 27 shows $\beta^*$ as a function of $T_c$ and the factor $\phi$ for $\omega_1 = 0.40$, corresponding to a typical coefficient of variation for visually graded dimension lumber in bending. Finally, Figure 28 shows the relationship between $\beta^*$, $\phi$, and $\omega_1$ for a fixed value of $T_c = 10$ years. A similar analysis has been carried out by computer simulation using the general model of Case A. Figure 29 shows the relationship between $\phi$ and $T_c$ for fixed probability-of-failure levels using $\omega_1 = 0.4$ and $\omega_2 = 1.15$.

The method outlined for constant loads can be extended to predict the probability of failure for any load history and design factor $\phi$. Barrett and Foschi (1978b) studied the reliability of single members under cyclic loads of constant and of random amplitude. The lattter were obtained from models for snow loading, using distributions for annual maximum snow loads and estimates for the period of ground snow to simulate each snow cycle as a triangular pulse. The amplitude was a random variable chosen from the appropriate snow-depth distribution, and the cycle duration was taken equal to the mean-annual period of recorded ground snow. Eq. (28) was integrated for the resulting load history, and computer simulation was used to determine the reliability of structural elements at selected lifetimes.

Results obtained for Cases A and B are shown in Figures 30 and 31 for $\omega_1 = 0.15$ and 0.40, based on a design life of 30 years and taking the snow records for the cities of Vancouver and Winnipeg. It is assumed that the design load is that snow load with a probability of 1/30 of being exceeded. The predicted-failure probability, for a given value of $\phi$, is generally higher in Winnipeg. This suggests that it should be necessary to adjust the design loads for different locations to achieve a constant level of safety.

The generalized damage model developed by Barrett and Foschi has been fitted to experimental data from small, clear bending specimens. Its application to realistic reliability analyses hinges on the development of data for load-duration effects in in-grade material. Studies are currently underway in Canada and the United States to characterize that behavior.

## III. Slow Crack-Growth Models

The concepts of linear-elastic fracture

mechanics were discussed previously in relation to the prediction of the effect of cracks on the short-term ultimate behavior. These concepts have been extended to allow prediction of the long-term behavior of cracked members in materials subject to delayed fracture. Predictions of the time to fracture for members is developed from a knowledge of the relationship between the applied-stress intensity factor and the corresponding crack velocity. A simple method for studying slow crack growth, based on the double torsion specimen, was presented by Williams and Evans (1973). This specimen has been used to study the K - V relationship for Douglas-fir (Mindess, Nadeau and Barrett, 1975). The relationship between stress-intensity factor and crack velocity was expressed as

$$K_I = \alpha V^n \quad (38)$$

where $K_I$ is the stress-intensity factor in the opening mode (Mode I),V the crack velocity and $\alpha$ and n are material parameters. A typical set of test results is shown in Figure 32 for cracks propagating parallel to the grain. Using the $K_I$ - V relationship and the relationship between applied loads and stress intensity, it is possible to derive a relationship between the initial stress intensity, $K_{Ii}$, the applied constant stress $\sigma$, and the time to fracture T. This is given as follows,

$$T = \frac{2}{\alpha \sigma^2 Y^2 (n - 2)} K_{Ii}^{2-n} \quad (39)$$

where Y is a correction factor for finite width. Fig. 33 shows the predicted time to fracture as a function of the applied stress ratio derived on the basis of the slow crack-growth tests for Douglas-fir.

Given a series of nominally similar specimens, the time-to-fracture result of Eq. (39) can be used to develop the following relationship between time to fracture and applied stress for constantly loaded specimens,

$$\sigma^n T = \text{Constant} \quad (40)$$

A similar relationship can be obtained between the fracture stress and the strain rate for ramp tests. Figure 34 shows the predicted relationships for constant- and ramp-load tests obtained from the slow crack-growth model. In each case, the slope of the trend line is a function of the parameter n. The results of constant-load tests are shown in Figure 33 with the predicted constant-load behavior. Figure 35 shows the results of a series of displacement-rate tests designed to test the slow crack-growth hypothesis. The slopes measured in these two tests agree well with the expected results for time to fracture to approximately one day. Beyond one day, the trend line in the constant-load data drops much more rapidly than predicted, indicating a possible change of process which is not accounted for in the current slow crack-growth models.

Preliminary investigations of the suitability of the slow crack-growth model for studying the delayed fracture of wood under constant and ramp loads suggest that the approach could be useful for developing a more fundamental model of the fracture process. Comparisons between predicted and observed behavior under constant load indicate that the range of applicability of the current slow crack-growth models may be limited to times to fracture of approximately one day. Extension of the approach to treat the effects of variability in time to fracture at a constant stress and variability in strength would be required to assess the general suitability of the approach for treating reliability problems in wood structures.

## STRENGTH AND RELIABILITY OF WOOD STRUCTURES

We want to discuss briefly the implications of the previous topics from the point of view of reliability of wood structures. In a probabilistic approach to design, it is recognized that both the loads and the strength of the material are not deterministic values. In the simplest approach, two random variables are defined: U, the "load effect" (e.g., the maximum bending stress produced by the loads) and R, the "resistance" (e.g., the bending strength of the member). Each random variable has its own distribution, and failure will occur if $U \geq R$. If the two distributions superpose, so that the failure criterion is satisfied for a certain range of the variables, there exists the possibility of failure and the probability of this occurrence can be calculated when the distributions are known. An exact knowledge of the distributions is normally difficult to obtain, particularly of their tails which are the determining factors for the calculation of failure probabilities. An alternative approach (on which probabilistic design codes for steel have been based, for example) is that of using a "safety index" $\beta$ for the evaluation of safety. Using the logarithms of U and R to write the failure criterion $\ell n(U) \geq \ell n(R)$, and further assuming that U and R are lognormally distributed, the safety index $\beta$ can be calculated from

$$\beta = \frac{\ell n(\bar{R} / \bar{U}) - \frac{1}{2}\ell n(1 + V_R^2) + \frac{1}{2}\ell n(1 + V_U^2)}{\sqrt{\ell n(1 + V_R^2) + \ell n(1 + V_U^2)}} \quad (41)$$

where $\overline{U}$ and $\overline{R}$ are the means of the corresponding variables and $V_U$ and $V_R$ are their coefficients of variation. If these coefficients of variation are sufficiently small, q. (41) can be approximated by

$$\beta = \frac{\ell n(\bar{R} / \bar{U})}{\sqrt{V_R^2 + V_U^2}} \quad (42)$$

which holds for any distribution (i.e., under the assumption of low variability, there is no need to specify lognormal distributions for R and U).

The safety index $\beta$ relates to the probability of failure: if U and R are lognormal variables, the failure probability can be obtained directly by using $\beta$ from Eq. (41) and entering normal probability tables. If the variability is low, $\beta$ from the approximation of Eq. (42) can also be used with normal probability tables for any distribution of U and R. As an example, $\beta = 3$ gives, approximately, a failure probability of $10^{-3}$ and so on. For a more detailed discussion of the safety index formulation and the assumptions behind the different definitions see Foschi (1978).

For materials with low variability (e.g., steel) Eq. (42) has been used to compute the safety index of different structural applications and to obtain, as much as possible, a constant index across applications. Note that the use of eq. (42) has eliminated the need for distribution assumptions, which has allowed this method to be called "distribtuion free". A "target index" is adopted according to the desired level of safety and/or past experience, and for steel a target of $\beta = 3.0$ has been chosen. Ideally, the same target index should apply to all materials, as safety should be, from the consumer's point of view, independent of material. Can wood match steel's performance and can we analyze the safety of wood structures following the same procedures? We think that these are questions that must be carefully considered.

First, we have to deal with large variability and, therefore, have to make a statement about distributions. Second, and perhaps a more important problem, it is impossible to define "strength" or "resistance" in wood without specifying the load history, as we have already discussed. The variables U and R are not "independent", but their relationship can be quantified by using the damage-accumulation models. We have seen that these models depend on distribution assumptions for the damage-accumulation law, and that they allow a direct calculation of failure probabilities. Can we still use the concept of safety index? To answer this question, consider the case of cyclic loading corresponding to snow loads. If U is the amplitude of the cycle for the 20th year, the distribution of U will be the distribution of annual maxima. The distribution of R to be used in conjunction with U must take into account the effect of the previous 19 years and, assuming that this distribution can be obtained through use of the damage accumulation models, a safety index can be calculated, in principle, at the 20th year. The important conclusion is that the safety index $\beta$ is now a function of time and, since its calculation is dependent on distribution assumptions for the damage models, it presents no clear advantage over direct calculation of failure probabilities.

## REFERENCES

Barrett, J.D. 1974. Effect of Size on Tension Perpendicular-to-Grain Strength of Douglas-fir. *Wood Fiber* 6 (2): 126-143.

Barrett, J.D. 1976. Effect of Crack-Front Width on Fracture Toughness of Douglas-fir. *Eng.Fract. Mech.* 8:711-717.

Barrett, J.D., Foschi, R.O. and Fox, S.P. 1975. Perpendicular-to-Grain Strength of Douglas-fir. *Can. J. Civ. Eng.* 2 (1): 50-57.

Barrett, J.D. and Foschi, R.O. 1977a. Mode II Stress Intensity Factors for Cracked Wood Beams. *Eng. Fract. Mech.* 9:371-378.

Barrett, J.D. and Foschi, R.O. 1977b. Shear Strength of Uniformly Loaded Dimension Lumber. *Can. J. Civ. Eng.* 4 (1):86-95.

Barrett, J.D. and Foschi, R.O. 1978a. Duration of Load and Failure Probability in Wood. Part I: Modelling Creep Rupture. *Can. J. Civ. Eng.* 5(4):-505-514.

Barrett, J.D. and Foschi, R.O. 1978b. Duration of Load and Failure Probability in Wood. Part II: Constant, Ramp and Cyclic Loadings. *Can. J. Civ. Eng.* 5(4):515-532.

Bolotin, V.V. 1969. *Statistical Methods in Structural Mechanics.* Holden-Day Inc., San Francisco.p. 49-53.

Foschi, R.O. 1979. A Discussion on the Application of the Safety Index Concept to Wood Structures. *Can. J. Civ. Eng.* 6(1):51-58

Foschi, R.O. and Barrett, J.D. 1976a. Longitudinal Shear Strength of Douglas-fir. *Can. J. Civ. Eng.* 3 (2):198-208.

Foschi, R.O. and Barrett, J.D. 1976b. Stress Intensity Factors in Anisotropic Plates Using Singular Isoparametric Elements. *Int. J. Num. Meth. Eng.* 10 (6):1281-1288.

Foschi, R.O. and Barrett, J.D. 1977. Longitudinal Shear in Wood Beams: A Design Method. *Can. J. Civ. Eng.* 4 (3): 363-370.

Gerhards, C. 1977. Effect of Duration and Rate of Loading on Strength of Wood and Wood-Based Materials. U.S. D.A., Forest Products Lab., Madison, Wis., Research Paper FPL 283.

Leicester, R.H. 1971. Some Aspects of Stress Fields at Sharp Notches in Orthotropic Materials. I. Plane Stress. Aust. CSIRO, Div. Forest Prod. Tech., Paper No. 57.

Mindess, S., Nadeau, J. and Barrett, J.D. 1975. Slow Crack Growth in Douglas-fir. *Wood Science* 8(1):339-396.

Weibull, W. 1939. A Statistical Theory of the Strength of Materials. Proc. Roy. Swed. Inst. Eng. Res., Stockholm, No. 151.

Williams, M.L. 1952. Stress Singularities Resulting from Various Boundary Conditions in Angular Corners of Plates in Extension. *J. Appl. Mech.* 19:526-528.

Williams, D.P. and Evans, A.G. 1973. A Simple Method for Studying Slow Crack Growth. *J. Testing Eval.* 1 (4):264 - 270.

Wood, L.W. 1951. Relation of Strength of Wood to Duration of Load. US Forest Prod. Lab., Madison, Wis., Report R-1916.

## TABLE I

Effective Periods of Constant Load

| Cycle Shape Parameter<br>n | Load History | $T^*$ |
|---|---|---|
| 0 | 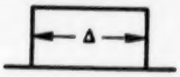 | $N_f \Delta$ |
| 0.25 | 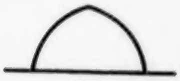 | $N_f \Delta/10$ |
| 1.0 | 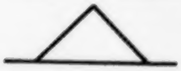 | $N_f \Delta/37$ |
| 4.0 | 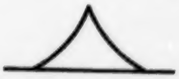 | $N_f \Delta/145$ |

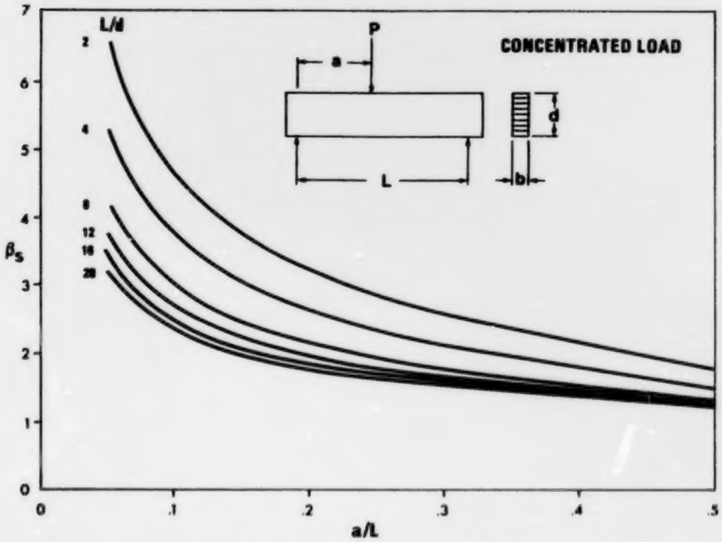

Figure 1. Stress distribution factor for a single concentrated load.

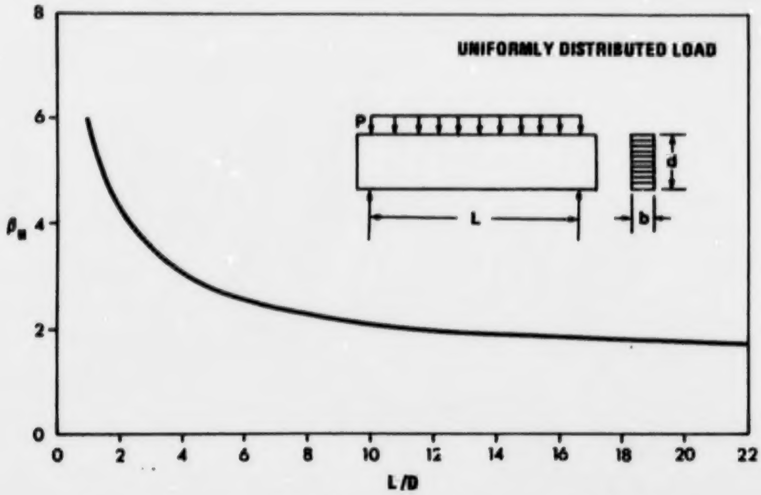

Figure 2. Stress distribution factor for uniformly distributed load.

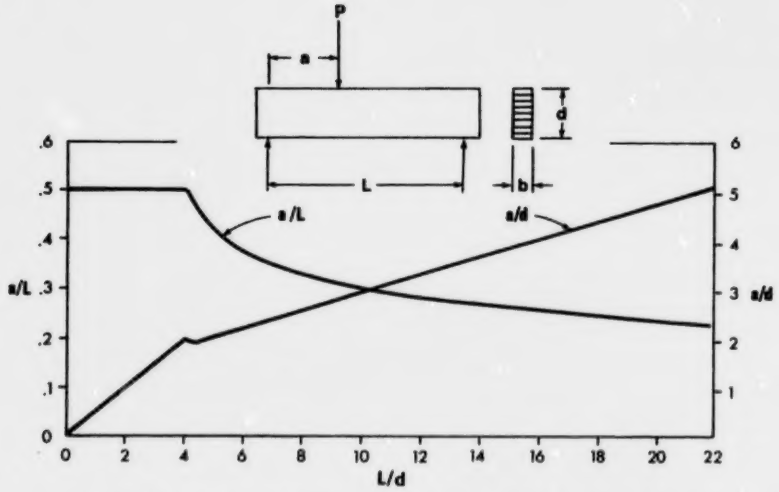

Figure 3. Most unfavorable position for a single concentrated load.

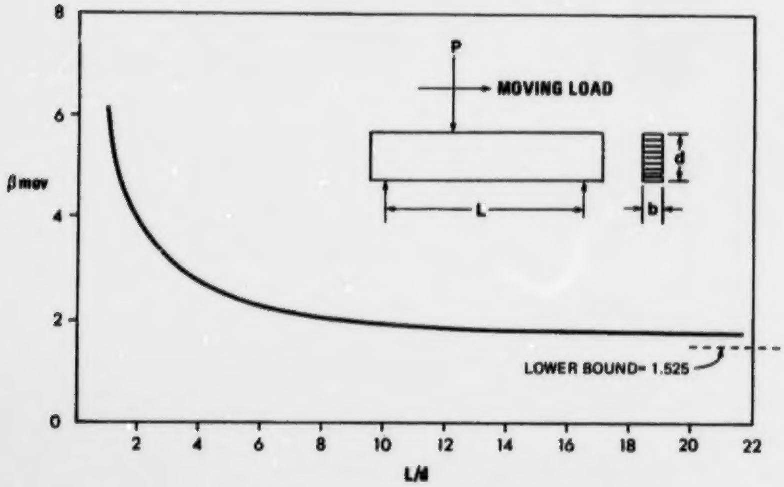

Figure 4. Stress-distribution factor for a moving concentrated load.

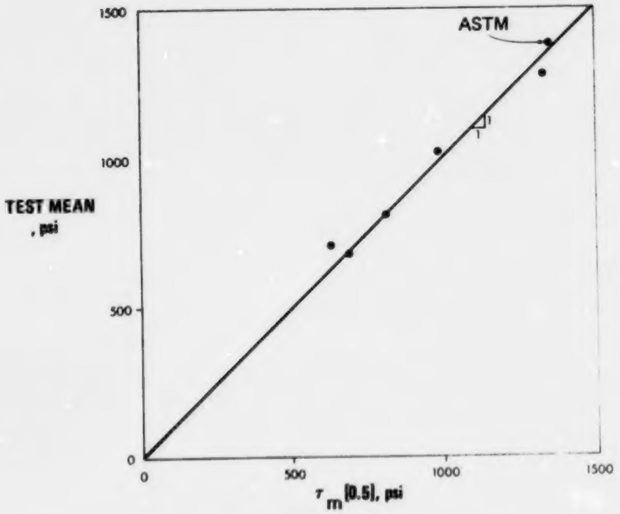

Figure 5. Comparison of fitted and observed strengths, fit of k and $\tau^*$ (0.5).

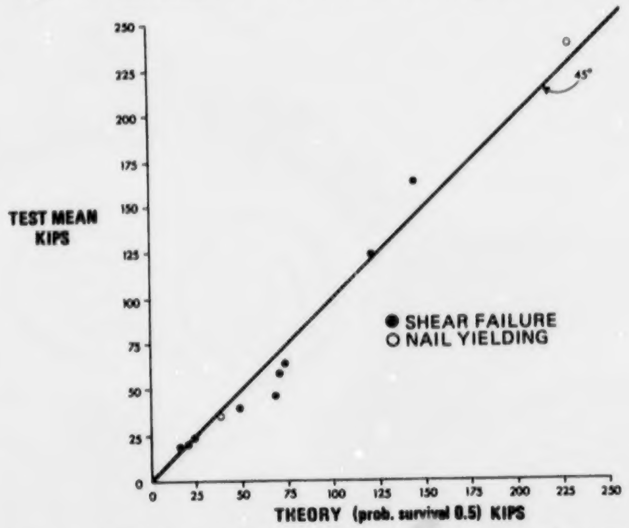

Figure 6. Comparison of predicted and measured failure loads, nailed connection.

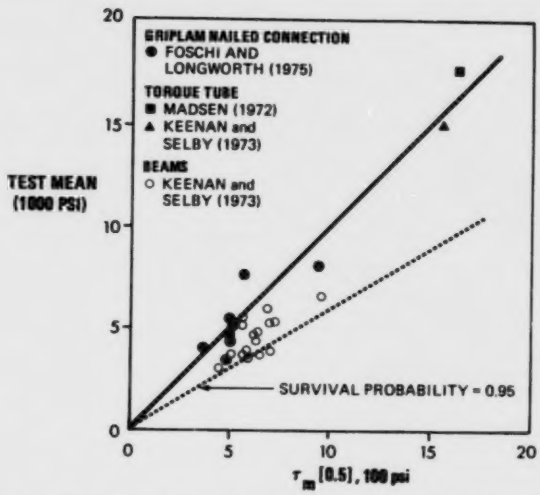

Figure 7. Comparison of predicted and measured stregnths for other configurations.

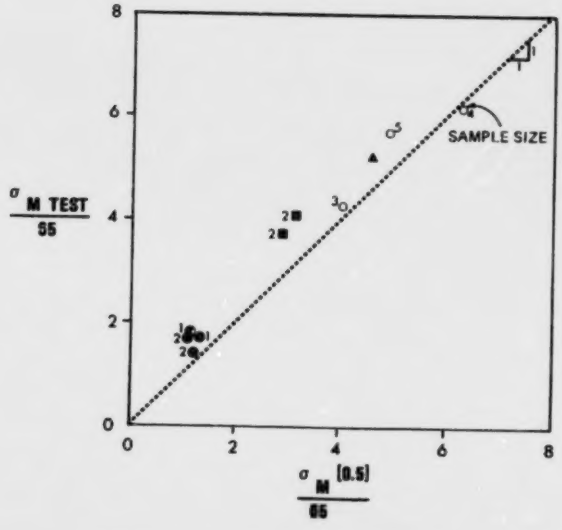

Figure 8. Comparison of predicted and measured strengths, tension perpendicular to the grain.

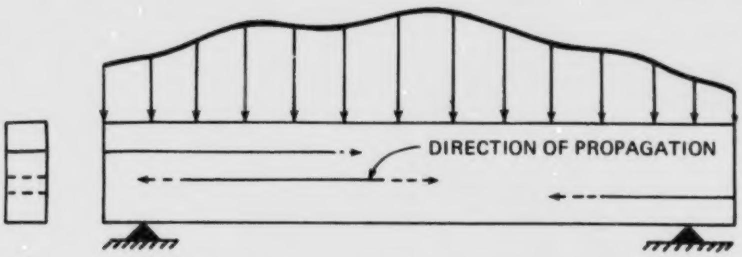
DIRECTION OF PROPAGATION

Figure 9. Example of a cracked beam.

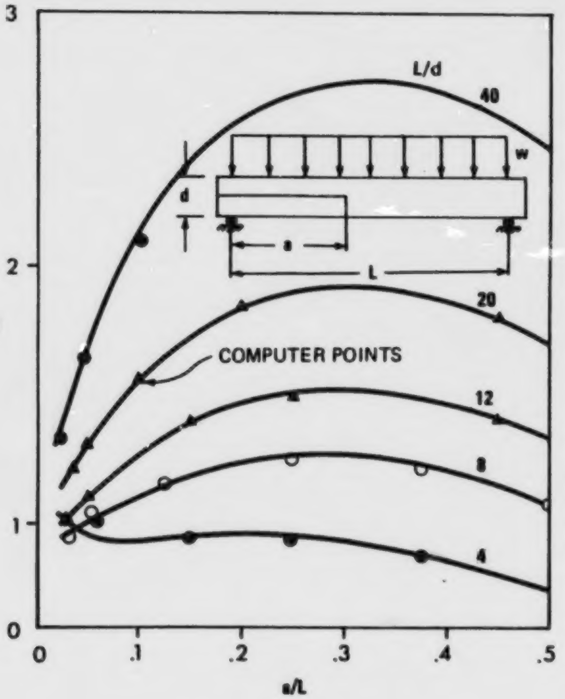

Figure 10. Stress-intensity factors, end-cracked beam under uniform load.

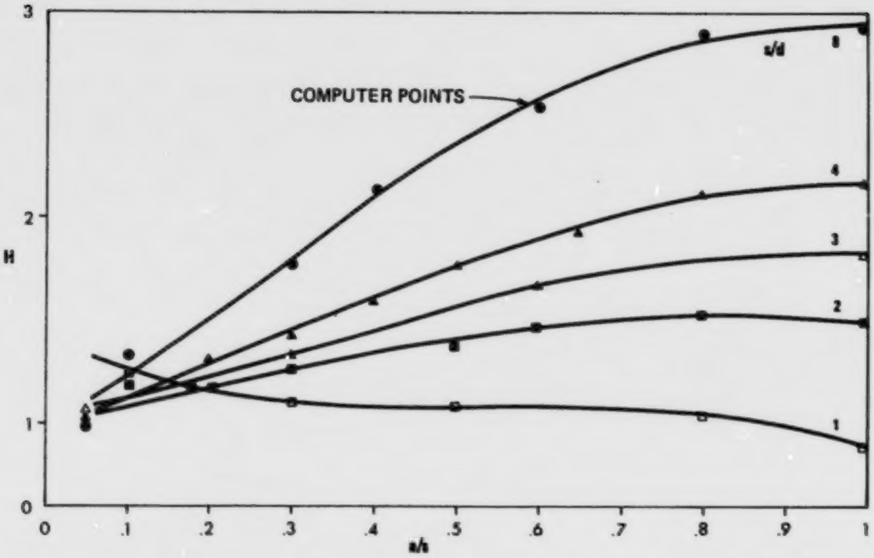

Figure 11. Stress-intensity factors, end-cracked beam under a concentrated load.

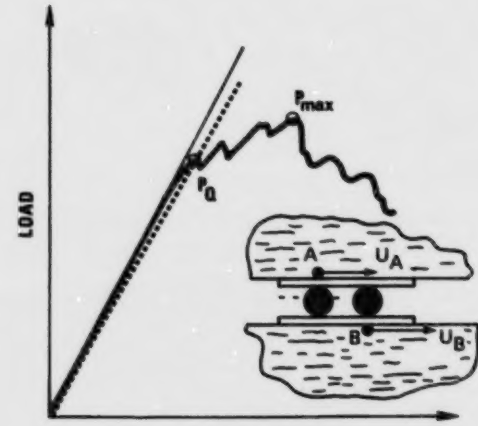

LOAD
$P_{max}$
$P_Q$
A
$U_A$
B
$U_B$
$U_B - U_A$

Figure 12. Load-crack opening displacement experimental curve.

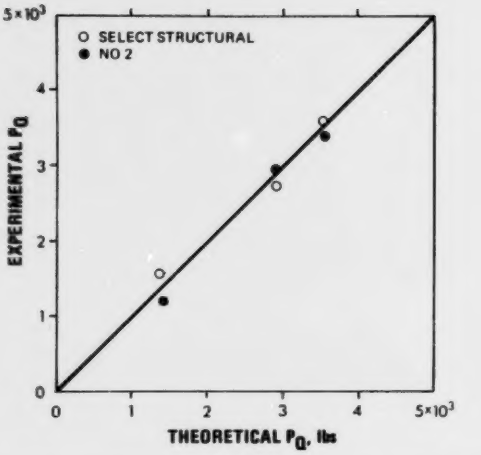

Figure 13. Comparison of predicted and measured failure loads, end-cracked dimension lumber.

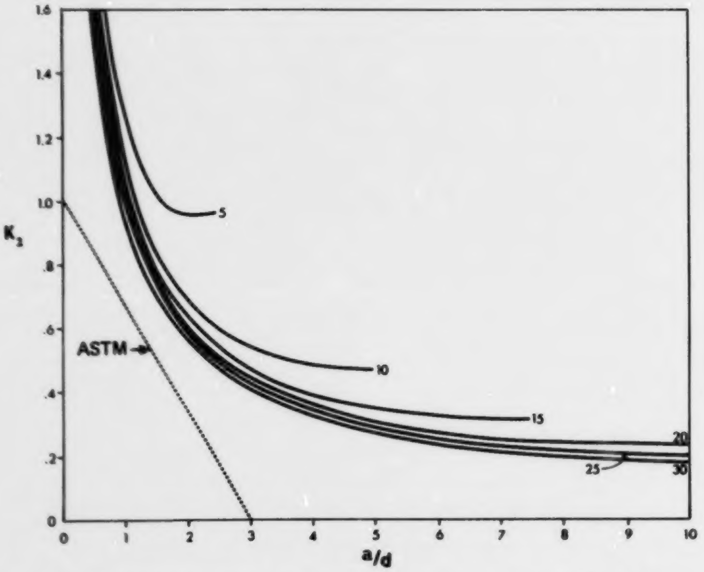

Figure 14. Strength-reducing factor, end-cracked beams under uniform load.

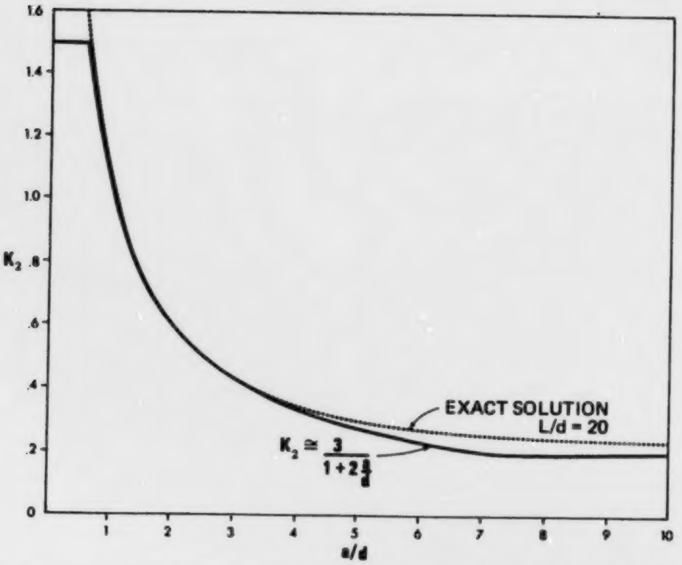

Figure 15. Strength-reducing factor, end-cracked beams under uniform load (approximation).

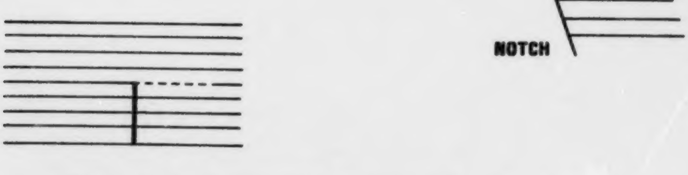
INITIAL CRACK
CRACK PROPAGATION
GRAIN
NOTCH

Figure 16. Crack propagation in sharp cracks and notches.

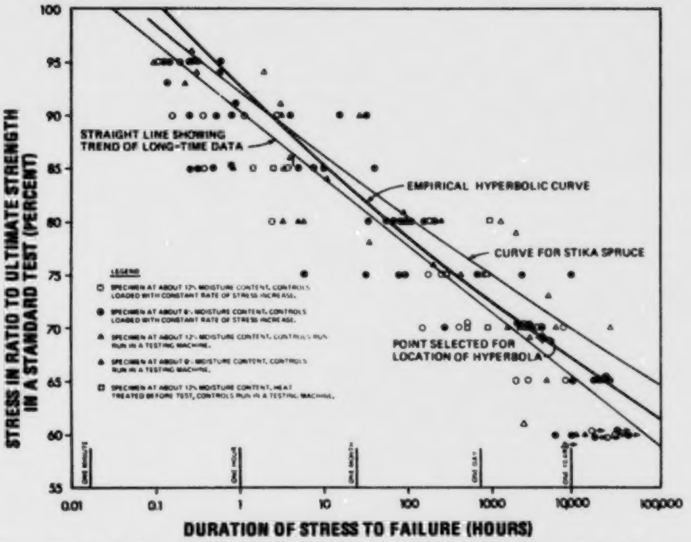

Figure 17. Relation of duration of constant stress to level of stress in long-time loading of Douglas-fir bending specimens (Wood, 1951).

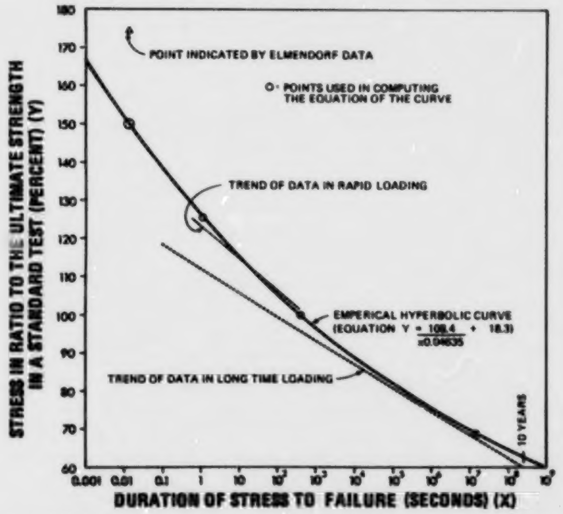

Figure 18. Relation of duration of stress to level of stress in long-time loading and rapid loading of Douglas-fir bending specimens (Wood, 1951).

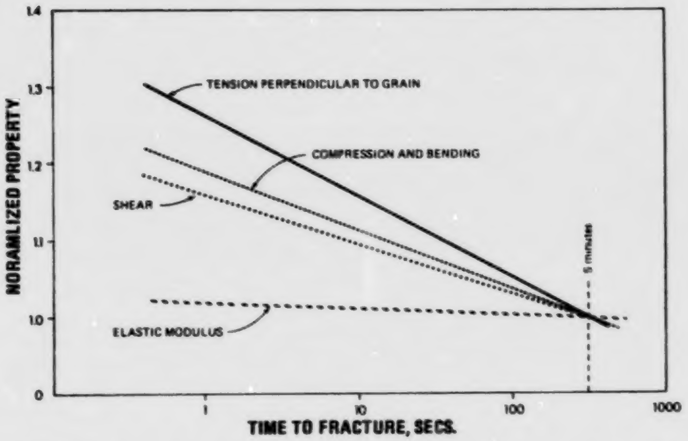

Figure 19. Effect of rate of loading on strength and elastic properties of small, clear specimens.

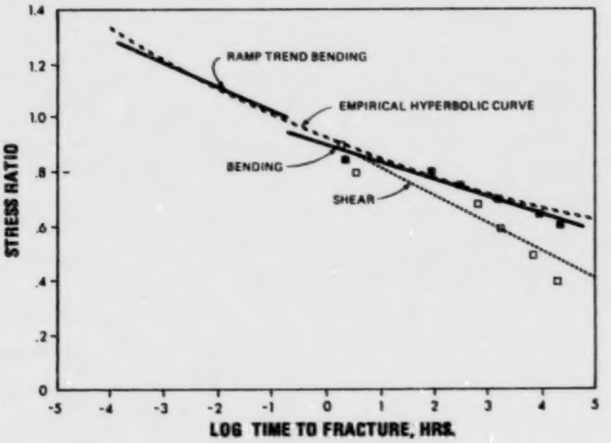

Figure 20. Trend lines for ramp and constant load tests of small, clear specimens.

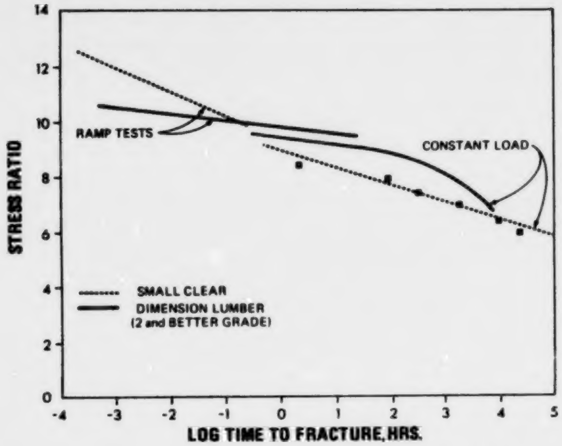

Figure 21. Comparison of trend lines for ramp and constant-load tests of small, clear and dimension-lumber specimens.

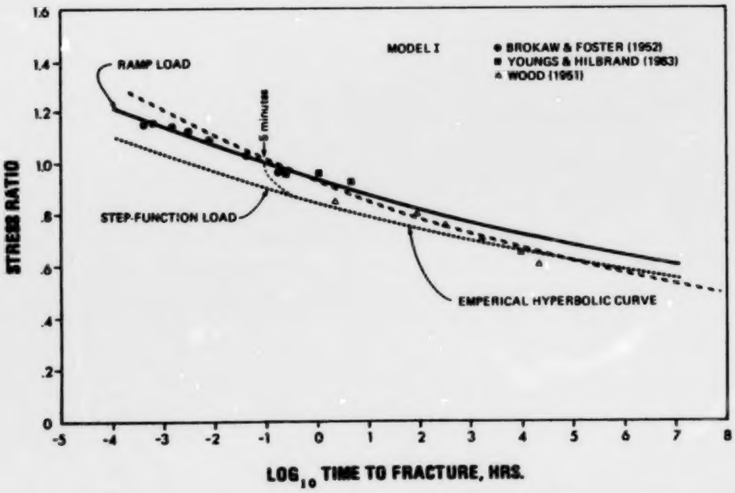

Figure 22. Fit of damage model (Case B) to small, clear bending strength results.

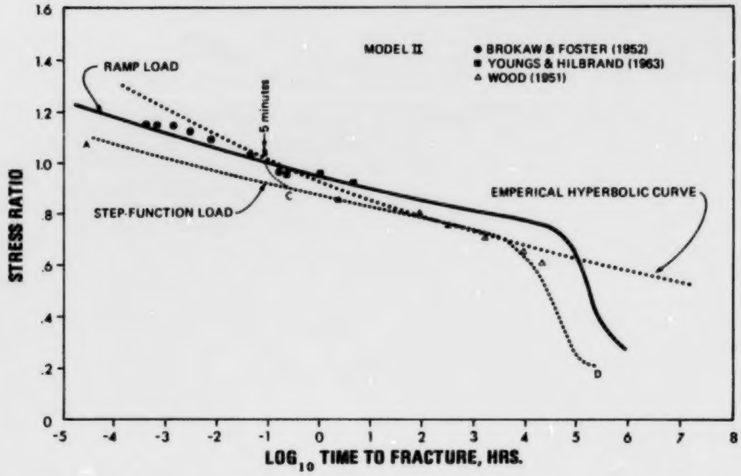

Figure 23. Fit of damage model (Case A) to small, clear bending strength results.

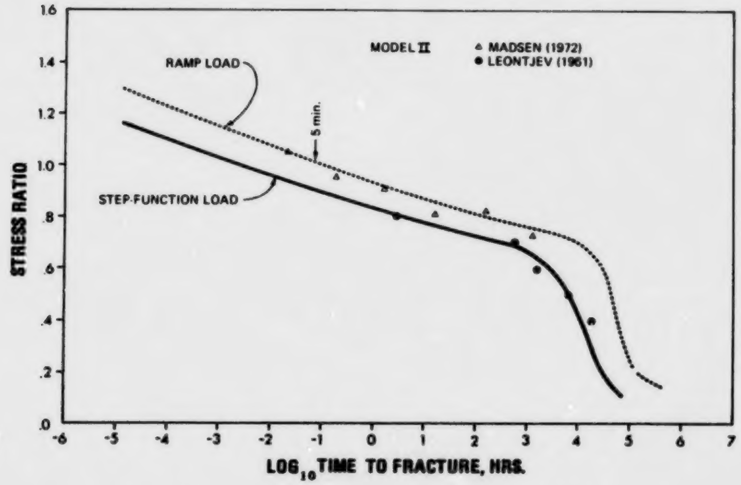

Figure 24. Fit of damage model (Case A) to small, clear shear strength results.

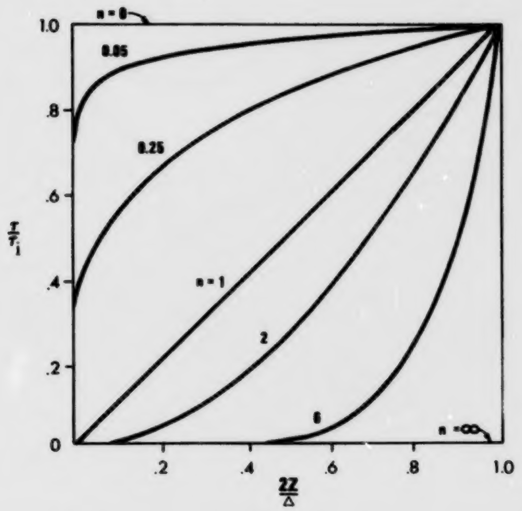

Figure 25. Cycle shape as influenced by the shape parameter n.

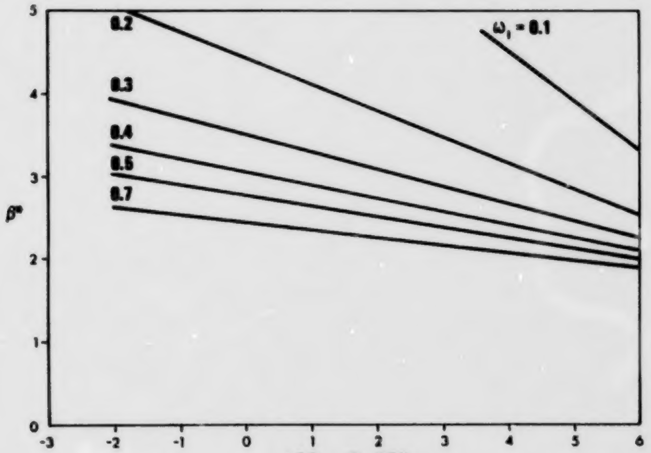

Figure 26. Relationship between time to fracture $T_c$ under constant load and the safety measure $\beta^*$ for different $\omega_i$; $\phi = 2.1$.

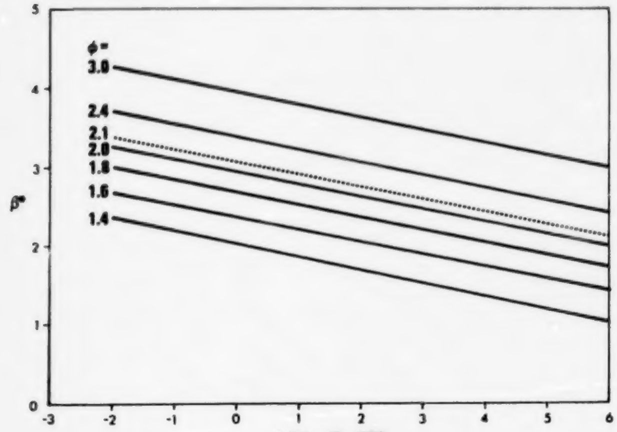

Figure 27. Relationship between time to fracture $T_c$ under constant load and the safety measure β*, for different φ; $\omega_1$ = 0.40.

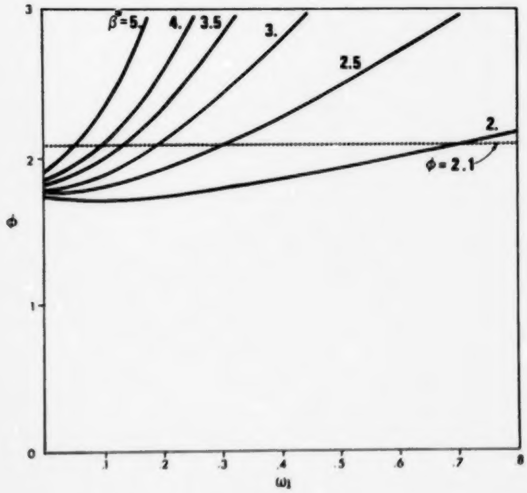

Figure 28. Relationship between the safety measure β*, φ, and $\omega_1$ for a time to fracture under constant load $T_c$ = 87600 hours (10 years).

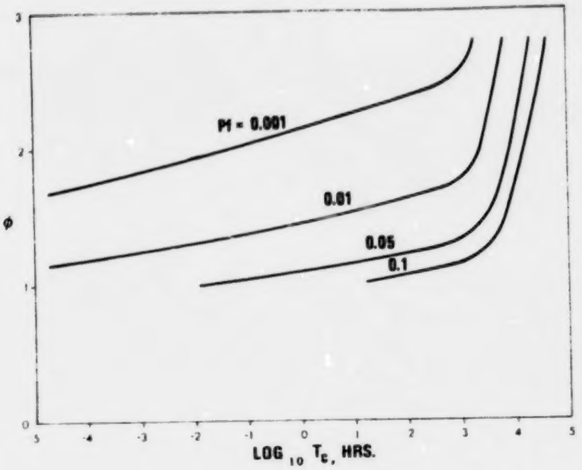

Figure 29. Relationship between $\phi$, probability of failure $P_f$ and time to fracture $T_c$ under constant load. Case A: $\omega_1 = 0.40, \omega_2 = 1.00$.

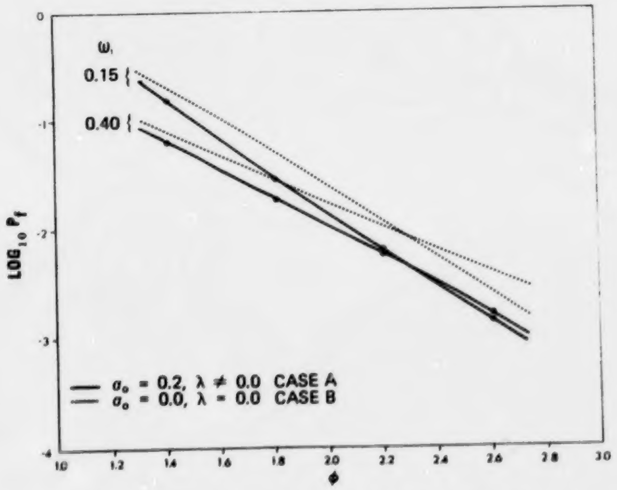

Figure 30. Probability of failure $P_f$ as a function of $\phi$ for Vancouver. Snow load only, Cases A and B.

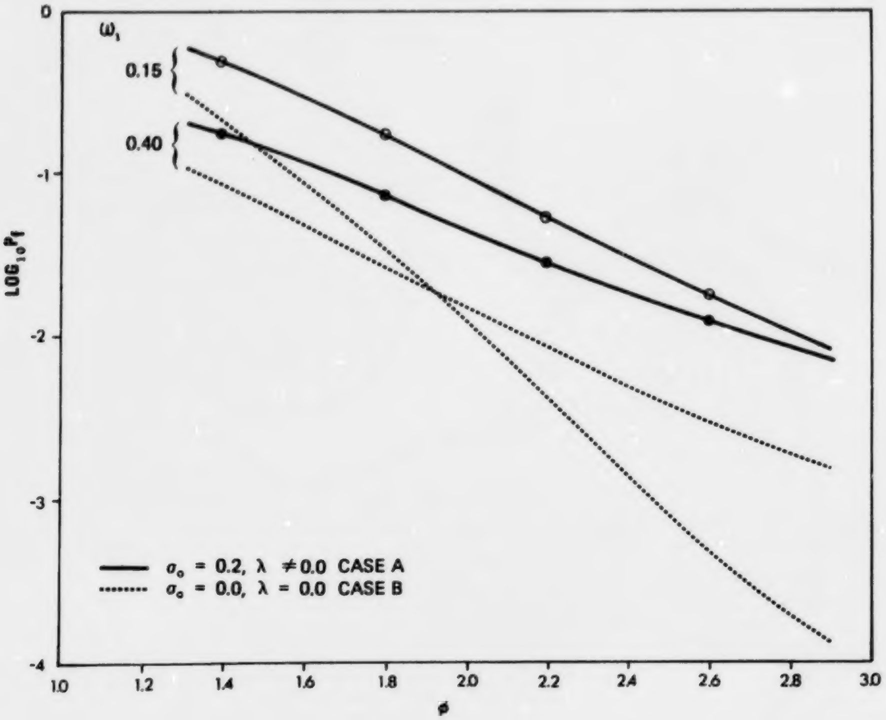

Figure 31. Probability of failure $P_f$ as a function of $\phi$ for Winnipeg. Snow load only, Cases A and B.

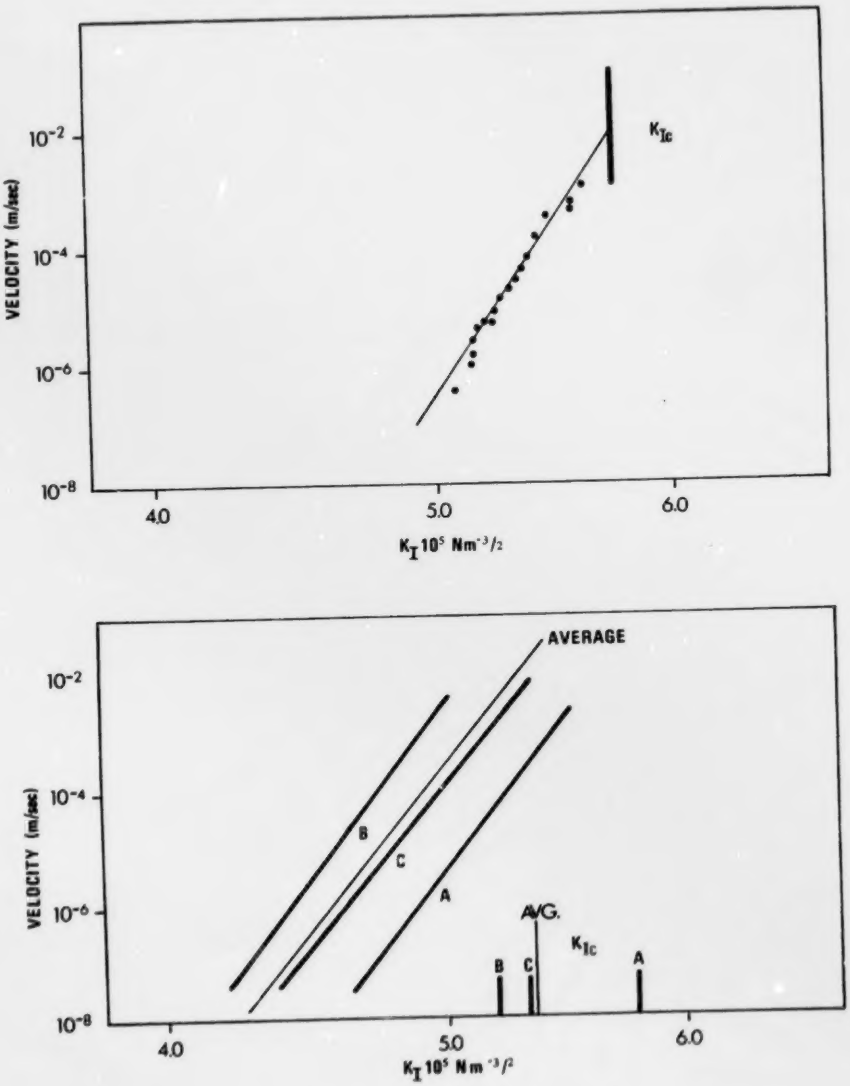

Figure 32. $K_I$ vs. V curves for Douglas-fir.

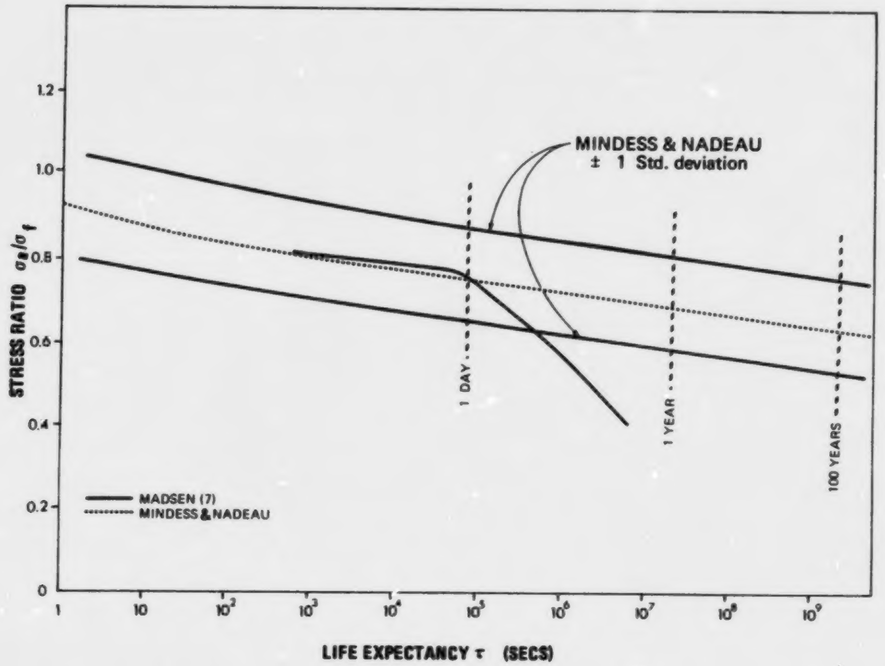

Figure 33. A comparison of the predicted constant-load behavior using slow crack growth models with the results of constant-load tests.

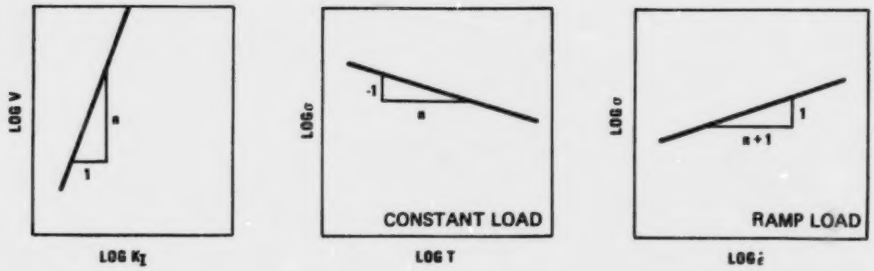
LOG V
n
1
LOG $K_I$
LOG σ
-1
n
CONSTANT LOAD
LOG T
LOG σ
1
n + 1
RAMP LOAD
LOG $\dot{\varepsilon}$

Figure 34. Constant-load and ramp-load behavior predicted using slow crack growth model.

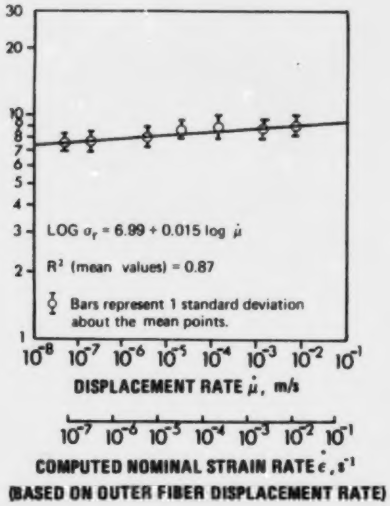

Figure 35. Modulus of rupture vs. displacement rate and nominal strain rate.

# ORTHOTROPIC AND MIXED MODE FRACTURE IN WOOD

By

C.L. CHOW & C.W. WOO

---

Department of Mechanical Engineering, University of Hong Kong, Hong Kong

## ABSTRACT

It is well known that wood is a highly anisotropic, heterogeneous and porous material with variable mechanical properties. Although the anisotropy is originated from the tree stem, wood may be considered orthotropic if specimens are taken at a sufficient distance from the centre of the stem to avoid excessive curvature effect.

Wood as a constructional material is often subjected to the combined loading of both opening mode ($k_1$) and edge-sliding mode ($k_2$). However, recent investigation by Williams and Birch expressed concerns on the independence of $k_2$ and $k_1$ in the mixed mode fracture in wood.

Examination of the William's analysis revealed that the geometrical correction factor used for the mixed mode fracture should only be applied to mode I fracture. A set of geometrical correction factors which incorporated mixed mode effects is derived and applied to characterize fracture behavior of Kapur and Gagil (both classified as hardwood) at three different slanted angles. The results agree with those by other investigators that the mixed mode fracture in an orthotropic media is governed by mode I ($k_1$) as well as mode II ($k_2$). The timbers known as Kapur and Gagil are chosen because they have been observed to possess markedly different fracture toughness values. The tests were carried out with the DCB specimen for $K_{Ic}$ evaluation and with side-edge notch under uniform loading for mixed mode fracture.

## INTRODUCTION

For materials other than wood, there have been considerable developments in the characterization of fracture behavior (1) which is based on the linear elastic fracture mechanics (LEFM) propounded principally by Irwin (2). Although the history of applying the LEFM to wood fracture is relatively short, it has in the recent years received increasing attention and acceptance, and has been developed as a useful tool, not only for studying catastrophic failures by rapid crack propagation, but also for the design analysis for wooden structures ( 3 – 10).

Although wood is a highly anisotropic, heterogenous and porous material with variable mechanical properties, the anisotropy is originated from the tree stem. If the wood specimen is taken at a sufficient distance from the centre of the stem to avoid excessive curvature effect, wood may then be considered as an orthotropic plate. Although wooden structures are often subjected to the combined loading of both tension (mode I or $k_1$) and shear/torsion (mode II or $k_2$), information on the behaviors of wood fracture under the mixed mode loading is limited. The subject was first theoretically treated by Wu (4) who derived an empirical relation of $(k_1/k_1c) + (k_2/k_2c)^2 = 1$ for balsa wood.

In a recent publication by Williams and Birch (9), Utile and Scots pine were tested under the mixed mode loading. The results were analyzed and it was found that these timbers satisfied a constant $k_1c$ fracture criterion independent of $k_2$. This paper is intended to re-examine the constant $k_1c$ fracture criterion on the mixed mode behaviors of two types of timber known as Gagil (Hope segal, Morawan) and Kapur *(Dryobalanops* spp.) which are used extensively in Hong Kong as structural materials. The materials were chosen because they have been observed to possess markedly different $k_1c$ values. Side-notched specimen was used for the convenience of testing under the mixed mode while the geometrical correction factors associated with the specimen geometry are derived from the finite element analysis.

## MODE I FRACTURE IN ORTHOTROPIC MEDIA

There are three principal directions of material anisotropy in wood, viz along the axis of the trunk termed longitudinal (L), along the radial direction (R) and along the tangential direction (T) as shown in Fig. 1. Orthotropic system requires the determination of twelve elastic constants (11), namely three components of Young's moduli, $E_L$, $E_R$ and $E_T$, three components of moduli of rigidity, $\mu_{LR}$, $\mu_{RT}$ and $\mu_{TL}$ and six components of Poisson's ratios, $\nu_{LR}$, $\nu_{RT}$, $\nu_{TL}$, $\nu_{RL}$, $\nu_{TR}$, and $\nu_{LT}$. Of those components, none are independent and the Poisson's ratios and Young's moduli are related by

$$\frac{\nu_{LR}}{E_L} = \frac{\nu_{RL}}{E_R} \quad ; \quad \frac{\nu_{RT}}{E_R} = \frac{\nu_{TR}}{E_T} \quad ; \quad \frac{\nu_{TL}}{E_T} = \frac{\nu_{LT}}{E_L}$$

In this investigation, only the tangential and longitudinal directions (TL system) are considered as Porter (3) found little if any difference between crack-extension force values obtained from RL and TL systems and the same result pertained to a comparison of RT and TR system.

In the determination of the stress intensity factor in mode I ($k_1c$) or its equivalent $G_1c$ for metals, different testing methods and specimen geometries have been developed and well documented (12, 13, 14). Recently, the quasistatic energy method has received considerable attention, as the method is not only valuable in the $G_1c$ determination, but also in the characterization of different crack parameters such as stability, crack path, environmental effects, strain rate, etc. (15, 16, 17).

By the consideration of work theorem, it can be shown that

$$G_c = \left(\frac{\partial \Lambda}{\partial A}\right)_u = -\left(\frac{\partial \Omega}{\partial A}\right)_p \qquad (1)$$

where G is fracture toughness, A is crack surface area, p is load, u is displacement, $\Lambda$ is strain energy function and $\Omega$ is complimentary energy function.

Eqn. (1) provides simple experimental technique for the evaluation of $G_c$ which is defined as the energy required for an incremental crack growth as shown in Fig. 2.A. The specimen geometry chosen for the test is double-cantilever beam (DCB) which is depicted in Fig. 2.B together with the dimensions of the specimen used.

The tests were carried out with an Instron Universal testing machine which provides autographic recordings of the load and displacement. Crosshead speed of 2 mm/min was selected. Difficulty was experienced in determining the exact boundary of the crack tip, since the crack front appeared to be highly irregular. The difficulty was removed by pre-calibrating the compliance curve of the specimen at different crack lengths.

Since stability of crack propagation was observed during the quasistatic process, this agrees with the analytical prediction of the DCB specimen (17). Advantage of the geometrically stable specimen allows several fracture toughness values to be measured from one specimen, thus minimizing possible experimental errors.

For the orthotropic media with a crack in the direction of principal modulus, the stress intensity factors were found to be the same as the isotropic case and the fracture toughness G is related to K as (18)

$$G_I = K_I^2 \left[\frac{1}{2E_L E_T}\right]^{1/2} \phi \qquad (2.a)$$

$$G_{II} = \left[\frac{K_{II}^2}{1.4142E_L}\right] \phi \qquad (2.b)$$

$$Gc = \left[\frac{1}{2 E_L \; E_T}\right]^{1/2} \left[K_I^2 + \left(\frac{E_T}{E_L}\right)^{1/2} K_{II}^2\right] \phi \qquad (2.c)$$

where

$$K = \sqrt{\pi k}$$

and

$$\phi = \left[\left(\frac{E_L}{E_T}\right)^{1/2} - \frac{E_L\left(\frac{2\nu_{LT}}{E_T} - \frac{1}{\nu_{LT}}\right)}{2}\right]^{1/2}$$

It can therefore be seen that knowledge about the mechanical properties of the wood materials in the TL plane is necessary in order to obtain the stress intensity factor (K) from the measured fracture toughness (G). Separate specimens according to the ASTM standards (19) were then produced and tested. Their respective mechanical properties were measured and shown in Table 1.

A total of eight specimens were used for the $G_1c$ determination and an average of about three values were able to be obtained from each specimen due to the inherited stable characteristic of the DCB specimen described earlier. The measured fracture toughness values and their corresponding stress intensity factors are summarized in Table II for the timbers of Gagil and Kapur.

## MIXED MODE AND GEOMETRICAL CORRECTION FACTOR

Structural components of engineering interest are often loaded under the combined mode of opening (I) and edge-sliding (II). The mixed mode problem was first analytically treated by Sih *et al.* (20) who considered a crack inclined at an angle $\theta$in an infinite solid under a remote uniform stress $\sigma$ (Figure 3.A) and derived the following expressions:

$$\begin{aligned} k_1 &= \sigma\sqrt{a}\cos^2\theta \\ k_2 &= \sigma\sqrt{a}\cos\theta\sin\theta \end{aligned} \qquad (3)$$

Since it is experimentally desirable to initiate a crack from the side-edge of a specimen, dimensions shown in Fig. 3.B were chosen with the crack angles oriented at 15, 45 and 60 degrees along the "principal" modulus or grain direction of the timbers. Eqn. (3) may then be expressed for the specimen geometry as

$$\begin{aligned} k_1 &= \sigma Y_1\sqrt{a}\cos^2\theta \\ k_2 &= \sigma Y_2\sqrt{a}\cos\theta\sin\theta \end{aligned} \qquad (4)$$

For the determination of $k_1$ and $k_2$, Eqn. (4) requires the knowledge of the geometrical correction factors $Y_1$ and $Y_2$. This was accomplished with the finite element method by computing the state of displacements in the vicinity of the crack tip. The stress intensity factors can in turn be evaluated with the following expressions:

$$\begin{aligned} u &= \frac{k1}{\mu}\left(\frac{r}{2}\right)^{\frac{1}{2}} \cos\frac{\beta}{2}\left[\frac{1-\nu}{1+\nu} + \sin^2\frac{\beta}{2}\right] \\ &\quad + \frac{k2}{\mu}\left(\frac{r}{2}\right)^{\frac{1}{2}} \sin\frac{\beta}{2}\left[\frac{2}{1+\nu} + \cos^2\frac{\beta}{2}\right] \\ v &= \frac{k1}{\mu}\left(\frac{r}{2}\right)^{\frac{1}{2}} \sin\frac{\beta}{2}\left[\frac{2}{1+\nu} - \cos^2\frac{\beta}{2}\right] \\ &\quad + \frac{k2}{\mu}\left(\frac{r}{2}\right)^{\frac{1}{2}} \cos\frac{\beta}{2}\left[\frac{\nu-1}{1+\nu} + \sin^2\frac{\beta}{2}\right] \end{aligned} \qquad (5)$$

A typical finite element network used for the analysis is depicted in Fig. 4 and the geometrical correction factors $Y_1$ and $Y_2$ at 15, 45 and 60 degree angles are presented in Fig. 5. The results compare well with those by Bowie (21) who made use of the conformal mapping technique.

In the mixed mode tests, specimens were manufactured with grain at the above mentioned three angles to the specimen axis as shown in Fig. 3.B in which the dimensions of the specimen are also described. A total of three specimens each for a particular angled crack was used and loaded under the uniform loading with an Instron Universal testing machine. The cross-head speed of 2 mm/min was chosen for the tests. Meticulous attention was taken to assess accurately the critical fracture load which was recorded and plotted at different crack lengths. The averaged load was further checked by plotting the product of the uniform stress and the corresponding geometrical correction factor ($\sigma Y$) versus the reciprocal of the square root of the crack length ($1/\sqrt{a}$). The results are shown in Fig. 6 and good linearity can be observed at different angles for the types of timber considered.

The measured data can then be applied to evaluate the stress intensity factors of $k_1$ and $k_2$ of Eqn. (4) and the ratio of $k_1/k_2$ is shown to vary with a/W (Fig. 7).

## DISCUSSIONS AND CONCLUSIONS

The quasistatic energy method which has been found to be valuable in the characterization of fracture behaviors of materials other than wood is observed to apply equally well to that of Gagil and Kapur. Since stable crack propagation has been observed for the determination of mode I fracture, the use of the DCB specimen may be recommended for the testing of wood fracture as the specimen provides favourable geometrical stability factor, thus enabling several measurements of fracture toughness to be made from one specimen and providing savings for the costly machine time.

In the mixed mode fracture of Gagil and Kapur, constant $k_1c$ fracture criterion independent of $k_2$ has not been observed as that by Williams and Birch (9). Examination of the William's analysis revealed that the geometrical correction factor used should only be applied to mode I fracture. Although Williams based his justification on the finite element results by Mandell *et al.* (22), no conclusive agreement can be drawn from Mandell's work that the geometrical correction factors under the mixed mode loading for the orthotropic media with cracks along the grain direction should be the same as for mode I loading.

A set of geometrical correction factors which incorporate the mixed mode effects has been presented and applied successfully to the fracture behaviors of Gagil and Kapur. It is found that for orthotropic media under the mixed mode loading, the ratio of $k_1/k_2$ decreases with the increase of crack length, a phenomenon which agrees with similar findings by Wu (4).

## REFERENCES

1. Liebowitz, H., Fracture, Vols. I – VII, Academic Press, New York, 1968.
2. Irwin, G.R., Structural Mechanics. Pergamon Press, London, 1960.
3. Porter, A.W., On the Mechanics of Fracture in Wood. Forest Products J. 14(8): 325 – 331, 1964.
4. Wu, E.M., Application of Fracture Mechanics to Anistropic Plates, J. App. Mechanics, Series E 34: 967 – 974, 1967.
5. Schneiwind, A.P. and Pozniak, R.A., On the Fracture Toughness of Douglas Fir Wood. Engineering Fracture Mechanics 2: 223 – 233, 1971.
6. DeBaise, G.R., Morphology of Wood Shear Fracture. J. of Materials 7: 568 – 572, 1972.
7. Barrett, J.D., Effect of Crack-front Width on Fracture Toughness of Douglas-Fir. Engineering Fracture Mechanics 8: 711 – 717, 1976.
8. Barrett, J.D. and Foschi, R.O., Mode II Stress-Intensity Factors for Cracked Wood Beams. Engineering Fracture Mechanics 9: 371 – 378, 1977.
9. Williams, J.G. and Birch, M.W., Mixed Mode Fracture in Anisotropic Media, Cracks and Fracture. STP 601, American Society for Testing and Materials: 125 – 137, 1976.
10. Standards Association of Australia, AS CA65-1972. SAA Timber Engineering Code, Sydney, 1972.
11. Lekhnitskii, S.G., Anisotropic Plates, translated from Russian 2nd ed. Gordon and Breach, New York, 1957.
12. Fracture Toughness Testing and its Applications. STP 381, American Society for Testing and Materials, 1965.
13. Plain Strain Crack Toughness Testing of High Strength Metallic Materials. STP 410, American Society for Testing and Materials, 1966.
14. Kobayashi, A.S., Experimental Techniques in Fracture Mechanics. Society for Experimental Stress Analysis, U.S.A., 1973.
15. Gurney, C. and Hunt, J., Quasistatic Crack Propagation. Proc. Roy. Society, London, A299, 1957, pp. 508 – 524.
16. Gurney, C. and Ngan, K.M., Quasistatic Crack Propagation in Non-linear Structures. Proc. Roy. Society, London, A325, 1971, pp. 207 – 222.
17. Chow, C.L. and Ngan, K.M., Crack Propagation with Quasistatic Energy Analysis. J. Strain Analysis 12: 45 – 52, 1977.
18. Sih, G.C., Paris, P.C. and Irwin, G., On Cracks in Rectilinearly Anisotropic Bodies. International J. Fracture Mechanics 1: 189 – 203, 1965.
19. Testing Plywood in Tension, American Society for Testing and Materials D 3500, 1976.

20. Sih, G.C., Paris, P.C. and Erdogan, F., Crack-Tip, Stress-Intensity Factors for Plane Extension and Plate Bending Problems. J. Appl. Mechanics, 29:306 – 312, 1962.

21. Bowie, O.L., Solutions of Plane Crack Problems by Mapping Technique, Methods of Analysis and Solutions of Crack Problems, edited by G.C. Sih. Noordhoff, The Netherlands, 1973.

22. Mandell, J.F., McGarry, F.J., Wang, S.S. and Im. J., Stress Intensity Factors for Anisotropic Fracture Test Specimens of Several Geometries, J. Composite Materials 8: 106 – 116, 1974.

## TABLE I

## MECHANICAL PROPERTIES OF TIMBER

| | Young's Modulus GN/m$^2$ | | Poisson's Ratio | | Shear Modulus MN/m$^2$ |
|---|---|---|---|---|---|
| MATERIAL | $E_L$ | $E_T$ | $\nu_{LT}$ | $\nu_{TL}$ | $\mu_{LT}$ |
| Kapur | 12 | 0.65 | 0.44 | 0.0238 | 560 |
| Gagil | 12 | 0.53 | 0.32 | 0.0141 | 674 |

## TABLE II

## FRACTURE TOUGHNESS OF KAPUR AND GAGIL

**(Moisture content 15% ± 2%)**

| MATERIAL | Fracture Toughness $G_{Ic}$, kN-m/m$^2$ | Stress Intensity Factor $K_{Ic}$, MN/m$^{3/2}$ |
|---|---|---|
| Kapur | 1.157 | 1.32 |
| Gagil | 0.553 | 0.833 |

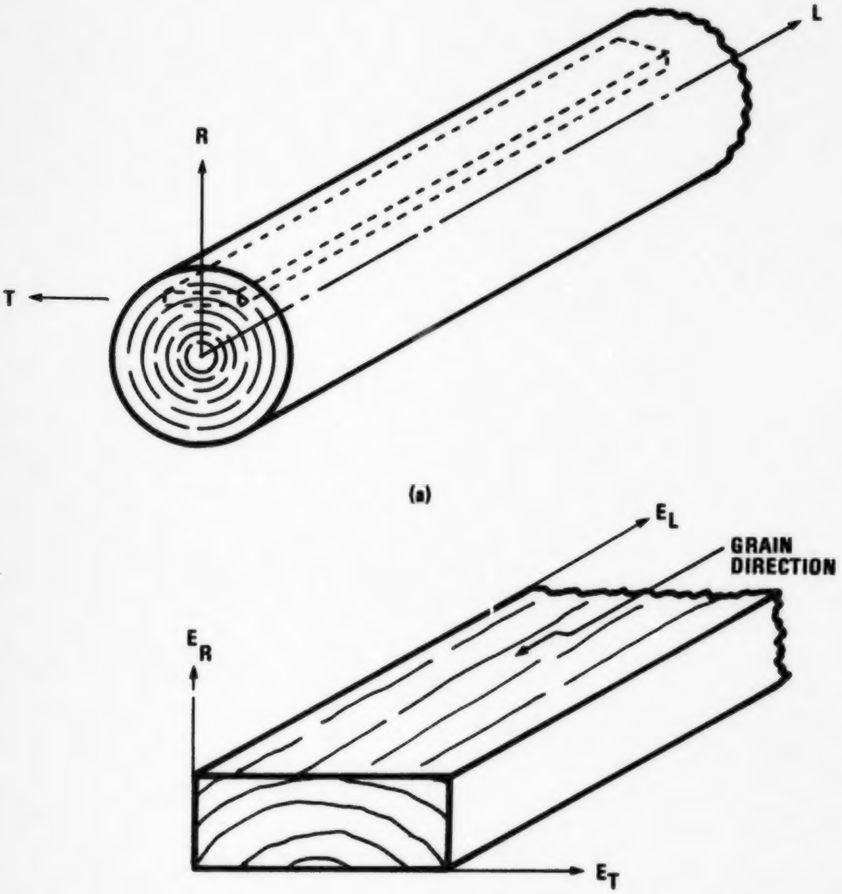
L
R
T
E_L
GRAIN DIRECTION
E_R
E_T

(a)

(b)

Figure 1. Anisotropy direction of wood

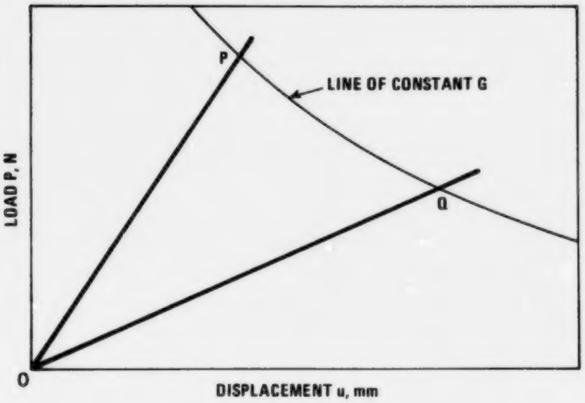

Figure 2.A. Load-displacement diagram

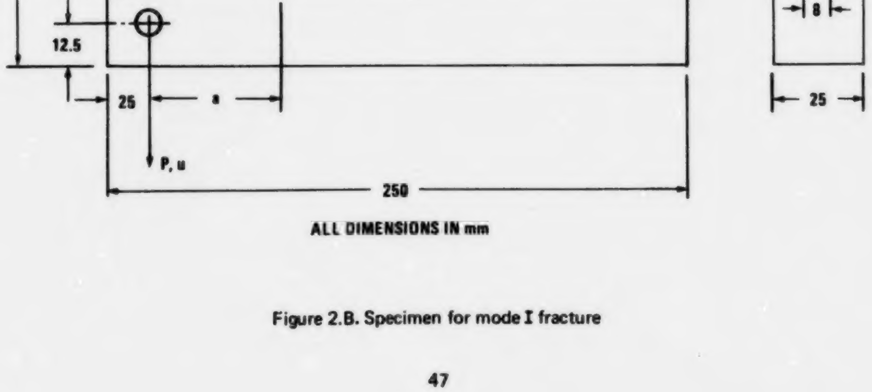
P, u
ϕ10
12.5
50
12.5
25
a
P, u
250
8
25
ALL DIMENSIONS IN mm

Figure 2.B. Specimen for mode I fracture

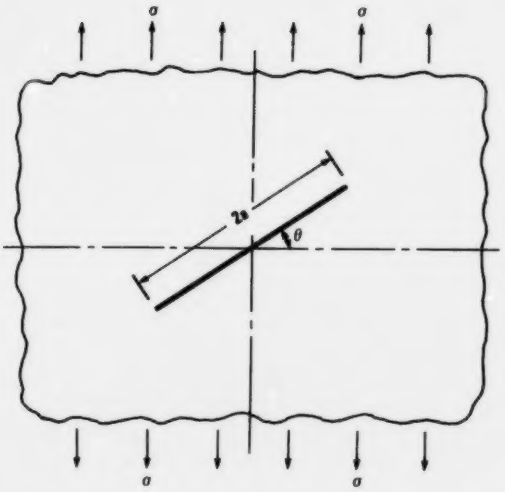

Figure 3.A. Inclined crack in an infinite solid

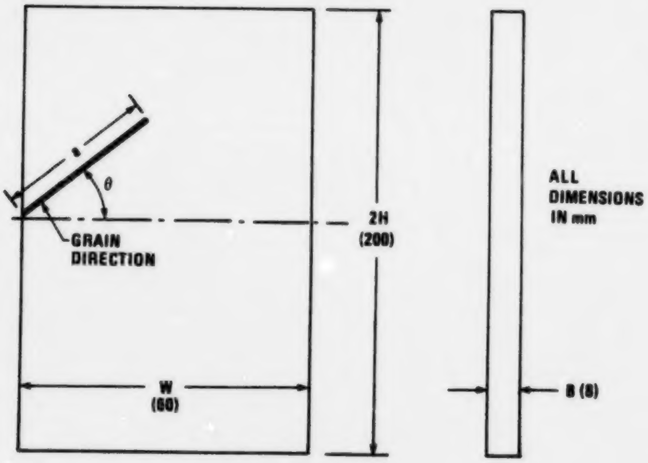
a
θ
GRAIN
DIRECTION
2H
(200)
W
(60)
B (8)
ALL
DIMENSIONS
IN mm

Figure 3.B. Specimen geometry for mixed mode fracture

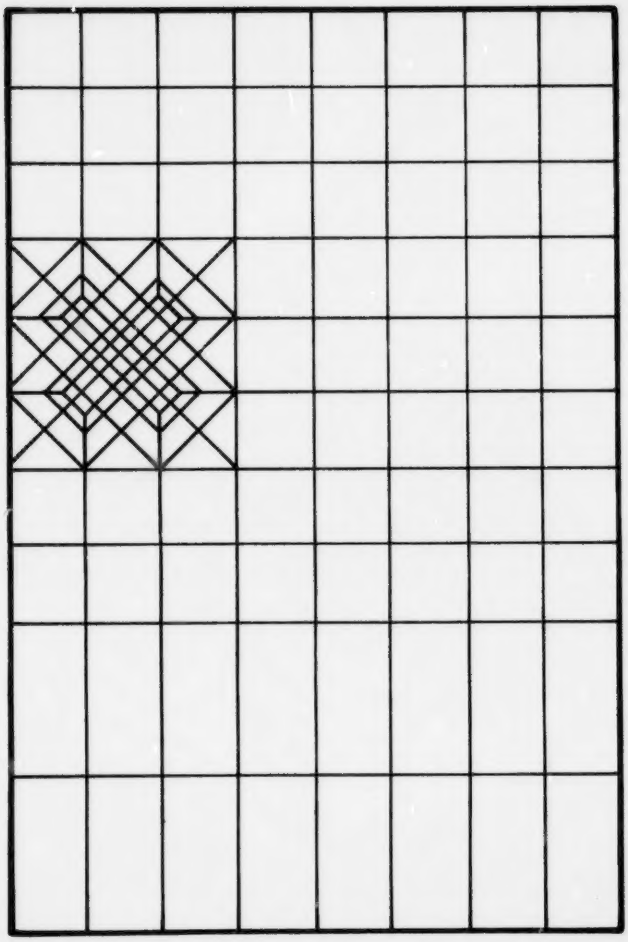

Figure 4. Finite element network used to compare the geometrical correction factors

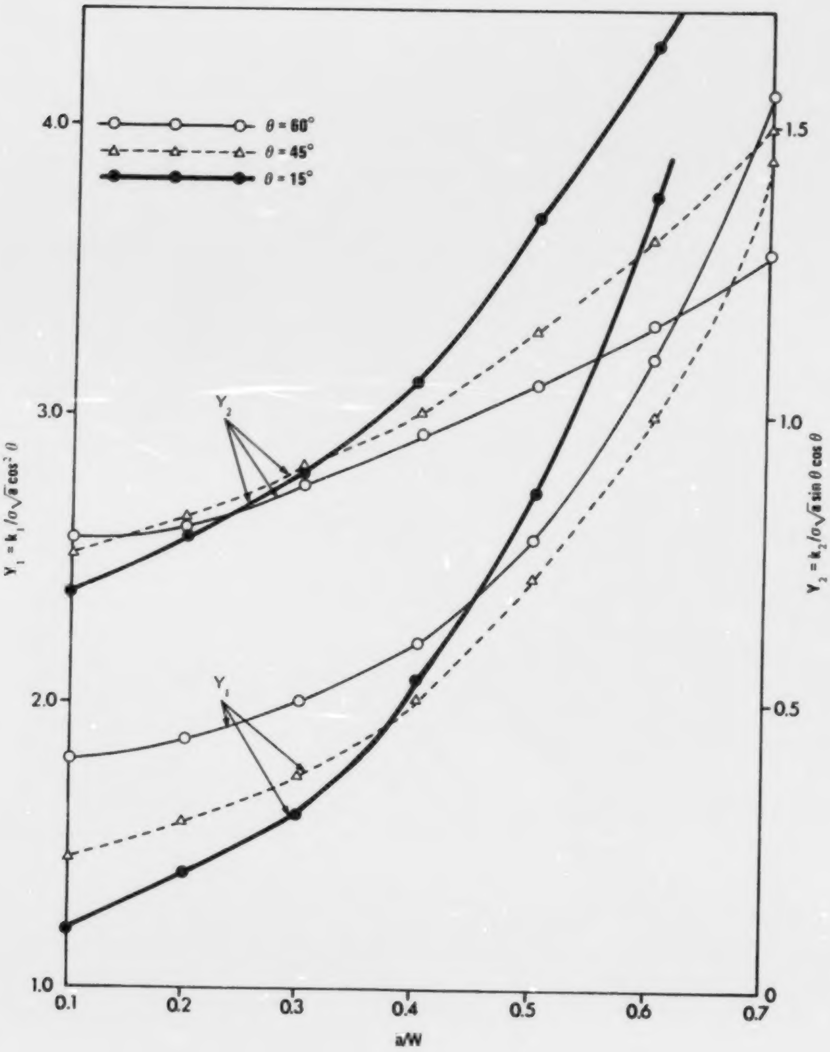

Figure 5. Geometrical correction factor of mixed mode with side-edge crack

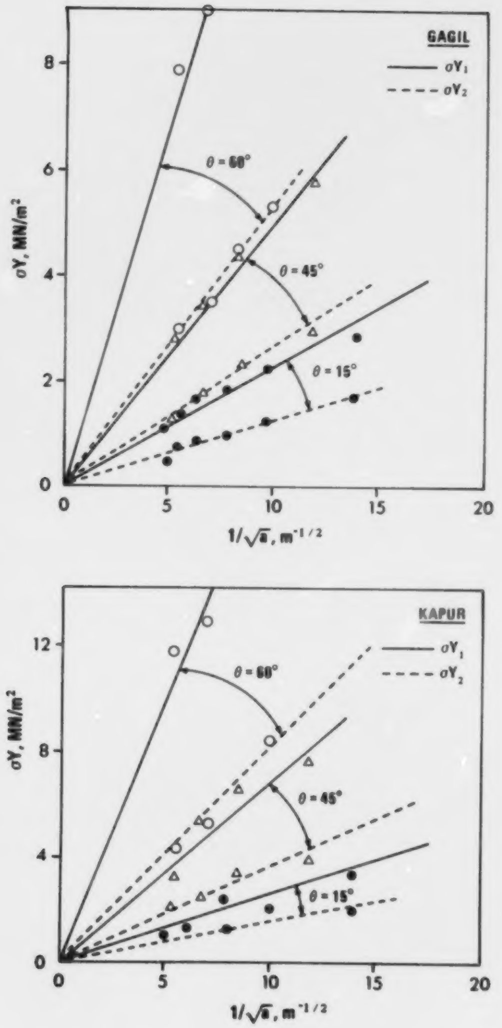

Figure 6. $\sigma Y$ versus $1/\sqrt{a}$ for Gagil and Kapur

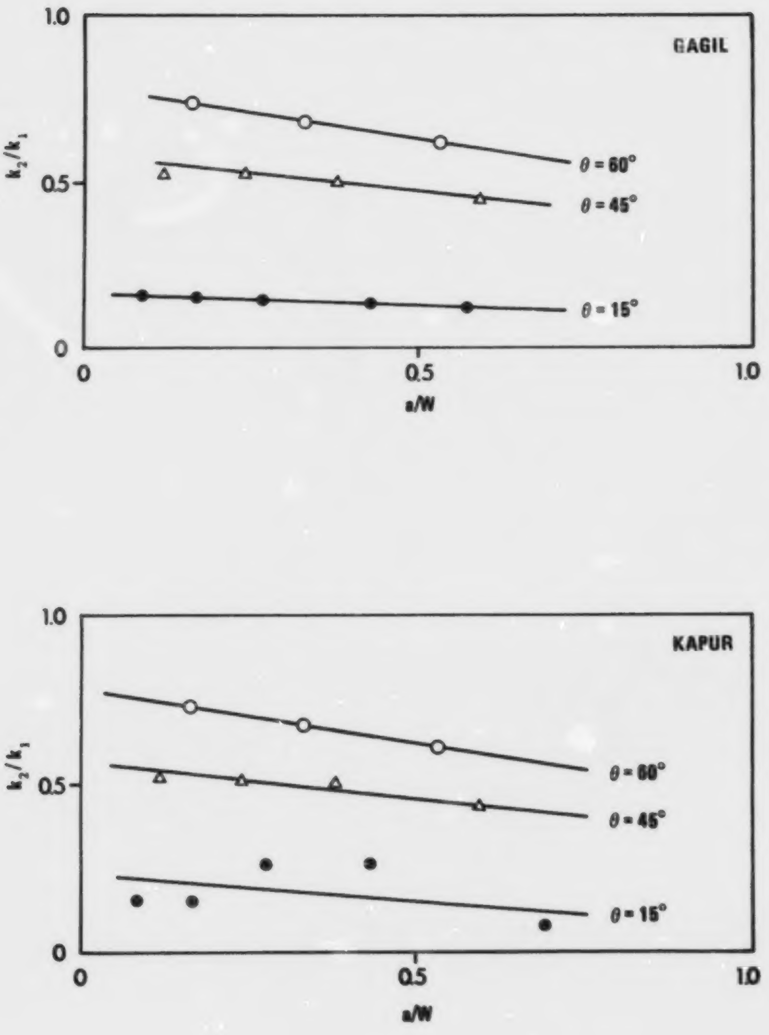

Figure 7. Effect of $k_1$ and $k_2$ on crack angles

# MATHEMATICAL MODEL OF THE TENSION BEHAVIOR OF WOOD WITH KNOTS AND CROSS GRAIN

By

James R. Goodman[1] and Jozsef Bodig[2]

---

[1] Professor of Civil Engineering, Colorado State University, Fort Collins, Colorado.

[2] Professor of Wood Science and Technology, Department of Forest and Wood Sciences, Colorado State University, Fort Collins, Colorado.

## 1.0 INTRODUCTION

The better utilization of wood depends heavily on increased knowledge of its basic behavior under load and the development of means to evaluate this behavior prior to structural applications. The objective of the paper is to describe current research efforts of the authors, which include the study of the tension behavior of wood as affected by knots and associated grain distortion.

## 2.0 MATHEMATICAL MODELING METHODS

### 2.1 Closed-Form Solutions

Existing solutions of two- and three-dimensional elasticity problems for orthotropic materials are limited to simple problems with simple boundary conditions, such as those given by Hearmon (17) and Lekhnitskii (18). In addition, the solutions are usually for the case when the direction of loading coincides with one of the orthotropic axes of the materials. For cases of a general direction of loading with a general orientation of orthotropic axes, such as a wood member with a slope of grain, the closed-form elasticity solution seldom, if ever, exists. When problems are further complicated, such as the behavior of a wood tension member with a cross grain and knots, the closed-form solutions appear to be impractical due to their complexity.

### 2.2 Finite Element Method

Since the mid-fifties, with the development of large digital computers, numerical solution techniques have become increasingly available for the solution of complex structural problems. In particular, the development of the finite element method opened the door for the study of evermore complex problems. The wide range of applications of this method [see Zienkiewicz (25) or Cook (6)] now permits the study of many interesting and useful problems concerning the behavior of structural materials and systems under load.

Since early work by Levy (19), Turner *et al.* (23), Wilson (24) and Argyris (3), the applications of the finite element method to all types of structural problems have been very extensive. Special applications in wood have not been so numerous, however. Work by Al-Dabbagh (1) for anisotropic three-dimensional solids, particularly as related to experimental studies of the elasticity of wood, is one of the early investigations. Applications to structural problems include the extensive work of Fox (9), Foschi (7), Thut (22) and Foschi and Fox (8) on glulam beams with taper and curvature. This work was followed by extensive experimental and extended finite element work by Gopu (13) and by Gopu and Goodman (14). Some other studies which involved the use of the finite element method for solving problems in the structural behavior of wood have been conducted by Shuldt (21) and Penney (20).

At this point in time, large structural computer programs exist, such as SAP IV, STRUDL, NASTRAN, etc., which generally include some level of anisotropic element. These programs provide a readily available means to analyze the more common problems in the structural behavior of wood members. However, certain problems, particularly those associated with dealing with the prevalent characteristics of wood, such as knots, checks and cross grain, are yet to be considered.

### 2.3 Fundamentals of Applying the Finite Element Method to Wood

The obvious requirements of application of the finite element method to wood are needs for proper geometric representation and input data on properties of materials. While the property aspect is obvious, it is far from trivial. The availability of the orthotropic elastic parameters is very limited (11,16) and, unless extensive measurements for the particular wood used can be justified, one is forced to use a predictive technique or other estimating method (5).

When the problem to be studied is more detailed, such as investigations of the influence of knots and cross grain on the behavior of wood, even more extensive input is needed. To apply the finite element method to such problems, a proper transformation of orthotropic properties to account for angle-to-the-grain stress application is needed. Use of tensor transformation concepts is the only method available currently for such needed calculations. Strength properties for angle-to-grain loading present even more problems and some form of the Hankinson's formula seems to be about all that is available at this time (12,15).

Considering the influence of knots, the fact that their orthotropic directions are different from the piece which contains the knot, their marked density difference and resinification, the problems of defining appropriate properties for these elements are clearly very difficult. However, the finite element method offers promise in providing an analysis which can recognize the differences in knot properties.

Perhaps of even greater concern than the knot itself, is the distortion of the grain surrounding the knot. The primary problem here concerns a means to define this distortion so that it may be accommodated in the finite element model.

## 3.0 FINITE ELEMENT ANALYSIS OF TENSION BEHAVIOR OF WOOD

### 3.1 Introduction

Applications of the finite method to nonhomogeneous problems, such as the tension behavior of wood with knots and checks as well as cross grain, have not been extensive. Some attempts have been made, such as those by Al-Dabbagh *et al.* (2), and there have been some fracture-mechanics applications.

To illustrate the potential of applying the finite element method to tension behavior of wood, a description of a current research effort by the authors is presented. The project description demonstrates the steps involved in such a study and serves also to define the problems encountered. A flow diagram of the tasks envisioned to complete a verified two-dimensional, nonhomogenous model for the tension behavior of wood members with knots is given in Fig. 1. Four main research components are defined and the subtasks are listed below. Those items shown in script type are not now in progress, but are considered essential to the completion of the effort.

### 3.2 Geometric Characterization

The goal of this component of the research is to develop a method for mathematically modeling the deviation of orthotropic axes; namely, the grain direction in wood due to defects, such as the existence of cross grain and knots. This part of the research is an essential component which, when verified, will allow reliable stress analysis for the tension behavior of structural members of wood and other nonhomogeneous, anisotropic materials.

A significant breakthrough has been achieved in the mathematical modeling of the grain deviation in wood due to the presence of cross grain and knots. The hypothesis was developed that grain directions around knots might follow paths similar to those of laminar flow lines around an object. This "flow-grain analogy" between hydrodynamics and growth phenomena of wood structure has been developed and verification studies are continuing currently to validate the concept. Studies to date are very encouraging and suggest that the "flow-grain analogy" is a valid method of characterizing the geometry of grain direction surrounding a knot. Proper geometrical characterizations of grain directions are essential to stress analysis procedure for wood, which must account for the anisotropic character of the material.

Briefly stated, the mathematical procedure involved utilizes elliptical coordinates and results in the following equations:

$$\psi = V\,(a+b)\sinh(\xi-\xi_0)\sin(\eta-\alpha) \qquad (1)$$

$$\phi = V\,(a+b)\cosh(\xi-\xi_0)\cos(\eta-\alpha) \qquad (2)$$

where:

$\psi$ - stream function (grain direction in analogy);

$\phi$ = potential function (perpendicular-to-grain direction in analogy);

V = constant involving flow rate (taken as unity in analogy);

a,b = length of major and minor axes of ellipse of flow obstacle (represents knot in analogy);

$\alpha$ = angle of attack of flow (cross-grain angle for wood member in analogy);

$\xi_0$ = constant.

Simplification for plotting is obtained by converting into rectangular coordinates. Computer programs have been developed to aid in handling the calculations and to provide automatic plotting of resulting models of wood members with knots and the associated cross grain. An example of the results obtained using the developed mathematical model is shown in Fig. 2. The calculated grid is superimposed over a photograph of a piece of wood which has had its grain directions inscribed for reference with the "flow analogy" results. The general agreement shown is an exciting result and promises a new era in capability to perform meaningful analyses of the behavior of wood under load.

### 3.3 Material Properties

The techniques to determine the elastic parameters of wood will utilize previously developed techniques (4,5,11,17,21) with modifications to determine the elastic parameters of knots. Preliminary tests have been completed to work out the details of the needed testing procedures. Tests to evaluate the parameters of the clear wood require the measurement of in-plane elastic parameters and strength properties. Due to the small physical size of the knot specimens, special testing techniques are being studied involving the use of disk or ring shapes to evaluate the properties of the knots.

### 3.4 Stress Analysis

The finite element stress analysis method is being developed in a special form to allow proper analysis of the tension behavior of wood members with knots and cross-grain defects. The key to the use of the finite element method is the geometrical characterization of the test specimens, described previously. The geometrical layout of the element mesh is automatically assigned by the mathematical model for grain deviation developed using the "flow-grain analogy". Element size in the mesh can be altered as desired to allow for more detailed analysis around the knot or at other critical locations. Automation of this procedure will allow a wide range of computer simulation studies to be conducted.

The versatility of the finite element method being developed allows the proper variation of material properties from element to element to account for changes due to load angle to the grain and the presence of knots. As described previously, the properties of the knots are being measured to allow for the proper inclusion of their effects on the behavior of the member. Parameter studies of the influences of defect properties are anticipated to further enhance the knowledge gained by the use of the finite element program developed.

### 3.5 Experimental Verification

Experimental verification of the developed model is the last phase of the study. However, some testing has to be done in advance to determine the input parameters of the model. The necessary test apparatus is being assembled at this time.

Once the elastic parameters of the clear wood and the knot are determined experimentally (or predicted through correlation with other known input variables) and the proper grain pattern is generated, the load-deformation behavior will be predicted through the finite element model. To assess the acceptability of the model, i.e. its representation of the real behavior or wood, experimental verification is necessary.

To experimentally verify the model, it is necessary to apply stress to a real specimen which the model represents and measure the corresponding strains. Since the strain varies from location to location in a nonhomogeneous anisotropic specimen, a large number of strain measurements are needed at various locations. These requirements lead to the problems of whole-field strain measurement of wood under load.

Since green specimens will be used in the first phase of the study to eliminte the possibility of material discontinuity, some of the most often used techniques, such as the Moire' fringe technique, are not easily applicable. High-magnification photographic technqiues promise usable results and this approach will be employed for the strain measurement.

Depending on the closeness of the results predicted by the model and the experimental measurements, the model may be accepted or further modified to take into account additional variables not now judged to be significant. After an acceptable model is verified, it is expected the work will proceed to the additional studies, such as fracture analysis listed in Fig. 1.

## 4.0 SUMMARY

As stated at the beginning of this paper, better utilization of wood depends heavily on increased knowledge of its basic behavior under load. Various components of basic knowledge concerning the behaviour of wood under load, its failure mechanisms, its variability, and the effects of environmental changes are emerging. Many of these aspects are currently under study. However, much additional work is needed before the complete picture can be assembled.

The use of finite element models, such as outlined in this paper, offer many advantages to the researcher and to the structural designer seeking practical solutions to a myriad of problems. While the understanding of the behavior of wood under load is a complex problem, the use of the finite element method promises to reduce this complexity to a tractable result. In addition, new concepts, such as fracture mechanics and Monte Carlo simulation, can be easily accommodated using this approach. Only limited studies using these techniques have been conducted to date and extended research in these areas is badly needed (10). Significant contributions to research on wood behavior, with proper application to construction problems, can markedly contribute to proper utilization of timber resources.

## 5.0 REFERENCES

1. Al-Dabbagh, A.M.A. 1970. Finite Element Stress Analysis for Anisotropic Solids. Ph.D. Dissertation, Dep. Civil Eng., Colo. State Univ., Fort Collins.
2. Al-Dabbagh, A.M.A., Goodman, J.R. and Bodig, J. 1972. Finite Element Methods for Wood Mechanics.J.Struct. Div., ASCE 98(ST3):569-586.
3. Argyris, J.H. 1965. Continua and Discontinua. Proc. Conf. Matrix Methods Struct. Anal. Wright-Patterson Air Force Base, AFFDL-TR-66-80, Dayton, Ohio. p. 11-189.
4. Bodig, J. and Goodman, J.R. 1969. A New Apparatus for Compression Testing of Wood. Wood and Fiber 1(2):146-153.

5. Bodig, J. and Goodman, J.R. 1973. Prediction of Elastic Parameters for Wood. Wood Sci. 5(4):249-264.

6. Cook, R.D. 1974. Concepts and Applications of Finite Element Analysis. John Wiley, New York.

7. Foschi, R.O. 1968. Plane Stress Problem in a Body with Cylindrical Anisotropy, With Special Reference to Curved Douglas-fir Beams. Can. Forest Serv., Western Forest Prod. Lab., Dep. Pub. No. 1244, Ottawa.

8. Foschi, R.O. and Fox S.P. 1970. Radial Stress in Curved Timber Beams. J. Struct. Div. ASCE 96(ST10):1977-2008.

9. Fox, S.P. 1970. Stress Analysis of Double-Tapered Pitched, Glued-Laminated Beams. Eng. J. 13(A-2):I-VI.

10. Goodman, J.R. 1977. Important Research Needs in Wood. 1977 ASCE Fall Conv., Preprint No. 2948, San Francisco, CA.

11. Goodman, J.R. and Bodig, J. 1970. Orthotropic Elastic Properties of Wood. J. Struct. Div. ASCE 96(ST11):2301-2319.

12. Goodman, J.R. and Bodig, J. 1971. Orthotropic Strength of Wood in Compression. Wood Sci. 4(2):83-94.

13. Gopu, V.K.A. 1976. Behavior and Design of Double-Tapered, Pitched and Curved Glulam Beams. Ph.D. Dissertation, Dep. Civil Eng., Colo. State Univ., Fort Collins.

14. Gopu, V.K.A. and Goodman, J.R. 1974. Analysis of Double-Tapered, Pitched and Curved Laminated Beam Section. Wood Sci. 7(1):52-60.

15. Hankinson, R.L. 1921. Investigation of Crushing Strength of Spruce at Varying Angles of Grain. Air Serv. Inf. Cir., Vol. III, No. 259 (Mater. Sec. Paper No. 130).

16. Hearmon, R.F.S. 1948. Elasticity of Wood and Plywood. U.K. Dep. Sci. Ind. Res., Forest Prod. Res. Spec. Rep. No. 7, London.

17. Hearmon, R.F.S. 1961. An Introduction to Applied Anisotropic Elasticity. Oxford Univ. Press, Amen House.

18. Lekhnitskii, S.G. 1963. Theory of Elasticity of an Anisotropic Elastic Body. Holden-Day, San Francisco, CA.

19. Levy, S. 1953. Structural Analysis and Influence Coefficient for Delta Wing. J. Aeronaut. Sci. 20(7):449-454.

20. Penney, D.T. 1977. Fracture Mechanics Analysis of Butt Joints in Laminated Wood Beams. Master's Thesis, Dep. Mech. Eng., Colo. State Univ., Fort Collins.

21. Shuldt, J.P. 1972. Unified Testing Procedure for Determining the Elastic Parameters of Wood. Ph.D. Dissertation, Dep. Forest Wood Sci., Colo. State Univ., Fort Collins.

22. Thut, W.K. 1970. Stresses in Pitched-Cambered Glulam Beams. Master's thesis, Dep. Civil Eng., Univ. B.C., Vancouver, B.C.

23. Turner, M.J., Clough, R.W., Martin, H.C. and Topp, L.J. 1956. Stiffness and Deflection Analysis of Complex Structures. J. Aeronaut. Sci. 23(9):805-823.

24. Wilson, E.L. 1965. Structural Analysis of Axisymmetric Solids. AIAA Journal 3(12):2269-2274.

25. Zienkiewicz, O.C. 1971. The Finite Element Method in Engineering Science, McGraw-Hill, London.

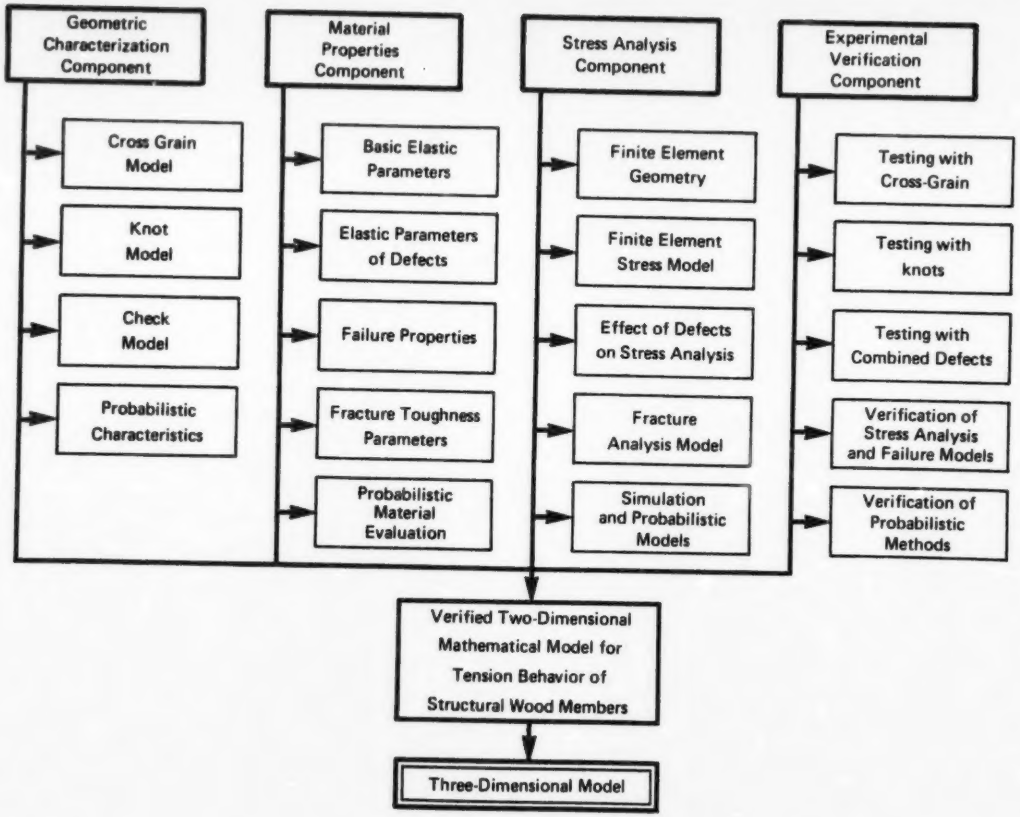
Geometric Characterization Component
Cross Grain Model
Knot Model
Check Model
Probabilistic Characteristics
Material Properties Component
Basic Elastic Parameters
Elastic Parameters of Defects
Failure Properties
Fracture Toughness Parameters
Probabilistic Material Evaluation
Stress Analysis Component
Finite Element Geometry
Finite Element Stress Model
Effect of Defects on Stress Analysis
Fracture Analysis Model
Simulation and Probabilistic Models
Experimental Verification Component
Testing with Cross-Grain
Testing with knots
Testing with Combined Defects
Verification of Stress Analysis and Failure Models
Verification of Probabilistic Methods
Verified Two-Dimensional Mathematical Model for Tension Behavior of Structural Wood Members
Three-Dimensional Model

Figure 1. Flow diagram of research tasks

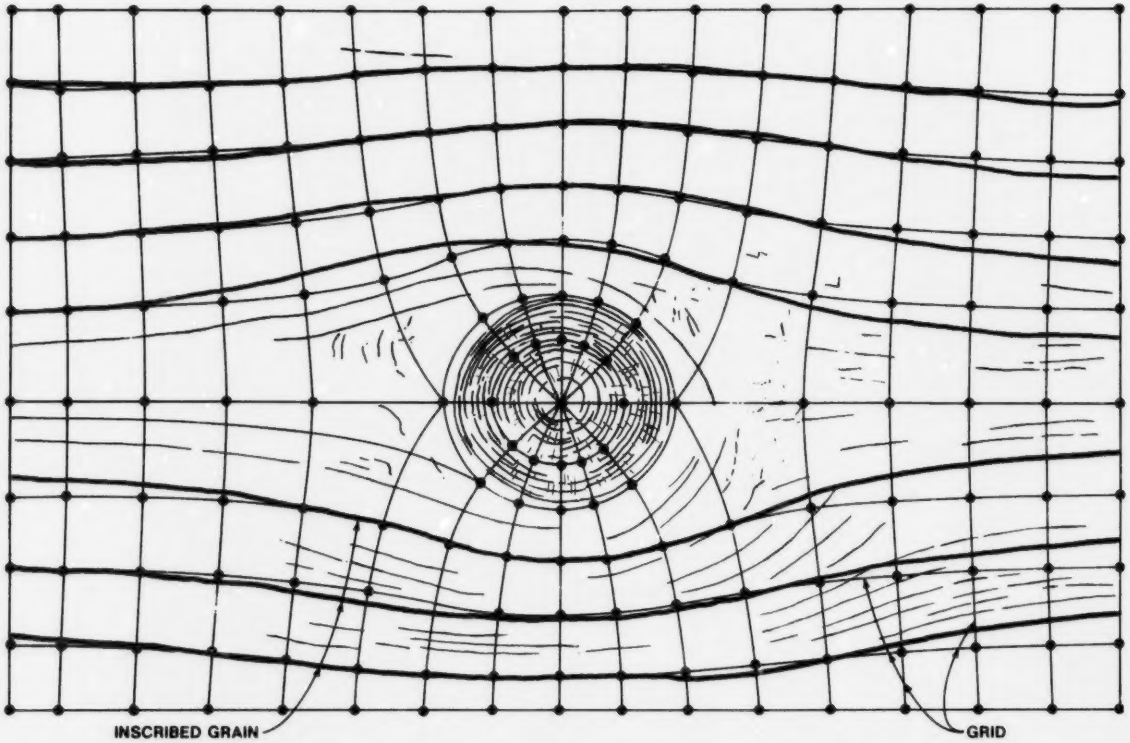
INSCRIBED GRAIN
GRID

Figure 2. Example of "flow-grain analogy"

# EVALUATION OF LONG-TERM BEARING CAPACITY OF WOOD STRUCTURES BY THEIR PERFORMANCE UNDER SHORT-TERM LOADING

By

Yuri M. Ivanov

---

Professor, Dr.Sc., Central Research Institute for Building Structures, Gosstroi U.S.S.R., Moscow

## INTRODUCTION

A peculiarity of wood is to alter its strain and strength under the load that involves a decrease of bearing capacity of structure in duration of time. Therefore, a calculation of wood structure to guarantee its reliable work during a given term has to consider the end state of a structure. Thus the structure ought to have to its service end the bearing capacity not less than the minimum required. This task is actually performed in designing by design stresses established to ensure long work of a structure under load. Then design bearing capacity of a structure $D_d$ ought to be equaled theoretical long-term bearing capacity $D_\tau$ in the end of service life, i.e. $D_d = D_\tau$.

According to the notion of a design as a long-term bearing capacity of wood structure, we can define as the major aim of the test a forecast of long-term bearing capacity $U_\tau$ of a structure by its ultimate load $U_t$ and time characteristic t obtained from testing and using the factor

$$K_1(t) = \frac{U_t}{U_\tau} \qquad (1)$$

As strength of wood increases when duration of load gets shorter, the ultimate load $U_t$ of the structure obtained from short-time testing exceeds its long-term bearing capacity $U_\tau$. The influence of time on strength of wood has been known for a long time. But only recently, in connection with the achievements in studying strength of solids, it was ascertained that to the temperature-time relation of long-term strength of solids of various composition including polymers[2] follows also wood[3]. This relationship,

$$t = A e^{-\alpha\sigma}, \qquad (2)$$

where t is time up to failure, $\sigma$ is stress, A and $\alpha$ are constants (at constant temperature), shows that strength of a solid depends, not only on stress value, but also on its duration and temperature. On the basis of the data of experiments with long-term tests of wood, we obtained an average straight line 3,6

$$1g\ t = 17.1 - 0.166\sigma, \qquad (3)$$

(here $lg_s = 17.1$; $\alpha = (2.3.1gA)/\sigma_o$; $\sigma_o = 103$ percent) which was plotted according to the data of long-term tests during five years carried out in the USSR by N.L. Leontiev[4] at bending and shear along the grain of air-dry spruce wood (Fig. !a - average times up to failure t). A correctness of the straight line (3) was checked by comparison of calculated according to (2) values of $\sigma_1$ (at duration $t_1$ of machine testing similar specimens reduced to the time t of an invariable action of the maximum stress) with actual value of $\sigma_{ul}$ of machine testing the same specimens - the difference was found to be within 5 percent (for bending 4.7; for shear 4.9 percent). Later on L.W. Wood's data[5] were plotted on the same graph for bending samples of air-dry Douglas-fir (moisture content 6 and 12 percent). These data were preliminarily counted relatively to $\sigma_{ul}$ for the same duration t of machine testing as that according to GOST USSR (t = 19.2 sec; t = 0.513 s; lg t =-0.290). The points plotted according to these data are shown in Fig. Ib. The points of the testing with different speed of loading were plotted (with reduced $t_1$ to time t) on the same graph for pine wood air dried and water saturated at bending and compression along the grain[6]. These points are near the straight line[3] (Fig. Ic) what proves a general relationship of long-term strength of wood for different species, moisture content, stress state, long-term and machine testing[7].

Let us reduce (3) to more convenient form

$$\sigma = \sigma_0 \frac{(1 - 1g\ t)}{17.1}. \qquad (4)$$

On dividing both parts of (4) by $\sigma_{ul100}$, which is taken for 100 percent, we will obtain the relative strength of wood decreased during the time t of the action of stress

$$\frac{\sigma}{\sigma ul100} = 1.03 \left(1 - \frac{\lg t}{17.1}\right) \qquad (5)$$

Having the straight line $\sigma(\lg t)$ on Fig. 1 based on the data of long-term wood testing by the duration of five years[4,5], we can extrapolate for a period $\tau$ of normal service of structures. Let us transform (4) by dividing both sides by $\sigma_\tau$ in[3]

$$\sigma_\tau = \frac{\sigma_t}{B - C\lg t} \qquad (6)$$

where

$$B = \frac{17.1}{17.6 - 1,03\lg\tau}\ ; \quad C = (B-1)\frac{1}{\lg\tau}$$

Since in a rightly designed and manufactured structure invariability of scheme of calculation and stability of members and of structure as a whole are ensured, then the initial properties of material are retained and gluelines have sufficient strength and steadfastness to provide a solidity of glued members, hence on this ground we can suppose that the long-term bearing capacity of a wood structure $U_\tau$ is in the same relation to the ultimate load $U_t$ as the long-term strength of wood $\sigma_\tau$ is to its ultimate strength $\sigma_t$ according to (6), i.e.

$$U\tau = \frac{U_t}{B - C\lg t} \qquad (7)$$

In accordance to (1) and (7)

$$K_1(t) = B - C\lg t, \qquad (8)$$

where t = time of the action of ultimate load $U_t$ on the structure. In order to determine $U_t$ it is necessary to put on test some limitations. The process of deformation of wood structure displays the significant influence of after-effect[8]. The latter is connected with load change and more clearly appears just after an application or on removal of load. Therefore, it is important that the test loading will be uniform in time, being nearer to one with constant speed. At the same time, it is necessary to maintain the structure periodically under constant load of gradually growing load steps (Fig. 2). The test mentioned begins after the effect from action of previous loading on the structure has ceased.

The structure ought to be fastened according to design, but it is not allowed any restraint of it by members of test installation. Replacements are measured in characteristic points of structure. The test process ought to be fixed during the time, so as it will be possible to put on a graph the relation of strain to load as well as to time.

The time $t_1$ of loading up to maximum load must be reduced to invariable action of ultimate load $U_t$. In general case, at change of stress, the time up to failure $t_p$ must answer the well-known ratio[9,10]

$$\int_0^{t_p} \frac{dt}{t[\sigma(t)]} = 1. \qquad (9)$$

Let us assume the load and stress grow by the constant rate, i.e. $w = \sigma/t$. Then time up to failure[10]

$$t = \frac{1}{\alpha w} \qquad (10)$$

A lower value of $K_1(t)$ we will take equal unit with the upper ones for uninterrupted action of total design load on structure during 25 and 50 years 2.02 and 2.10. (Table 1) Intermediate magnitudes of $K_1(t)$, which correspond to testing finite spaces of time, we can calculate from (8). In order to guarantee the reliable work of the structure, the value of the ultimate load $U_t$ must be more than the long-term bearing capacity $K_1(t)$ if only the time factor is considered.

Bearing structures in buildings are not subjected to uninterrupted action of the design load P. The long-term load on roofs are the constant load P' and, according to the

URSS-norm, a long-term part of norm snow load which acts two months in the end of winter (Fig. 3). The relative decreased strength of wood can be determined by substituting in (5) a time $t_{eq}$ which is equivalent to action of invariable load replaced service load.

For a periodical action of the same load of equal duration $\Delta t$ according to (9) we have $n \Delta t = t(\sigma)$, where $n = \tau$ in years. Time $t_{eq}$ of the action of load $P_d$

$$t_{eq} = \left(\frac{2}{12} + \frac{10}{12} \psi\right) \tau, \qquad (11)$$

where according to (9) $\psi = \frac{t(\sigma a)}{t(\sigma b)}$ for stress $\sigma a$ under the load $P_d$ and $\sigma_b$ under the load P'. Taking logarithm of $\psi$ we find

$$\lg \frac{t(\sigma a)}{t(\sigma_b)} = (\sigma b - \sigma a) \frac{\lg A}{\sigma_o}$$

An average roof weight according to the design analysis made for bearing wood glued structures of mass application is ~0.43 P with its reliable factor 1.1 and the weight of bearing structure gives (0.43 1.1 + 0.07) P= 0.54P. At an ultimate load~2.5P we have

$$\lg\psi = \frac{(0.54 - 0.80)P}{2.5P} \times \frac{17.1}{1.03} = 0.104 \times 16.6 = -1.73; \psi = 0.0187$$

That is the part of an effect of the constant load P' on the decrease of wood strength we can neglect. Then according to (11), time $t_{eq}$ of the action of load $P_d$: $t_{eq} = 0.167\tau$ and for periods of time 25 and 50 years makes 4.16 and 8.32 years (Table 2), at upper values of $K_1(t)$ equaled 1.85 and 1.92.

However, the value of long-term load $U_\tau$ forecasted by the test data is characterized by dispersion. Therefore the ratio

$$\frac{U_\tau}{D_d} = K_2 > 1.$$

The dispersion mentioned depends on the variability of the material and manufacturing quality of the structure. The magnitude of $K_2$ can be determined from statistical analysis of small samples of $U_t$ values from the population of $U_t$ - values for finished structures.

At last it is to take into account imperfections of calculation assumptions as idealization of material properties, inaccuracy of calculation scheme, peculiarities of limit state of structure, etc., which we shall cover by introducing coefficient $K_3$. In the end, we come to the inequality which shall be satisfied by tested structure:

$$\frac{U_t}{P} > K, \qquad (12)$$

where

$$K = K_1 \beta K_2 K_3 \; ; \; \beta = \frac{P_d}{P}$$

K is a general index (an adimensional quantity more than unity) which defines the state of material science, development level of theory and methods of calculation, as well as a culture of structure manufacturing. This index in the end does show a degree of resource use of material in structure. Up to now, value of K for structures of various materials required was established intuitively. Recently this factor was named as "coefficient of ignorance" since its analysis was difficult enough at design of structures by allowable stresses. After in the USSR the limit state method of calculation was adapted, it appeared a basis for study and scientific analysis of, not only variability of external forces on structures and material quality, but also the very nature and composition of safety factor of structures.

The values K required can be calculated for load bearing roof structures of buildings by following formulae (for service life 50 years):

at plastic type of failure $(K_3 \approx 1)$

$$K_{p1} = K_2 \times K_3 \times \beta \times K_1(t) = K_2 K_3$$
$$\beta \; (1.92 - 0.108 \lg t)$$

at fragile type of failure

$$K_{fr} = K_2 \times K_3 \times \beta \times K_1 (t) = K_2$$
$$K_3 \beta (1.92-0.1081 g t).$$

$K_2 = 1.42$ and $K_3 = 1.30$[11] were recommended.

## REFERENCES

1. Ivanov, Yu. M. 1975. Analysis of safety factor of wood structures. Izv.vuz'ov Stroi.a.architect. No. 7.

2. Jurkov, S.N. 1968. Kinetics conception of strength of solids. Vestnik Akadmii Nauk USSR, No. 3.

3. Ivanov, Yu. M. 1972, 1975. Long-term strength of wood. Izv.vuz'ov-Lesnoi jurnal, No. 4, No. 5.

4. Leontiev, N.L. 1957. Long resistance of wood.M.

5. Wood, L.W. 1951. Relation of stregnth of wood to duration of load. US Forest Products Laboratory, NR 1916.

6. Liubosiz, M.I. 1950. Effect of rate of loading on the limit of plastic flow of pine wood. Dissertation. Minsk.

7. Ivanov, Yu.M. 1976. Uber die einheitliche GesetzmäBigkeit für die Dauerfestigkeit von Holz. Holztechnologie, Dresden. 17, No. 1.

8. Ivanov, Yu.M. 1977. After effect in wood of structural members. Izv.vuz'ov Stroit.a. architect. No.1.

9. Bailey, J. 1939. An attempt to correlate some tensile strength measurements of glass. Glass Industry, No.3.

10. Jurkov, S.N., Tomasevskiy, E.E. 1959. In book: "Nekotorye problemy procnosty tverdyh tel".Izd.AN SSSR,M-L.

11. Ivanov, Yu.M. 1976. Test principles and evaluation of bearing capacity of wood structures. Intern. Symposium on timber structures. Kiev. 7-12.

Table 1

| $\tau$ |  | lg$\tau$ | B | C | $K_1(t)$ |
|---|---|---|---|---|---|
| years | sec |  |  |  |  |
| 50 | $1.58 \times 10^9$ | 9.2 | 2.10 | 0.120 | 2.10−0.120 lg t |
| 25 | $7.9 \times 10^8$ | 8.9 | 2.02 | 0.115 | 2.02−0.115 lg t |

Table 2

| $\tau$ | $t_{eq}$ |  |  | B | C | $K_1(t)$ |
|---|---|---|---|---|---|---|
| years | years | sec | 1g |  |  |  |
| 50 | 8.32 | $2.64 \times 10^8$ | 8.42 | 1.92 | 0.109 | 1.92−0.109 lg t |
| 25 | 4.16 | $1,32 \times 10^8$ | 8.12 | 1.85 | 0.105 | 1.85−0.105 lg t |

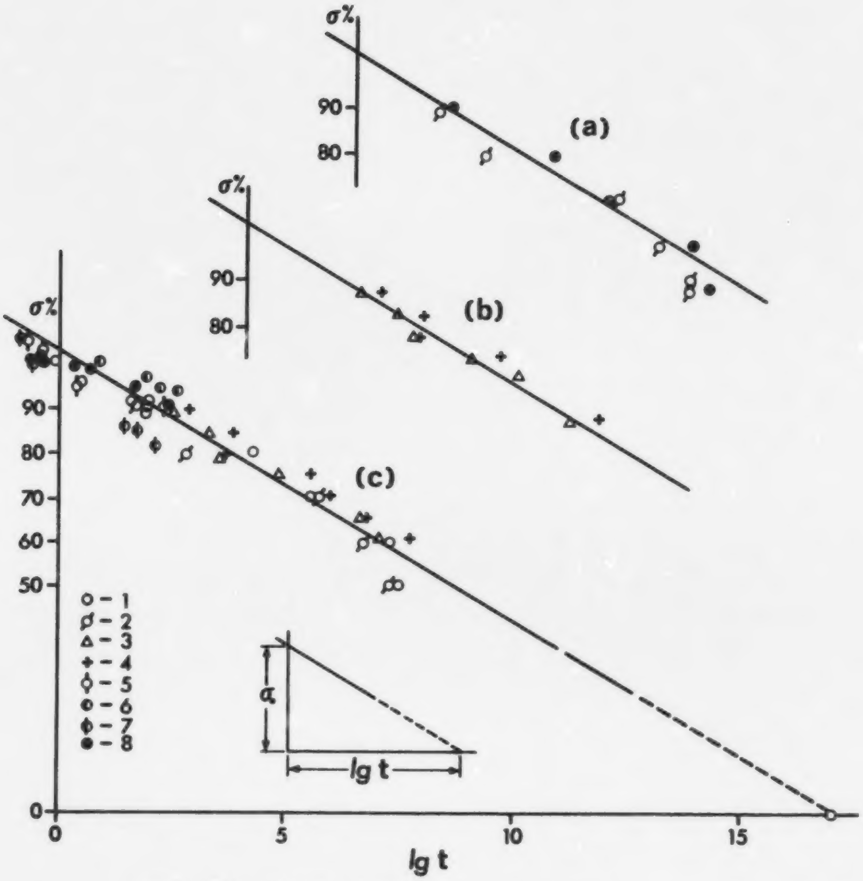

Fig. 1a. The straight line (3) plotted by points from work[4]

Fig. 1b. The location near line (3) of points plotted by data from work[5]

Fig. 1c. The straight line (3) with points for different species of wood: 1, 2 – spruce[4]; 3, 4 – Douglas-fir[5]; 5 – 8 – pine[6]; moisture content (percent) 1, 2 – 13.5; 3 – 12; 4 – 6; 5 – 15; 6 – 8 – 30; stress state, 1, 3, 4, 7, 8 – bending; 2 – shear; 5, 6 – compression along the grain; 1 – 4 – long-term tests; 5 – 8 – machine tests.

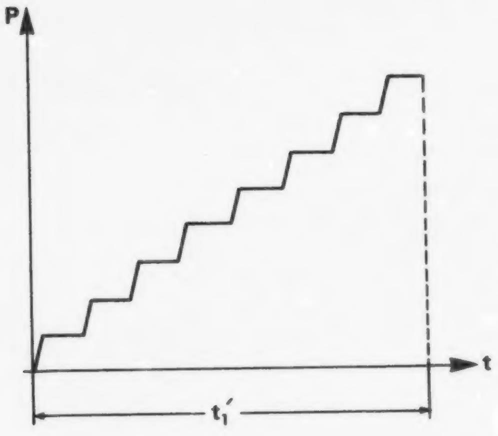

Fig. 2. Rate of loading on testing structure

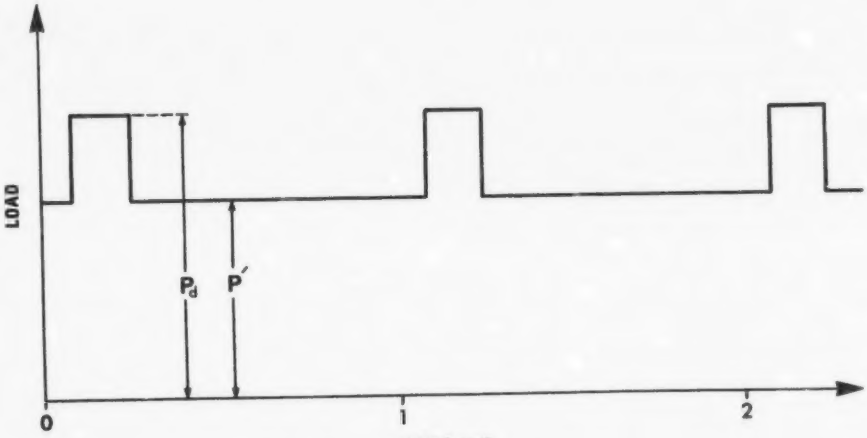
LOAD
$P_d$
$P'$
0
1
2
TIME (years)

Fig. 3. Scheme of design load for bearing roof structures in buildings

# EFFECT OF TRANSVERSE STRESS ON SHEAR STRENGTH AND FAILURE MECHANISM OF DOUGLAS-FIR

By

F.J. Keenan[1] and T.A. Jaeger[2]

---

[1] Faculty of Forestry and Landscape Architecture,
University of Toronto, Toronto, Ontario.

[2] Eastern Forest Products Laboratory,
Forintek Canada Corp., Ottawa, Ontario.

## ABSTRACT

It has been hypothesized that the shear strength of wood parallel to the grain is increased by the application of compression stress perpendicular to the grain, in a manner analogous to the effect of a normal compression force increasing the frictional resistance between two surfaces. This hypothesis was examined by mechanical testing, and the morphology of the failure surfaces were studied using both light and scanning-electron microscopy. The experiments involved the application of stress perpendicular to grain to three different types of dry Douglas-fir specimens: ASTM shear blocks, oblique-grain compression specimens and torsion tubes. The test results showed that the hypothesis appears to hold only when radial-plane shear strength is considered; in contrast, the shear strength of the tangential plane is virtually insensitive to the presence of transverse stress. In all cases involving transverse-compression stress, the tangential-plane strengths were found to be lower than the radial-plane strengths. Thus, when a shear failure in dry Douglas-fir is free to seek its plane or surface of minimum resistance - as is usually the case in large timber beams - it occurs predominantly along tangential surfaces and its shear strength is not significantly increased by the application of compression stress perpendicular to the grain. The anatomical studies showed failure modes which were consistent with the test results: the radial-plane specimens had mainly intrawall failures, in which tracheids had slid longitudinally past each other near the middle lamella. This sliding suggested that the frictional analogy was apt. In contrast, the tangential-plane failures displayed transwall failures, in which the tracheid walls had been ripped longitudinally; this mode did not suggest a frictional analogy. Considering the four basic failure modes which were identified in this research, an overall model for the shear-strength mechanisms of dry Douglas-fir is proposed.

## INTRODUCTION

The shear strength of a glued-laminated timber beam is not a constant, but it increases as the location of an applied concentrated load comes closer to a support point (Huggins *et al.* 1966). In the past, one hypothesis advanced to explain this behaviour was that the shear strength of wood parallel to the grain increases when compression stress perpendicular to the grain is applied to the shear plane (Mandery 1969); that is, as the applied load approaches a support of the beam, the perpendicular-to-gain bearing stresses increase the shear strength of the beam, in a manner analogous to the effect of a normal compression force increasing the frictional resistance between two sliding surfaces.

This hypothesis was tested in three projects. The detailed aspects of the strength tests and their implications for the practice of timber engineering are reported elsewhere (Keenan and Selby 1973, Keenan 1974). This paper reports on some of the anatomical studies which were carried out on the fracture surfaces and, also, attempts to demonstrate the close correlation between shear strength properties and the morphology of shear-fracture surfaces.

## EXPERIMENTAL STUDIES - EFFECT OF TRANSVERSE STRESS ON SHEAR STRENGTH

Three different types of specimens - ASTM shear blocks (Project A), oblique-grain compression specimens (Project B), and torsion tubes (Project C) - were tested to investigate the effect of stress perpendicular to grain ("transverse stress") on shear strength parallel to grain. All specimens were air-dry Douglas-fir; sample sizes, moisture contents, and specific gravities are listed in Table 1. Specimen dimensions and methods of load application are shown schematically in Figure 1.

In Project A, the standard ASTM shear block was subjected to transverse stress (tension for some, compression for others) by means of an apparatus mounted around the specimen. The transverse stress was applied first; then the specimen was tested in shear. The specimens were manufactured so that half were tested in the tangential plane of the wood and the other half in the radial plane.

In Project B, the specimens were cut from planks so that 16 specimens had tangential planes of obliquity when tested in compression parallel to a specimen's axis and 68 specimens had radial planes of obliquity. From elementary mechanics, if the grain direction makes an angle greater than zero with the direction of the applied load, the applied axial compression stress induces both a shear stress parallel to grain and a compression stress normal to the grain. The relative proportions of these stresses are controlled by the selection of the angle of obliquity. The tangential-plane specimens had obliquity angles of 20, 25, and 30 degrees; the radial-plane specimens had obliquity angles of 0, 15, 20, 25, 30, 45, 60, 75, and 90 degrees. The specimens were loaded in compression until failure and each specimen was examined to determine the type of failure.

In Project C, thin-walled torsion tubes were turned on a lathe to the approximate dimensions shown in Figure 1. The specimens were tested in shear until failure by rotating one end of the specimen with respect to the other end. Twenty-two specimens were tested in torsional shear alone; another 22 had a hydraulic-pressure tank and thin latex sleeve applied over the region of minimum wall thickness. The hydraulic pressure induced a circumferential compression stress in a specimen which, of course, was perpendicular to the grain at all points in the wall of a specimen. Because of the geometry of the specimen, the induced perpendicular compression stress was equal to about seven times the applied hydraulic pressure.

The rate of application of the hydraulic pressure was proportional to the rate of application of torsional shear, with different ratios of stress being used to produce a variation of transverse compression stress with shear strength.

The test results for the three projects are shown in Figure 2. Each point plotted for Projects A and B, and the control point in Project C, is the average strength for specimens in a group; the group size is shown in parentheses under the point.

In Project A, two of the radial-plane specimens and four of the tangential-plane specimens failed at transverse-compression stresses between 750 psi and 1000 psi before shear could be applied. For the other specimens (which failed in shear), a distinct difference is seen between the tangential-plane and the radial-plane shear strengths: the shear strength of the radial plane varied markedly with changes in transverse stress, but the tangential-plane shear strength was virtually insensitive to changes in transverse stress.

All the compression specimens were cut form one plank and all the tension specimens from another plank, so that essentially two different populations are plotted on the graph. Nevertheless, the graph hints strongly at continuity of behaviour when passing from perpendicular compression to perpendicular tension.

In Project B, as expected, failure type was dependent upon angle of obliquity: at 0 degrees, failures were solely in compression parallel to the grain; between 15 and 25 degrees, failure was by shear; at 30 degrees, the specimens showed transverse compression-failure wrinkles before finally failing in shear; and for angles greater than 30 degrees, failures were by transverse compression with some shear distortion. As in Project A, the radial-plane shear strength was more responsive to transverse compression than was the tangential-plane shear strength.

Thus, in terms both of relation between shear strength and transverse compression, and of onset of transverse compression failure, the trends found in Project B were consistent with those in Project A.

In Project C, it was possible to differentiate between specimens which failed in shear and those which failed in a combination of shear and transverse compression, as described below. Since all points on the circumference of each specimen were equally stressed in both shear and transverse compression, it was expected that the failure surface would seek the plane of minimum strength. From Projects A and B, the shear strength of this plane (the tangential plane) responded very sluggishly to the influence of transverse compression; the Project C response was consistent with this expectation, as shown in Figure 2.

The observation drawn from these three projects is that, when a shear failure in dry Douglas-fir is free to seek its plane of minimum strength, as is usually the case in large timber beams, its shear strength parallel to the grain is not significantly increased by the application of transverse-compressive stress. This helps to explain why the present results differ from those of Mandery (1969); an examination of his paper suggests that his specimens were not able to seek their plane of minimum strength.

## ANATOMICAL STUDIES

After the testing, the failure surfaces of the specimens in Projects A and C were examined, using incident-light microscopy and scanning-electron microscopy in an attempt to see whether or not the failure modes observed were consistent with the experimental results.

When a shear-failure plane passes through wood, its location at the cellular level can be described as being in one of two broad categories: "intrawall" or "transwall". "Intrawall" failure describes a failure surface which remains *within* the double cell wall of two adjoining cells; "transwall" failure cuts *through* the double cell wall so that the lumen and the S3 layer are exposed. The transwall failure mode is relatively easy to detect in Douglas-fir because the S3 layer is characterized by spiral thickenings.

### Project A

Each specimen was examined first using incident-light microscopy and then small samples of wood which appeared to be representative were cut from the surface for electron microscopy.

#### (a) Radial Plane

Figures 3 to 6 are photomicrographs of radial-shear planes in blocks tested under different levels of compressive and tensile transverse stress. The following is a summary of the information gained from these photographs. Latewood tracheids showed intrawall failures almost exclusively, with the failure plane in each band of latewood remaining in a particular ray plane. Earlywood tracheids showed both intrawall and transwall failures, with the exception of the specimens to which high tensile stress was applied; these showed mainly intrawall failures. The failure plane in earlywood did not remain in a particular ray plane, but moved from one ray plane to another. Ray crossings on the latewood tracheids seemed to be slightly squashed on the specimens subjected to high transverse compression.

The test data and the photographs suggested the following mechanism of shear failure in the radial plane. The major zone of weakness appeared to be within the double cell wall in the compound middle lamella between adjoining tracheids; the presence of rays contributed to this weakness by interrupting the contact between tracheids. Failure seemed to take place by sliding at or near this interface, with the ray cells twisting or rolling between the two sliding surfaces. With a sliding mode of failure, it seemed natural to think of the behaviour as being similar to friction between two fairly smooth surfaces. The shear-strength test results are in line with a frictional analogy: high resistance with high transverse compression and lower resistance with lower stress. This is borne out by the appearance of the specimen with high transverse tension (Figure 6): the "friction" in the interface between the tracheids has been reduced by the high tension to the extent that the failure type of the earlywood tracheids has changed from mixed transwall-intrawall to predominatly intrawall.

It is possible that the ray cells, in addition to their function as interrupters of the contact between adjacent tracheids, may have had another role to play. Figure 5 hints that ray cells rolled or twisted between the sliding surface and might be thought of as "sticky roller bearings". However, with the application of lateral compressive stress, the ray cells functioned less well as roller bearings, until at high pressures they deformed so that the sliding surfaces had to grind these cells as shear deformation took place; in this way, ray cells at high pressures may have added to the friction between the surfaces. Figure 4 shows ray crossings in a specimen which had had high compression stress applied; the areas where the rays had been in contact with the tracheids (the ray crossings) appear to be more mashed-looking than in the other figures.

In summary, the concept of intrawall friction for the shear strength of the radial plane seemed to be consistent with the shear strength results and with the appearance of the failure surfaces.

### (b) Tangential Plane

The tangential-plane failures were examined next. Macroscopic examination of each failure surface indicated that the surfaces had distinct regions which were either light or dark to the naked eye. On closer examination with a hand lens and with incident–light microscopy, the "dark" surfaces turned out to be failures at or very near the boundary between the last-formed latewood tracheids of one annual ring and the first-formed earlywood tracheids of the next annual ring, and were either intrawall or earlywood transwall. The "light" areas were transwall failures in earlywood tracheids further away from the annual-ring boundary than the dark areas. An interesting trend was noticed: the specimens with no transverse stress seemed to be almost completely dark, but specimens with either transverse tension or transverse compression had some light areas, with the specimen with the most light area being the one examined which had experienced the highest compression stress. In an attempt to quantify this trend, photographic enlargements were made of the entire failure surfaces of all tangential specimens. The light and dark areas were outlined in pencil on the prints and a planimeter was used to calculate the percentage of the total surface which was dark. These "percent darkness" values are plotted in Figure 7 against the transverse stress which had been applied. The graph shows that lightness was associated with transverse stresses and that at zero stress the surfaces had the greatest average dark area. In other words, the failure plane in the tangential specimens was at or very near the annual-ring boundary (i.e. in the first-formed earlywood cells) when the transverse stresses were absent or low; at higher stresses, the failure plane migrated some distance into the earlywood. This was confirmed using scanning-electron microscopy.

Figures 8 to 10 are photomicrographs of tangential shear plane in blocks tested under different transverse stresses. The observations made from these photographs, and from others not shown, are summarized as follows. Failure invariably seemed to be either in earlywood or at the annual-ring boundary. Specimens with zero stress and low tension or compression stress exhibited both ring boundary intrawall and earlywood transwall failures; specimens with higher compression and tension stress showed mainly transwall failures. The transwall failures at high compression showed flattened tracheids and cleancut fractures in the cell walls; transwall failures at high tension were not flattened and the cell-wall fractures appeared to be torn rather than cleancut.

On the basis of this information, an attempt can be made to describe a possible failure mechanism for tangential shear planes. In the case of radial shear planes, the analogy of friction between two fairly smooth sliding surfaces seemed to be appropriate, since radial-plane behaviour was dominated by the intrawall mode. However, tangential plane behaviour is largely characterized by the transwall mode in the relatively weak earlywood tracheids; in this mode, the friction analogy comes to mind only reluctantly, since the cell walls seem to rip or tear and sliding is more difficult to conceptualize. Some sort of internal frictional effect may exist in transwall mde, but it is suggested that it is less significant than it would be in intrawall mode.

At zero or low stress, both intrawall and earlywood transwall modes exist and thus it is felt that their shear strengths are roughly equal. However, if the suggestion in the above paragraph is valid, then the intrawall mode would increase in strength more quickly than the transwall mode when perpendicular compression is increased and, thus, transwall strength should become the dominant mode. This is supported by Figure 8 which shows mainly transwall mode in a specimen with high compression. There is another possible reason why transwall mode characterizes Figure 8; the flattened cells and the cleancut walls suggest that the high compression may have damaged the earlywood tracheid walls, making them easier to shear and counter-balancing any increase in shear strength due to transwall friction. The specimen shown in Figure 8 had a transverse compression stress of 750 psi applied to it before testing in shear. That this level of stress may be damaging to the tracheid walls is supported by the fact mentioned earlier that six test specimens in Project A failed in compression perpendicular to the grain, before they could be tested in shear, at stresses between 750 and 1000 psi; four of these six were tangential plane specimens.

In the case of applied transverse tension, it is felt that intrawall and transwall modes have about the same strength at low stress levels (as mentioned earlier), until the application of the tension stress damages the earlywood tracheid walls making them easier to shear. For example, Figure 10, which is typical of the appearance of specimens with high transverse tension, shows mainly transwall failure.

In summary, the tangential-shear plane fails in both earlywood transwall and intrawall modes and appears to experience only a minor frictional effect, until the transverse tension or compression stress is high enough to damage the earlywood tracheid walls, at which time the failure is mainly transwall.

### Project C

The failure surfaces of specimens subjected to transverse-compression stresses less than about 370 psi sought a tangential orientation and occurred largely in earlywood tracheids, but showed no strong preference for any particular failure location around the circumference of the specimen; the failure surfaces appeared essentially the same as the tangential-plane failure surfaces of Project A. Above 370 psi, however, a distinct change was noted in the failure location and appearance: the failures were transwall in the earlywood tracheids and showed a "lateral shearing" distortion of the tracheid walls, as well as longitudinal ripping (Figure 11). Moreover, the failure surface had a strong tendency to seek the point on the circumference of the specimen where the annual rings made an angle of about 60° - 75° with the tangent drawn to the specimen wall, i.e., with the direction of circumferential compressive stress perpendicular to grain (Figure 12). The authors found this to be puzzling until it was recalled that it is approximately this annual-ring orientation which produces the smallest strengths of wood in compression perpendicular to the grain (Kennedy 1968, Kollmann 1959). The lateral movement on the failure surface was then thought to be the same as the diagonal shearing movement seen in a piece of wood tested in compression perpendicular to the grain when the annual-ring orientation is neither perpendicular nor parallel to the direction of load, i.e. "rolling shear". This agrees with Figure 2, in which the onset of transverse compression failure occurs earlier in Project C than in either Project A or Project B.

Figure 13 is an attempt to tie together all of the previous data, observations, and suggestions. It is a graphical representation of the overall shear-strength response of the various failure modes to the application of transverse stress. The ordinates to the four curves are purely conceptual in nature and not quantitative, but the general shapes of the curves and the abscissae bear a general relationship to the test data and to the photomicrographs.

## SUMMARY AND CONCLUSIONS

Three experimental projects were carried out to investigate the effect of transverse stress on the shear strength parallel to grain of air-dry Douglas-fir. Three different types of specimens were used -- ASTM shear blocks, oblique-grain compression specimens and torsion tubes -- in Projects A, B and C, respectively. After the testing, the failure surfaces of the specimens in Projects A and C were examined using incident–light and scanning-electron microscopy in an attempt to see if the appearances of the failure surfaces were consistent with the experimental results.

### Project A

(a) When transverse compression is applied to a specimen, the radial plane is generally stronger in shear than the tangential plane. The opposite is true when transverse tension is applied.

(b) The shear strength of the radial plane increases as transverse compression is applied and decreases as transverse tension is applied.

(c) The shear strength of the tangential plane is virtually insensitive to the application of either transverse tension or transverse compression.

(d) The shear strength of the radial plane is dominated by interwall failure in the latewood tracheids and the analogy of friction between two relatively smooth sliding surfaces appears to be consistent with the test results and with photomicrographs of the failure surfaces.

(e) Shear failure of the tangential plane is composed of varying amounts of intrawall and earlywood transwall failures and it is possible to conceive of friction being of only minor importance. At zero and low transverse stresses, failure is by intrawall failure at the annual-ring boundary and by transwall failure in the first row of earlywood tracheids. At higher stresses, the failures move farther into the earlywood and are mainly transwall.

### Project B

The trends observed in Project B agreed with those of Project A in regard to the following:

(a) When transverse compression is applied to a specimen, the radial plane is generally stronger in shear than the tangential plane.

(b) The shear strength of the radial plane increases much more rapidly with the application of transverse compression stress than does that of the tangential plane.

(c) There appears to be a value of transverse compression stress (approximately 750 psi) below which the application of transverse compression increases shear strength, and above which the specimens are susceptible to compression perpendicular-to-grain failures, which in turn reduce the shear stresses that can exist simultaneously with the compression stress.

### Project C

(a) When no perpendicular-to-grain compressive stress was applied to a torsion tube specimen, there was no definite preferred location on the specimen for shear failures to take place, although, in the main, the failures remained in the earlywood portions of annual rings. This seems to indicate that the tangential plane is only slightly weaker in shear than the radial plane when no transverse stress is applied. In this, the results agree with a trend found in Project A that the tangential and radial failure trends tended to converge as transverse stress approached zero.

(b) Shear strength increased very slightly with transverse compression in the interval zero to 370 psi of compression stress; the failures had the same appearance as the specimens to which no transverse stress was applied.

(c) At transverse stresses more than 370 psi, shear strength decreased and the shear failures showed inelastic deformation in compression perpendicular to the grain in the failure zone. The failures had a strong preference for the points on the circumference where the annual rings made an angle of 60 - 75 degrees with the tangent to the tube's wall; the failures were exclusively in the earlywood and passed diagonally, not normally, through the wall of the specimen. The decrease in shear strength at more than 370 psi is in marked contrast to the behaviour seen in Project A and, it is suggested, that it is due to wood's particular weakness in compression perpendicular to grain when the orientation of the annual rings is at an angle of 60 - 75 degrees to the direction of the perpendicular compression stress. The failure mode seems to be similar to "rolling shear" in the earlywood and photomicrographs of the failure surfaces are consistent with this suggestion. This was the weakest failure mode observed: earlywood trans-wall for longitudinal plus lateral shear, which is more critical than those observed in Project A.

The general conclusion from all these projects is that, when a shear failure in dry Douglas-fir is free to seek its plane of greatest weakness, as is usually the case in glued-laminated timber beams, its shear strength is not significantly increased by the application of compressive stress perpendicular to grain.

## REFERENCES

Huggins, M.W., J.H.L. Palmer and E.N. Aplin. 1966. Evaluation of the effect of delamination. Engineering Journal 49(2):32-41.

Keenan, F.J. 1974. The shear strength of wood beams. Forest Products Journal 24(9):63-70.

Keenan, F.J. and K.A. Selby. 1973. The shear strength of Douglas-fir glued-laminated timber beams. Department of Civil Engineering, University of Toronto, Publication 73-01, Toronto, Ont.

Kennedy, R.W. 1968. Wood in transverse compression. Forest Products Journal 18(3):36-40.

Kollmann, F.F.P. 1959. The problem of transverse compressive strength of timber. Translated by D.S.I.R. (Great Britain) from Holzforschung und Holzverwertung 11(5):109-121.

Mandery, W.L. 1969. Relationship between perpendicular compressive stress and shear strength of wood. Wood Science 1(3):177-182.

## ACKNOWLEDEMENTS

This research was supported by the National Research Council of Canada and by the Ontario Department of University Affairs. The assistance of Messrs. W. Glover, J. Knight, F. Pfaff, P. Swindle, J. Whittaker and D. Yamasaki in the preparation and testing of the specimens is gratefully acknowledged. The authors also greatly appreciate the production of scanning-electron photomicrographs by Mr. E.E. Quinn at the Division of Building Research, National Research Council, and the several contributions to this research by Professors K.A. Selby and J.J. Balatinecz of the University of Toronto.

TABLE 1 - Test Specimens

| Project | Number of Specimens | Specimen Type | Moisture Content (%) | Basic Specific Gravity |
|---|---|---|---|---|
| A | 33 | ASTM shear blocks | 6.1 ± 0.4 | 0.50 ± 0.02 |
| B | 90 | Oblique-grain compression specimens | 10.4 ± 0.5 | 0.50 ± 0.04 |
| C | 47 | Torsion tubes | 8.0 ± 1.0 | 0.38 ± 0.06 |

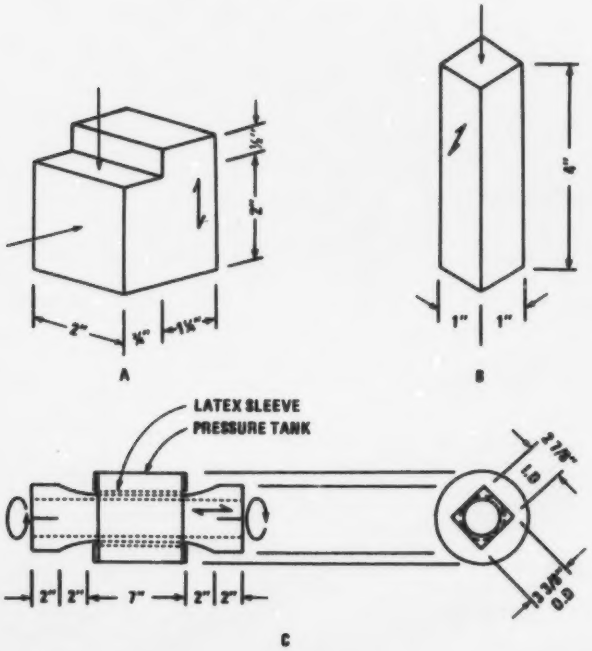
½"
2"
2"
½"
1½"
A
4"
1"
1"
B
LATEX SLEEVE
PRESSURE TANK
2 7/8"
I.D
3 3/8"
O.D
2"
2"
7"
2"
2"
C

Figure 1. Test specimens and schematic representation of loading methods: A – ASTM shear block; B – oblique-grain compression specimen; C – torsion tube. The one-sided arrows indicate the grain direction, i.e. the longitudinal direction of the wood.

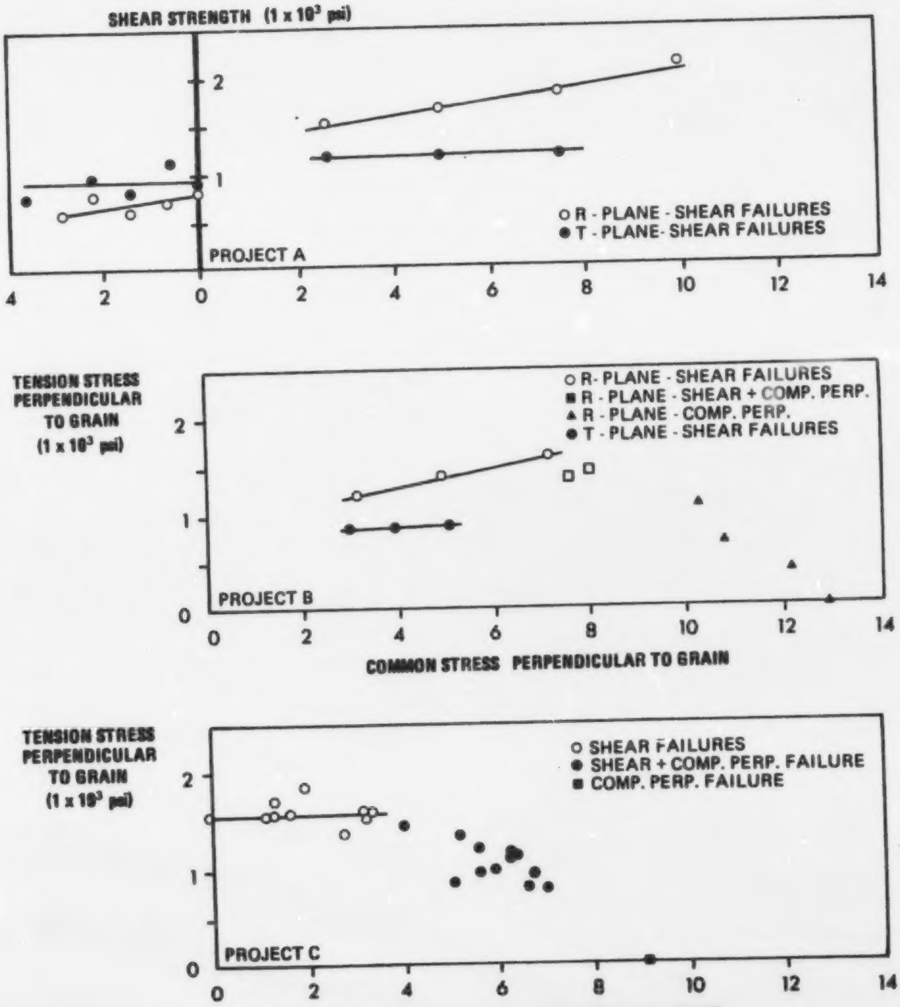

Figure 2. Test results - effect of transverse stress on shear strength.

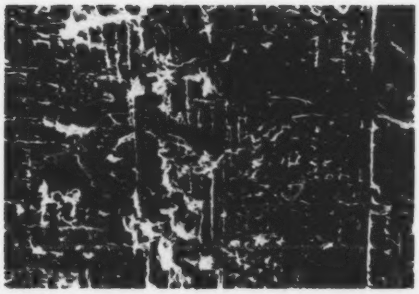

Figure 3. Radial shear plane - no transverse stress. (magnification = 233x). The latewood exhibits intrawall failure almost exclusively. The ray crossings (and some ray cells) are visible; the failure plane in a band of latewood stays largely in the plane of a particular ray. The earlywood shows both intrawall and transwall failures and is much rougher than the latewood. The failure plane in earlywood does not always remain associated with a particular ray, but may jump back and forth in the tangential direction.

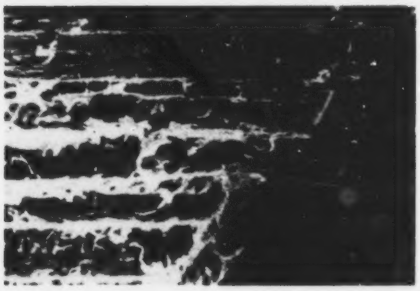

Figure 4. Radial shear plane - high transverse compression (magnification = 240x). Beyond a large "curl" of wood that has been pushed up during shear failure, can be seen the radial shear failure plane of a specimen to which 750 psi of transverse compression had been applied. The latewood shows intrawall failure in one particular ray plane, although the tracheids and ray crossings seem to be slightly "mashed" or deformed when compared with Figure 3, as would be expected. The earlywood again shows both intrawall and transwall failure.

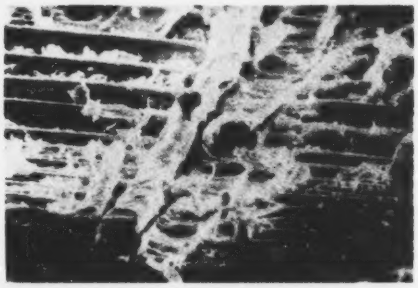

Figure 5. Radial shear plane - low transverse tension (75 psi) (magnfication = 1,110x). A few ray cells seem to have been pulled or rolled away from the adjoining tracheids. The latewood exhibits largely intrawall failure at a particular ray plane and the earlywood has both intrawall and transwall failures.

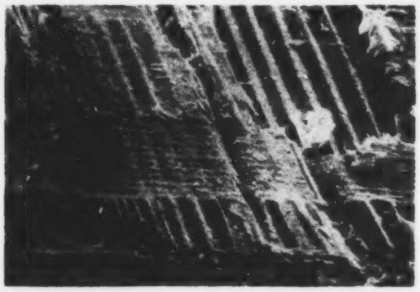

Figure 6. Radial shear plane - high transverse tension (300 psi) (magnification = 138x). In contrast to those in Figures 3 to 5, both earlywood and latewood tracheids have intrawall failures although some earlywood tracheids have transwall failures.

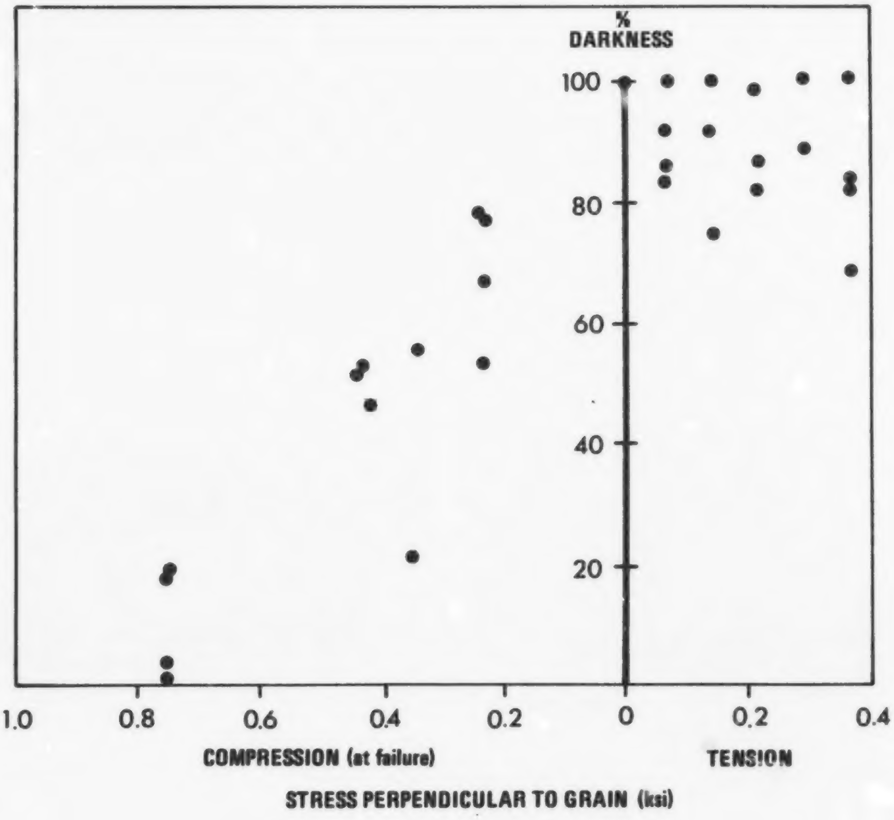

Figure 7. Effect of transverse stress on "darkness" of the tangential shear plane. "Dark" areas occurred at or very near the annual-ring boundary, either as ring boundary intrawall or earlywood transwall failures. "Light" areas were transwall failures in earlywood a few rows of tracheids away from the annual-ring boundary. Each point represents one specimen with the exception of the zero stress point which is the average of 100, 100, 100, 94 and 100%.

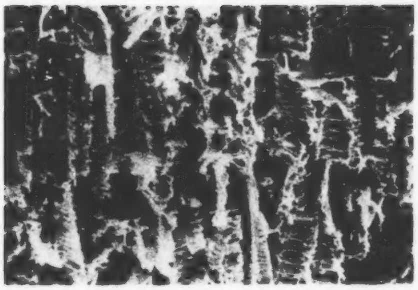

Figure 8. Tangential shear plane - high transverse compression (750 psi) (magnification = 72x). The failure is in earlywood and is mainly transwall. Spiral thickenings are clearly visible. Note the flatness of the tracheids and the relatively clean-cut fractures of the cell walls. (For contrast see Figure 10, which is a photograph of a specimen to which transverse tension had been applied.)

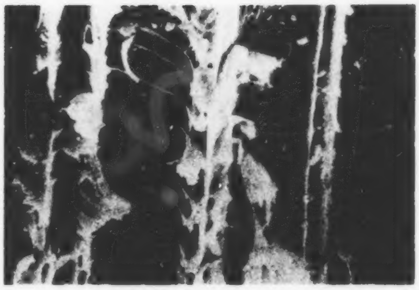

Figure 9. Tangential failure plane - low transverse compression (magnification = 830x). The intrawall failures at the annual-ring boundary and transwall failures are typical of specimens with low compression stress, no stress, and low tension stress.

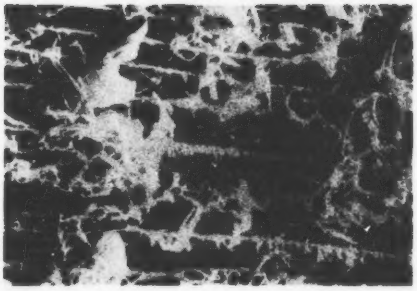

Figure 10. Tangential failure plane - transverse tension (magnification = 72x). The failure is in the earlywood and is mainly transwall. The fractured edges of the cell walls are not as clean cut as in Figure 8, but seem to be somewhat torn.

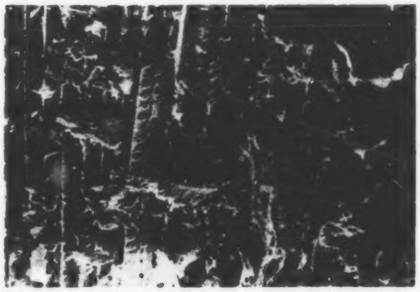

Figure 11. Tangential failure plane - high transverse compression. The failure surface is similar to that seen in Figure 8 except that some lateral shearing distortion of the tracheid walls is also present. The transwall failures often follow the baseline of serial bordered-pit pairs.

Figure 12. Cross-section of a torsion tube subjected to high compression stress. The diagram shows the typical location of the shear failure crack when the compression stress exceeded 370 psi.

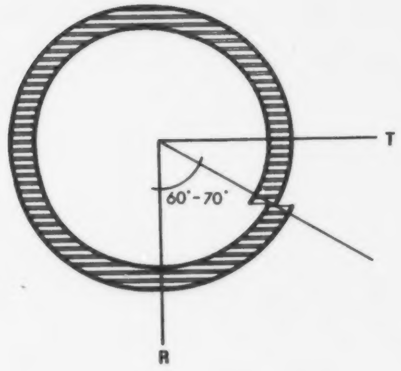

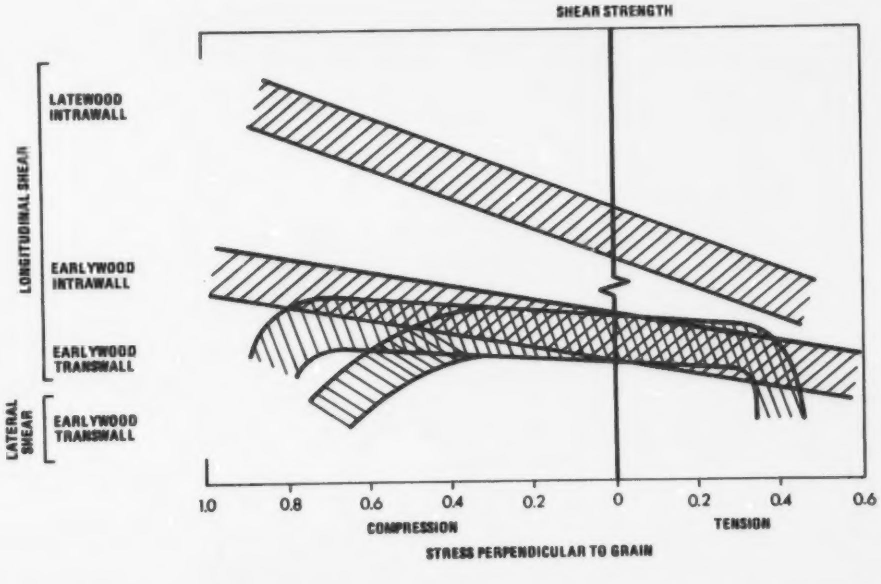

Figure 13. Failure modes. The earlywood intrawall mode is considered to include intrawall failures at the annual-ring boundary. Tangential plane failures involved only the earlywood modes, but all modes are involved in radial-plane failures. The lower branch of the earlywood transwall mode occurred only in Project C.

# A MODEL FOR FRACTURE TOUGHNESS OF ORIENTED FLAKEBOARD

by

Young-kong Lei[1] and James B. Wilson[2]

---

[1] Graduate Research Assistant and [2] Assistant Professor of Forest Products, School of Forestry, Oregon State Univ., Corvallis, Oreg. 97331. This is paper 1343 of the Oregon Forest Research Laboratory, OSU.

## INTRODUCTION

Elastic and strength properties are highly uniform throughout the plane of flakeboard because its production from solid wood reduces the size of all natural defects, such as knots, and uniformly distributes them throughout the board. However, manufacturing usually introduces processing defects, such as interflake voids and nonbonded areas, into the flakeboard (Fig. 1). Because board strength depends on the voids and nonbonded areas (4), mechanical properties such as tensile strength normal to the board (internal bond strength) are lower for flakeboard than for better grades of solid wood of the same species.

This paper establishes a model for predicting the fracture toughness ($K_{Ic}$) of flakeboard based on the $K_{Ic}$ and inherent flaws of the original solid wood, as well as the length of voids and nonbonded areas in the board. Assuming that voids and nonbonded regions in flakeboard form surfaces for cracks, we applied fracture mechanics to analyze flakeboard as a cracked body. We also tested the validity of our model using oriented flakeboards of differing densities.

## ANALYTICAL MODEL

Our approach used classical fracture mechanics to determine the $K_{Ic}$ of a material, assuming that the $K_{Ic}$ for solid wood is a material parameter (2, 5). We also assumed that cracks in the flakeboard cause its $K_{Ic}$ to differ from the $K_{Ic}$ of the solid wood used to make the flakes. The size of the cracks can be predicted using probability theory. Then, based on the $K_{Ic}$ of the original wood used to make the flakes and the expected crack length due to voids and nonbonded areas in the flakeboard, we can calculate the predicted $K_{Ic}$ of a given flakeboard.

To calculate $K_{Ic}$, we adopted an equation for a single-edge-notched plate in normal tension (1):

$$K_{Ic} = \sigma_c \; a^{1/2} \; Y\left(\frac{a}{W}\right) \text{ for } \left(\frac{a}{W} < 0.6\right) \quad (1)$$

where: $K_{Ic}$ = the fracture toughness for the opening mode (psi$\sqrt{\text{in}}$);

$\sigma_c$ = the critical stress to fail the cracked specimen (psi);

$a$ = the crack length (in.);

$W$ = the specimen width (in.);

$$Y\left(\frac{a}{W}\right) = 1.99 - 0.41\left(\frac{a}{W}\right) + 18.7\left(\frac{a}{W}\right)^2 - 38.48\left(\frac{a}{W}\right)^3 + 53.85\left(\frac{a}{W}\right)^4$$

Examination of our edge-notched specimen of oriented flakeboard (Fig. 2) shows that the initial notch (crack) in the specimen will lengthen if it contacts an interflake void, a nonbonded region, or both. This will lengthen the crack from a to a + Δa, thus reducing the maximum stress needed to fail a fracture-toughness specimen. This effect can be shown by rearranging equation 1 for the critical stress:

$$\sigma_c = K_{Ic} \; a^{-1/2} \left[Y\left(\frac{a}{W}\right)\right]^{-1} \quad (2)$$

Assuming the same $K_{Ic}$ for the original wood and the flakes, then, for a given value of $K_{Ic}$ and an increased crack length a + Δa, the critical stress, $\sigma'_c$, for the flakeboard can be calculated:

$$\sigma'_c = K_{Ic}(a + \Delta a)^{-1/2}\left[Y\left(\frac{a + \Delta a}{W}\right)\right]^{-1} \quad (3)$$

$$Y\left(\frac{a + \Delta a}{W}\right) = 1.99 - 0.41\left(\frac{a + \Delta a}{W}\right) + 18.7\left(\frac{a + \Delta a}{W}\right)^2 - 38.48\left(\frac{a + \Delta a}{W}\right)^3 + 53.85\left(\frac{a + \Delta a}{W}\right)^4$$

However, this equation cannot predict a flakeboard strength greater than the strength of the original solid wood. This analysis must be modified to account for this case because our earlier experiments (4) have shown that flakeboard can be stronger than its original solid wood.

Evaluating $K_{Ic}$ of any material with a similar specimen geometry (a/W) and a constant initial crack length (a) automatically assumes a direct relationship between any two pairs of $\sigma_c$ and $K_{Ic}$ values, such as

$$\frac{K'_{Ic}}{K_{Ic}} = \frac{\sigma'_c}{\sigma_c} \qquad (4)$$

However, another relationship must be assumed if the $K_{Ic}$ of two different materials are calculated using different crack lengths in equation 1. The relationship may be

$$\frac{K'_{Ic}}{K_{Ic}} = g \cdot \frac{\sigma'_c}{\sigma_c} \qquad (5)$$

or some other form. The proportionality variable, g, is determined empirically as a function of the material fracture properties and crack length. It is used to correct our analysis when the flakeboard is stronger than the original solid wood used to make the flakes.

Our analysis assumed that the solid wood was flawless, whereas most materials have inherent flaws. In Douglas-fir, these range from 0.1 to 0.12 in. in length (6).

To determine g in terms of the effect of inherent flaws in the solid wood, we assumed a state in which an oriented flakeboard becomes equivalent to its original solid wood in terms of flaw size, flaw distribution, and fracture resistance. This occurs when the variable, g, equals one. We assumed that this state is reached if the average length of the interflake crack ($1/\mu$) in the flakeboard equals the average inherent flaw ($\Omega$) in the solid wood. The simplest mathematical form to depict this state is:

$$g = \exp\left(\Omega - \frac{1}{\mu}\right) \qquad (6)$$

Substituting equations 2, 3, and 6 into 5, we have an expression to predict the fracture toughness ($K'_{Ic}$) of flakeboard:

$$K'_{Ic} = \exp\left(\Omega - \frac{1}{\mu}\right) K_{Ic}\, a^{1/2} \left(a + \Delta a\right)^{-1/2}$$
$$\left[Y \quad \frac{a}{W} \quad Y\left(\frac{a + \Delta a}{W}\right)\right]^{-1} \qquad (7)$$

To predict the $K'_{Ic}$ of the flakeboard, we have to know the average size of the inherent flaws ($\Omega$), the fracture toughness of solid wood used to make the flakes, the initial crack length (a) for an edge-notched specimen, and the expected increase in crack length ($\Delta a$) due to interflake voids and nonbonded areas in the flakeboard. A similar analysis can be developed to predict the critical stress for flakeboard.

## EXPECTED INTERFLAKE CRACK INCREMENT ($\Delta a$)

When an edge notch is introduced into a fracture specimen of flakeboard, the tip of the notch has a probability of occurring somewhere in an interflake void, a nonbonded area, or both. Thus, the length of the introduced crack could increase by an increment, $\Delta a$, which can be determined by considering the distributions of the interflake voids and the nonvoid lengths. These approximated exponential distributions (Fig. 5). The probability of the notch tip being in a void is (3):

$$P\left\{\text{void at tip} \mid \text{void at } a=0\right\} =$$
$$\frac{\lambda}{\lambda + \mu} + \frac{\mu}{\lambda + \mu} e^{-(\lambda + \mu)a} \qquad (8)$$

where: $\frac{1}{\lambda}$ = average nonvoid length and

$\frac{1}{\mu}$ = average void length.

Following the analysis through (4) shows that the expected increase in crack length due to the interflake void is:

$$\Delta a = \frac{1}{\mu} \cdot \frac{\lambda}{\lambda + \mu} \qquad (9)$$

The length of the initial crack (a) does not affect the value of the crack increment ($\Delta a$). Thus, the expected increase in the initial crack length can be determined by measuring the interflake void lengths, nonvoid lengths, and nonbonded lengths for a given flakeboard. The expected increase in crack length can be calculated for two possible cases: where $\Delta a$ is based on $1/\mu$ equal to the average interflake void length; and where $1/\mu$ is equal to the average interflake void plus nonbonded lengths. For each case, $1/\lambda$ is suitably adjusted.

## EXPERIMENTAL VERIFICATION

To experimentally verify equation 7, our model for $K'_{Ic}$ of flakeboard, we tested matched samples of Douglas-fir solid wood and flakeboard made from parallel-oriented edge-grain flakes. An edge-notched specimen was selected to measure fracture toughness in the TL mode for both solid wood and flakeboard because earlier experiments (4) showed that this mode was the least variable. The TL mode refers to a tensile load applied in the tangential direction, T, and a crack extension in the longitudinal direction, L (Fig. 3). Other data that must be evaluated for the theoretical model are: the fracture toughness ($K_{Ic}$) for the solid wood fracture; the average length of inherent flaws in solid wood ($\Omega$); the average length of interflake cracks ($1/\mu$); and the average length between interflake cracks ($1/\lambda$).

Four flakeboards (1/2 x 12 x 12 in.) with nominal densities of 37, 40, 43, and 47 lb./ft.$^3$ were made from parallel-oriented edge-grain flakes. For both the solid wood and flakes, clear old-growth Douglas-fir averaging 20 rings/inch was selected. To minimize wood damage, the flakes were individually sawn to 1/32 x 11/16 x 2 in., then sprayed with phenol-formaldehyde resin (42% solids) at a spread rate of 1.35 lb./1000 ft.$^2$ of flake surface area. The flakes were individually hand aligned in mats and hot pressed for 10 minutes at 325°F and 250 psi.

Fracture toughness specimens were cut to 1/2 x 1 x 2 in. Each specimen was edge notched 0.75 ± 0.01 in. with a bandsaw blade ground to a sharp edge, then glued to aluminum blocks and subjected to a tensile load applied at 0.04 in/min.

To calculate the expected crack length increase ($\Delta a$) for flakeboard, we measured the void, nonvoid, and nonbonded lengths using a scanning line 1/32 in. wide and 8 in. long (Fig. 4). Void and nonvoid lengths were measured directly on the edge of the board, whereas the interflake voids were pried open with a knife so nonbonded areas could be measured. The nonbonded areas – void lengths plus nonbonded lengths – could be easily identified by the dark color of the phenolic resin that uniformly coated the flake surface. In bonded areas, wood surfaces would fracture when the voids were opened. The nonbonded lengths occurred at the corners of interflake voids (Fig. 1).

Five scanning strips were used for each board. Frequency of occurrence for each void length was then plotted versus void length (Fig. 5). An exponential curve of the form, $f(x) = \mu \exp(-\mu x)$, was fit to the histogram; thus giving a value for $1/\mu$. The same procedure was used for determining $1/\lambda$. Using the data in Table 1, the expected increase in crack length, $\Delta a$, can then be calculated from equation 9. Fig. 6 shows the variation of the expected increase in crack length with board density.

The fracture toughness values were experimentally measured and determined using equation 1 and an edge-notch depth of 0.75 in. for both the solid wood and the respective flakeboards (Table 2). Due to the variability of $K_{Ic}$ for wood, the $K'_{Ic}$ values for flakeboard must be normalized by dividing them by the $K_{Ic}$ of their matched samples of solid wood. Thus, the $K'_{Ic}$ for flakeboard is plotted as the $K_{Ic}$ retention of the original solid wood (Fig. 7).

From Fig. 7, we determined the average flaw size in the solid wood. In determining the proportionality variable, g, we assumed that g equalled one when the average length of the interflake crack equalled the average inherent flaw. The experimental data (Fig. 6) shows that flakeboard $K_{IcTL}$ retention is 100% of the original solid wood when the average crack length is approximately 0.1 in. Thus, the length of the inherent flaw ($\Omega$) in Douglas-fir solid wood is approximately 0.1 in. which matches published values (0.1 to 0.2 in.) of inherent crack length for Douglas-fir (6).

## RESULTS AND DISCUSSION

The $K_{Ic}$ values in the TL mode for the different density flakeboards were predicted using equations 7 and 9. The accuracy of our model was assessed by averaging the differences between the predicted and actual values. The error for our predictions averaged 12.2%, if only the interflake void length is used to calculate the expected crack extension. However, if the interflake void length plus the nonbonded length are used for the calculation, then the error averaged only 6.9%.

In Fig. 6, the flakeboard with a zero crack length is our "idealized flakeboard" made of parallel-laminated veneers with veneers of the same thickness as the flakes and the same amount of resin. Again, the predicted values closely agree with the actual values.

## CONCLUSIONS

Assuming that the flakes were not severely damaged and that the resin was adequately applied, our analytical model and the experimental verification for the $K_{Ic}$ of oriented flakeboards show that:

1. The $K_{Ic}$ of oriented flakeboard is determined by the interflake crack length and the distance between cracks.
2. The model proposed in equation 7 can be used to estimate the $K_{Ic}$ of flakeboard within 6.9% when the reference point is the TL mode of fracture toughness ($K_{IcTL}$) of original solid wood.
3. Starting with the concepts of linear-elastic fracture mechanics, we can determine the fracture strength of oriented flakeboards based upon the fracture toughness and inherent flaws in solid wood, as well as the void, nonvoid, and nonbonded lengths in the board.

## LITERATURE CITED

1. Brown, W.F. and J.E. Srawley. 1966. Plane strain crack toughness testing of high strength metallic materials. Am. Soc. Test. Mater., Philadelphia, PA, ASTM Spec. Tech. Publ. 410.

2. Johnson, J.A. 1973. Crack initiation in wood plates. Wood Sci. 6(2):151 - 158.

3. Karlin, S. and H.M. Taylor. 1975. A First Course in Stochastic Processes. Academic Press, New York.

4. Lei, Young-kong. 1978. On the fracture mechanics of oriented flakeboard. Ph.D. thesis, Oreg. State Univ., Corvallis. 149 p.

5. Porter, A.W. 1964. On the mechanics of fracture in wood. Forest Prod. J. 14(8): 325 - 331.

6. Schniewind, A.P. and D.E. Lyon. 1973. A fracture mechanics approach to the tensile strength perpendicular to grain of dimension lumber. Wood Sci. Tech. 7:45 - 59.

Table 1. Size of cracks in oriented flakeboard of four densities

| FLAKEBOARD DENSITY | | AVERAGE LENGTH | | | | | VOIDS WITHOUT NONBONDED LENGTHS |
|---|---|---|---|---|---|---|---|
| Nominal | Actual[1] | Void (a) | Nonbonded (b) | Nonvoid | a + b | b/a | |
| (lb./ft.$^3$) | | (in.) | | | | (%) | (%) |
| 37 | 38.18 | 0.4449 | 0.0584 | 0.6278 | 0.5033 | 13.13 | 43.33 |
| 40 | 39.43 | 0.1784 | 0.0476 | 0.4315 | 0.2260 | 26.67 | 38.46 |
| 43 | 42.06 | 0.1152 | 0.0314 | 0.4542 | 0.1466 | 27.30 | 36.00 |
| 47 | 48.28 | 0.0745 | 0.0007 | 0.7058 | 0.0752 | 0.88 | 71.43 |

[1] Based on weight and volume at a moisture content of 5 to 6 percent.

Table 2. Actual and predicted fracture toughness in the TL mode ($K_{IcTL}$) for oriented flakeboards of four densities.

| EXPERIMENTAL | | | | FLAKEBOARD $K_{IcTL}$ PREDICTED FROM CRACK EXTENSION DUE TO | |
|---|---|---|---|---|---|
| Original solid wood | | Flakeboard | | | |
| Density (lb./ft.$^3$) | $K_{IcTL}$ (psi $\sqrt{in.}$) | Density (lb./ft.$^3$) | $K_{IcTL}$ (psi $\sqrt{in.}$) | Void length | Void + nonbonded lengths |
| | | | | (psi $\sqrt{in.}$) | |
| 37.31[1] | 294 ± 16 | 38.18 | 126 ± 38 | 139 | 116 |
| 32.33 | 260 ± 20 | 39.43 | 189 ± 36 | 213 | 190 |
| 32.33 | 260 ± 20 | 42.06 | 206 ± 32 | 240 | 226 |
| 33.36 | 305 ± 13 | 48.28 | 345 ± 42 | 313 | 313 |

[1] Based on weight and volume at a moisture content of 9 to 10%.

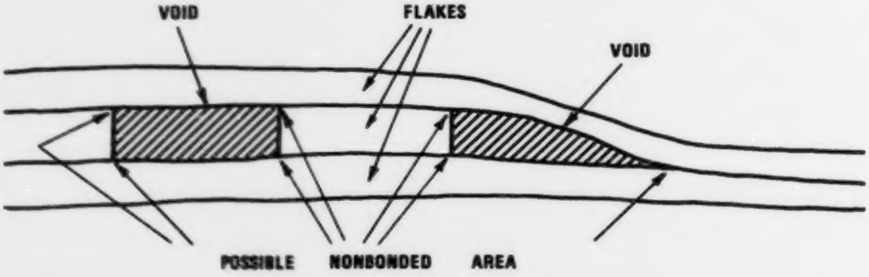

Figure 1. Triangular and rectangular interflake voids and possible nonbonded areas in flakeboard.

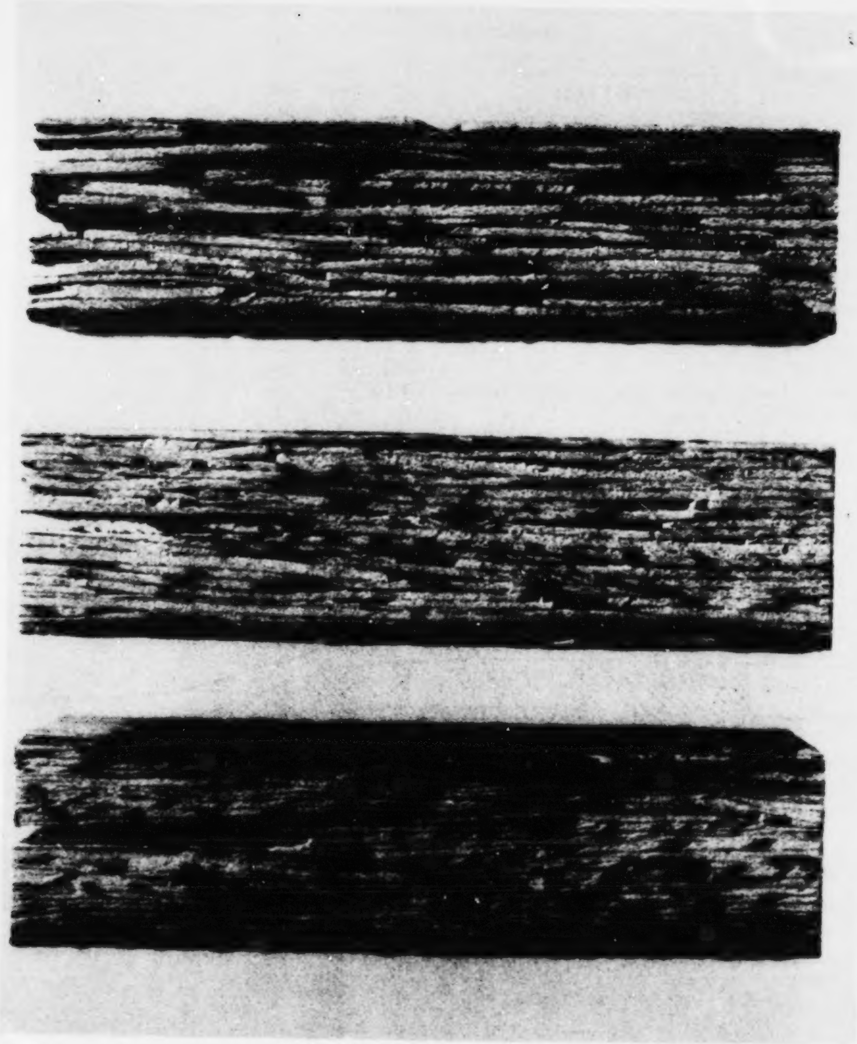

Figure 2. Fracture toughness specimens for oriented flakeboard of (top to bottom) low, medium, and high density.

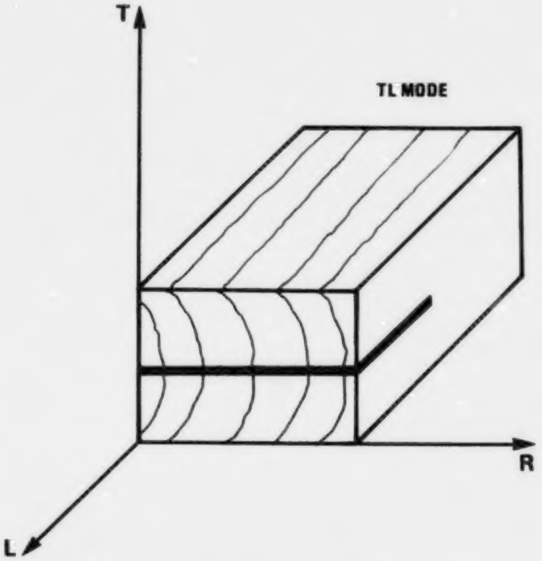

Figure 3. Opening mode (I) fracture toughness specimen for a tensile load applied in the T direction and a crack extension in the L direction.

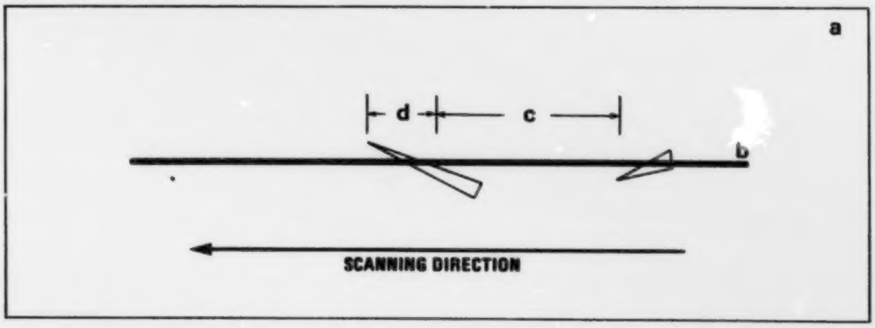

Figure 4. Measurement of interflake void and nonvoid lengths on a scanning strip; (a) cross section of an oriented flakeboard, (b) scanning line 1/32 in. wide and 8 in. long, (c) distance between voids (non-void length), and (d) interflake void length.

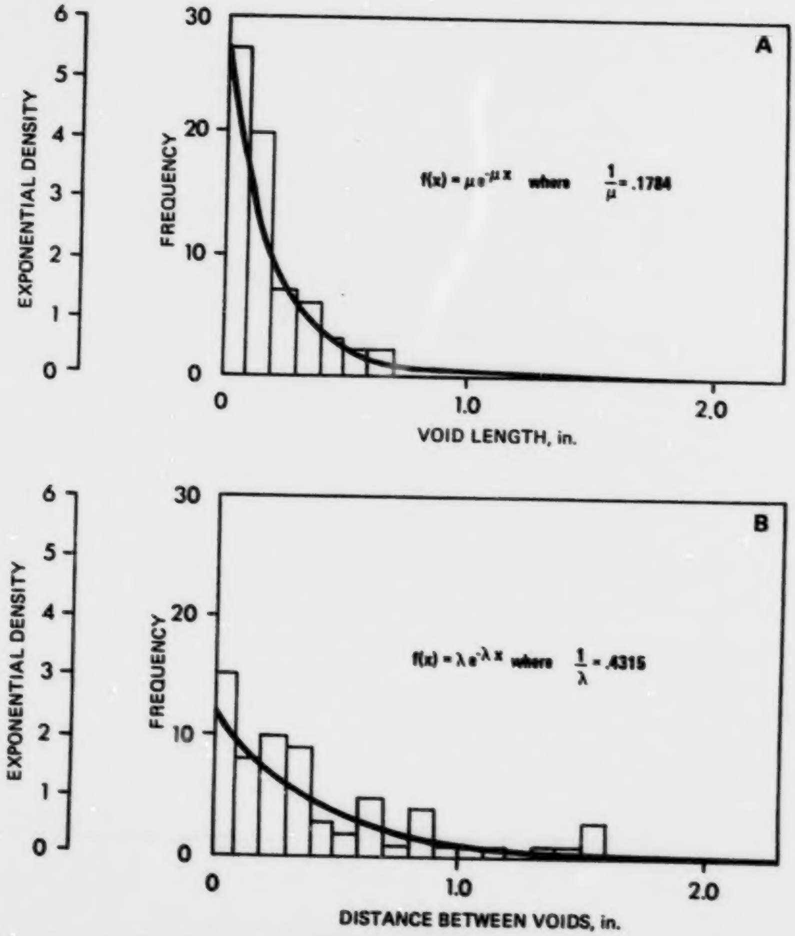

Figure 5. Frequency histogram and exponential density function of 39 lb./ft.$^3$ oriented flakeboard determined from five 8-in. scanning strips; (A) interflake void lengths ($1/\mu$ = average length); (B) distances between voids ($1/\lambda$ = average distance).

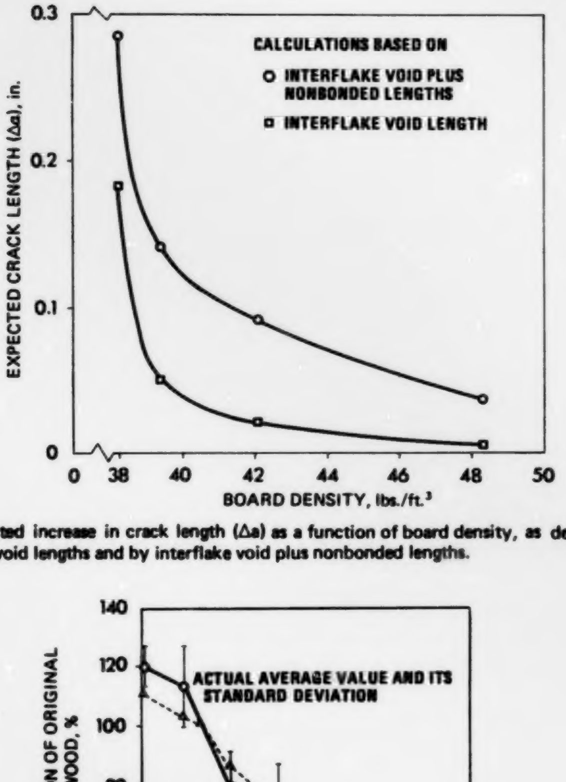

Figure 6. Expected increase in crack length (Δa) as a function of board density, as determined by inter flake void lengths and by interflake void plus nonbonded lengths.

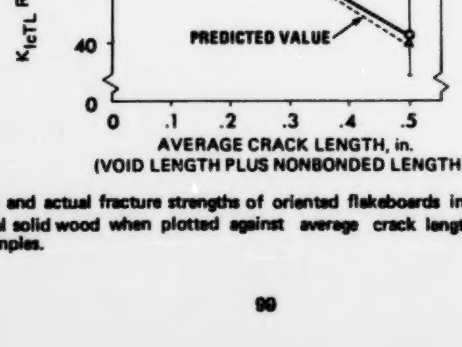

Figure 7. Predicted and actual fracture strengths of oriented flakeboards in terms of $K_{IcTL}$ retention of original solid wood when plotted against average crack length. Each point is an average of 20 samples.

# SIZE EFFECT IN LUMBER FOR BENDING

By

**Borg Madsen**

---

Department of Civil Engineering, University of British Columbia, Vancouver, B.C.

Brittle fracture has been shown to lead to size effects which can be expressed as a function of the stressed volume. Such material exhibits a strength distribution which has the form of a Weibull distribution which, in turn, has been developed using the weakest-link principle. Drs. Barrett and Foschi have shown that the brittle-fracture theory can be applied to wood for both tension perpendicular to grain and shear. In these cases, it is thought that microflaws in the general wood substance are responsible for this behaviour and natural growth characteristics, such as knots, are not responsible for the onset of failure.

In commercial lumber, the mentioned microcracks occur in the clear wood material but, in addition, knots and other defects cause specific stress concentrations which are often the apparent cause of failure when the material is subjected to bending or tension. The size of knots and similar defects are different for the different commercial grades.

The strength aspects of the grading rules have been developed by a knot-area concept developed by the Forest Products Laboratory in Madison, Wisconsin, and it was thought that this could be assigned to lumber regardless of width; i.e. a constant ratio would give the same reduction in strength regardless of width of the lumber.

### In-Grade Testing

In conjunction with a large testing program carried out in Canada, it was possible to investigate the influence of width on the strength at the 5th percentile level.

The in-grade testing method deviates in several respects from current ASTM testing methods for wood. It deals with full-size members and part of the philosophy is to use many replications in each test, at least 200. This, for practical reasons, necessitates a rapid load application of 10 seconds. It also employs the idea of a proof-load level to which all the pieces are subjected, but the proof-load level is selected such that only about 10% of the pieces are destroyed. The material which does not fail is returned to the sawmill. For this reason, it has been found most practical to conduct the tests in the sawmill using portable testing machines.

### Testing

Three species groups were tested: Douglas fir-Larch, Hem-Fir and Spruce-Pine-Fir. The sizes used in inches were 2 x 4s, 2 x 6s, 2 x 8s and 2 x 10s. Select Structural grade and #2 grade were tested extensively, but #1 grade and #3 grade material were also included in limited amounts. Both bending tests and tension tests were conducted. Each test consisted of 200 specimens of which roughly 10% were destroyed, but in addition 25 pieces were randomly picked from each sample and tested to destruction to get an estimate of the mean value and the general shape of the distribution.

### Results (Bending)

The 5th percentile was estimated using a ranking method and the results are shown in Fig. 1 for Hem-Fir. Straight lines have been fitted to the data and the $r^2$ values are shown. Similarly, the Douglas fir-Larch data is shown in Fig. 2. Because of more data available, the S-P-F species group results are represented grade by grade in Figs. 3-5 for Select Structural grade, #1 grade and #2 grade, respectively. The $r^2$ values are somewhat lower, but this could be caused by the fact that the data were obtained from several different mills.

The data from the different species groups are very similar, indicating that the observed size effect is insensitive to species. The species combined regression lines have been calculated. It is also observed in this test and others that the difference in strength between #1 grade and #2 grade is insignificant; therefore, the regression lines for these two grades have been combined. The results are as follows:

SS grade $y = -232x + 4908$
$r^2 = 0.60$

#1 & #2 grade $y = -177x + 3689$
$r^2 = 0.48$

#3 grade $y = -160x + 3076$
$r^2 = 0.56$

Correction factors for size can be developed and the 2 x 8 size was chosen as the base because the majority of tests in the overall program were conducted on 2 x 8s.

**Size Adjustment Factors**

| | 2x4 | 2x6 | 2x8 | 2x10 |
|---|---|---|---|---|
| SS | 1.31 | 1.13 | 1.00 | 0.86 |
| #1 & #2 | 1.28 | 1.13 | 1.00 | 0.85 |
| #3 | 1.31 | 1.15 | 1.00 | 0.83 |

From the above it would appear that the same factors can be used for the three grades.

Since the thickness is constant for all of the sizes and a constant span-to-depth ratio was used, a plot of log strength vs. log width should be a straight line if the weakest-link principle was operating. Such plots were made, but the fits were not quite as good as the ones shown above. However, the range of width was narrow and it cannot be disproven that a brittle-fracture concept cannot be applied.

As mentioned, it was not possible in this test to sort out a possible component caused by grading from a size effect in the weakest-link connotation, since only the overall effect is observed. However, from a design point the findings are significant because they show that high stresses can be applied to the narrower widths of lumber, while some decreases in stresses may be necessary for wider widths.

Another experiment pertaining to the size effect in bending was carried out using 2x6 Hem-Fir material. Three matched samples, each consisting of 116 pieces, were generated from a larger group of material. One sample was tested to destruction using a single load applied in the center. The other two were subjected to two concentrated loads with different spacing. The test span was the same for all three load configurations which are shown in Fig. 6. It will be noted that the volume subjected to high stresses varies for the different load configurations.

The strength distributions found are shown in Fig. 7 and, as expected, the concentrated load resulted in higher strength values. This experiment shows quite clearly that the stressed volume is important in determining the strength properties.

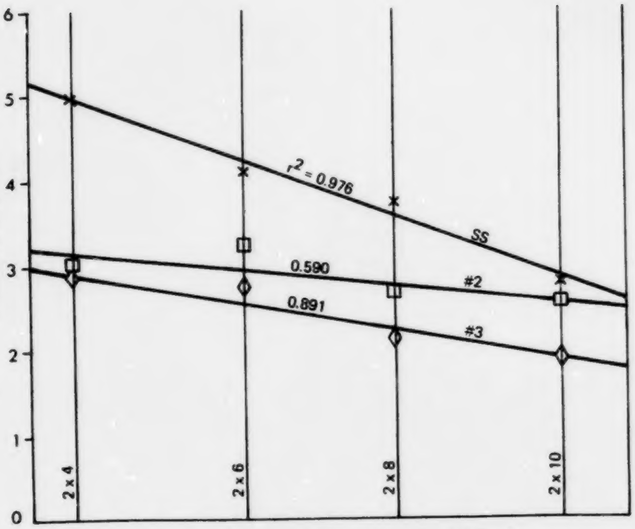

Figure 1: Size Effect, Bending. Hem-Fir All Grades

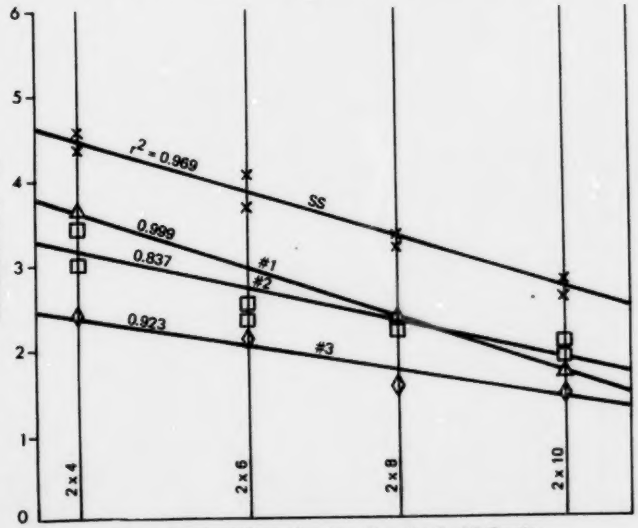

Figure 2: Size Effect, Bending. Douglas-fir All Grades

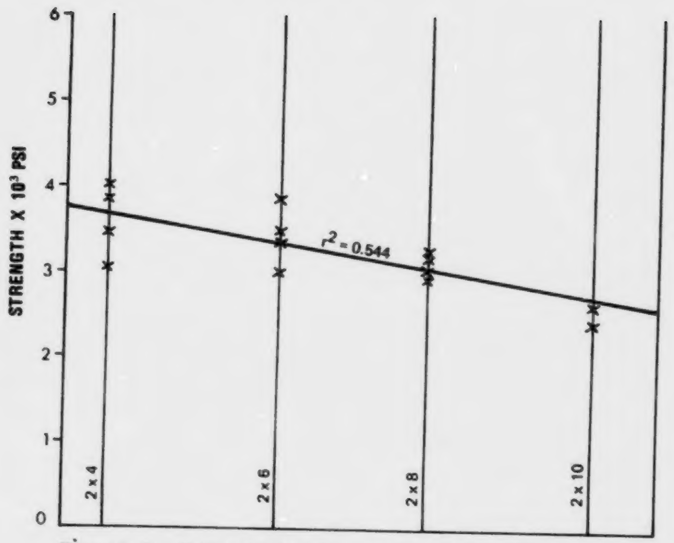

Figure 3: Size Effect, Bending. Spruce-Pine-Fir Select Structural Grade

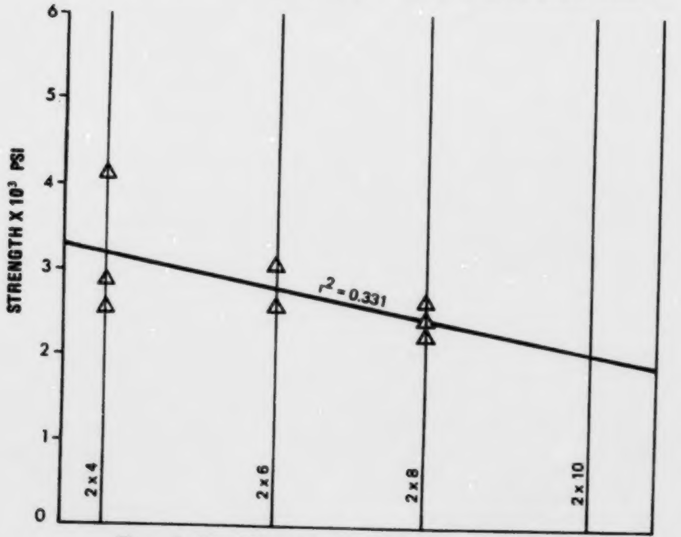

Figure 4: Size Effect, Bending. Spruce-Pine-Fir #1 Grade

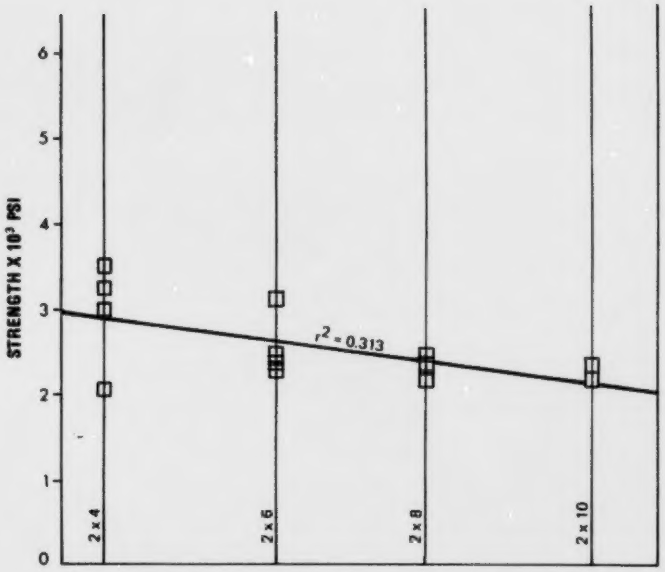

Figure 5: Size Effect, Bending. Spruce-Pine-Fir #2 Grade

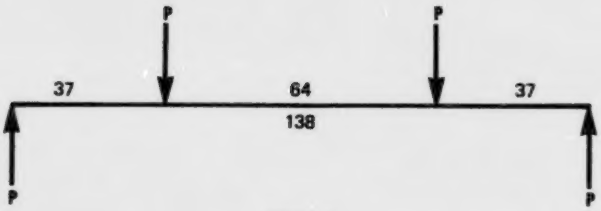
P
P
37
64
37
138
P
P

GROUP A

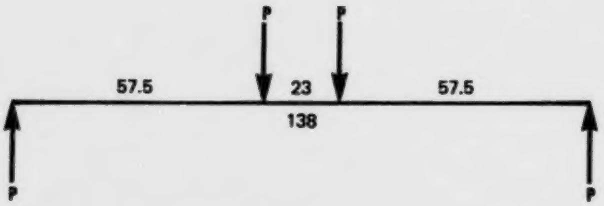
P
P
57.5
23
57.5
138
P
P

GROUP B

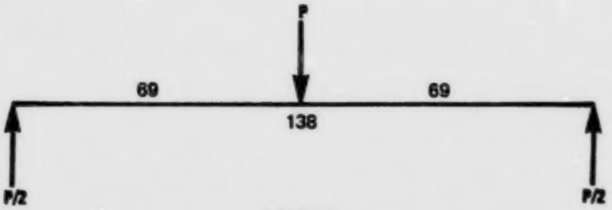
P
69
69
138
P/2
P/2

GROUP C

Figure 6: Dimensions For Tests

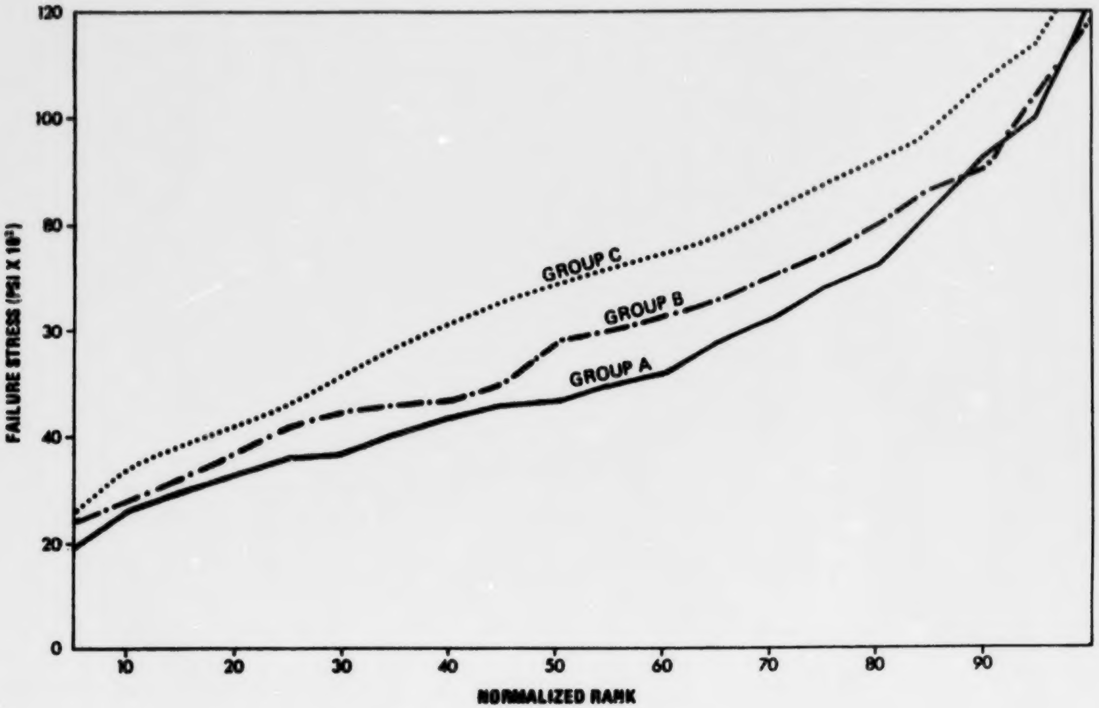

Figure 7: Failure stress vs. Normalized Rank

# TIME-STRENGTH RELATIONSHIP FOR LUMBER

By

**Borg Madsen**

---

Department of Civil Engineering, University of British Columbia, Vancouver, B.C.

The present concept of duration of load, which is based on testing of small clear specimens, greatly influences the determination of allowable stresses because a factor of 0.6 is used to reduce short-term test results to the 10-year-loading period used as the base for allowable stresses.

However, it is questionable if one can use tests with small clear specimens to predict the behaviour of lumber. For one thing, the strength of small clear specimens is in the range of 10,000 - 14,000 psi, while the low end of the strength distribution for lumber is about 2,000 psi. Also the failure mode of small clear specimens is commonly compression, while tension is the predominate failure mode for commercial lumber.

In order to investigate this question, a test program was developed in which it was envisaged that about 4,000 specimens would be subjected to a constant load for varying periods of time.

The present duration-of-load concept is depicted in Fig. 1. Here the strength at one minute has been shown as 100% and it can be seen that 80% of the total anticipated strength loss takes place in the first two months of the loading period. Therefore, tests with commercial material lasting for that length of time would be useful to verify the duration-of-load concept.

### Materials

It was not possible to use the matched-specimen technique used for small clear specimens in conjunction with commercial lumber. Instead, a matched-sample approach was developed. The idea was to divide a large shipment of material into samples which have similar strength distributions using modulus of elasticity and knot sizes as an indicator of strength. This method is described in detail in (1).

Due to the inherent variability of the material it was, through a computer analysis, found necessary to have a sample size of at least 80 specimens for each test. Kiln-dried Douglas-fir 2 x 4-inch x 12-foot long lumber of "No. 2 & Better" grade was used.

### Testing Method

Due to space constraints, it was necessary to use a loading frame as shown in Fig. 2. A steel tube equipped with cross beams was attached to the floor in an upright position. Two test specimens were placed in the frame and a pulley system applied a dead load to the specimen at the third points.

### Selection of Load Levels

Three groups of material were used to assess the strength distribution under short-term loading. The 240 pieces were tested in an Olson testing machine using a loading rate which would cause failure after about one minute.

The test results were ranked as shown in Fig. 3 and four load levels selected as 71% of the 5th, 10th, 25th and 50th percentile levels, respectively, were established. The number 71% was selected since it was the anticipated strength after 10,000 minutes, see Fig. 1.

### Testing

Each group was then placed in turn in the test frame and loaded to its designated load level and left until the designated time period had elapsed. The number of boards which broke while the load was being applied was recorded (B.O.L.) and the time to failure was observed for any of the pieces which broke during the test period. The boards were unloaded, after the designated time period had elapsed, and a week thereafter the surviving boards were broken in the Olson machine using the previously mentioned loading rate.

### Results

An example of the test results is shown in Fig. 4. Here the abscissa is the log of time and times to failure are indicated with solid circles. The figure shows that five tests were conducted at 1,070 psi, one lasting seven hours, two seven days, one 70 days and one test longer than one year. This latter test was conducted slightly differently and is described later.

The strength distribution of the two tests lasting seven days is shown in Fig. 5. The dotted line shows the strength distribution of the control, while the solid line represents the distribution of the test. The load increments used in reading the desired load level is shown and it can be seen that about 15% of the sample reached the desired load level. Twenty-eight percent of the pieces broke while this load was being applied. It should be noticed that the strength distribution of the surviving boards coincides very well with the control sample, indicating that the short-term strength of the surviving boards had not been changed.

The overall results are shown in Fig. 6 where the abscissa is log time in hours and the ordinate is the estimated strength ratio. The strength ratio is the applied stress divided by the estimated short-term strength of the board (1). Also shown is the Madison curve with the diamond shapes indicating the points used in design (two months, seven days, etc.). A solid line has been drawn through all the points indicating the general trend. The large scatter in the data is to some extent caused by the different load levels used and the trend line has been redrawn in Fig. 7, where a trend line has been produced for each load level. The number of test specimens used for establishing the curves are indicated on top of the figure. The high number for the shorter times are, of course, caused by the fact that a test lasting for 70 days automatically yields information for seven days. Some very important observations should be made here.

Firstly, the loss of strength is dependent on load level. This may not be surprising, but it is something which has not been recognized before, since we have assumed that the behaviour was the same regardless of stress. This trend of greater strength loss with greater stress is interesting and it could be visualized that the Madison curve, which has been developed with strong material (12,000 psi), represents the upper end of the progression. As mentioned earlier, the weak material (1,070 psi) is governed by tension failures and the change in behaviour as function of stress could possibly be caused by a change from predominately tension failures to predominately compression failures.

Secondly, it should be observed that the slope of the trend lines at short times is almost flat, while the Madison curve shows the relative increase in strength for shorter load periods. This is very important because the Madison curve has led to a large increase for impact loads and this cannot be justified by our test results. A secondary experiment dealing with rate of loading, described in (1), confirmed this finding.

Thirdly, it should be noted that the trend lines are substantially above the Madison curve, indicating that our present concept is very conservative for periods up to one year, but it cannot, from this experiment, be concluded that the same is the case for longer periods such as 10 years.

## Long-Term Test

As mentioned, the tests lasting longer than one year were carried out differently from the rest. A special test frame containing about 180 specimens was built in a building 20 miles from the university.

The specimens were loaded as shown in Fig. 8, using a pulley system which would load nine specimens simultaneously. An end view of the overall setup is shown in Fig. 9. The test has now been running for 3 1/2 years and the results are shown in Fig. 10.

The data is similar to what is reported above except it would appear that the slope, which is increasing until about six months, now diminishes and would appear to be asymptotic to a stress level of about 50%.

## Creep

Even though creep information was not part of the objective of this investigation, some time deformations were obtained in this latter test. Since the whole setup was very compact, it was difficult to get very accurate deformation readings, but it is thought that the information presented is adequate for engineering purposes.

Fig. 11 shows average deformation of about 10 boards for each stress level as function of time. Again a logarithmic scale is used. The same information is presented in Fig. 12 where the deformation at time t is divided by the initial elastic deformation. The deformation after 3 1/2 years is about 1.6 times the initial deformation regardless of load level.

## Conclusions

The presently held concept of duration of load as expressed by the Madison curve cannot be confirmed.

The increase used for impact loading would appear to be unconservative and should not be permitted.

For loading periods up to one year the strength losses are less than presently allowed for.

The total deformation after 3 1/2 years amounts to 1.6 times the initial deflection.

## Reference

1. Madsen, B. and Barrett, J.D. 1976. Time-Strength Relationship for Lumber. Structural Research Series, Report No. 13, University of British Columbia, Department of Civil Engineering, Vancouver.

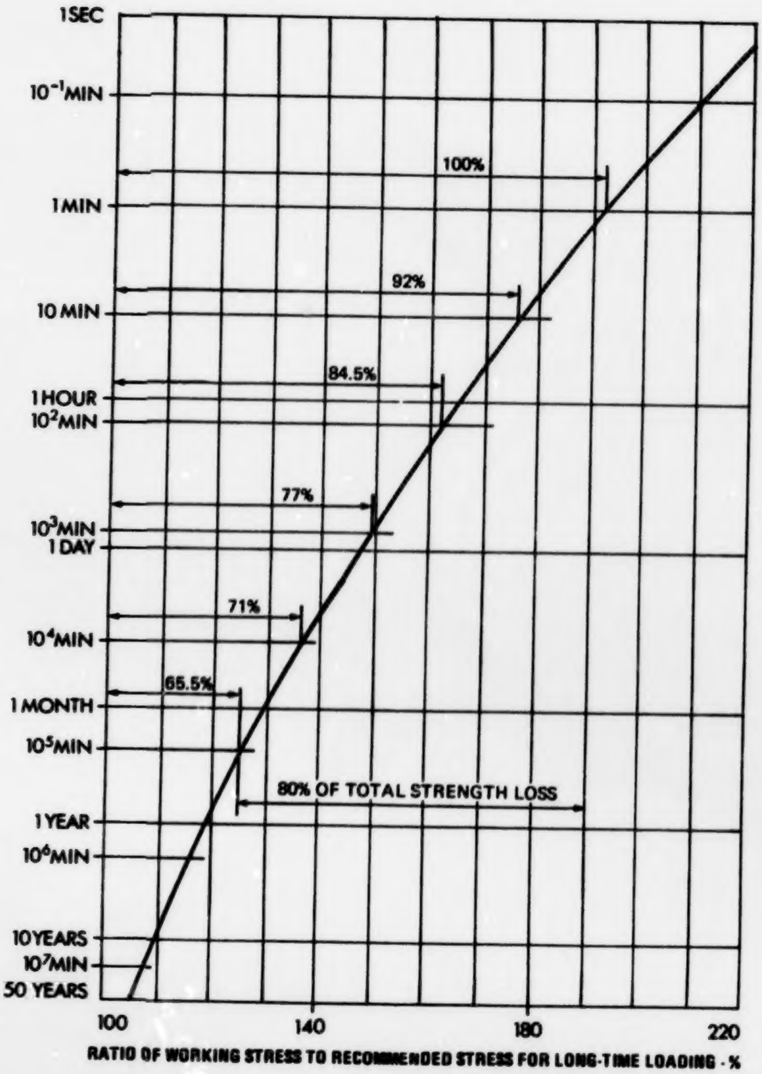

Fig. 1. Duration of maximum load.

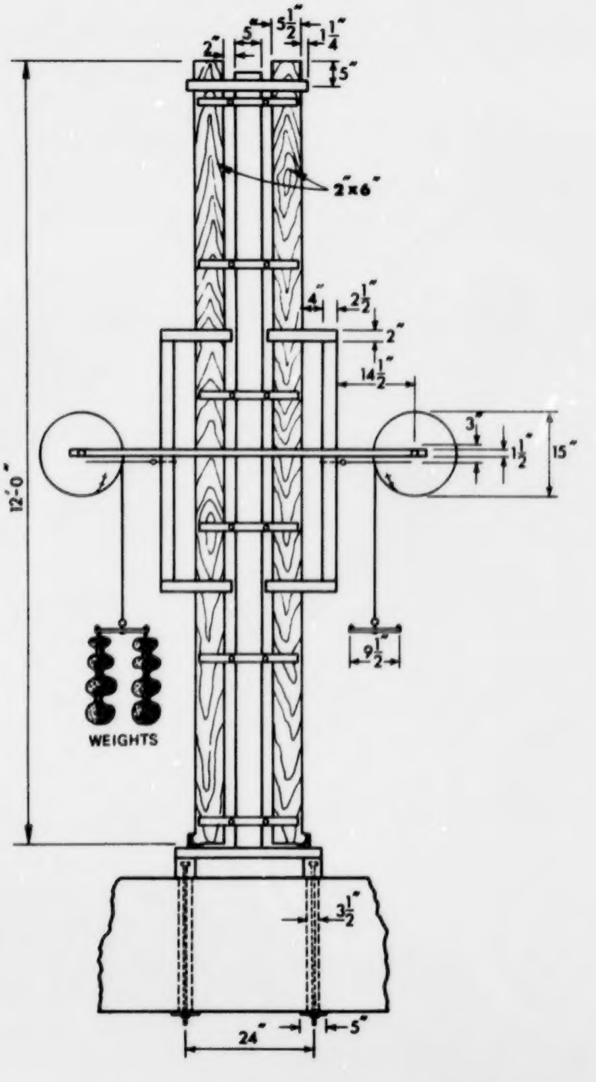
2"
5
5½"
1¼"
5"
2"x6"
4"
2½"
2"
14½"
3"
1½"
15"
12'-0"
9½"
WEIGHTS
3½"
24"
5"

Fig. 2. Test setup for constant stress 2" x 6" x 12' bending.

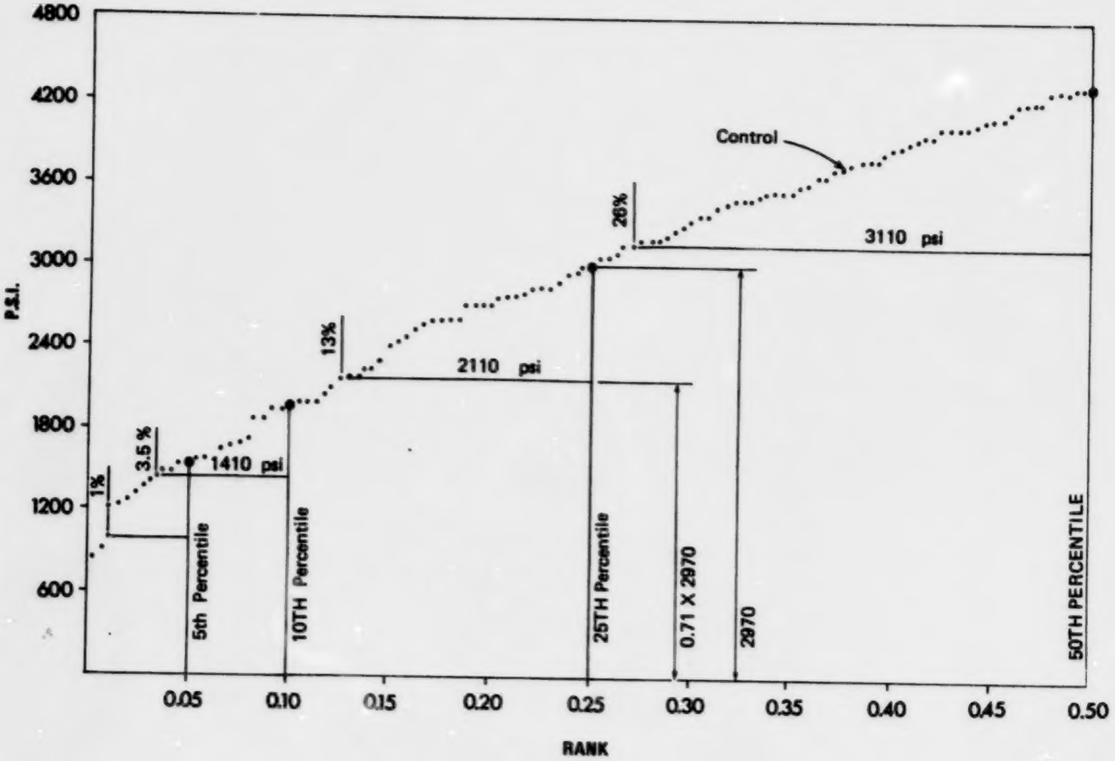

Fig. 3. Selection of stress levels

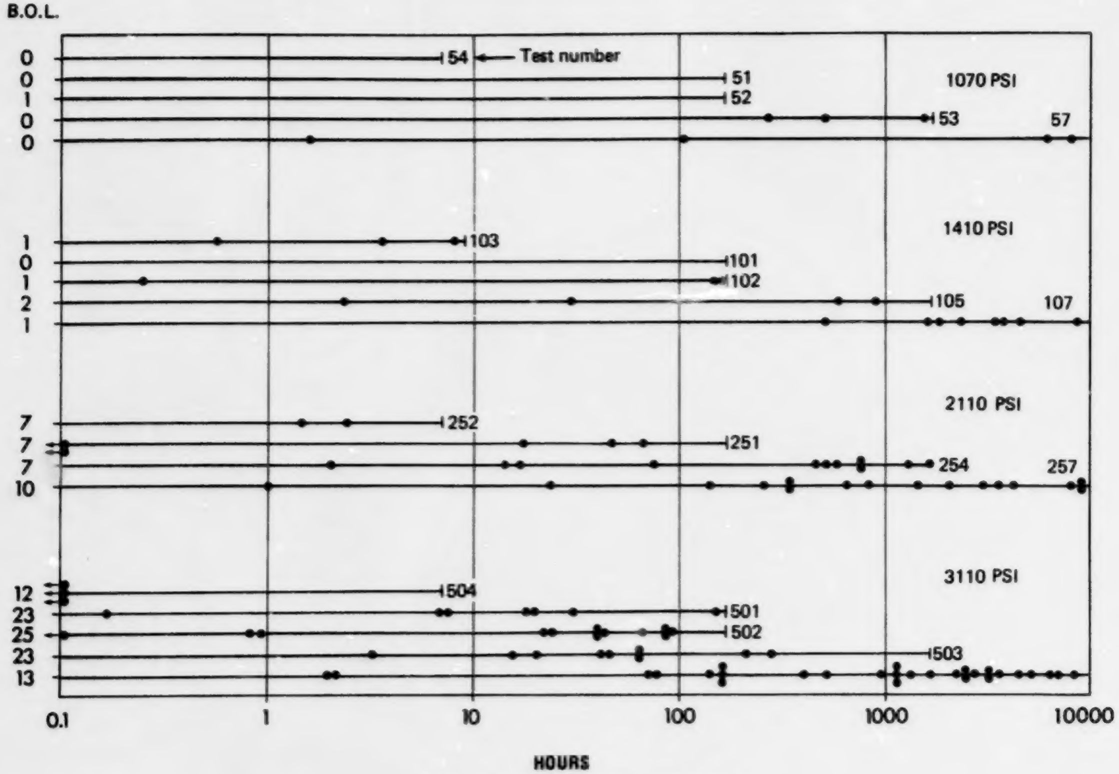

Fig. 4. Time to failure -- population I.

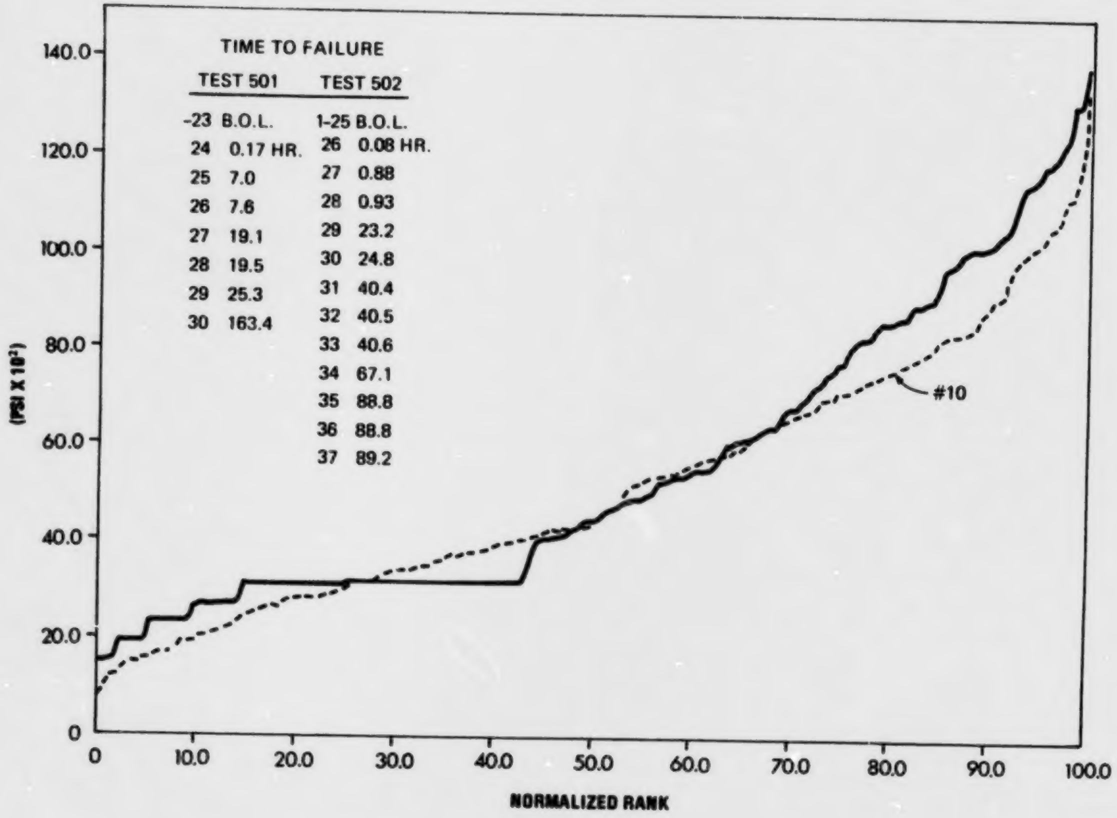

Fig. 5. Example of ranked presentation.

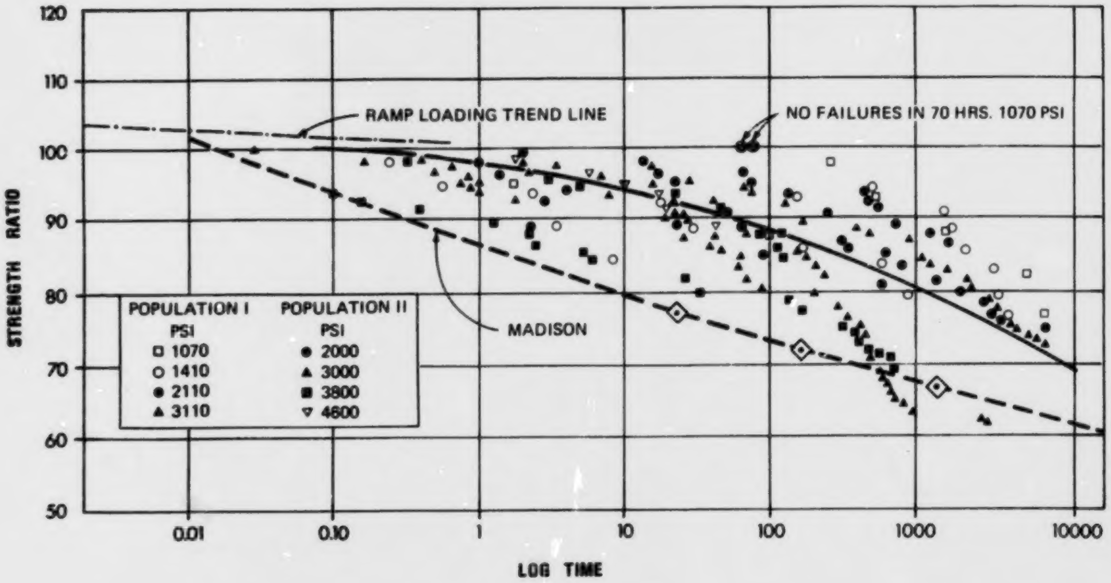

Fig. 6. Overall view of strength ratios.

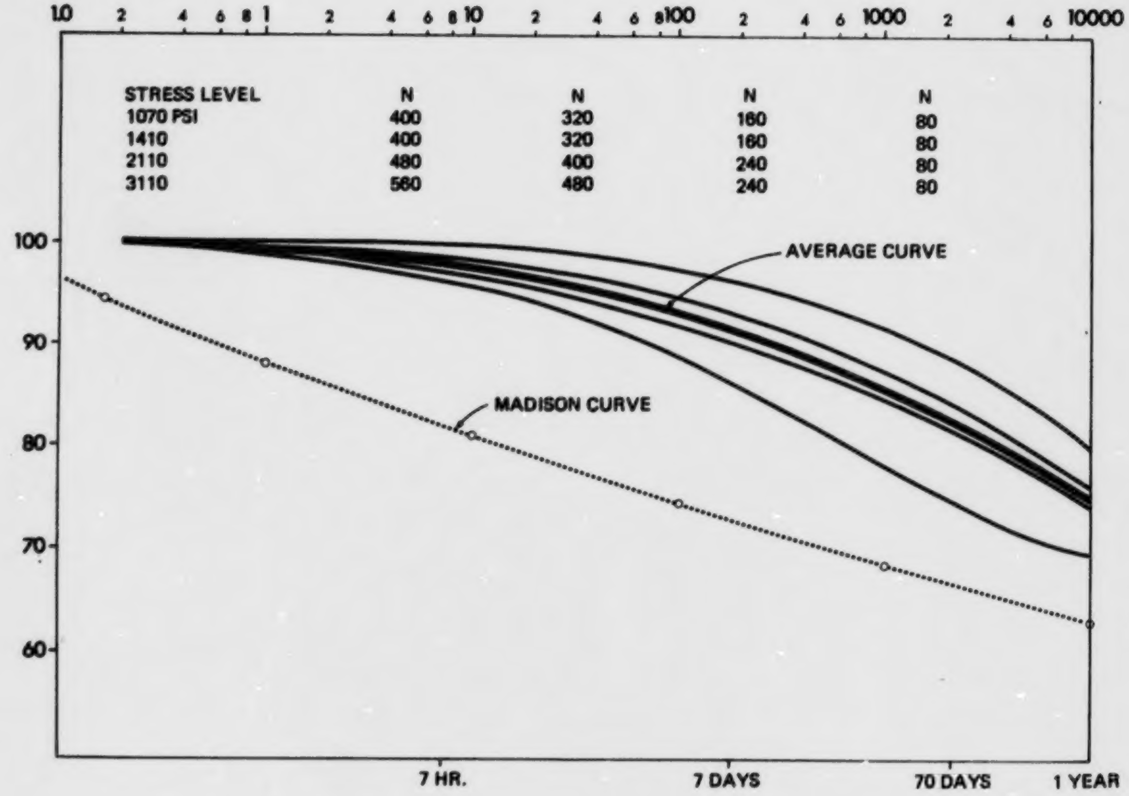

Fig. 7. Composite curves for $F_{time}$'

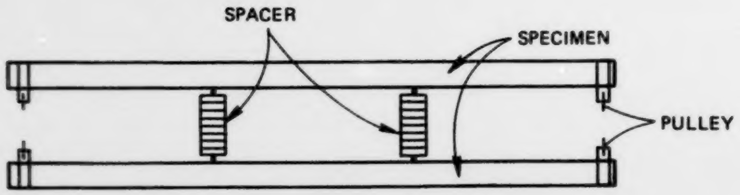
SPACER
SPECIMEN
PULLEY

**SIDE VIEW OF TEST SET-UP**

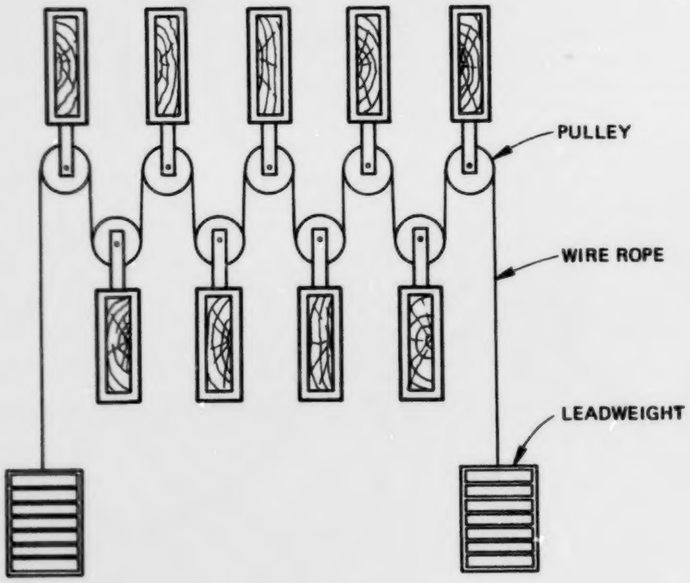
PULLEY
WIRE ROPE
LEADWEIGHT

**END VIEW**

Fig. 8. Test setup for Surrey test.

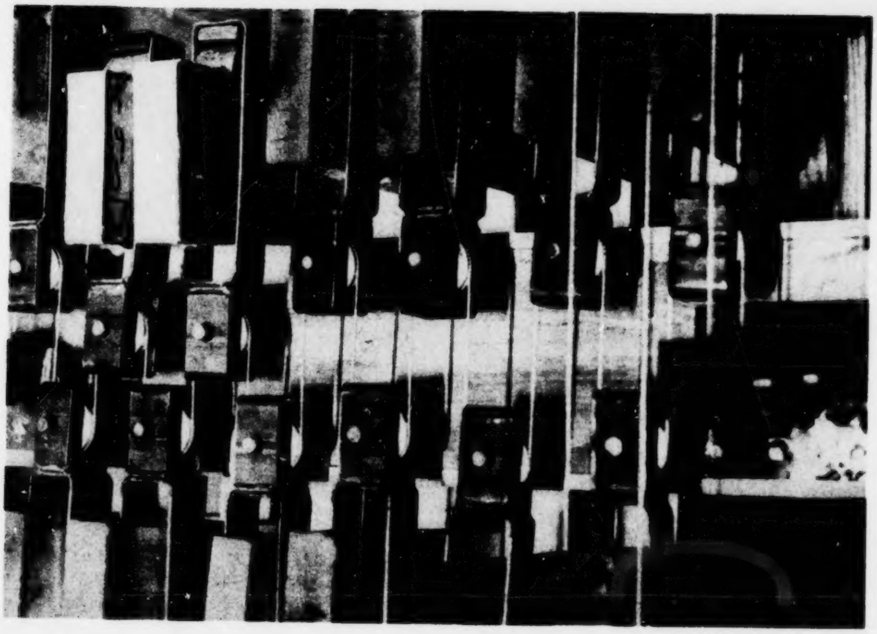

Fig. 9. Test setup for Surrey test.

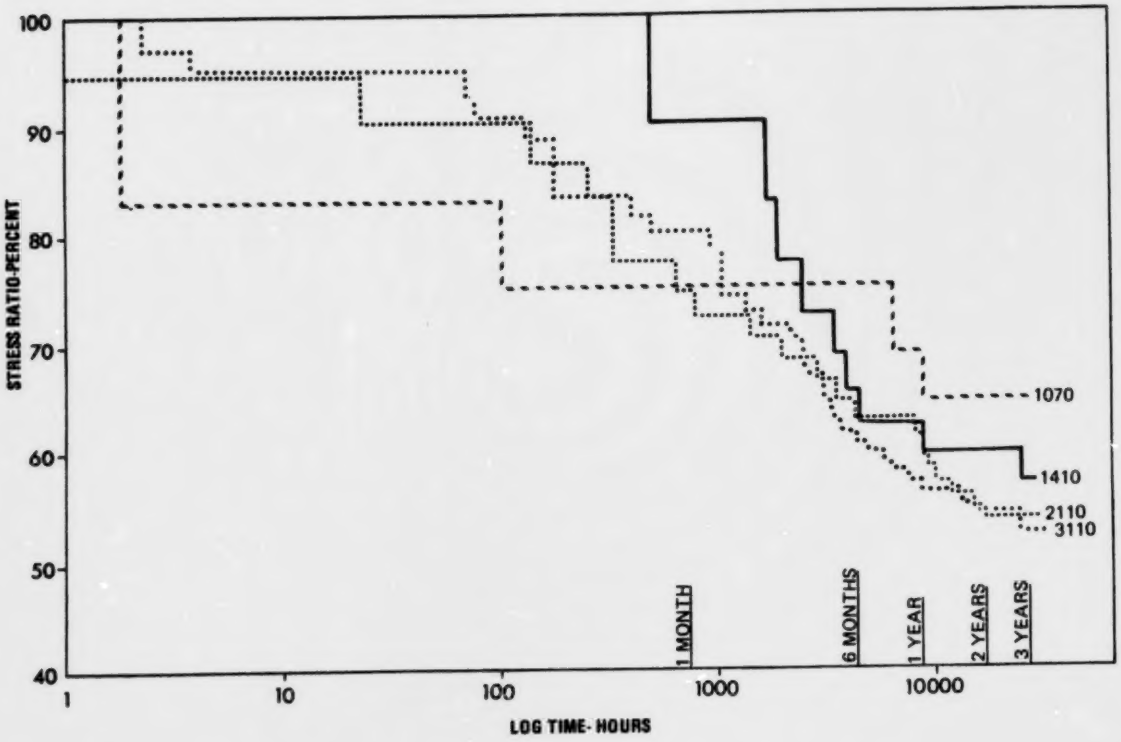

Fig. 10. Long-term results.

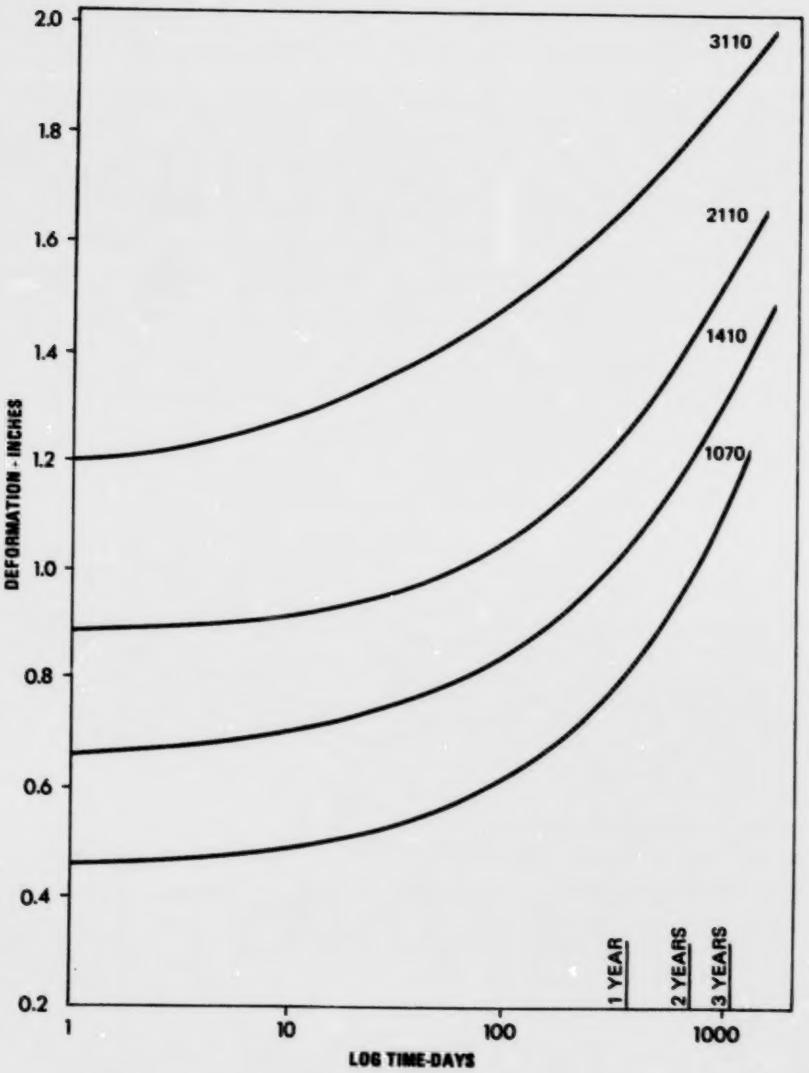

Fig. 11. Creep deformation.

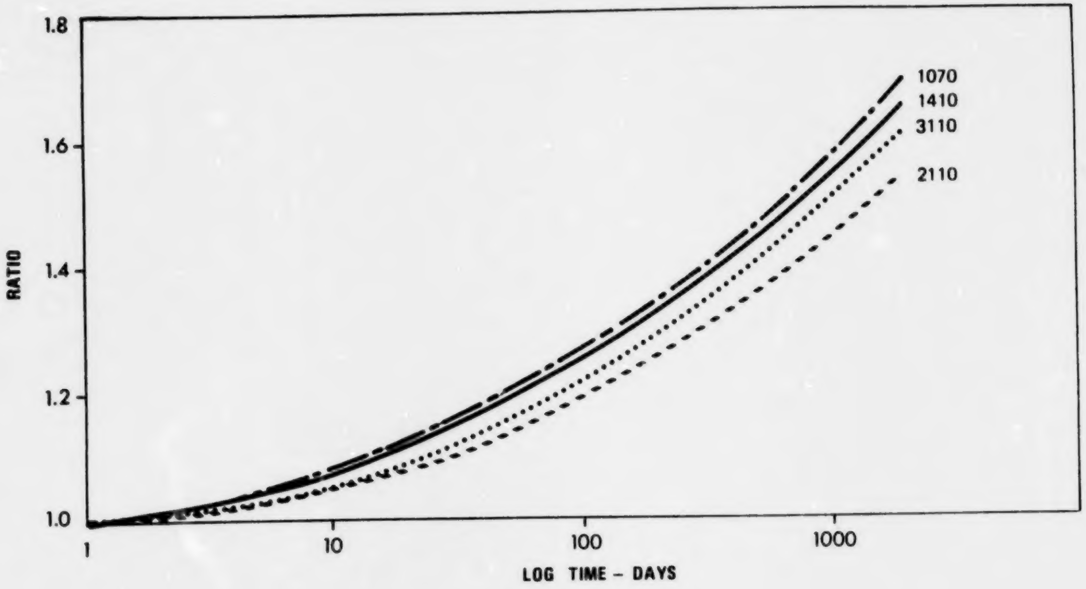

Fig. 12. $\frac{\text{Creep deformation}}{\text{Initial deformation}}$ vs. time

# CLIMATIC STRESSES OF WOODEN CONSTRUCTION ELEMENTS

By

Ulrich A. Meierhofer

---

Wood Section, Swiss Federal Laboratory for Testing Materials and Research (EMPA), Dübendorf.

## INTRODUCTION

Great efforts have been made to investigate the mechanical properties of wood and the behaviour of timber constructions (and structural elements) under mechanical stress. When a timber construction is being designed, most attention is paid to the calculation of the forces and stresses, while the climatic effects are usually considered to be of less importance.

On the other hand, a survey of the construction damages and defects, made by the Wood Section of the EMPA, shows that at least three-quarters of all timber construction damages are related to climatic factors; i.e. in the first-line moisture induced processes. Other investigations lead to similar conclusions (Verall 1966). Of this investigated damage, a major part is caused by water, such as fungal attack, condensation phenomena, etc. Most of these damages and many other construction defects are in connection with the capability of wood to absorb and desorb water from the surrounding air, a process which is accompanied by the well-known swelling and shrinking of the wood. The possible defects related to these processes range from deformation (bowing, warping, etc.) to the forming of checks and opening of joints, to the buildup of internal stresses, destruction of connections, etc.

For this reason it is important, for a defect-free timber construction, to consider the moisture conditions (MC) at the location of the individual wooden-construction element and to control carefully the MC of the applied timber. These requirements are, however, not very easy to fulfill. Firstly, the moisture and its variation at the place of application are often difficult to predict with any accuracy and, furthermore, the MC of the wood, which is influenced by many factors during fabrication and erection, is hard to keep under control.

The time-dependent moisture conditions in wooden-construction elements have occasionally been the subject of research work (Staudacher 1936; Trendelenburg 1939; Kollmann, Schneider and Serrand 1966; Tibbetts and Robson 1971; etc.). Mostly, however, only the average MCs have been recorded at relatively large intervals. Also, the moisture values found occasionally in standards, building codes, etc., are mostly not very specific; sometimes they are even to be doubted.

Considering these occurrences, the Wood Section of the EMPA is performing various investigations to evaluate, under working conditions, the physical behaviour of wooden-construction elements under the influence of moisture. Among other investigations, the behaviour of glued-laminated beams placed in an open shelter has been measured and recorded during a period of one year. The following report describes these tests and summarizes the principal results of the measurements.

## CLIMATIC STRAIN OF GLULAM BEAMS

Glulam beams find for various reasons increased application in construction. Architects appreciate the many possibilities provided by this versatile construction system. Unfortunately, they sometimes disregard that this construction system also has its limits and inappropriate applications cause consequent defects or damages (Figure 1).

Most of these defects could easily be avoided by taking into account the climatic stresses at the place of application. Preliminary results of presently running investigations of directly weathered glulam beams show a predominance of solar radiation as climatic strain.

In an open shelter, the main factors of the climatic strain are variations of relative humidity (RH) and temperature of the surrounding air, which cause the phenomena described in the first paragraphs.

One of the big advantages of laminated timber compared with solid wood is the possibility of an easier and better seasoning of the relatively thin lamellae and the homogenizing effect of mixing the lamellae. This refers, not only to irregularities in the wood structure (knots, slope or grain, variation of density, etc.), but also to the angle of annual rings within the individual lamellae. Due to the shrinking anisotropy of the wood, this latter factor may considerably influence the cracking tendency. However, the angle of the annual rings is generally disregarded in the workshop out of operating considerations.

Laminated timber allows the assemblage of cross sections of considerable size. Large wooden cross sections are, however, far more susceptible to changes in the surrounding climate than smaller ones; small cross sections adapt relatively quickly to climate changes; i.e. to changes in the relative humidity. Big wooden cross sections – laminated timber as well as solid wood – however, show a considerable inertia in this regard. This MC may change rapidly (minutes, hours) only in the zones close to the surface. The MC of the central part of the cross section remains at the same time practically unchanged (Figure 5); i.e. it adapts to the variation in moisture only within longer periods (weeks, months).

This phenomenon may be observed with wood as well as with other construction materials. In contrast to other construction materials, the change of the MC of wood is connected with considerable shrinking or swelling or, if inhibited, with the buildup of internal forces. This happens when the surface of a large timber element changes in MC faster than the internal zones. If the moisture gradient is directed from the outside inwards – i.e. when the surface zones are under compressive stress – no defects are to be expected. A gradient in the opposite direction, however, leads to tensile stresses at the surface and, because of the low resistance of wood in tension perpendicular to the grain, to the formation of checks. Joints may also open in the glueline of laminated timber.

The above-mentioned phenomena are of high complexity due to the number of influencing factors and their dynamic and statistical character, and various methods have been tried for their investigation. Thus, Schniewing (1963) investigated the check formation by photoelastic models followed by an anatomical interpretation. Recently, Möhler and Steck tried to comprehend the phenomena by calculations of the elastic behaviour of the wood. Based on a measured MC distribution, with a difference of only 4% between the surface and the center of glulam beams of 16 x 45 cm cross section, they calculated a maximum tensile stress at the surface of 1.2 N/mm$^2$. This value considerably exceeded the simultaneously evaluated 5% exclusion limit of the perpendicular to the grain strength. For a similar specimen with some surface treatment, on the other hand, a maximum tensile stress of only 0.6 N/mm$^2$, approx. the 1% exclusion limit of the tensile strength, was calculated.

As the stress relaxations have been disregarded in these calculations, a comparison with working conditions is difficult. The obvious impossibility of matching the complexity of the natural conditions with physical or mathematical models leads to the preference of a phenomenalogical test method for the described investigations.

## EXPERIMENTAL DATA

Three identical glulam beams of European spruce (*Picea abies* [L] Karst.) were used for the investigation. The cross section of approx. 170 x 350 mm was composed of 25-mm thick lamellae which were glued with urea-formaldehyde resin.

The principal test beam was equipped with various transducers, as shown in Figure 2, at both ends and at the center of the beam measuring continously the temperature, relative humidities (RH) and linear expansion. In addition, the RH and the temperature of the surrounding air were recorded. In the middle of the beam, the measurements were made at three different depths: 10 mm, 40 mm and 85 mm (i.e. at the center). To study the influence, one of the ends was protected with a thin water-repellent coating (approx. 150 g/m$^2$). The paint had a solids content of approx. 25% (mainly alkyd resin) and an admixture of 2% paraffin.

The second beam was weighed periodically to check the total amount of adsorbed (and desorbed) water. The third beam was loaded flatwise, as shown in Figure 3, to a maximum bending stress of 7.2 N/mm$^2$ and the deflection (creep) of the central part of the beam, with constant maximum stress, was continuously recorded.

The measurement of temperatures was performed with NiCr/Ni thermocouples and a reference temperature of 0°C (ice water).

Inductive linear-displacement transducers were applied to register the linear expansions, as well as the deflection changes of the "creep beam".

The continuous measurement of the MC at a specific location of a wooden element is difficult to realize. It was, therefore, decided to measure the RH and the temperature of the air in boreholes of the test beam and to calculate the MC based on this data with the formula described by Simpson (1971). Commercial, slim transducers were available for the measurement of the RH.

Readings were taken at all measuring points on the test beam every eight minutes.

The primary measured values from the chart recorder had to run through various stages of data processing consecutively before reaching the final values.

The test beams were placed from September, 1975, to August, 1976, in a laterally open shelter at the site of the EMPA laboratory at Dübendorf, Switzerland. The beams were thus protected from precipitation as well as from direct sunchine, but exposed to the natural variation of temperature and RH of the air. It should be pointed out that this is a quite common type of exposure and climatic stress for constructive timber elements.

The beams had already been stored at the test place for many years and were thus adapted to the specific climate. The climate at Dübendorf may be considered more or less typical for central Europe.

Purely by chance, the weather in the test period included an extraordinarily dry period, specifically in June, 1976. This allowed us to study the (negative) effects of a pronounced drying-out period.

## TEST RESULTS

The principal test results are summarized in Figures 4 to 10. Figure 4 shows the variation of RH of the air, the main factor influencing the place and time-dependent MC of the wood. It should be noted that the short-period variation of the RH, mainly the daily variation, is not smaller than the long-period variation; i.e. the seasonal fluctuations.

Figure 5 shows the plot of the MC at the very center of the test beam and 10 mm under the surface. The damping effect of the increased depth – i.e. the reduction of the amplitude and a delay – is clearly visible. The slow adaption of the MC at the center, especially in the winter months, is remarkable. The average MC at the center during the measuring period was 13.7%, the maximum 15.5%, the minimum 12.0%. The corresponding values at 10 mm depth were 15.6%, 19.2% and 11.4%. During the measuring period, the center was thus, on the average, nearly 2% drier than the zones close to the surface. The maximum difference between the MC at the center (humid) and the surface (dry) was 2% at the beginning of July, 1976 (cracking).

Figure 6 compares the MC at the painted end and at the unprotected end of the beam. It is interesting to note that the damping effect of the (rather permeable) surface treatment is not very pronounced in the short-period fluctuations of the MC. The seasonal variations are, however, clearly influenced by the protective coating. Thus, the minimum reached at the unprotected end was 9.5%, i.e. 2% less than at the opposite end. The corresponding average MCs of the test period were 13.3% and 13.4%.

Similar to Figure 6, Figure 7 displays the effect of the surface treatment by means of the development of the linear expansion at both ends. The absolute amounts of the observed linear expansions (resp. retractions) are about $6.10^{-3}$ corresponding to a MC change of 3 to 4%. This is considerably less than the MC changes measured at the corresponding location (about 7%) and may be explained by internal stresses, the forming of checks within the measuring span (of 10-cm length).

It should be added that the correlation between the linear expansion and the MC is extremely bad, the correlation coefficients being generally less than 0.5.

Figure 8 demonstrates the cracks which occurred at the unprotected end of the test beam towards the end of the dry period; i.e. at the beginning of July, 1976. The unfavourable effect of the lamellae containing pith is easily recognized.

Figures 9 and 10 are detailed graphs of the temperature and the MC outside and the three measuring points at the center of the test beam on three consecutive days in June, 1976. It is evident that the damping effect is much more effective for moisture movements than for temperatures. Even at the surface measuring point (10 mm below the surface), the daily fluctuation of the MC in the wood is small (less than 1 percent) and the general level of humidity decreases very slowly, in spite of extreme dryness of the outside air.

The change in the deflection of the "creep beam" as a multiple of the initial value is shown in Figure 11. The beam was exposed to the same climatic fluctuations as the main test beam and the measurements confirm the results of earlier investigations (Meierhofer 1976), in particular in regard of the deflection during drying periods, followed by a partial recovery when the MC rises again. Figure 11 also demonstrates that the deflection/time curve may be reasonably well approximated by a power function, in our case:

$$\delta/\delta_{init} = (1/40.39)\ (t \exp 0.363)$$

where t = time in days

It has to be stressed again that the test (as opposed to most other investigations) represents normal working conditions and it is, therefore, interesting to see that the extrapolation of the indicated formula leads to an increase in the deflection of approx. 50% within 10 years and a doubling in approx. 100 years.

## ASSESSMENT OF THE RESULTS

Various conclusions may be drawn from the results of the weathering tests on glulam beams placed in an open shelter.

- A great number of very complex factors and interdependencies influence the temporal and spatial distributions of the MC. The MC therefore cannot be deducted from the course of the RH and temperature of the surrounding air, as had been done by Tsoumis (1964) based on the observations made with small specimens.
- Wooden-construction elements of larger cross section adapt their MC, as a whole, very slowly to the fluctuations in the climate in an open shelter. In the element central part, MC changes of any significance may only be observed during the lapse of a few months (seasonal changes). If the wood surface is unprotected, the zones close to the surface (mainly the first few mm of depth), however, follow the rapid changes of the RH of the air.
- The variation as well as the average MC is influenced by the distance to the timber surface; the greater the distance, the lower the MC and its variations.
- The occurring MC distributions – i.e. the steep non-linear moisture gradients, due to the shrinking and swelling of the wood – cause dynamic internal stresses, which may lead to the formation of checks during the drying stage (compression at the center, tensile stresses at the surface).
- Without special protective measures, even in an open shelter – i.e. protected from solar radiation – the formation of checks during the summer cannot be avoided.
- A surface treatment, even if relatively permeable, has a definite damping effect on the moisture exchanges (see also Böttcher 1977).
- For various types of constructions, it is important to take into account a linear expansion due to the annual shrinking and swelling cycles. For glulam beams of 16 to 20 cm thickness in the climatic conditions of central Europe, the dimensional variation to be considered should not be less than 1%.
- According to the magnitude of the observed long-term deflection, a consideration in many structural circumstances seems indispensable. For the time being, systematic investigations in this field are still lacking.

Even if the described investigations leave many questions unanswered, it shows the principal reasons for the formation of checks in glulam beams and the necessary measures to avoid them:

- careful selection of the raw material;
- uniform seasoning (preferably 2% less than the average MC in working conditions);
- control of the MC during the fabrication;
- application of a protective surface treatment in the workshop;
- reduction of the transport and erection time to a minimum (avoiding especially the storing of finished elements at a damp working site for long periods);
- careful usage of heaters and dehumidifiers (especially when drying out new buildings), etc.

It would appear useful to fix these precautions within the framework of rules or specifications for the timber trade, as has been done in Switzerland (EMPA 1978).

While the application of glulam beams in open shelters, with the necessary precautions, is certainly safe and durable, the direct exposure to the weather poses problems which are not yet solved. With suitable tests, similar to those performed and described in this report, the Wood Section of the EMPA is presently studying these problems.

## LITERATURE CITED

Böttcher, F. 1977. Schutz von Holzleimbindern gegen Feuchtigkeitsaufnahme während der Bauzeit (Protection of glulam beams against the adsorption of moisture during construction). Bauen mit Holz 79(6).

EMPA. 1978. Klimabeanspruchung von Brettschichtholz – Empfehlung für Schutzmassnahmen (Climatic stresses of glulam beams – recommendations for protective measures). EMPA und Schweiz Studiengruppe für Holzleimbau.

Kollmann, F., A. Schneider and W. Serrand. 1966. Untersuchungen über den Einfluss der Abmessungen und von Feuchteschutzbehandlungen von Holzteilen auf die Geschwindigkeit der Feuchteänderung im Konstantklima und auf Feuchtigkeitsschwankungen im natürlichen Wechselklima (Investigations of the influence of the size and protective coatings on the speed of moisture changes). Forschungsbericht des Landes Nordrhein-Westfalen Nr. 1647.

Meierhofer, U.A. 1976. Zeitäbhangige Verformungen von Holzbauteilen unter mechanischer und klimatischer Beanspruchung (Time-dependent deformations of timber elements subjected to mechanical and climatic stresses). Schweiz. Bauzeitung 94 (25): 348 – 351.

Schniewind, A.P. 1963. Mechanism of Check Formation. Forest Prod. J. 13(11): 475 – 480.

Simpson, W.T. 1971. Equilibrium Moisture Content Prediction for Wood. Forest Prod. J. 21(5): 48 – 49.

Staudacher, E. 1936. Der Baustoff Holz (The construction material timber). Thesis, Swiss Federal Institute of Technology, Zürich.

Tibbetts, D.C., and D.R. Robson. 1971. Moisture Content of Exposed Painted Wood Panels. Build. Res. Note No. 79, Can. Nat. Res. Council, Ottawa.

Trendelenburg, R. 1939. Das Holz als Rohstoff (Wood as raw material). Verlag J.F. Lehmanns, München.

Tsoumis, G. 1964. Estimated moisture content of air-dry wood exposed to the atmosphere under shelter, especially in Europe. Holzforschung 18: 76 – 81.

Verrall, A.F. 1966. Building decay associated with rain seepage. Forest Service, U.S. Dep. Agric., Tech. Bull. 1356.

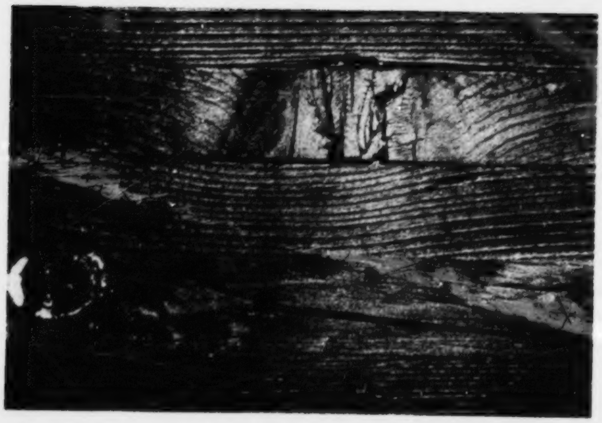

Figure 1. For architectural reasons, glulam beams often remain directly exposed to the weather. If such beams are not protected by an effective and carefully maintained surface treatment, the weathering causes in a short time serious checking of the beam. Above is a directly weathered glulam beam with insufficient maintenance after six years of exposure.

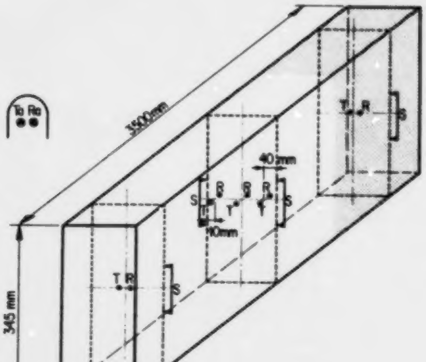

Figure 2. Location of the sensors on the test beam: T for temperature, R for relative humidity, and S for expansion; index "a" means open air. The shaded part represents the surface treatment (paint).

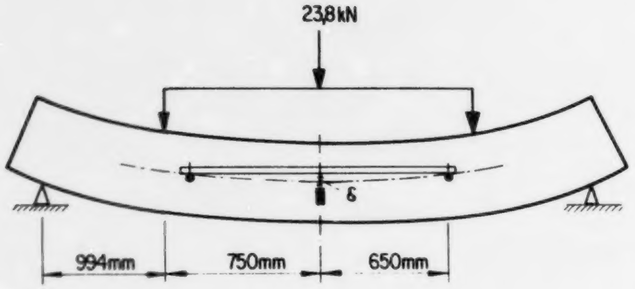

Figure 3. Setup of the "creep beam". Measurement of the deflection only in the central part of the beam with constant, maximum bending moment.

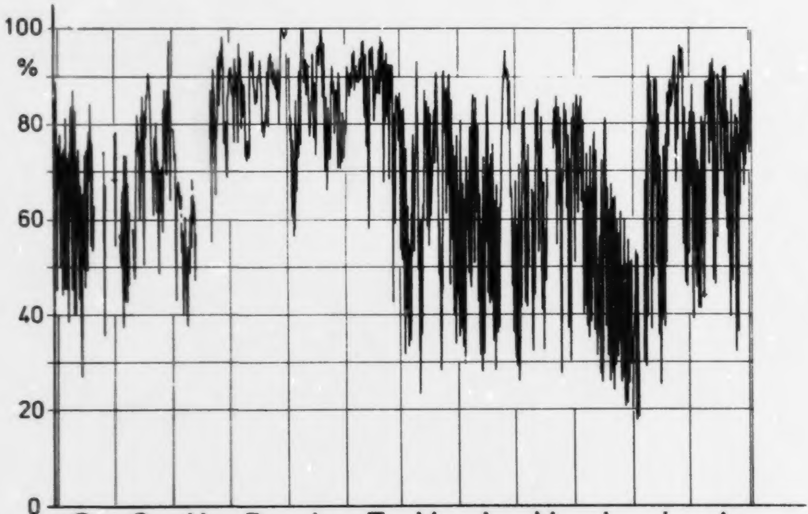

Figure 4. RH-time curve. The RH (%) of the surrounding air is the main factor influencing the climatic strain of timber-construction elements situated in open shelters.

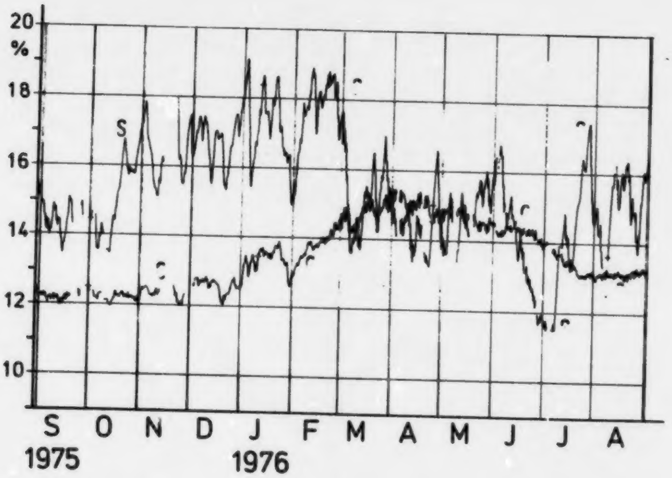

Figure 5. Moisture content(%)—time curves of the measuring points at the center of the test beam (C) and at 10 mm below the surface (S).

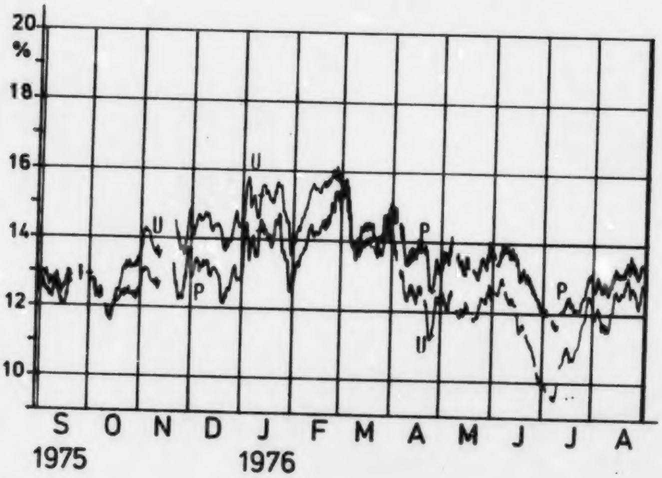

Figure 6. Moisture content(%)—time curves of the measuring points at the painted (P) and unpainted (U) ends of the test beam.

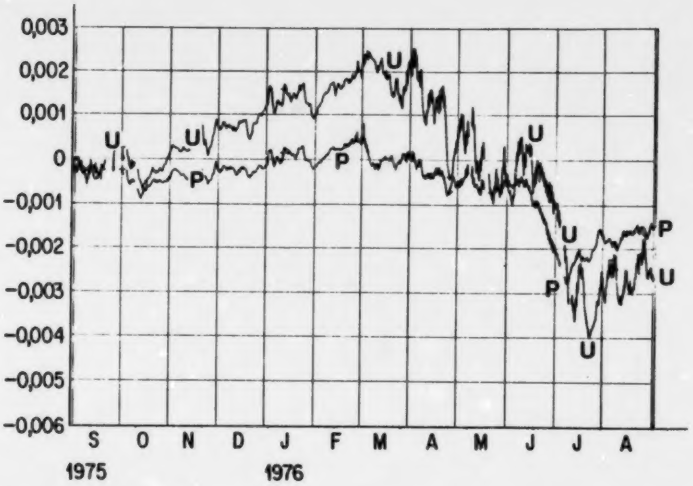

Figure 7. Expansion-time curves of the measuring points at the painted (P) and unpainted (U) ends of the test beam.

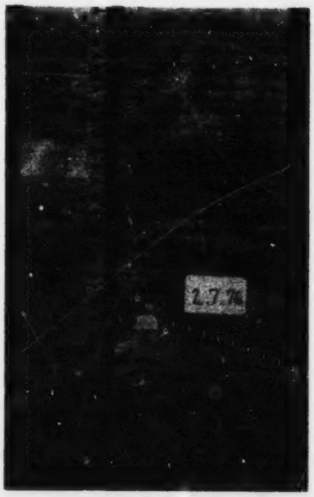

Figure 8. Checks at the unpainted end of the test beam after a pronounced drying period.

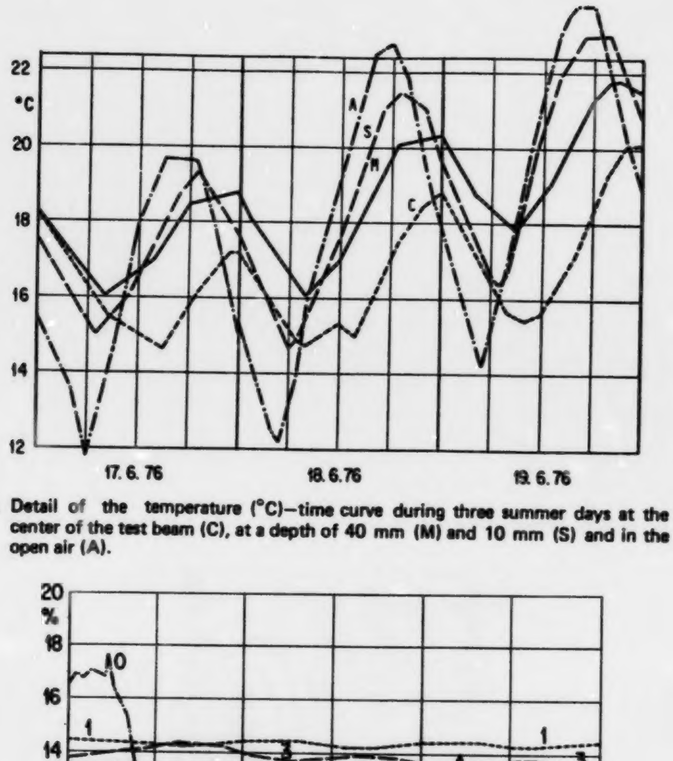

Figure 9. Detail of the temperature (°C)–time curve during three summer days at the center of the test beam (C), at a depth of 40 mm (M) and 10 mm (S) and in the open air (A).

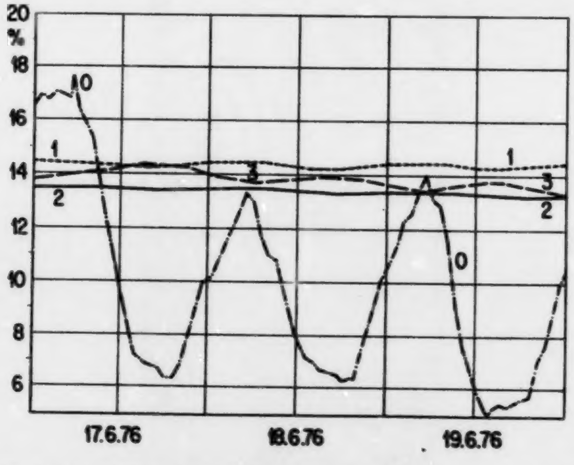

Figure 10. Detail of the relative humidity(%)– time curve during three summer days at the center of the test beam (C), at a depth of 40 mm (M) and of 10 mm (S), and in the open air (A).

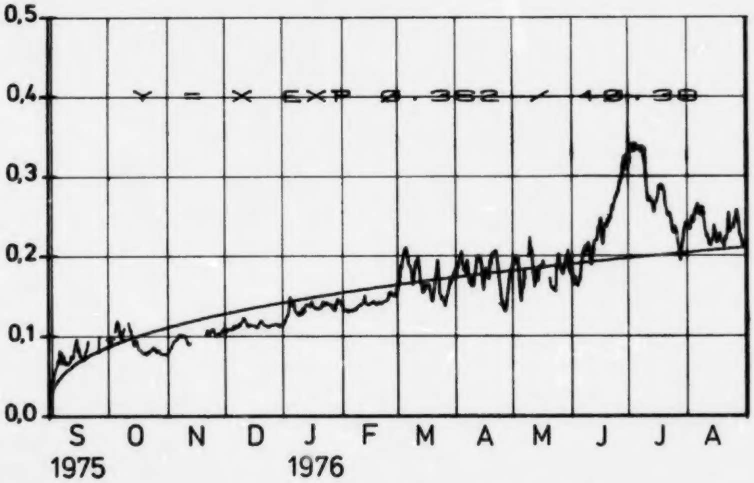

Figure 11. Deflection as a multiple of the initial deflection of the test beam according to Figure 2. The power function approximates the average deflection-time

# RATE OF LOADING AND DURATION OF LOAD TESTS ON DOUGLAS-FIR IN TENSION PERPENDICULAR TO THE GRAIN

By

**Sidney Mindess[1], Borg Madsen[1] & J.D. Barrett[2]**

---

[1] Department of Civil Engineering, University of British Columbia, Vancouver, B.C.

[2] Western Forest Products Laboratory, Forintek Canada Corp., Vancouver, B.C.

## ABSTRACT

Two series of tests were carried out on matched groups of specimens of Douglas-fir. The first series involved rate-of-loading tests in both direct tension and flexure. The second series consisted of duration-of-load (i.e., time to failure under constant load) tests on similar specimens. The results indicate the rate of loading has no effect on the apparent strength of wood. The current failure theories for wood suggest that, therefore, no duration-of-load effects should be observed. However, the second series of tests indicate that there is a definite effect due to a constant load; the time to failure decreases as the stress increases. This brings into question the application of the slow crack growth model for prediction of time to failure for wood.

## INTRODUCTION

It has long been known that the strength of wood depends upon the load history. A number of experimental studies have shown that the strength of wood increases as the stress rate increases (1-4) and that the time to failure at constant stress decreases with increasing stress levels (5). It has recently been suggested (4) that the dependence of the strength of wood upon the loading history is a consequence of subcritical crack growth; that is, the slow growth of cracks that are too small to cause failure instantaneously under the applied stress. Such a process would not only explain delayed failure, but would also lead to a dependence of the failure stress on the loading rate since, in specimens loaded slowly, more time is available for subcritical crack growth than in specimens loaded rapidly.

It has been shown (6) that the relationship between the velocity of cracks and stress for Douglas-fir stressed in tension perpendicular to the grain fits the expression:

$$\log V = n \log K_I + \log A \qquad (1)$$

where V is the crack velocity, $K_I$ the mode I (crack-opening mode) stress intensity, and n and log A are constants. On a log-log graph, n is then the slope of a V - $K_I$ plot.

However, it has been shown by Evans (7) and by Wiederhorn (8) that equation (1) can be integrated to give expressions for the effect of strain rate upon strength, and also the effect of constant load upon strength. Thus, three independent methods of evaluating the slope of a log V - log $K_I$ plot are available, as shown in Figure 1:

1. direct observation of controlled crack growth in stressed plates;
2. in constant load tests, by plotting log T versus log $\sigma_a$, where T and $\sigma_a$ are the time to failure and the applied stress, respectively; the slope of this plot is -1/n;
3. in specimens loaded at a constant rate of strain to failure, the logarithm of fracture strength, $\sigma_r$, plotted against the logarithm of strain rate, $\dot{\epsilon}$, is a straight line with a slope of 1/(n + 1).

The agreement between values of n determined by the three methods is a test of the assumption that delayed failure and the stress-rate dependence of strength are manifestations of subcritical crack growth. In previous work (4,6), it was shown that the first and third methods gave values of n that were within 6 percent of each other. However, these results were not in agreement with the results previously reported in the literature of conventional constant load tests.

It was the purpose of the present study to try to compare the results of the second and third methods (constant load and rate of loading) directly, using matched groups of specimens of Douglas-fir in both tension and flexure.

### Experimental Procedure

The test specimens consisted of glued-laminated blocks as shown in Figure 2. The cross sections of both the tension and flexure specimens were the same, 4.0 inches deep by 1.4 inches wide. The flexural tests (third-point loading) were on a span length of 22.5 inches; the tension specimens were 22.0

inches long. For both types of test, the specimen configurations were such that failure occurred essentially in tension perpendicular to the grain.

The types of tests carried out are summarized in Table 1. As may be seen, three loading rates were used in the direct tension tests and four in the flexural tests. For the constant load tests, three different stress levels were used in tension and four in flexure. In each test series, 39 specimens were used for a total of 546 specimens. For the constant load tests, the loading apparatus for tension is shown in Figure 3 and the loading arrangement for flexure is shown in Figure 4. After about one year, the remaining unfailed specimens were removed from the apparatus and tested to failure in conventional short-term tests.

### Experimental Results

For the rate-of-loading tests, the average stresses at failure, the times to failure and their standard deviations are given in Table 2. The coefficients of variation were higher for the direct tension tests than for the flexural tests, probably due to the experimental difficulties inherent in trying to carry out pure tension tests. However, as may be seen, there is no apparent effect of loading rate on ultimate strength in either tension or flexure. This is also shown in Figure 5 and 6, which show the ranked data for these tests.

For the constant load tests, the percentage surviving versus load level are given in Figure 7 for tension and in Figure 8 for flexure. This data may also be presented by the conventional stress-ratio versus duration-of-load curves, Figures 9 and 10, for tension and flexure, respectively. The stress ratios were obtained by comparing the applied stresses on the constant load specimens to the ranked short-term strength curves at the same normalized rank (Figures 5 and 6).

The number of specimens in each group that were broken on loading and the number surviving at the end of about one year are given in Table 3. Figures 11 and 12 show the ranked data for the surviving constant load specimens, tested to failure at the end of the loading period. It may be seen that these are similar to the average curves of Figures 5 and 6. Thus, a substantial time under load appears to have little effect on the short-term strength distribution of specimens that do not fail during the test.

It should also be noted here that, during the constant load tests, it was not possible to keep the environment in the test area completely constant. No doubt, some temperature and relative humidity fluctuations did take place. This is indicated by the typical deflection-time curve shown in Figure 13 for one of the tensile specimens. The curve should be smooth; the scatter in the data is probably due to changes in the relative humidity over the period of the test. It is assumed that these fluctuations did not have a significant effect on the test data.

### Discussion of Results

As we have stated earlier, one of the basic assumptions of fracture mechanics is that time-dependent failure is governed by the kinetics of crack growth. This would imply that, as there is no apparent effect of the rate of loading upon strength, then there also should be no apparent effect of constant load upon strength. That is, if the rate-of-loading data plotted according to Figure 1(b) has very little slope, then the constant load data plotted according to Figure 1(c) should also have very little slope. However, an examination of the present data reveals that this is not the case. A plot of the rate-of-loading data (Table 2) does have almost a zero slope; the data of Figures 9 and 10, even if redrawn as log-log plots, would clearly have a considerable slope.

In developing the slow-crack-growth model, it was envisaged that the model could be used to predict the effects of an arbitrary load history, given a knowledge of the parameters A and n of equation {1}. However, contrary to the fracture model predictions, the rate of loading and constant load tests do not appear to give results which can be considered to confirm the model that was assumed. These findings are also not in agreement with the study cited above (4), which indicated that linear-fracture-mechanics concepts could indeed be applied to wood. Some possible causes for the disagreement are:

1. The ramp-loading and constant-load results obtained in the present study are not truly comparable. Comparing Figures 9 and 10 with the ramp-loading results, it may be seen that at times to failure of less than 10 hours, the slope of the stress-ratio versus time-to-failure plot is small, and agrees qualitatively with the results of the rate-of-loading tests in which the times to failure ranged only up to about five hours. However, at longer times to failure the results of the constant load tests show an increasing slope which is not predicted by the fracture-mechanics model. Explanations for the observed non-linearity have not been found, but could reflect changes in the failure mechanism due to the longer periods of loading in constant-load tests at low stress ratios.

2. The earlier work was carried out on small, clear specimens. The present work was carried out on larger specimens which were not clear. It is possible that the existing flaws in the wood were of a sufficient magnitude to mask the rate-of-loading results that were noted with the small, clear specimens.

3. The fluctuations in laboratory temperature and relative humidity during the constant-load tests may have resulted in more rapid failure, as has been suggested by Schniewind (9).

Nevertheless, the observed differences underscore the need for verification of predictions of the long-term behaviour of large specimens or structural members based on short-term tests of small specimens. A general model to describe the time-dependent failure of wood still remains to be found.

## Bibliography

1. Keeton, J.R. 1968. Dynamic properties of small, clear specimens of structual-grade timber. Technical Report R573, Naval Civil Engineering Lab., Port Hueneme, Ca.

2. Liska, J.A. 1950. Effect of rapid loading on the compressive and flexural strength of wood. Report No. R1767, USDA Forest Service, Forest Prod. Lab., Madison, Wis.

3. Madsen, B. 1972. Duration of load tests for wood in tension perpendicular to grain. Structural Research Series Report No. 7, University of British Columbia, Dep. of Civil Engineering, Vancouver, B.C.

4. Mindess, S., Nadeau, J.S., and Barrett, J.D. 1976. Effect of constant deformation rate on the strength perpendicular to the grain of Douglas fir. Wood Sci. 8(4):262-266.

5. Clauser, W.S. 1959. Creep of small wood beams under constant bending loads. Report 2150, USDA Forest Service, Forest Prod. Lab., Madison, Wis.

6. Mindess, S., Nadeau, J.S., and Barrett, J.D. 1975. Slow crack growth in Douglas fir. Wood Sci. 8(1):289-396.

7. Evans, A.G. 1974. Slow crack growth in brittle materials under dynamic conditions. Int. J.Fracture 10:251.

8. Wiederhorn, S.M. 1973. Subcritical crack growth in ceramics. In: Fracture of Ceramics, II. R.A. Bradt, D.P.H. Hasselman and F.F. Lange (eds.). Plenum Press, New York.

9. Schniewind, A.P. 1967. Creep-rupture life of Douglas fir under cyclic environmental conditions. Wood Sci. and Tech. 1:278.

## TABLE 1

Schedule of Tests

| Type of test | Rate of Loading<br>Rate of cross-head motion (in/sec) | Constant Load<br>Stress level (psi) | % of short-term failures corresponding to the stress level |
|---|---|---|---|
| tension | $2.20 \times 10^{-3}$ | 134.4 | 50 |
| tension | $1.12 \times 10^{-4}$ | 91.8 | 30 |
| tension | $6.00 \times 10^{-6}$ | 36.7 | 10 |
| flexure | $5.49 \times 10^{-2}$ | 350 | 54.4 |
| flexure | $2.13 \times 10^{-3}$ | 300 | 35.6 |
| flexure | $1.31 \times 10^{-4}$ | 250 | 17.9 |
| flexure | $1.18 \times 10^{-5}$ | 200 | 10.5 |

NOTE: Each group consisted of 39 specimens initially.

## TABLE 2

### Rate-of-Loading Data

| Type of test | Rate of loading (in/sec) | Ultimate Stress Level<br>Mean (psi) | Ultimate Stress Level<br>Standard deviation (psi) | Ultimate Stress Level<br>Coefficient of variation (%) | Time to Failure<br>Mean (sec) | Time to Failure<br>Standard deviation (sec) | Time to Failure<br>Coefficient of variation (%) |
|---|---|---|---|---|---|---|---|
| tension | $2.20 \times 10^{-3}$ | 134.3 | 72.9 | 54.3 | 28.4 | 13.9 | 48.9 |
| tension | $1.12 \times 10^{-4}$ | 151.3 | 81.0 | 53.5 | 701.8 | 289.0 | 41.2 |
| tension | $6.00 \times 10^{-6}$ | 143.7 | 65.2 | 45.4 | 16788.5 | 6475.4 | 38.6 |
| flexure | $5.49 \times 10^{-2}$ | 337.5 | 99.3 | 29.4 | 2.25 | 0.69 | 30.7 |
| flexure | $2.13 \times 10^{-3}$ | 315.2 | 110.7 | 35.1 | 54.1 | 15.1 | 27.9 |
| flexure | $1.31 \times 10^{-4}$ | 339.4 | 103.2 | 30.4 | 1061.0 | 296.8 | 28.0 |
| flexure | $1.18 \times 10^{-5}$ | 333.5 | 101.8 | 30.5 | 12737.8 | 3952.3 | 31.0 |

## TABLE 3

Summary of Constant-Load Data

| Type of test | No. of specimens | Stress level (psi) | Broken on loading | No. of specimens surviving | Minimum load time of surviving specimens (hours) |
|---|---|---|---|---|---|
| tension | 36 | 134.4 | 10 | 9 | 8400 |
| tension | 39 | 91.8 | 6 | 10 | 4100 |
| tension | 36 | 36.7 | 4 | 27 | 8200 |
| flexure | 39 | 350 | 24 | 0 | – |
| flexure | 39 | 300 | 16 | 1 | 18500 |
| flexure | 39 | 250 | 10 | 2 | 18100 |
| flexure | 39 | 200 | 3 | 18 | 14200 |

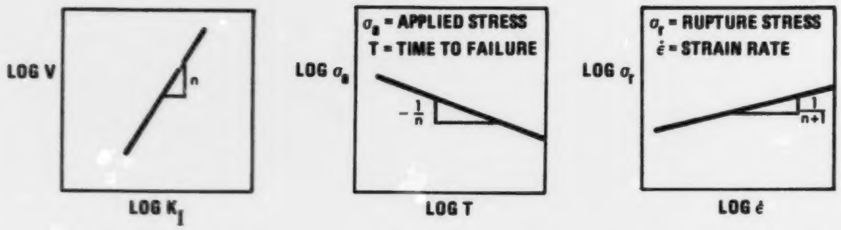

(a) Direct observation of cracks in plates.

(b) Duration of load tests.

(c) Stress rate tests.

Fig. 1: Three ways of determining the parameter n, the slope of the log crack velocity V versus log stress intensity $K_I$ plot.

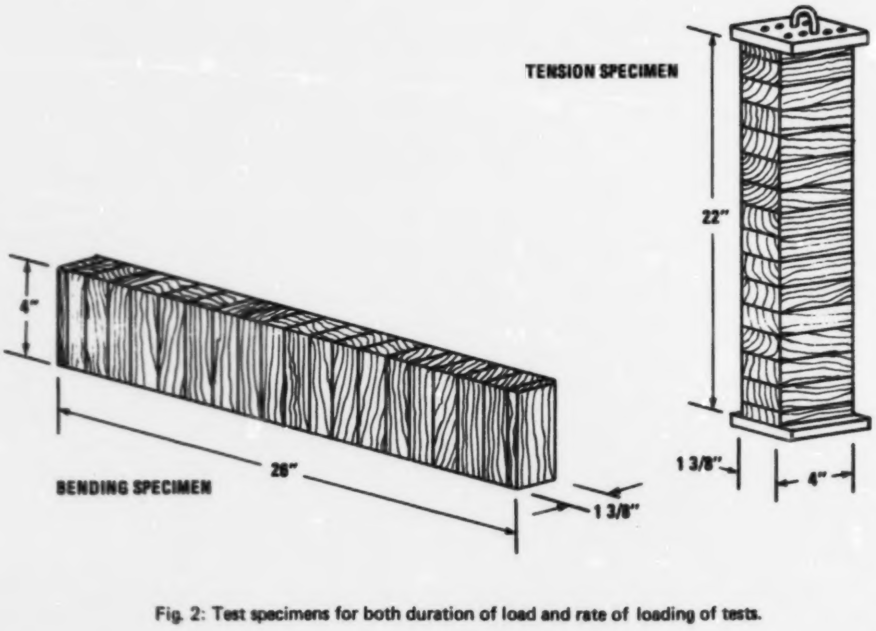
TENSION SPECIMEN
22"
1 3/8"
4"
4"
26"
BENDING SPECIMEN
1 3/8"

Fig. 2: Test specimens for both duration of load and rate of loading of tests.

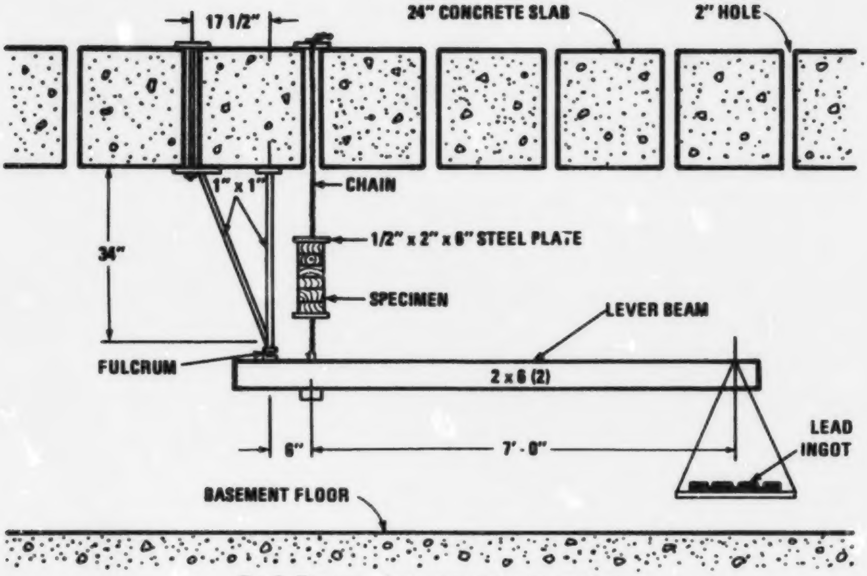
17 1/2"
24" CONCRETE SLAB
2" HOLE
1" x 1"
CHAIN
1/2" x 2" x 6" STEEL PLATE
34"
SPECIMEN
LEVER BEAM
FULCRUM
2 x 6 (2)
6"
7'-0"
LEAD INGOT
BASEMENT FLOOR

Fig. 3: Test setup for long-term tension specimens.

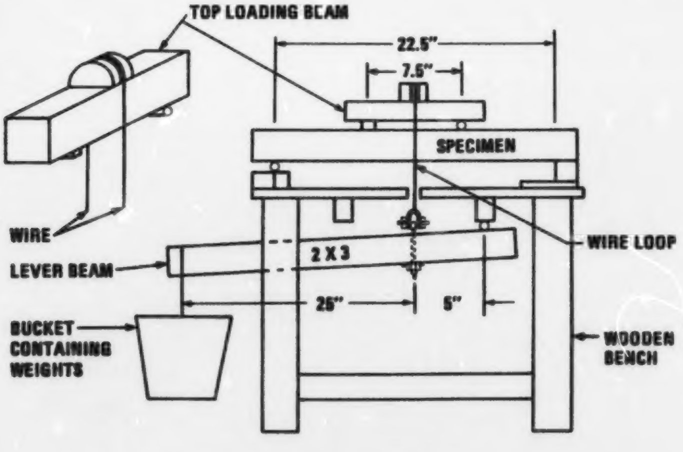
TOP LOADING BEAM
22.5"
7.5"
SPECIMEN
WIRE
WIRE LOOP
LEVER BEAM
2 X 3
26"
5"
BUCKET CONTAINING WEIGHTS
WOODEN BENCH

Fig. 4: Test setup for long-term bending specimens.

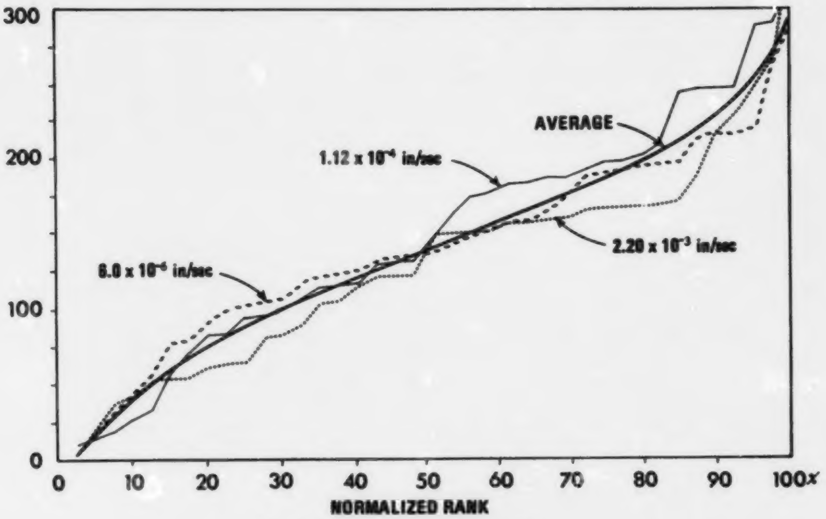

Fig. 5: Short-term tensile strength.

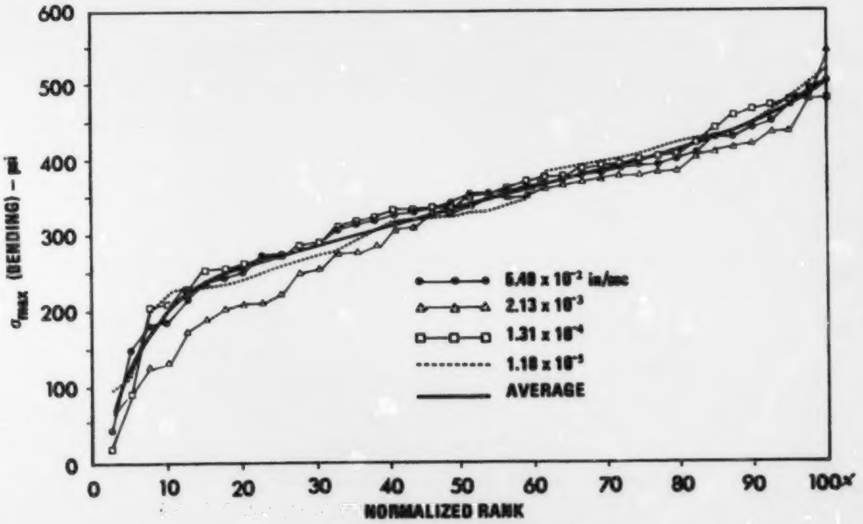

Fig. 6: Short-term bending strength.

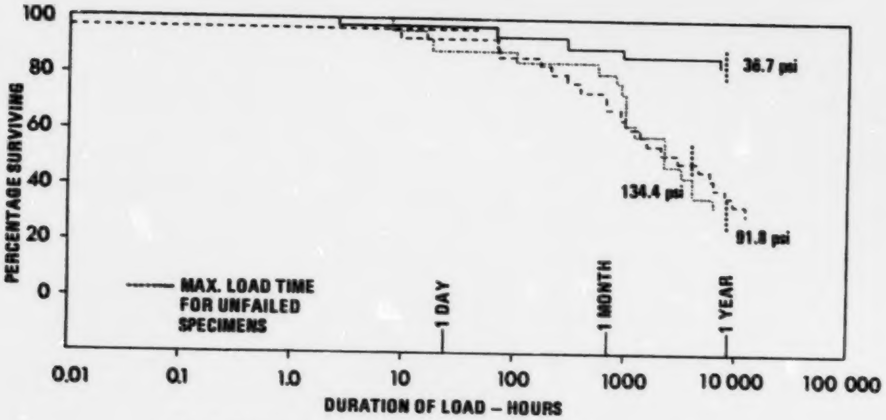

Fig. 7: Long-term tension: percentage surviving vs. load duration.

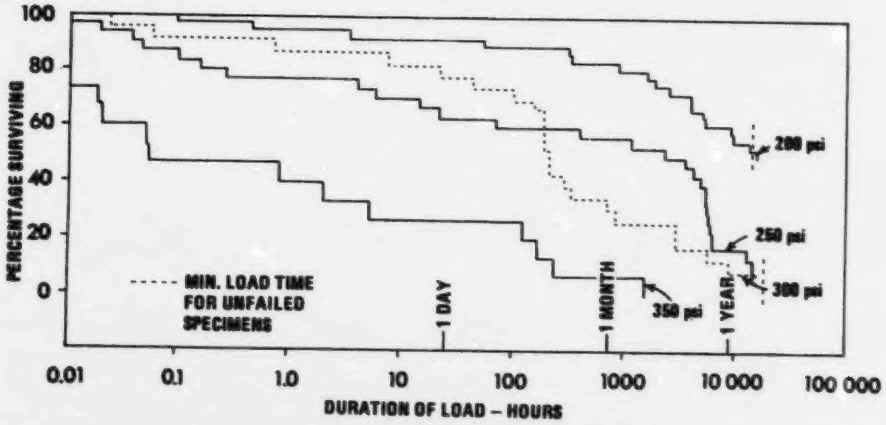

Fig. 8: Long-term bending: percentage surviving vs. load duration.

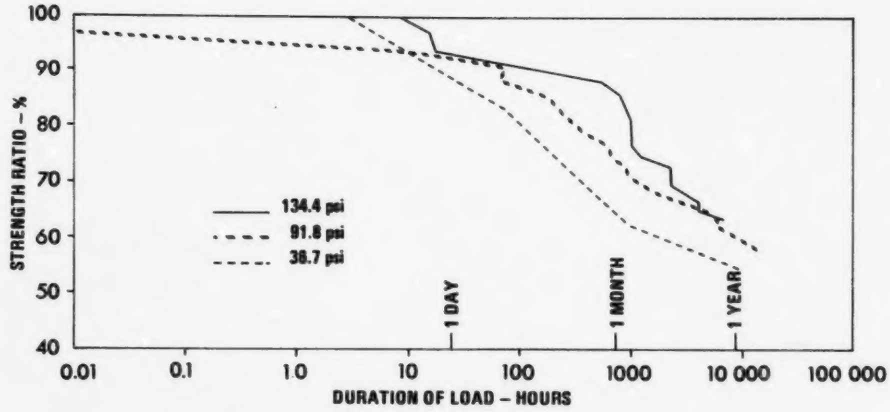

Fig. 9: Long-term tension: strength ratio vs. load duration.

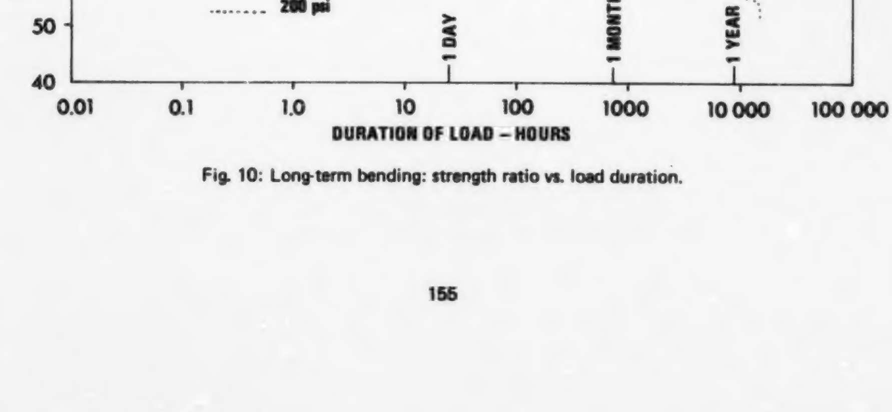

Fig. 10: Long-term bending: strength ratio vs. load duration.

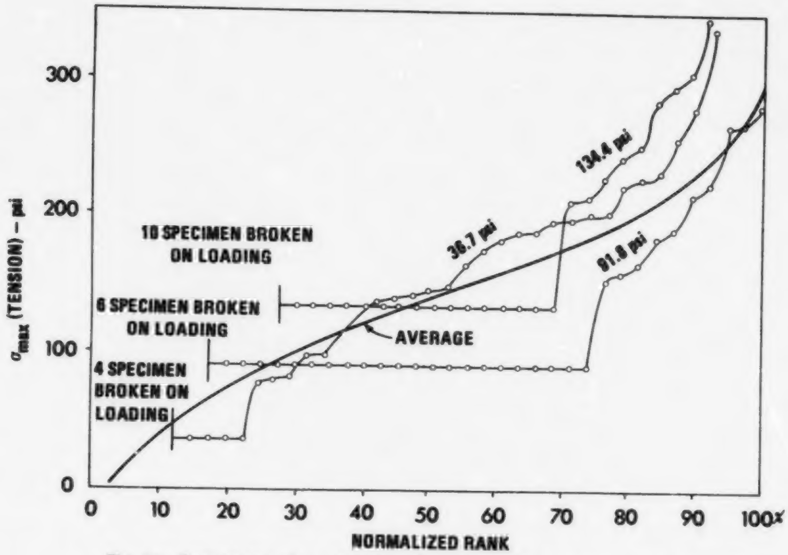

Fig. 11: Ranked data for unfailed specimens tested after about 1 year (tension).

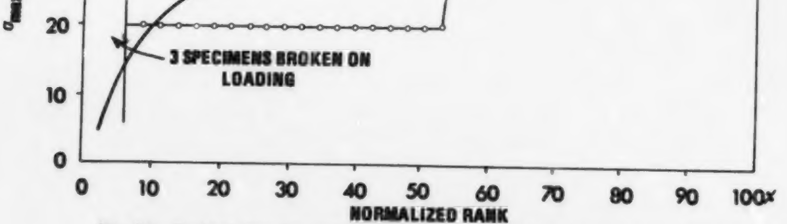

Fig. 12: Ranked data for unfailed specimens tested after about 1 year (flexure).

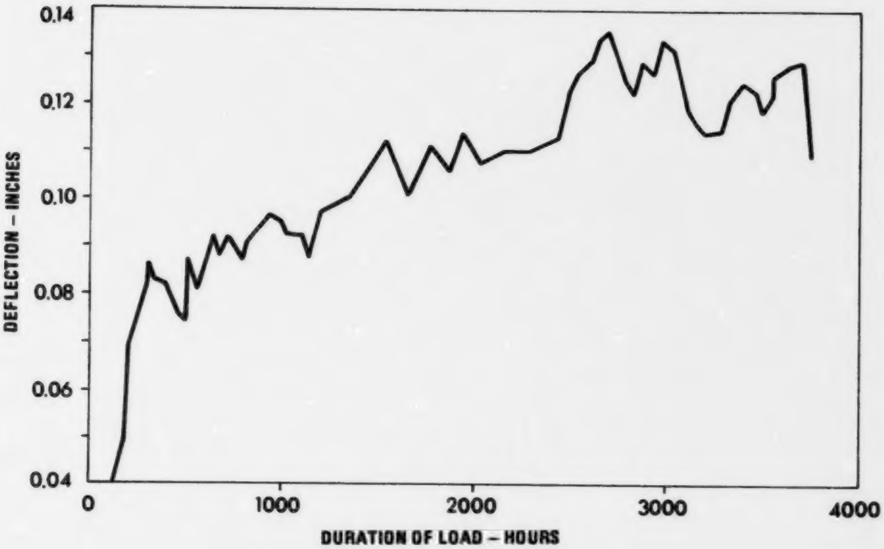

Fig. 13: Deflection versus time; long-term tension

# USING FRACTURE MECHANICS TO PREDICT FAILURE IN NOTCHED WOOD BEAMS

By

**Joseph F. Murphy**

---

Engineer, Forest Products Laboratory, Forest Service,
U.S. Department of Agriculture, Madison, WI.

## ABSTRACT

Failure loads of small (1 by 1 by 16 in.) rectangular-notched beams (center, off center, and end) are compared with failure loads of slit-notched (saw kerf) beams and controls. All the notches are on the tension side, and only the center-notched beams are subject to two-point symmetric loading. The experimental results show the conservativeness of design criteria based on slit notches when used for rectangular-notched beams. Also, a combined mode failure criterion is tested using transformed theoretical stress-intensity factors. The transformation computes "equivalent" stress-intensity factors in the rupture plane parallel to grain and perpendicular to the slit notch.

## INTRODUCTION

Bending stresses in beams with notches can be calculated using a reduced net depth. This method does not, however, take into account stresses caused by the stress concentration at the notch corner. Steida (1966) has shown that, for a beam with a slit notch (saw kerf wide) half its depth, the failing load (corresponding to load at proportional limit and visible crack initiation at the corner) is less than 10 percent of the unnotched-beam failing load. This compares to 25 percent that the net section method would predict. As the width (span direction) of the notch becomes very small, a crack-like manmade flaw would result.

Linear-elastic fracture mechanics (LEFM) methodology was developed to analyze the stress field around cracks in metal. Fracture-mechanics principles are also being applied to wood (Wu, 1967; Schniewind and Pozniak, 1971; Schniewind and Lyon, 1973; Leicester, 1974; Walsh, 1974; Barrett and Foschi, 1977, to list a few).

This paper shows how LEFM principles can predict failure of notched beams in general; specifically, (1) failing loads of beams with wide notches will be compared to failing loads of beams with narrow slit notches and (2) failure for slit-notched beams under combined loading will be explored.

Reviewing some LEFM basics, a planar crack can propagate in a coplanar fashion by the superposition of three basic modes of crack surface displacement (Fig. 1). In mode I propagation, the crack surfaces open normal to themselves; in mode II, the surfaces slide tangential to themselves in the direction of propagation; and in mode III, the surfaces slide tangential to themselves and perpendicular to the propagation direction in a tearing fashion. Mode I results from symmetric inplane loading; mode II, from skew-symmetric inplane loading; and mode III, from out-of-plane loading.

Sih *et al.* (1965) have derived formulae, using LEFM methodology, for the stresses in a small region surrounding a cracked tip in an orthotropic body. They used stress-intensity factors to describe conditions for crack extension and a complex variable approach for the stress functions. Their results for a slit notch or crack parallel to a material axis and coincident with the negative X-axis (Fig. 2) are:

Symmetric (about X-axis) plane loading

$$\sigma_x = \frac{K_I}{\sqrt{2\pi r}} \; \mathrm{Re}\left[\frac{-\beta_1\beta_2}{\beta_1-\beta_2}\left(\frac{\beta_2}{\beta_2} - \frac{\beta_1}{\beta_1}\right)\right] \qquad (1)$$

$$\sigma_y = \frac{K_I}{\sqrt{2\pi r}} \; \mathrm{Re}\left[\frac{1}{\beta_1-\beta_2}\left(\frac{\beta_1}{\beta_2} - \frac{\beta_2}{\beta_1}\right)\right]$$

$$\tau_{xy} = \frac{K_I}{\sqrt{2\pi r}} \; \mathrm{Re}\left[\frac{-\beta_1\beta_2}{i(\beta_1-\beta_2)}\left(\frac{1}{B_1} - \frac{1}{B_2}\right)\right]$$

and

Skew-symmetric (about X-axis) plane loading

$$\sigma_x = \frac{K_{II}}{\sqrt{2\pi r}} \; \mathrm{Re}\left[\frac{1}{i(\beta_1-\beta_2)}\left(\frac{\beta_1^2}{B_1} - \frac{\beta_2^2}{B_2}\right)\right] \qquad (2)$$

$$\sigma_y = \frac{K_{II}}{\sqrt{2\pi r}} \; \mathrm{Re}\left[\frac{1}{i(\beta_1-\beta_2)}\left(\frac{1}{B_2} - \frac{1}{B_1}\right)\right]$$

$$\tau_{xy} = \frac{K_{II}}{\sqrt{2\pi r}} \; \mathrm{Re}\left[\frac{1}{\beta_1-\beta_2}\left(\frac{\beta_1}{B_1} - \frac{\beta_2}{B_2}\right)\right]$$

where

$B_j = \sqrt{\cos\theta + i\beta_j \sin\theta} \qquad i = \sqrt{-1} \qquad j = 1,2$

Re = real part of

$$\left.\begin{aligned} \beta_1^2 &= \epsilon_2^2 = \frac{E_x}{E_y} \\ k &= \frac{\epsilon^2}{2} \left(\frac{E_y}{G_{xy}} - 2\nu_{yx}\right) \end{aligned}\right\} \text{for plane stress}$$

Directly ahead of the crack the stresses are:

$$\sigma_y = \frac{K_I}{\sqrt{2\pi x}} \quad \text{and} \quad \tau_{xy} = \frac{K_{II}}{\sqrt{2\pi x}}$$

where the Ks are stress intensity factors (SIFs) which are linearly dependent on remote boundary conditions, highly dependent on geometry, and slightly dependent on orthotropic parameters (for finite bodies). In single-mode loading, when the SIFs reach critical values (CSIFs), such as $K_{I_c}$ or $K_{II_c}$, crack propagation occurs. The stresses around a wide rectangular notch have been analyzed theoretically using a finite-element method by Walsh (1974). For notches one-third the beam's depth (1/3 d) and widths of 4/3 d and 16/3 d, Walsh computes the stresses along the grain (y < 0) to be:

$$\sigma_x(o,y) = \frac{0.133}{\left(2\pi\frac{r}{d}\right)^{0.45}} \quad \frac{6M}{bd^2};$$

$$\tau_{xy}(o,y) = \frac{0.020}{\left(2\pi\frac{r}{d}\right)^{0.10}} \quad \frac{6M}{bd^2} \qquad (3)$$

$$r = |y|$$

For the same orthotropic parameters[2] and using a modified boundary collocation method with complex variables, the author computed -- for a slit notch one-third the beam depth under pure moment -- the stresses along the grain (y < 0) to be:

$$\sigma_x(o,y) = \frac{0.138}{\left(2\pi\frac{r}{d}\right)^{0.50}} \quad \frac{6M}{bd^2}$$

$$\tau_{xy}(o,y) = \frac{0.275}{\left(2\pi\frac{r}{d}\right)^{0.50}} \quad \frac{6M}{bd^2} \qquad (4)$$

A comparison of equations (3) and (4) reveals that a slit notch has higher stress intensities; therefore, a beam with a slit notch should fail at a lower load than a beam with a rectangular notch. Experiments were conducted to compare the failing loads of beams which had rectangular notch widths more than twice the beam's depth to failing loads of slit-notched beams.

## Procedure

From two slow-grown, quarter-sawn, Douglas-fir 2 by 10s, 147 beam specimens were cut, 16 by 1 by 1 inch. Specimens were cut to minimize slope of grain and conditioned to 11 percent moisture content.

Seven geometries were chosen with 21 replications each. One was the control and was loaded in quarter-point bending to determine modulus of rupture (MOR). The six other geometries and loading positions are shown in Fig. 3.

All notches were 1/3-inch deep and cut on a table saw. The slit notches were one saw kerf wide, equal to 3/32 inch. Notches of beams B, C, and F (Fig. 3) were 2, 3, and 2-1/2 inches wide, respectively. The notches in A and B are symmetric about the centerline, while the center of the notch in C, D, E, and F is 4, 2-1/2, 5-1/2, or 1-1/4 inches from the support, respectively. Spans are 15 inches and loadings of A and B are symmetric quarter-point, while C, D, E, and F are loaded two-third span from the support closer to the notch.

Slit notches in beams D and E coincide with the ends of the wide notch in beam C.

---

[2] $E_y/E_x = 16$, $\nu_{yx} = 0.25$, $E_y/G_{xy} = 16.5$.

Also the slit notch in beam D coincides with the end of the wide notch in beam F. A conservative estimate of the failing load of beam C would be the minimum of three loads: (1) failing load of the net section; (2) failing load of beam D; and (3) failing load of beam E. Estimate of the failing load of beam B would be the lower load from net section theory and beam A. Also the estimated failing load for beam F would be the lower load from net section theory and beam D.

All loads were applied in the radial direction. Centerline deflection was measured using a linear-variable-differential transducer (LVDT) in all cases. A clip gage (Fig. 4A) was used to measure crack opening displacement (COD) on all slit-notched beams, while a LVDT measured displacement perpendicular to grain at the end of the rectangular-notches (Fig. 4B).

The specimens were loaded in a screw-type testing machine at a uniform rate of 0.1 inch per minute. Centerline deflection relative to span middepth and either COD or perpendicular expansion were plotted as a function of load automatically on an X-$Y_1$, $Y_2$ recorder. Two LVDTs were used for beam B because intitial failure could occur at either corner. Only one LVDT was needed for C as the crack always started at the corner closest to the load.

## Results

Experimental results are given in Table 1. All values represent average load at proportional limit for 21 specimens, except where otherwise noted. Proportional-limit load was used as failure load because it corresponds to crack initiation that precedes visible opening. Because the COD gage does not measure displacement across the initiated crack, the results were adjusted.

Note in Table 1 that the clip gage picks up approximately the same load as the yoke gage, but the notch gage is about 25 percent lower. To relate the various values, the ratio of the yoke-gage load to the load calculated from either the clip or notch gage was computed for each beam (Table 1, col. 5-6).

Because the clip gage did not measure displacements across the initiated crack, 10 more specimens were loaded in the beam A configuration, but with two LVDTs fastened as shown in Figure 4C. The average ratio of load computed from the yoke gage to the lower proportional limit of the two LVDTs was 1.377. Because this ratio is consistent with the y/n ratios, the average loads computed by the yoke gages for the slit-notched beams are divided by 1.377 (Table 1, col. 7) and compared with the notch-gage loads for the wide-notched beams (Table 1, col. 4).

Average modulus of rupture of the controls was 12,700 pounds per square inch, with an unbiased standard deviation of 1,780 pounds per square inch. (For an unnotched beam, failure load occurs at MOR).

## Discussion

Beams with slit notches fail ("proportional limit") at lower loads than those with wide rectangular notches. The conservativeness of using the failing (crack initiating) loads of a narrow slit-notched beam, compared with a wide-notched beam, can now be assessed quantitatively. Beam A failed at 91 percent of the load of beam B, beam E failed at 99 percent of the load of beam C, and beam D failed at 88 percent of the load of beam F.

Comparisons of beams A to B are consistent with Steida's (1966) results. He found that, for beams with notch depths of one-eighth and one-half of the beam depth under pure moment loading, slit-notched beams failed at 84 percent and 93 percent, respectively, of the load at which rectangular-notch beams failed.

Using the $K_{Ic}$ of Douglas-fir calculated by Schniewind and Centeno (1973), who used a clip gage on single edge-notched specimens, failing loads for the A beams would calculate to 186.7 pounds compared with this study's value of 163 pounds.

## Theoretical Considerations

Since a crack starts at a corner of a notch and propagates along the grain, stresses along the grain line were examined theoretically. The main idea here is that we know where the crack is going to occur; if we reference ourselves on this imminent fracture plane, the stresses at failure on this plane should be the same whether the original crack-like flaw is parallel or perpendicular to this plane.

When a crack is perpendicular to grain, the boundary conditions which would cause (refer to Fig. 2) the following stresses:

$$\sigma_y = \frac{K_I}{\sqrt{2\pi r}}, \quad \tau_{xy} = \frac{K_{II}}{\sqrt{2\pi x}}$$

$$\text{at } \theta = 0°$$

or immediately ahead of the crack (eq. (1) and (2)) would cause the following stresses:

$$\sigma_x = \frac{1}{\sqrt{2\pi r}} (0.12\ K_I \mp 0.82\ K_{II})$$

$$\tau_{xy} = \frac{1}{\sqrt{2\pi r}} (\mp 0.24\ K_I + 0.47\ K_{II}) \qquad (5)$$

$$\text{at } \theta = \pm 90°$$

or at right angles to the crack tip ($E_Y/E_x = 16$, $E_y/G_{xy} = 16.5$, $\nu_{yx} = 0.25$). The expressions in parentheses in equation (5) can be thought of as "transformed" stress-intensity factors or "equivalent" stress-intensity factors along the grain perpendicular to the original crack. Two points to consider are: (1) loadings that cause only pure tension or pure shear directly ahead of the crack, produce both shear and tension at a right angle to the crack;(2) when shear ahead of the crack is present, both shear and tension perpendicular are greater in the -90° direction than in the +90° direction. The first point corroborates Steida's 1966 work, recorded for notched beams under pure moment ($K_{II}$ = D), that "The initial failure at the notch was always a combination of shear and tension perpendicular to grain failure". The second point is important because, if $K_{II} \neq 0$, cracks should initiate in the -90° direction rather than the +90° direction. This was verified when all the asymmetrically loaded beams had a crack run toward the loading point.

Finally, equation (5) can qualitatively explain the difference for critical stress intensity factors in the RL and LR systems of crack propagation (the first letter refers to the direction normal to the crack plane and the second refers to the crack propagation direction). The RL system has the original crack parallel to grain and the LR has it perpendicular. Schniewind and Centeno (1973) report for Douglas-fir

$K_{I_c}$ = 2,450 psi $\sqrt{\text{in.}}$ for the LR system and

373 psi $\sqrt{\text{in.}}$ for the RL system.

Using equation (5) and the notion of transformed SIFs, they would obtain in the LR system:

$$\bar{\bar{K}}_I = 294 \text{ psi } \sqrt{\text{in.}}$$

$$\bar{\bar{K}}_{II} = 588 \text{ psi } \sqrt{\text{in.}}$$

where the double bar superscript refers to transformed SIFs along the grain. $\bar{K}_{Ic}$ is less than $K_{I_c}$ (373 psi $\sqrt{\text{in.}}$) for the RL system, but is of the same order of magnitude. Also shear is present along the fracture plane and would be expected to lower the failure $K_I$.

Before testing a combined SIF failure criterion, a theoretical analysis of $K_I$ and $K_{II}$ as a function of slit relative depth was completed. Fig. 5 gives the graphs of two loading conditions -- pure moment and balanced shear. The crack notch is perpendicular to grain, with elastic constants as noted previously. A modified boundary collocation method with complex variable stress functions was used.

Applying the concept of transformed SIF to the notched beams of this study, consider a beam with a slit notch one-third the beam depth. From Fig. 5:

$$K_I = 7.0 \frac{M}{bd^{3/2}} \text{ and } K_{II} = 1.03 \frac{V}{bd^{1/2}}$$

For the three slit-notch beams (A, D, E) tested, the SIFs and transformed SIFs are given as a function of load in Table 2. Using the loads at failure (Table 1, col. 7), the failing SIFs are given in Table 3. The transformed SIFs show a better grouping than the normal SIFs, encouraging the use of transformed SIFs to predict failure loads.

As a first approximation, consider a conservative combined SIF failure criterion (Leicester, 1974):

$$\frac{K_I}{K_{I_c}} + \frac{K_{II}}{K_{II_c}} \geq 1 \qquad (6)$$

where the critical SIFs are measured by collinear-crack propagation and the SIFs are calculated in the normal way, when the crack is parallel to grain, or transformed, when the crack is perpendicular. For beams A, D, and E, a $K_{I_c} = 247$ psi $\sqrt{\text{in.}}$ and $K_{II_c} = 1{,}705$ psi $\sqrt{\text{in.}}$ would predict conservative loads at which the crack would propagate, Table 4.

A $K_{I_c} = 247$ psi $\sqrt{\text{in.}}$ for Douglas-fir (RL system) is within the range of values reported by Mindess *et al.* (1975) of 234 to 493 psi $\sqrt{\text{in.}}$ Also $K_{II_c} = 1{,}705$ psi $\sqrt{\text{in.}}$ is the same order of magnitude as measured by Barrett (1976) for Douglas-fir (1,800 psi $\sqrt{\text{in.}}$).

The CSIFs used in Table 2 should not be considered as estimates for the CSIFs of Douglas-fir. These values (reasonable in comparison with published values) are used to show how, combined with a failure criterion and transformed SIFs, failure of notched beams might be predicted.

The effect of notch depth on beam strength can now be quantified as shown in Figure 6. The abscissa is relative notch depth $\frac{a}{d}$ and the ordinate is the ratio of failing moment of a notched beam ($M_n$ at proportional limit) to the failing moment of an unnotched beam ($M_o$ at MOR). The dashed curve is net section theory. The solid curves were constructed using Fig. 5 (moment loading), transformed SIFs, equation (5), and a failure equation (6) to get $M_n$ and a value of $M_o = 2116$ pound-inch. The lower solid curve uses $K_{I_c} = 234$ psi $\sqrt{\text{in.}}$ and $K_{II_c} = 1800$ psi $\sqrt{\text{in.}}$ and the higher uses $K_{I_c} = 493$ psi $\sqrt{\text{in.}}$ and $K_{II_c} = 1800$ psi $\sqrt{\text{in.}}$ Square data points are from Steida (1966), adjusted by dividing by 1.377, and triangular results are from the present study. The open data points are for slit-notched beams, while the closed ones are for rectangular-notched beams (all having d = 1 in.). As can be seen, failure can be better predicted using LEFM principles than net section theory.

## Conclusions

1. Notched beams with narrow notches fail at lower loads than wide-notched beams (everything else remaining the same).

2. A displacement gage positioned across the grain perceives crack propagation at 25 percent lower loads than a COD gage across a slit notch which is perpendicular to grain.

3. Examination of the stress field along an imminent fracture surface using fracture mechanics gives a theoretical basis for experimental observation (shear and tension perpendicular).

4. Transformation of stress-intensity factors for a crack perpendicular to the grain qualitatively explains the order of magnitude difference of $K_{I_c}$ in the LR system compared with the RL system.

5. Using transformed SIFs and a linear SIF failure equation with reasonable CSIFs, crack initiation can be conservatively predicted for notched beams under various moment and shear loadings.

6. The effect of notch depth on bending strength can be quantified using fracture mechanics.

## LITERATURE CITED

Barrett, J.D. 1976. Shear fracture of wood. Int. Union of For. Res. Organ. Congr., Oslo, Norway.

Barrett, J.D., and R.O. Foschi. 1971. Mode II stress-intensity factors for cracked wood beams. Eng. Fract. Mech. 9(2):371-378.

Leicester, R.H. 1973. Effect of size on the strength of structures. CSIRO Australia, Div. Build. Res., Technol. Pap. No. 71:1-13.

Leicester, R.H. 1974. Application of linear fracture mechanics in the design of timber structures. Proc. 1974 Conf. Australian Fract. Group 23:156-164, Melbourne, Australia. Oct.

Mindess, S., J.S. Nadeau, and J.D. Barrett. 1975. Slow crack growth in Douglas-fir. Wood Sci. 8(1):389-396.

Schniewind, A.P., and J.C. Centeno. 1973. Fracture toughness and duration of load factor I. Six principal systems of crack propagation and the duration factor for crack propagating parallel to grain. Wood and Fiber 5(2):152-159.

Schniewind, A.P., and D.E. Lyon. 1973. A fracture mechanics approach to the tensile strength perpendicular to grain of dimension lumber. Wood Sci. Technol. 7:45-59.

Schniewind, A.P., and R.A. Pozniak. 1971. On the fracture toughness of Douglas-fir wood. Eng. Fract. Mech. 2:223-233.

Sih, G.C., P.C. Paris, and G.R. Irwin. 1965. On crack in rectilinearly anisotropic bodies. Int. J. Fract. Mech. 1:189-203.

Steida, C.K.A. 1966. Stress concentrations around holes and notches and their effect on the strength of wood beams. J. Mater. 1(3):560-582.

Walsh, P.F. 1974. Linear fracture mechanics solutions for zero and right angle notches. CSIRO Australia, Div. Build. Res., Technol. Pap. (second ser.) No. 2:1-16.

Wu, E.M. 1967. Application of fracture mechanics to anisotropic plates. J. Appl. Mech. 34:967-974.

TABLE 1. - - RESULTS[1] OF TESTS ON SIX NOTCHED BEAMS AND COMPARISON OF FAILURE LOADS USING DIFFERENT GAGES.

| Beam | Yoke gage (y) load | Clip gage (c) load | Notch gage (n) load | y/c | y/n | y/1.377 |
|---|---|---|---|---|---|---|
| | Lb | Lb | Lb | | | |
| A | 167.9 | 163.0 | - - | 1.032 | - - | 121.9 |
| | 23.6 | 20.8 | - - | .099 | - - | - - |
| B | 182.1 | - - | 133.4 | - - | 1.370 | - - |
| | 27.5 | - - | 15.7 | - - | .162 | - - |
| C | 165.5 | - - | 125.7 | - - | 1.340 | - - |
| | 32.8 | - - | 28.0 | - - | .279 | - - |
| D[2] | 284.2 | 307.8 | - - | .924 | - - | 206.4 |
| | 50.2 | 37.2 | - - | .125 | - - | - - |
| E[3] | 171.3 | 163.7 | - - | 1.048 | - - | 124.4 |
| | 23.7 | 19.4 | - - | .092 | - - | - - |
| F | 338.6 | - - | 234.1 | - - | 1.430 | - - |
| | 56.3 | - - | 44.3 | - - | .300 | - - |

[1] First value for each test is average failing load (corresponding to load at proportional limit); value listed below it is unbiased standard deviation. All results are for 21 specimens unless otherwise noted.

[2] 19 specimens

[3] 20 specimens

Table 2. - - Normal and 'transformed' SIFs for slit-notched beams A, D, and E[1].

| Beam | $K_I$ | $K_{II}$ | $\bar{\bar{K}}_I$ | $\bar{\bar{K}}_{II}$ |
|---|---|---|---|---|
| A | 13.125P | 0 | 1.575P | 3.150P |
| D | 5.833P | .3433P | .973P | 1.561P |
| E | 12.833P | .3433P | 1.821P | 3.241P |

[1] SIFs are in psi $\sqrt{\text{in.}}$ when P is total load in pounds.

Table 3. - - Normal and 'transformed' SIFs (units of psi $\sqrt{\text{in.}}$) at failing loads for slit-notched beams A, D, and E

| Beam | $K_I$ | $K_{II}$ | $\bar{\bar{K}}_I$ | $\bar{\bar{K}}_{II}$ |
|---|---|---|---|---|
| A | 1,600 | 0 | 192 | 384 |
| D | 1,204 | 71 | 201 | 322 |
| E | 1,596 | 43 | 227 | 403 |

Table 4. - - Failing loads of slit-notch beams (A,D,E) experimental and theoretical.

| Beam | Measured load | Calculated load[1] | $\frac{\text{Calculated load}}{\text{Measured load}}$ |
|---|---|---|---|
| | Lbs | Lbs | Pct |
| A | 121.9 | 121.6 | 100.25 |
| D | 206.4 | 204.6 | 100.88 |
| E | 124.4 | 107.8 | 115.40 |

[1] Using the following equations:

$$\frac{\bar{\bar{K}}_I}{247 \text{ psi} \sqrt{\text{in.}}} + \frac{\bar{\bar{K}}_{II}}{1{,}705 \text{ psi} \sqrt{\text{in.}}} = 1$$

$$\bar{\bar{K}}_I = 0.12\, K_I + 0.82\, K_{II}$$

$$\bar{\bar{K}}_{II} = 0.24\, K_I + 0.47\, K_{II}$$

$$K_I = 7.0 \frac{M}{bd^{3/2}} \qquad K_{II} = 1.03 \frac{V}{bd^{1/2}}$$

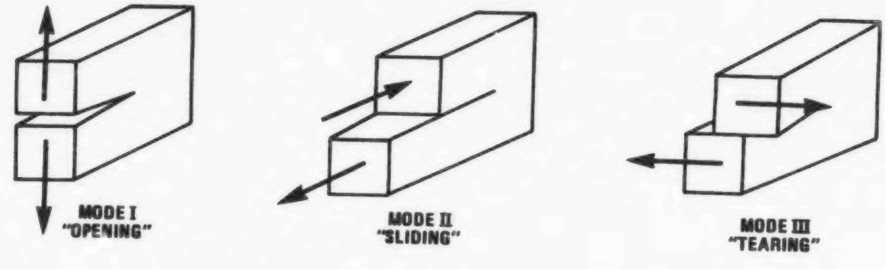
MODE I
"OPENING"
MODE II
"SLIDING"
MODE III
"TEARING"

Fig. 1. Three basic modes of crack surface displacement.

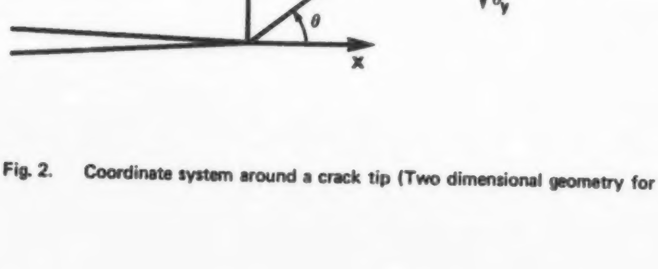
$\sigma_y$
$\tau_{xy}$
$\tau_{xy}$
$\sigma_x$
$\tau_{xy}$
$\sigma_x$
y
r
$\tau_{xy}$
$\sigma_y$
$\theta$
x

Fig. 2. Coordinate system around a crack tip (Two dimensional geometry for $K_I$, $K_{II}$).

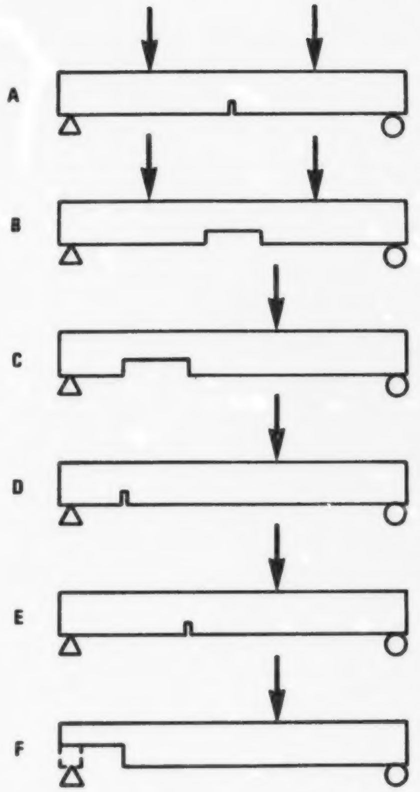

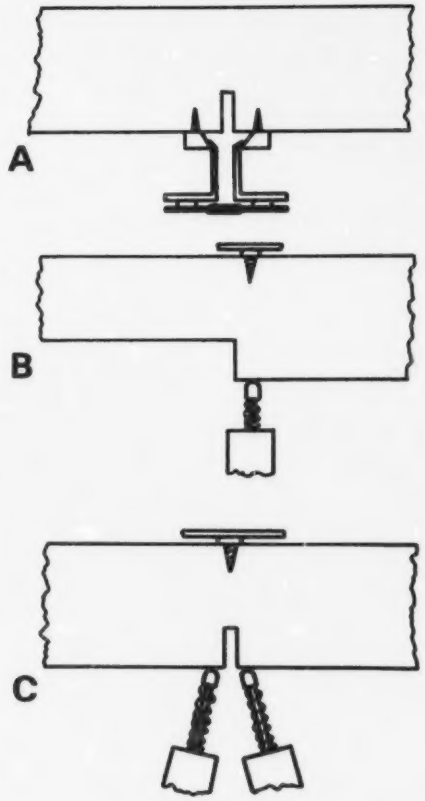

Fig. 3. Notched beam geometries and loading configurations.

Fig. 4. Gages to measure crack initiation:
(A) COD gage for a slit notch;
(B) LVDT gage for a rectangular notch; and
(C) Two LVDTs for a slit notch.

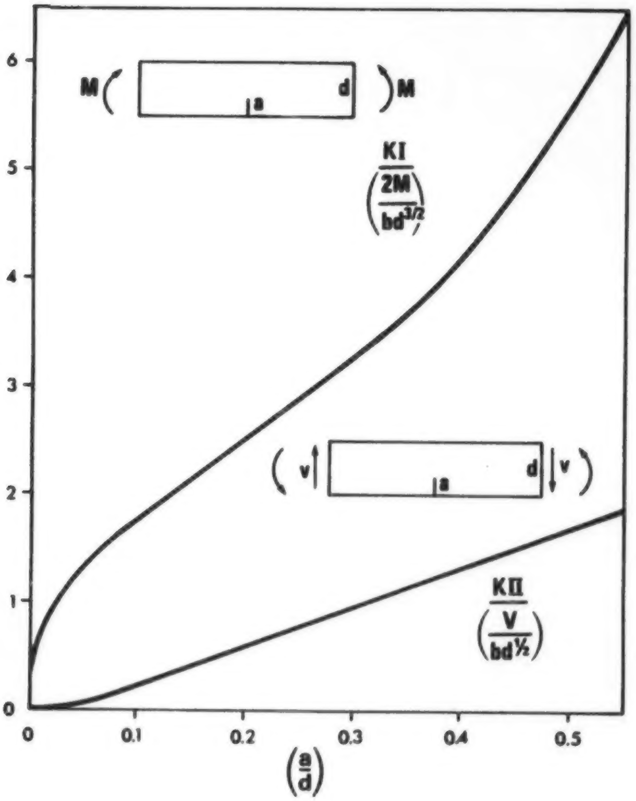

Fig. 5. Dimensionless SIFs for pure moment and balanced shear loadings as a function of relative slit-notch depth.

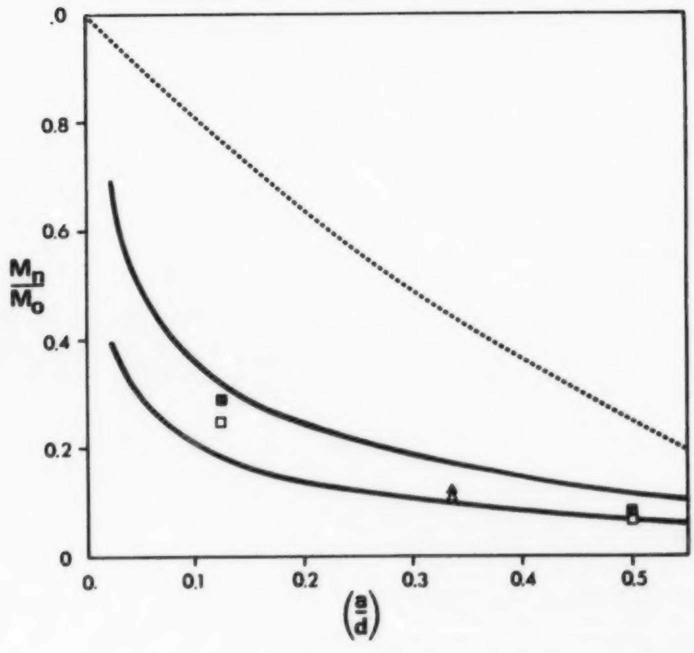

Fig. 6. Ratio of a notched beam's failing load to an unnotched beam's failing load as a function of relative notch depth. (Dashed line represents net section theory; solid lines are derived using LEFM principles. Open data points are from slit-notched beams and closed data points are from rectangular-notched beams.)

# FRACTURE MECHANICS: AN OVERVIEW

By

J.S. Nadeau

---

Department of Metallurgy, University of
British Columbia, Vancouver, B.C.

## INTRODUCTION

Fracture mechanics is the mechanics of cracked bodies. Thus it is a philosophical as well as a technical departure from traditional mechanics. It is based upon the premise that all structural components contain cracks, or incipient cracks, that can cause failure of the component by fracture. The elimination of cracks in structures is not regarded as an attainable goal in fracture mechanics. Instead, the objective is to specify the combination of stress and crack size that will cause failure, and to avoid this combination in practice. Two things are required for this method to succeed. First, there must be a critical crack-tip condition at which fracture will always ensue and, second, there must be a way of calculating the applied loads at which this condition is achieved. Much of the theoretical effort in fracture mechanics has been devoted to analysis of the crack-tip stress field, and to devising simple methods of characterizing it in terms of the applied loads. Experimental efforts have aimed to develop standard tests on small specimens, the results of which can be used to predict the failure conditions for large structures. This paper gives a brief summary of the methods used in fracture mechanics, especially in relation to wood fracture, and describes some cases in which it has been successfully applied.

## STRESSES AHEAD OF CRACKS

The concept of stress concentration is a familiar one and its mathematical formulation dates back to the early part of this century[1] . A simple equation for the tensile stress at the tip of an elliptical hole was given by Inglis in terms of the radius of curvature. When extended to the extreme case of a very flat ellipse, this expression showed that, for a crack having a tip radius of atomic dimensions, the crack-tip stress could be hundreds of times the applied stress. Griffith[2] proposed that it was this crack-tip stress intensification which caused the apparent strength of solids to be far below the theoretical cohesive strength. Using a thermodynamic argument, he derived the famous "Griffith equation" which is an archetype for all fracture criteria; i.e. it specifies the combination of applied stress and crack length at which failure will happen. Since it has a thermodynamic basis, it draws attention away from the crack-tip and concerns itself with the energy flows in the entire system of loads, specimen and crack surfaces. It has been successfully applied to many brittle, linear elastic materials.

The more recent trend in fracture mechanics has been to focus attention on the crack-tip stress field. Both classical and numerical methods have been used to compute the stress distribution ahead of a crack [3,4,5]. The initial objective of these calculations was to develop a fracture criterion, like the Griffith equation, but based upon a crack-tip condition rather than an energy balance in the system. This initial goal has been achieved and now there is a continuing fundamental interest in crack-tip stress fields in elastic-plastic materials[6,7] and in orthotropic materials like wood and composites[8]. An added focus for crack-tip stress field calculations is on complex geometries related to real structures.

The analytical expressions for the stresses ahead of a crack as given by Paris and Sih and, using the coordinate relations of Fig. 1, are:

$$\sigma_x = \frac{\sigma\sqrt{\Pi a}}{\sqrt{2\Pi r}} \cos\phi/2\,[1 - \sin\phi/2\,\sin 3\phi/2] \quad (1)$$

$$\sigma_y = \frac{\sigma\sqrt{\Pi a}}{\sqrt{2\Pi r}} \cos\phi/2\,[1 + \sin\phi/2\,\sin 3\phi/2] \quad (2)$$

$$\sigma_z = \nu\,(\sigma_x + \sigma_y) \quad (3)$$

Irwin[9] pointed out that if we define

$$K_I = \sigma\sqrt{\Pi a} \quad (4)$$

where $\sigma$ is the applied stress and a the crack length, the crack field stresses are related to the distance ahead of the crack by expressions of the form

$$\sigma_x = \frac{K_I}{\sqrt{2r}} \text{ [geometrical term]} \quad (5)$$

$$\sigma_y = \frac{K_I}{\sqrt{2r}} \text{ [another geometrical term]} \quad (6)$$

Thus the magnitude of the stress at a given point in the stress field depends only upon the value of $K_I$ which, in turn, depends only upon the applied stress and the crack length. $K_I$ was named the "stress intensity factor". It is a single-parameter representation of the crack-tip stress field.

## LINEAR-ELASTIC FRACTURE MECHANICS

The basic assumption of linear-elastic fracture mechanics is that fracture occurs at a critical value of K[9]. Thus a fracture criterion that is more general than the one derived by Griffith is:

$$K_{IC} = Y \sigma \sqrt{a} \qquad (7)$$

where $K_{IC}$ is the critical value of the stress-intensity factor, or the "fracture toughness", and Y is a factor that depends upon the geometrical arrangement of loads and crack. The value of Y has been calculated for many different geometries and compilations of these solutions are available[10].

The subscript I in equation (7) designates the opening mode of crack extension in which the crack arms are pulled apart by forces perpendicular to the crack faces. Cracks may also be extended by longitudinal shear (mode II) or tearing (mode III) forces[9].

$K_{IC}$ is a material property in much the same way that the yield stress is a property of metals. Thus one of the main activities in experimental fracture mechanics is to measure $K_{IC}$. Because of the rarity of mode II and mode III failures, $K_{IIC}$ and $K_{IIIC}$ are seldom measured. However, mode II failure in wood is of great importance and is now receiving some attention[11].

$K_{IC}$ is measured on standard specimens for which the relation between K, $\sigma$ and a has been calculated or experimentally calibrated. Two specimens that are used for this purpose are shown in Fig. 2. A test is conducted by loading a specimen until rapid crack propagation occurs and using the load at fracture to compute $K_{IC}$. For metallic specimens there is a standard method for measuring fracture toughness, ASTM E-399-72, and this specification is often used for other materials, including ceramics, wood, cement and concrete. One requirement of the method, which is not easily satisfied in non-metallic materials, is that there be a sharp crack in the specimen. This is achieved in metallic specimens by cyclic loading at a low value of $K_I$, thus producing a fatigue crack. The process that produces fatigue cracks in metals depends upon plastic deformation at the crack tip and thus does not operate in most non-metallic materials. As a result, it is difficult to produce sharp cracks in these materials and often saw cuts are used. This may cause the apparent value of $K_{IC}$ to be inflated.

Since wood is an orthotropic material, it is necessary to specify the crack geometry in relation to the wood structure. The two-letter convention of Schniewind and Pozniak[12] is used, in which the first letter refers to the direction normal to the crack plane and the second letter to the direction of crack propagation (Fig. 3). Thus an RL orientation has the crack in a plane normal to the radial direction in a tree and the crack propagates in the longitudinal direction, i.e. along the axis of a tree. A TR crack propagates in the radial direction and lies on a plane normal to the tangential direction in a tree.

Table I shows values of the fracture toughness for a variety of engineering materials. These values indicate the relative resistance to fracture. In the presence of cracks of equal size, the relative strengths of the various materials are directly proportional to the fracture toughness. All of the materials listed, except for wood, can be regarded as isotropic.

## SUBCRITICAL CRACK GROWTH

In some materials, including wood, cracks may grow slowly even when they are loaded far below the critical stress intensity. If they grow to critical size for the applied stress, rapid fracture follows. This phenomenon is called "stress corrosion cracking" in metals, "static fatigue" in ceramics and "duration of load effect" in wood. It is probably best termed "delayed failure". It appears to be the cause of the time dependence and also of the stress-rate dependence of the strength of brittle materials.

Fig. 4 shows three different ways of examining subcritical crack growth[13]. The most direct way is shown in Fig. 4a and simply involves measuring the rate of crack growth in a standard specimen with known loads. Often, however, it is difficult to see the crack tip in opaque substances and in these cases the changing specimen compliance with increasing crack length can be used as an indication of crack position.

Fig. 4b shows schematically the dependence of strength on duration of load. When slow crack growth is responsible for delayed failure, the slopes of the two plots are related to each other as shown in the figure. Because of this relationship, it is possible to calculate the duration of load curve from the V-K plot by integration between the initial value of stress intensity, $K_{Ii}$, and $K_{IC}$[14].

This integration yields, for the time to failure $\tau$:

$$\tau = 2 K_{Ii}^{(2-n)} / (n-2)\ Y^2 \sigma_a^2\ A \qquad (8)$$

where n is the slope of the log V - log $K_I$ plot, log A is the intercept, and $\sigma_a$ is the applied stress. Employing the relationship $K_{Ii}/\sigma_a = K_{Ic}/\sigma_f$, where $\sigma_f$ is the instantaneous fracture stress, we obtain

$$\tau = 2 \left[K_{IC} \frac{\sigma_a}{\sigma_f}\right]^{(2-n)} / (n-2)\, Y^2 \sigma_a^{\ 2}\ A \qquad (9)$$

Since this expression is based on a V - K plot having the form $V = AK_I^{\ n}$, it is only valid over the range where that form is obeyed. Thus it is not advisable to extrapolate beyond the range of the experimental data to obtain long-life strengths from short-time crack growth studies. However, the method can be used to measure the relative susceptibility to delayed failure of various materials, or of the same material in various environments. A delayed failure resistance index can be calculated by comparing the time to failure of a subject material to that of a standard material[15]. (An alternative method is to consider all materials with the same initial crack length.) The D.F.R.I. for a number of materials compared with soda-lime glass in water is given in Table II. The higher the value of the D.F.R.I., the greater is the resistance to delayed failure. The value shown for wood was obtained in tension perpendicular to the grain. There is evidence that for tension parallel to the grain, the more normal loading geometry, there is greater degradation of strength with time, that is the D.F.R.I. is lower[13].

Fig. 4c shows schematically the influence of subcritical crack growth on the strength of ramp-loaded specimens. At the higher loading rates, the crack has less time to grow and thus failure occurs at a higher stress. An excellent example of this effect was shown by Chandan *et al.*[16], with soda-lime glass in water, Fig. 5. Using conventional tests and instrumented impact tests, the stress rate was varied over six orders of magnitude. The fracture stress increased by a factor of about 3.4 over that range, but more significantly the slope of the plotted data was very close to the slope of the V - $K_I$ plot. Similar tests on Douglas-fir in tension perpendicular to the grain have produced the same kind of agreement between the two methods[13].

## THE USES OF FRACTURE MECHANICS

The information provided by fracture mechanics tests and its mathematical formalisms can be put to two purposes. They can be used in the design of structures and components or they can be used to understand and improve the fracture resistance of materials.

Traditional engineering design has been based upon the avoidance of tensile overload or of buckling. The avoidance of brittle fracture was generally achieved by certain design practices, based upon experience and knowledge about load distribution and stress concentration. Materials selection was also based upon a somewhat intuitive understanding of fracture resistance. Now it is possible to embed fracture mechanics principles in the design process. The simplest step is the quantitative specification of the fracture resistance of materials, as shown in a superficial form in Table I. Fracture toughness data on engineering materials are proliferating and the designer is now able to make his material selection accordingly. However, more information is needed about variations in toughness of wood before this property can become a useful design choice.

A second step in the application of fracture mechanics to design is to recognize the relation, as given in equation 7, between flaw size and failure stress. Since the stress in most structural members is dictated by a design code based upon the yield stress (in metals) or the fracture stess (in timber), equation 7 enables the designer to calculate the critical flaw size at the design stress. He can then specify the largest allowable flaw size in his structure and indicate suitable inspection methods to guarantee that no flaws exceed this size. The stress-flaw size relationship for Douglas-fir in tension parallel to the grain is shown in Fig. 5. The shaded area shows the range of recommended working stresses for dimension lumber. Since it is not possible to select lumber on the basis of fracture toughness, as is the practice with steel, for example, the selection must be based on this flaw-size strength plot.

The third step in integrating fracture mechanics with design is to adopt probabilistic methods. A combination of proof testing, Weibull statistics and fracture mechanics has been used to develop "Risk of Failure" diagrams[16,17,18]. This method is based upon equation 9, which gives the life expectancy of a stressed member as a function of the ratio of applied stress, $\sigma_a$, to the instantaneous breaking strength, $\sigma_f$. When plotted on log coordinates, equation 9 gives a single straight line as in Fig. 4b. However, we must recognize that the experimental quantities used to plot this line would typically be the mean values of a large number of tests. The plotted line would then represent the median specimens. Some specimens would fail at longer times and some at shorter times. If we consider the *distribution* of failure times at a given stress, i.e. if we use probabilistic methods, it is possible to plot a band, i.e. a range of times, within which a specified fraction of the specimen population will fail when subjected to a particular stress. This is shown schematically in Fig. 7. For many brittle materials, including wood, the distribution of initial flaw sizes is very broad and therefore the distribution of failure times at constant stress is also broad. This forces the designer, who aims for a very low failure probability, to treat the whole population as though it were no stronger than the weaker members. The way of more efficiently utilizing the strong members of a population of structural components is by removing the weak ones. This can be done by inspection, as in the grading of wood or by proof testing, i.e., applying a stress greater than the expected service stress and thus breaking the weaker specimens. The effect of both methods is to limit the maximum flaw size, although the inspection method will obviously miss flaws that are hidden.

Thus probabilistic methods, combined with inspection and proof testing, have two benefits. They allow more efficient use of the stronger members of a group of specimens and they allow the designer to choose the stress in his design on the basis of the failure probability at that stress.

## SUGGESTIONS FOR FUTURE WORK ON THE FRACTURE MECHANICS OF WOOD

1. The duration-of-load effect has great importance in the design of wood structures. Slow crack-growth studies should be conducted at very low stresses to permit predictions of the duration-of-load effect at long times.

2. Since mode II (longitudinal shear) is a common failure mode for wood, slow crack-growth studies should be conducted in this mode.

3. The failure origins in wood should be

identified and examined. This could lead to increased understanding of the failure mechanisms and to the development of improved inspection methods.

## REFERENCES

1. Inglis, C.E. 1913. Stresses in a Plate due to the Presence of Cracks and Sharp Corners. Proc. Inst. Naval Architects.
2. Griffith, A.A. 1920. The Phenomena of Rupture and Flow in Solids. Phil. Trans. Roy. Soc., London A. 221: 163-198.
3. Paris, P.C. and G.C. Sih. 1964. Stress Analysis of Cracks. ASTM Special Technical Publication 381 p. 30-81.
4. Knott, J.F. 1973. Fundamentals of Fracture Mechanics. Butterworth, London. p. 46-93.
5. Rice, J.R. 1968. Mathematical Analysis of the Mechanics of Fracture. Fracture, an Advanced Treatise, II, Academic Press, New York.
6. Rice, J.R. 1968. A path independent integral and the approximate analysis of strain concentration by notches and cracks. Journal of Applied Mechanics (trans. ASME), Series E 35:379-386.
7. Begley, J.A. and J.D. Landes. 1972. The J - Integral as a Fracture Criterion. ASTM Special Technical Publication 514, p. 1-20.
8. Foschi, R.O. and J.D. Barrett. 1976. Stress Intensity Factors in Anisotropic Plate Using Singular Isoparametric Elements. Journal for Numerical Methods in Engineering 10(6):1281-1287.
9. Irwin, G.R. 1958. Fracture: Encyclopedia of Physics VI, Springer, Heidelberg.
10. Hiroshi, Tada. 1973. The Stress Analysis of Cracks Handbook. Del Rio Corp., Hillertown, PA.
11. Barrett, J.D. and R.O. Foschi. 1977. Mode II stress-intensity factors for cracked wood beams. Engineering Fracture Mechanics 9(2):371-378.
12. Schniewind, A.P. and R.A. Pozniak. 1971. On the fracture toughness of Douglas-fir wood. Engineering Fracture Mechanics 2:223-233.
13. Mindess, S., J.S. Nadeau and J.D. Barrett. 1976. Effect of constant deformation rate on the strength perpendicular to the grain of Douglas-fir. Wood Science 8 (4):262-266.
14. Evans, A.G. and S.M. Wiederhorn. 1974. Proof Testing of Ceramic Materials: an Analytical Basis for Failure Prediction. Int. Journal of Fracture 10(3): 379-392.
15. Nadeau, J.S. and J.N. Hay. 1974. An index of resistance to delayed failure. Journal of Can. Ceram. Soc. 43:31-36.
16. Chandan, H.C., R.C. Bradt and G.E. Rindone. 1978. Dynamic fatigue of float glass. Journal American Ceram. Soc. 61 (5-6):209-210 .
17. Davidge, R.W. J.R. McLaren and G. Tappin. 1973. Strength-probability - time (SPT) relationships in ceramics. Journal Material Science 8:1699-1705.
18. Wiederhorn, S.M., E.R. Fuller, J. Mandel and A.G. Evans. 1976. An error analysis of failure prediction techniques derived from fracture mechanics. Journal American Ceram. Soc. 59:403-411.

Table I

SOME TYPICAL VALUES OF THE ROOM-TEMPERATURE FRACTURE TOUGHNESS, $K_{IC}$

| MATERIAL | $K_{IC}$ ($\mathrm{MNm}^{-3/2}$) |
|---|---|
| HY 130 STEEL | 249 |
| "CONSTRUCTION" STEEL | 110 |
| 7001 –T75 ALUMINUM | 20 |
| UNFILLED EPOXY | 6 |
| DOUGLAS-FIR WOOD (LT) | 2 |
| (RL) | 0.3 – 0.4 |
| WINDOW GLASS | 0.7 |
| CONCRETE | 0.4 – 1.0 |

Table II

DELAYED FAILURE RESISTANCE INDEX

$$\mathrm{DFRI} = \log(\tau_x/\tau_G) = -4.066 - n_x \log\left(\frac{K_{IC(x)}}{2}\right)$$

$$- \log(n_x - 2) - \log A_x$$

| MATERIAL | DFRI |
|---|---|
| SODA-LIME GLASS IN WATER | 0. |
| SODA-LIME GLASS IN TOLUENE | 4.21 |
| PORTLAND CEMENT PASTE IN WATER | 3.57 |
| DOUGLAS-FIR (RL) IN AIR | 13.8 |
| PYROLYTIC GRAPHITE IN AIR | 60.58 |

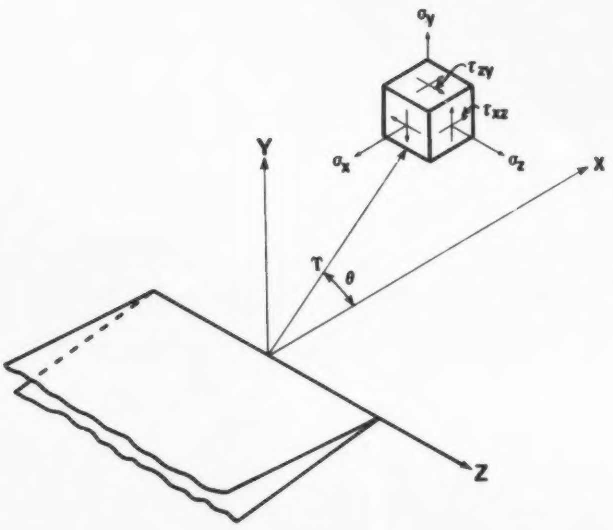
$\sigma_y$
$\tau_{zy}$
$\tau_{xz}$
Y
$\sigma_x$
$\sigma_z$
X
r
$\theta$
Z

Figure 1. Coordinate system used for describing the stresses ahead of a crack. From P.C. Paris and G.C. Sih[3].

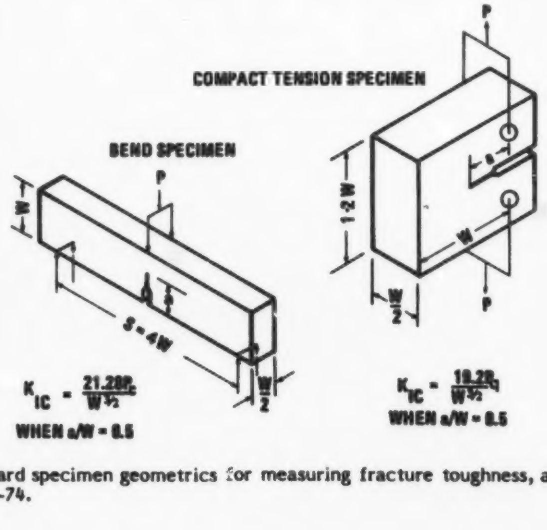
P
COMPACT TENSION SPECIMEN
BEND SPECIMEN
P
W
a
S = 4W
$\frac{W}{2}$
$K_{IC} = \frac{21.20P_c}{W^{3/2}}$
WHEN a/W = 0.5
1·2W
a
W
$\frac{W}{2}$
P
$K_{IC} = \frac{18.2P_Q}{W^{3/2}}$
WHEN a/W = 0.5

Figure 2. Standard specimen geometrics for measuring fracture toughness, according to ASTM, E-399-74.

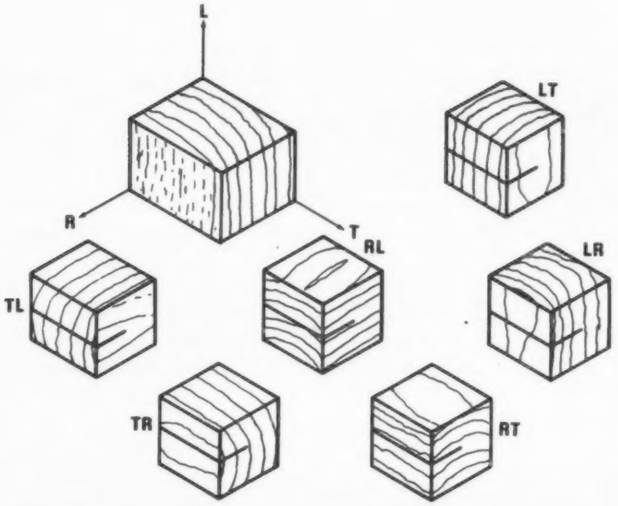

Figure 3. Three-letter system for designating orientation relations in wood, according to A.P. Schniewind and R.A. Pozniak[12]. The first letter gives the normal to the crack plane and the second, the direction of propagation.

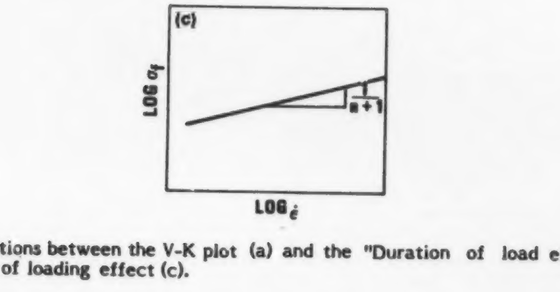

**Figure 4. Relations between the V-K plot (a) and the "Duration of load effect" (b) and the rate of loading effect (c).**

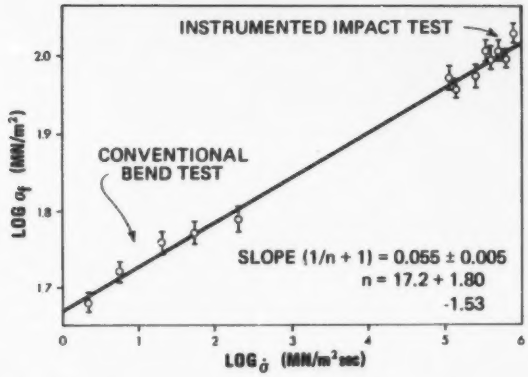

Figure 5. Effect of loading rate on strength for glass. Courtesy of H.C. Chandan, R.C. Bradt and G.E. Rindone[16].

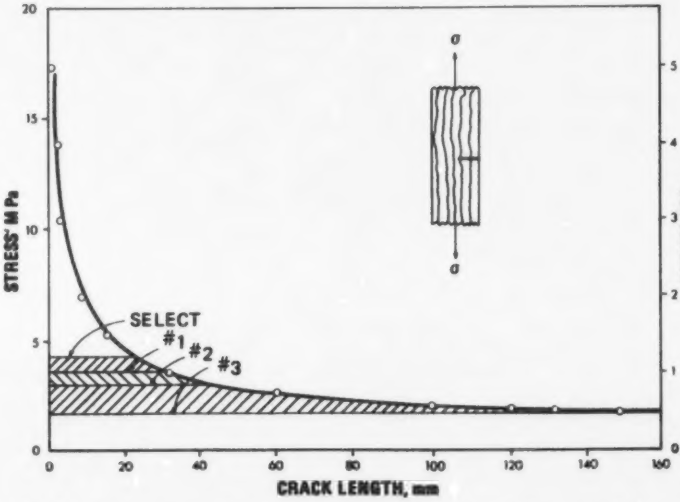

Figure 6. Breaking stress versus flaw size for Douglas-fir in tension parallel to the grain, according to the relation $K_{IC} = 1.12\,\sigma\sqrt{\pi a}$. Value of $K_{IC}$ from A.P. Schniewind and R.A. Pozniak[12], approximately 2.5 MN m$^{-3/2}$. Shaded area shows range of working stresses for dimension lumber.

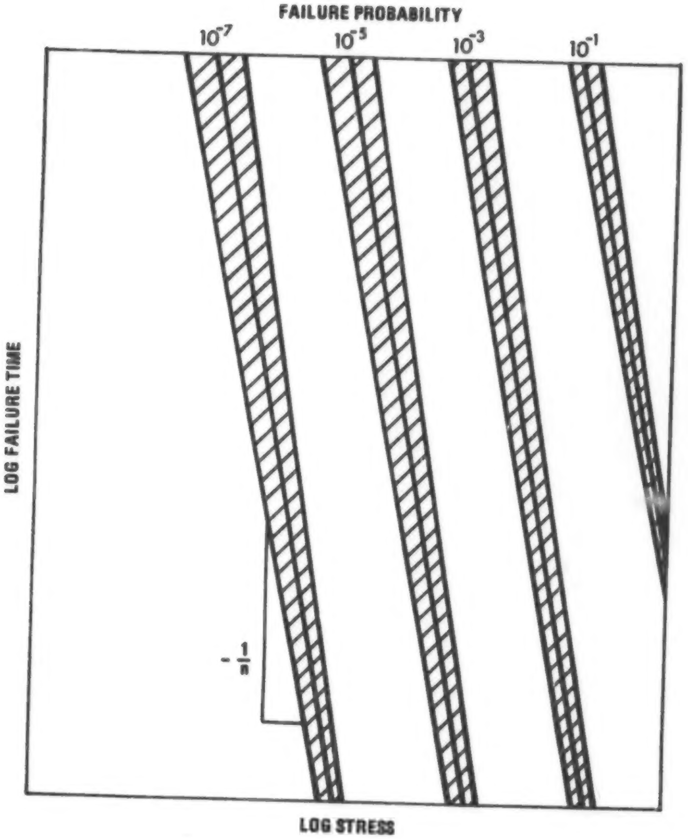

Figure 7. "Risk of failure plot" (schematic). The probability of failure is computed from the Weibull statistics of rapid fracture. Shaded bands show confidence limits at each probability.

# CRACK FAILURE OF DEAD-, RAMP- AND COMBINED-LOADED VISCOELASTIC MATERIALS

By

Lauge Fuglsang Nielsen

---

The Technical University of Denmark, Department of Civil Engineering, Building Materials Laboratory, Brygning, Denmark

## ABSTRACT

A method is developed which determines the lifetime of cracked, linear viscoelastic materials subjected to dead-, ramp- and combined loading. Two failure criteria are used: (1) failure is the state where cracks start propagating, (2) failure is the state where the rate of crack propagation increases catastrophically - leaving no load capacity back.

## INTRODUCTION

Mechanical tests of materials are often performed applying a combination of two types of loading histories, namely dead- and ramp loading. Mathematically we define

*Dead load:*

$$\sigma = \sigma^x H(t) \qquad (1)$$

*Ramp load:*

$$\sigma = ktH(t) \qquad (2)$$

where the meanings of the symbols are given in Figure 1. Heaviside's step function is denoted by H(t).

While ramp loading is relatively easy to establish, the true dead loading exists only in theory (at any rate when static situations are considered). It always takes a certain time, $t_0^x$ to apply a constant load. We will assume that the constant load level is reached by ramp loading. Compare Figure 1 the load history is now defined by

*Combined load:*

$$\sigma = \frac{\sigma^x}{t_0^x}\left\{tH(t) - (t - t_0^x)\, H\,(t - t_0^x)\right\} \qquad (3)$$

In the following we will analyze how the above defined loading types influence the time to failure of a cracked, linear viscoelastic test specimen. Primarily we will think of plane stress situations where the stress picture around the crack may be approximated to be similar to the one which applies to a central crack in an infinite sheet or an edge crack in a semi-infinite sheet subjected to tension, σ perpendicular to the crack plane (opening mode I). Other situations, however, may be analyzed in a manner quite analogous - giving results strongly familiar with those developed in the paper. The material is homogeneous and isotropic, or orthotropic with the crack plane coinciding with two materials principal axes. In the latter case, the creep functions associated with the elastic moduli must be congruent to each other (balanced creep). The Young's modulus and the creep function applied in the theory may be thought of as applying to the stress direction. At the same time, the critical energy release rate used should be considered as the orthotropic one associated with the crack plane - multiplied by a dimensionless factor which depends on all four elastic coefficients. However, as both the Young's modulus and the critical energy release rate in the final results exclusively appear in the "critical stress" introduced, the calculations need not differentiate between the orthotropic and the isotropic situation.

Time to failure is defined in two different ways: (1) failure is the state where materials damage (crack propagation) starts. This criterion may be considered to give a lower limit and thus a "safe" time to failure estimation; (2) failure is the state where the damage has reached a level where no load capacity is left back. The failure develops catastrophically because the rate of crack propagation has become very high. The time to reach this state may be considered as the upper-limit estimation of time to failure.

Both criteria are treated according to a theory given by the present author in (1). The first criterion is relatively easy to handle - and as the results are easy seen through, this criterion is used to illustrate the general consequences of applying the three loading types previously described. The mathematics of handling the second criterion is in general somewhat more complicated. Therefore, the discussion of this criterion is partly related to a specific creep function which allows for relatively simple solutions. In principle, however, the methods described are valid for arbitrary creep functions.

Figure 2 shows in principle the failure curves expected and the stress and time terminology applied in the following.

## THEORY

According to the linear-crack theory, the stress intensity factor, $K_I$, is expressed in the following way by the stress, $\sigma$, and the crack length, $2x$:

$$K_I^2 = \sigma^2 \pi x \qquad (4)$$

The crack is just about to propagate when the intensity factor reaches a critical value, $K_{I,cr}$, which is related to the so-called critical energy release rate, $\xi_{cr}$, by the following relation:

$$K_{I,cr}^2 = E\xi_{cr} \qquad (5)$$

where E is the Young's modulus. Thus, for a given crack length $2x_0$ the critical stress, $\sigma_{cr}$, at which the crack is just about to propagate is determined by:

$$\sigma_{cr} = \sqrt{\frac{E\xi_{cr}}{\pi x_0}} \qquad (6)$$

Introducing eq. 6 into eq. 4, the stress intensity factor may be written as:

$$K_I^2 = \left(\frac{\sigma}{\sigma_{cr}}\right)^2 \frac{x}{x_0} E\xi_{cr} \qquad (7)$$

### Time to start of crack propagation

According to (1) a crack starts to propagate at $t = t_s$ when:

$$\int_0^{t_s} c(t_s - \theta) \frac{dK_I^2}{d\theta} d\theta = \xi_{cr} \qquad (8)$$

where $K_I$ is given by eq. 7 with $x = x_0$. The creep function, $c(t)$, is given by:

$$c(t) = \frac{1}{E}\left\{1 + \mu t + \sum_1^N \alpha_q (1 - e^{-\mu_q t})\right\} \qquad (9)$$

where $\mu$, $\mu_q$ and $\alpha_q$ are materials constants. (In the mechanical analogy, the first and second terms correspond to a spring and a dashpot, respectively. Together they describe a Maxwell model. The summation term describes the behavior of a number of Kelvin elements in series. The Burger material is characterized by N=1).

Introducing the abbreviations

$$Y = \left(\frac{\sigma_{cr}}{\sigma^x}\right)^2 \text{ and } Y_{os} = \left(\frac{\sigma_{cr}}{\sigma_{os}}\right)^2 \qquad (10)$$

and combining eq. 8 with eqs. 1-3, we get the following expressions determining the time to start of crack propagation:

*Dead load:*

$$Y = Ec(t_s) \; ; \; (t_s = F(Y), \text{compare eq. 18}) \qquad (11)$$

*Ramp load:*

$$Y_{os} = \frac{2}{t_{os}^2} \int_0^{t_{os}} \theta E c(t_{os} - \theta) \, d\theta \qquad (12)$$

*Combined load:*

$$Y = \frac{2}{(t_0^x)^2} \int_0^{t_0^x} \theta E c(t_s - \theta) \, d\theta \qquad (13)$$

where the time, $t_0^x$ at which the load becomes constant is determined by $t_{os}$ from eq. 12 and

$$t_0^x = \frac{\sigma^x}{\sigma_{os}} t_{os} = \sqrt{Y_{os}/Y} \cdot t_{os} \qquad (14)$$

### Time to catastrophic failure

For a *constant* load, $\sigma^x$, the following expression determining the crack velocity may be developed (1).

$$K_I^2\, c \left\{ \frac{\pi^2}{8(1+Q)} \left(\frac{\sigma^x}{\sigma_1}\right)^2 \frac{x}{v} \right\} = \xi_{cr}\ ; \left(v = \frac{dx}{dt}\right) \quad (15)$$

Here Q is a constant, the theoretical value of which is 2-3. $\sigma_1$ is the limiting strength of the material, i.e. the strength of a very clean, uncracked specimen.

Introducing $K_I$ from eq. 7 together with the abbreviations 10 and

$$P = \frac{8(1+Q)}{\pi^2} \left(\frac{\sigma_1}{\sigma_{cr}}\right)^2 \quad (16)$$

eq. 15 may be rewritten as

$$Ec\left(\frac{x}{PYv}\right) = \frac{Yx_o}{x} \quad (17)$$

Defining a new function, F as the inverse of the creep function times E, i.e.

$$F\{Ec(t)\} = t \quad (18)$$

the crack velocity may be described explicitly by eq. 17. We get

$$\frac{1}{v} = PY \frac{F(Yx_o/x)}{x} \quad (19)$$

By integration of this expression, we get the period of time between crack position $x_{n-1}$ and $x_n$ as

$$t_n - t_{n-1} = PY \int_{Yx_o/x_n}^{Yx_o/x_{n-1}} F(\theta)/\theta \; d\theta \quad (20)$$

The period of time between the start of crack propagation, $t_s$, and catastrophic failure is obtained by setting $(x_{n-1}, x_n) = (x_o, Yx_o)$. The result is

$$t_{cat} - t_s = PY \int_1^Y \frac{F(\theta)}{\theta}\, d\theta \quad (21)$$

It should be noticed that the above equations apply irrespective of the load history before the time at which it becomes constant. Thus the time to catastrophic failure for dead- and ramp-load situations may be determined by eqs. 11, 12 and 13, 21 respectively. For the latter case, however, we must require $\sigma^x \leq \sigma_{os}$. Above this level, cracks propagate while ramp loading - and we must use the following procedure.

When a crack propagates *under varying* load, we may apply eq. 20 in a step by step procedure, i.e.

$$\Delta_n t = P\bar{Y} \int_{\bar{Y}x_o/x_n}^{\bar{Y}x_o/x_{n-1}} F(\theta)/\theta \; d\theta \quad (22)$$

where $\bar{Y}$ is determined by eq. 10 at a mean stress, $\bar{\sigma}^x$ between $t_{n-1}$ and $t_n$. A presumption for the use of eq. 22 is that $x_n \geq x_{n-1}$, i.e. the crack velocity must be non-negative. First time the lower limit of integration becomes greater than 1, catastrophic failure has just occurred.

The factor P applied in the above equations has been discussed in (1). It was found by deductions from results of experiments on polyurethan elastomer that the values of Q and $\sigma_1$ in practice may differ considerably from what is expected theoretically ($Q = 2\text{-}3$, $\sigma_1 = 0.1\text{-}0.01E$). It was concluded, for several reasons, that $(1+Q)\sigma_1^2$ for the present must be taken as a materials constant which characterize the "real" effect of the shape of and the coherence in the crack tip. The effect of changing P is practically a translantional shift along the log(time) axis.

## EXAMPLES: TIME TO START OF CRACK PROPAGATION

### General Solutions

If we define failure as the state where crack propagation starts, the relationships between lifetime, $t_s$, loading history and load level are determined through the eqs. 9 and 11-13. The results are:

*Dead load:*

$$Y = Ec(t_s) \tag{23}$$

*Ramp load:*

$$Y_{os} = 1 + \frac{1}{3}\mu t_{os} + \sum_{1}^{N}\alpha_q \left\{1 - \frac{2}{\mu_q t_{os}} + \frac{2}{(\mu_q t_{os})^2}(1 - e^{-\mu_q t_{os}})\right\} \tag{24}$$

*Combined load:*

$$Y = 1 + \mu t_s \, {}^{2}/_{3} \, \mu t_o^x + \sum_{1}^{N}\alpha_q \left(1 - \frac{2}{(\mu_q t_o^x)^2} e^{-\mu_q t_s}\left\{1 + (\mu_q t_o^x - 1)\, e^{\mu_q t^x_o}\right\}\right) \tag{25}$$

where $t_o^x$ is determined by eq. 24 and 14.

**Small time solutions**

For small times, the creep function may be written

$$c(t) = \frac{1}{E}(1 + \rho t) \quad ; \quad (\rho = \mu + \sum_{1}^{N}\alpha_q \mu_q) \tag{26}$$

In fact, this is the creep function for a Maxwell material with $\mu = \rho$. Therefore the following solutions apply exactly to this material. From eqs. 23-25 or directly from eqs. 11-13 we get

*Dead load:*

$$\rho t_s = Y - 1 \tag{27}$$

*Ramp load:*

$$\rho t_{os} = 3(Y_{os} - 1) \tag{28}$$

*Combined load:*

$$\rho t_s = Y - 1 + 2(Y_{os} - 1)\sqrt{Y_{os}/Y} \tag{29}$$

From eqs. 27 and 29 we get the following relation between failure time, $t_s^C$ for combined load and failure time, $t_s^D$ for dead load

$$\frac{t_s^C}{t_s^D} = 1 + 2\sqrt{Y_{os}/Y}\;\frac{Y_{os} - 1}{Y - 1} \tag{30}$$

For pure ramp load ($Y \to Y_{os}$), eq. 30 tells us that failure time is three times greater than the corresponding time for dead load. Together with $Ec(t_{os})$, eq. 30 is illustrated in Figure 3. The figure may be used in the following way: In the ramp load experiment the short time "strength", $\sigma_{os}$ has been reached in a period of time, $t_{os}$ for which the creep function has developed a value corresponding to $Ec(t_{os}) = 1.12$. Now we read that the strength measured ($\sigma_{os}$) is 98% of the max. obtainable strength, i.e. the critical value, $\sigma_{cr}$. At the same ramp loading rate, a combined load of $\sigma^x/\sigma_{cr} = 0.9$ ($\sigma^x/\sigma_{os} = 0.92$) will produce failure after a time, $t_s^C$, which is 1.32 greater than the corresponding time for dead load, $t_s^d$.

It may also be observed that results from combined load experiments are practically equal to those from dead load experiments, if the short time strength ($\sigma_{os}$) has been measured in a period of time for which the creep function does not increase more than approximately 5% ($Ec(t_{os}) < 1.05$).

The results of an analysis of a Burger material are shown in Figures 4 and 5. The equations applied are 23-25, (N=1). The Burger material has been chosen because this model illustrates in the simplest way all the features which apply to the failure criterion used. The materials constants have been given values as to give a reasonable picture of the behavior of wood for loading periods less than about 10 years, $(\alpha = \alpha_1,\ \mu/\mu_1 = \mu/\mu_K) = (.75, .001)$.

For the example chosen, we notice: (1) $t_s^R/t_s^D$ is approximately 3 at early and late times, where the material acts as a Maxwell material. This is in agreement with eq. 30 above. (2) The "Kelvin plateau" is approximately $\log_{10}(\mu/\mu_K)$ decades wide, starting at $\log_{10}(\mu_K t) = 0\text{-}1$. (3) Combined-, ramp- and dead-load capacities are nearly coinciding at the middle of the plateau mentioned. (4) Combined load curves drop from ramp to dead-load curve in approximately one decade. (5) For $\mu_K t_{os}$ (time to short-time failure) less than about 0.1, all combined load curves are practically equal to the dead-load curve. This agrees with the above comments to eq. 30 and Figure 3.

## EXAMPLE: TIME TO CATASTROPHIC FAILURE

In the preceding section, we have determined the time to crack propagation starts, $t_s$. The real (catastrophic) failure, however, takes place at a later time, $t_{cat}$ which - for constant load after $t_s$ - is determined by eq. 21. In general, numerical procedures have to be applied. An exception, however, is found when the creep function may be expressed by

$$c(t) = \frac{1}{E}(1 + At^{1/m}) \qquad (31)$$

where A and m are materials constants. We will choose this creep function to demonstrate some aspects of the difference between the results of the two failure criteria in question.

The inverse function of the creep function times E is derived as

$$F(t) = \left(\frac{t-1}{A}\right)^m \qquad (32)$$

which - through eq. 21 - produces the time to catastrophic failure by

$$A^m(t_{cat} - t_s) = P \cdot Y \int_1^Y \frac{(\theta - 1)^m}{\theta}\, d\theta \qquad (33)$$

The expression is valid for combined load at $\sigma^x \leq \sigma_{os}$ - and for dead load. For some m we may develop eq. 33 analytically. For example.

$$A^4(t_{cat} - t_s) = PY\left(\frac{1}{4}Y^4 - \frac{4}{3}Y^3 + 3Y^2 - 4Y + \ln(Y) + \frac{25}{12}\right) \;;\; (m = 4) \qquad (34)$$

Time to start of crack propagation is determined by eqs. 11-13:

*Dead load:*

$$t_s = F(Y) = A^{-m}(Y - 1)^m \qquad (35)$$

*Ramp load:*

$$t_{os} = \left\{\frac{(1+m)\ (1+2m)}{2Am^2}\ (Y_{os} - 1)\right\}^m \qquad (36)$$

*Combined load:*

$$Y = 1 + \frac{2Am}{(1+m)(1+2m)(t_o^x)^2} \left\{mt_s^{(1+2m)/m} - (t_s - t_o^x)^{(1+2m)/m} \left(\frac{(1+2m)t_s}{t_s - t_o^x} - 1 - m\right)\right\} \qquad (37)$$

where the time, $t_o^x$, at which the load becomes constant is determined by eq. 36 and eq. 14.

For (A,m,P) = (1/3,4,50) Figure 6 shows the life-time curves corresponding to dead load (eqs. 34,35). The numerical values of A and m are chosen as to get some relevance to the behavior of wood (at approximately 2 days and 10 years eq. 31 coincides with the creep function applied in the preceding section). The factor P (which is only needed for the analysis of running crack situations) is calculated from eq. 16 with Q=3 and a presumed critical stress of about 25% of the limiting stress, $\sigma_1$.

Figure 6 also shows the ramp load life time curves. The results are here obtained by eqs. 36 and 22. (The numerical integration in eq. 22 has been performed using only one step and letting $\sigma^x = \sigma_n$. This is a safe solution.)

It is noticed that the time difference between start of crack propagation and the final failure may be quite considerable. Further, it may be noticed that the ramp-load curves are practically shifts of the dead-load curves. The factor may be taken as approximately 3 which is the value previously derived for small time (and Maxwell) solutions.

The thin lines in Figure 6 refer to combined load experiments on wood (2,3). Assuming a creep behavior similar to the one theoretically applied - and assuming that the constant load has been established for $Ec(t_o) \leq 1.05$, the experimental values may be compared directly with the theoretical dead-load results. (It should be noticed that a creep function, as the one theoretically applied, has an infinite initial developing rate. At very early ages this may cause a strength decrease which might be somewhat overestimated).

## SOME OTHER FAILURE CRITERIA

Quite a number of failure criteria are available. Many - like the two demonstrated below - predict failure to occur when different types of energy transformed in the material reach some critical values. Such criteria, which are not directly based on failure mechanisms (ex. crack), are often referred to as phenomenological failure criteria. When linear constitutive equations are assumed, such criteria cannot count for the effect of progressing damage. Consequently, the results of the two "liner" criteria treated below should be compared with crack criterion (1) mentioned in the introduction, which predict failure when a crack starts running. Therefore a terminology similar to this criterion has been chosen.

*Critical total energy:*

$$W_{cr} = 1/2 \frac{\sigma_{cr}^2}{E} = 1/2 \frac{\sigma^2}{E} + \int_0^{t_s} \sigma \frac{d\epsilon}{d\tau} \, d\tau \tag{38}$$

where

$$\epsilon(t) = \int_0^t c\,(t-\tau) \frac{d\sigma}{d\tau} d\tau \tag{39}$$

This criterion tells us that failure occurs when the total energy transformed in the material reaches the critical value, $W_{cr}$, which may be expressed by the critical stress, $\sigma_{cr}$ (max. load capacity in dead-load experiment). We may rewrite eq. 38 as follows

$$\left(\frac{\sigma_{cr}}{\sigma}\right)^2 = 1 + \frac{2E}{\sigma^2} \int_0^{t_s} \sigma \frac{d\epsilon}{d\tau} \, d\tau \tag{40}$$

which yields the following special solutions.

*Dead load:*

$$Y = 1 + 2\mu t_s + 2\sum_1^N \alpha_q \left(1 - e^{-\mu_q t_s}\right) = 2Ec(t_s) - 1 \tag{41}$$

*Ramp load:*

$$Y_{os} = 1 + \frac{2}{3}\mu t_{os} + \sum_1^N \alpha_q \left(1 + \frac{2}{\mu_q t_{os}} e^{-\mu_q t_{os}} - \frac{2}{(\mu_q t_{os})^2} \{1 - q^{-\mu_q t_{os}}\}\right) \tag{42}$$

where Y and $Y_{os}$ are defined by eq. 10.

**Critical reversible energy**

$$W_{cr} = 1/2 \frac{\sigma_{cr}^2}{E} = 1/2 \frac{\sigma^2}{E} + \frac{1}{2E} \sum_1^N \alpha_q \left\{ \int_0^{t_s} \left(1 - e^{-\mu_q (t_s - \tau)}\right) \frac{d\sigma}{d\tau} \, d\tau \right\}^2 \tag{43}$$

This criterion tells us that failure occurs when the elastically stored energy (in the springs of the mech. model) reaches a critical value expressed by the critical stress defined in the preceding section. This concept is often referred to as the Reiner-Weisenberg failure criterion, see (4,5). We may rewrite eq. 43 as follows

$$\left(\frac{\sigma_{cr}}{\sigma}\right)^2 = 1 + \frac{1}{\sigma^2} \sum_1^N \alpha_q \left\{ \int_0^{t_s} \left(1 - e^{-\mu_q (t_s - \tau)}\right) \frac{d\sigma}{d\tau} \, d\tau \right\}^2 \tag{44}$$

The following special solutions apply to eq. 44.

*Dead load:*

$$Y = 1 + \sum_{1}^{N} \alpha_q \left(1 - e^{-\mu_q t_s}\right)^2 \qquad (45)$$

*Ramp load:*

$$Y_{os} = 1 + \sum_{1}^{N} \alpha_q \left(1 - \frac{1}{\mu_q t_{os}} \left(1 - e^{-\mu_q t_{os}}\right)\right)^2 \qquad (46)$$

where $Y$ and $Y_{os}$ are defined by eq. 10.

In Figure 7 the critical energy criteria just described are compared with the criterion based on initiating crack propagation. It is noticed that the crack criterion determines a time to failure which lays between the values predicted by the other criteria. The failure time gap for the total energy criterion is considerably greater than described by the other methods. Contrary to the other criteria, the reversible energy criterion predicts a load level below which no failure can occur - irrespective of deformation. All curves - except the total energy dead-load curve - nearly coincide at the "Kelvin plateau". The exception has a plateau at $\sigma^x/\sigma_{cr} = 1/\sqrt{1+2\alpha}$.

## FINAL REMARKS

In connection with Figure 3, it was proposed that combined- and dead-load results are practically equal, if the latter are based on a time-to-max.-load capacity for which the creep function does not increase more than about 5%. The conclusion was based on the start of crack propagation criterion. However, it is even more relevant for the catastrophic failure criterion because the life-time curves in this case lay above those associated with the first-mentioned criterion.

In general, we may think of a ramp-load life-time curve which is practically a simple shift of the dead-load curve. The factor may be taken as approximately 3. The combined load curves are placed in between, starting on the ramp-load curve and dropping to the dead-load curve in about one decade of time. This indicates an easy way of constructing life-time curves.

Figure 6 indicates a reasonable agreement between experiments on wood and the theory presented. It must, however, be emphasized that comparing theory with experiments - or experiments with experiments - without knowing the actual creep functions may be somewhat questionable. A variation of the parameters A and m used for the theoretical results of Figure 6 will show that it is certainly not enough comparing two sets of data by scaling or shifting according to short-time behavior (see also Figure 5).

It has been intimated that the factor P, which practically shifts the life-time curves along the time axis, may have a value different from (greater than) the theoretical value. The factor has to be determined by experiment. The factor P = 50 used in the paper is considered to be a minimum; i.e., in practice we may, for example, expect the catastrophic failure curves in Figure 6 to be shifted to the right - eventually by one decade.

## LITERATURE

1. Nielsen, L.F. 1978. Crack propagation in linear viscoelastic materials. Bygningsstatiske Meddelelser (Copenhagen) *49* (1).

2. Pearson, R.G. 1972. The effect of duration of load on the bending strength of wood. Holzforschung *26(4)*.

3. Madsen, B. and Barrett, J.D. 1976. Time-strength relationship for lumber. Univ. B.C., Dep. Civil Eng., Struct. Res. Series Rep. No. 13, Vancouver, B.C.

4. Reiner, M. and Weisenberg, K. 1939. A thermodynamic theory of the strength of materials. Rheological Leaflet *10* (12).

5. Bach, L. 1973. Reiner-Weisenberg's theory applied to time-dependent fracture of wood subjected to various modes of mechanical loading. Wood Science 5 (3).

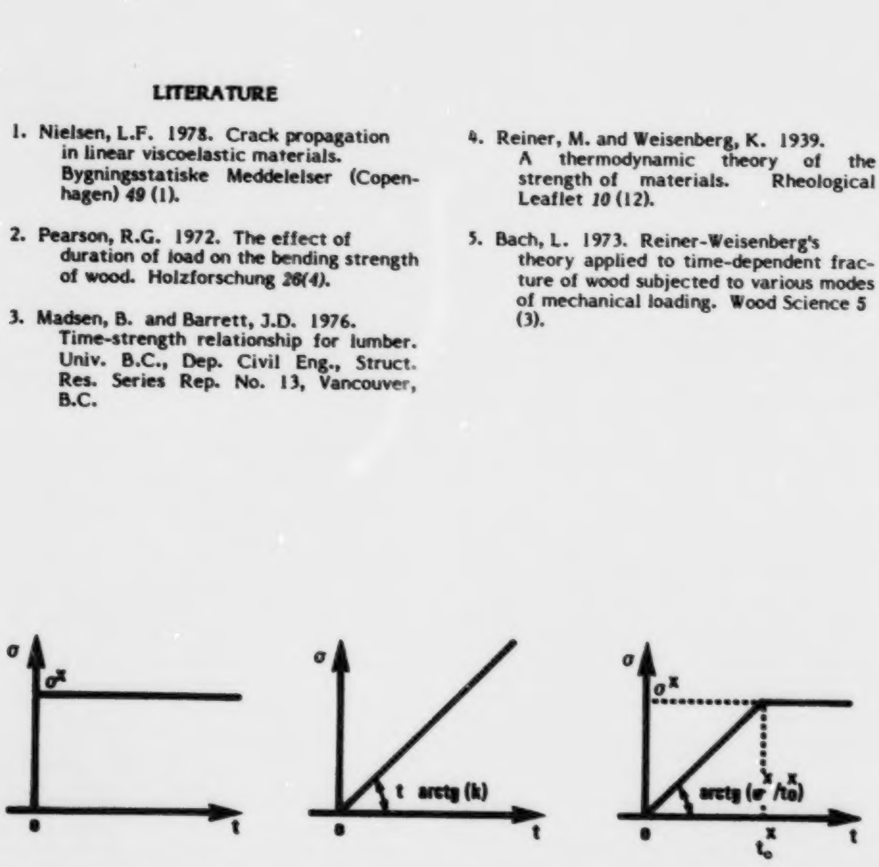

Figure 1. Dead load, ramp load and combined load, respectively.

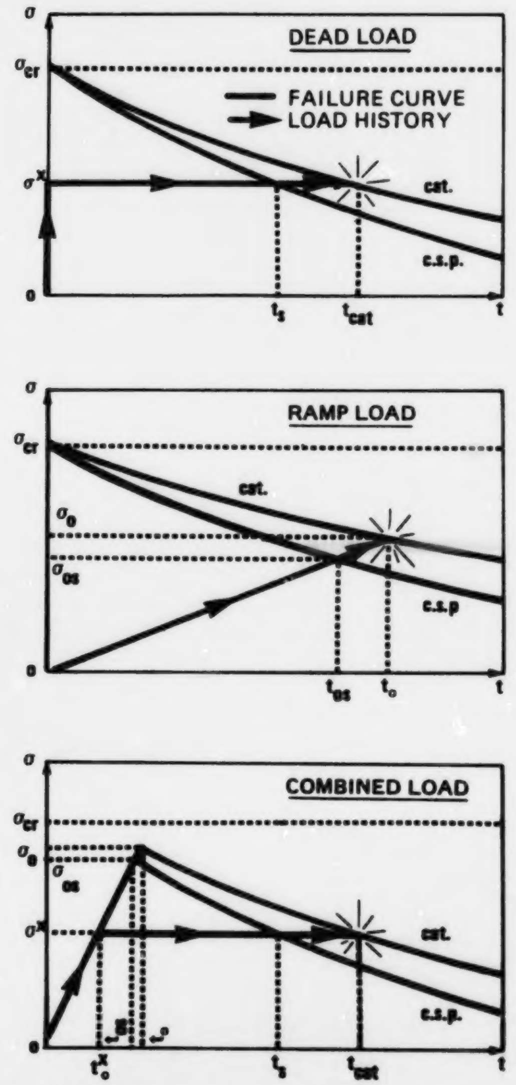

Figure 2. Load histories and life-time curves in principle. "C.s.p." means "Cracks start propagating". "Cat." means "Catastrophic failure".

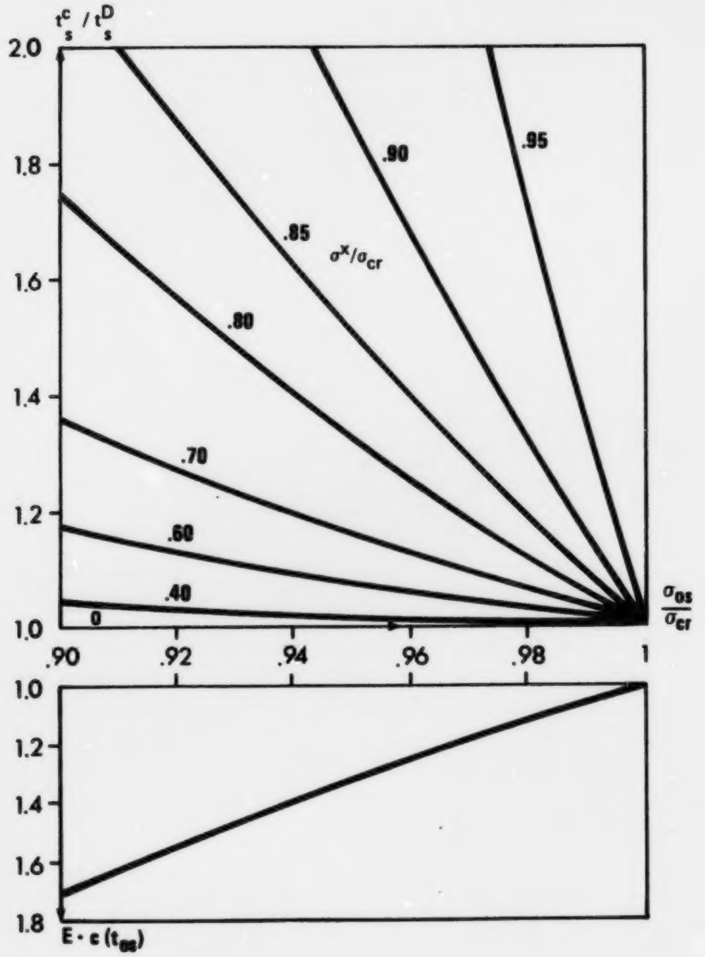

Figure 3. Conversion of combined-load results to dead-load results and vice versa at small times. (For a Maxwell material the figure applies in general).

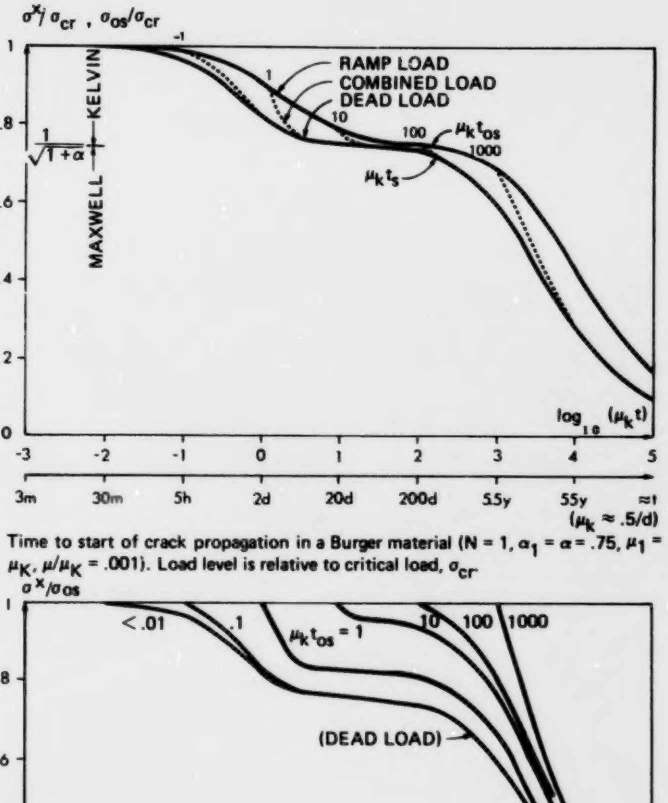

Figure 4. Time to start of crack propagation in a Burger material (N = 1, $\alpha_1 = \alpha = .75$, $\mu_1 = \mu_K$, $\mu/\mu_K = .001$). Load level is relative to critical load, $\sigma_{cr}$.

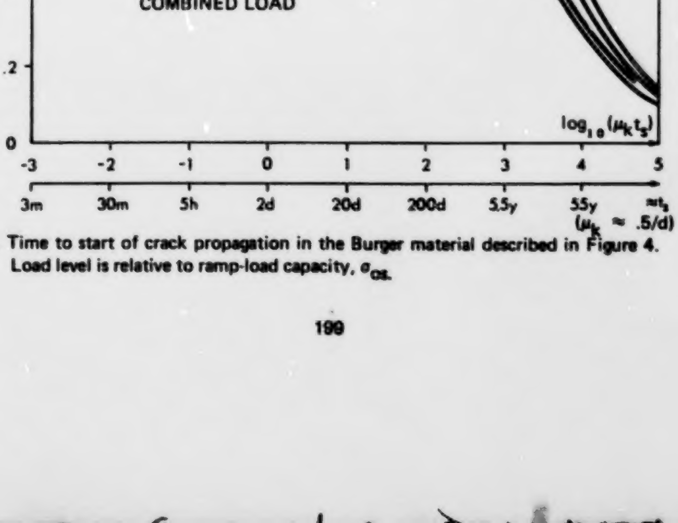

Figure 5. Time to start of crack propagation in the Burger material described in Figure 4. Load level is relative to ramp-load capacity, $\sigma_{os}$.

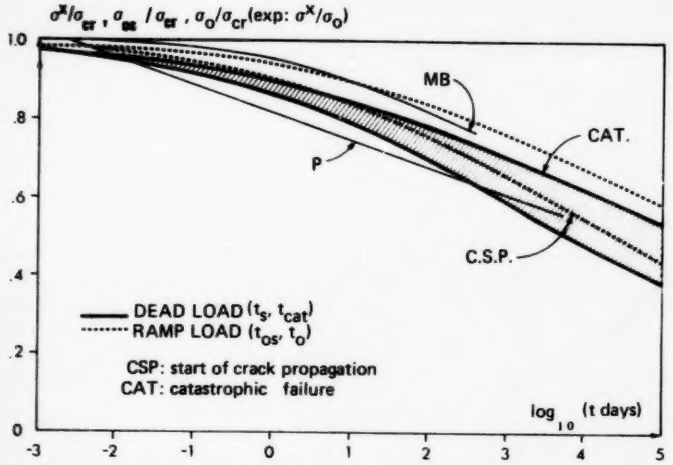

Figure 6. Failure curves for wood. Results indicated by heavy lines are due to the present theory assuming the following creep function: $c(t) = 1/E\ (1 + 1/3\ t^{1/4})$ with T in days. Results indicated by thin lines are due to combined load experiments. P = Pearson (2), $t_o \approx 4$ min., MB = Madsen and Barrett (3), average curve $t_o \approx 1$ min.

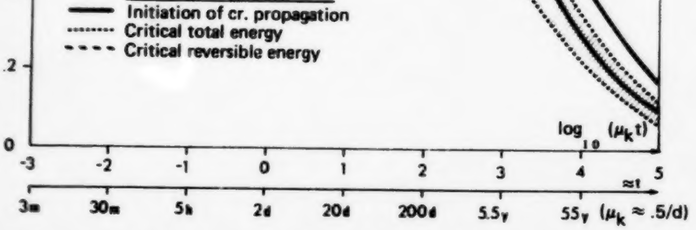

Figure 7. Comparison of load capacities according to different failure criteria applied to the Burger material described in Figure 4.

# GLUELINE FRACTURE OF WOOD ADHESIVE COMPACT-TENSION SPECIMENS AT VARIOUS GRAIN ORIENTATION CONFIGURATIONS

By

Tom C. Ruedy and Jay A. Johnson

---

Weyerhaeuser Company, Tacoma, WA.

## ABSTRACT

Fracture toughness and critical-strain energy release rates were determined for compact-tension specimens manufactured from seven species of wood and four adhesives. Five crack lengths were used to verify the dependence of the critical load at instability on initial crack size. Three types of load-deflection diagrams were noted. The results indicated that theories of fracture mechanics can be applied to wood-adhesive systems. Fracture toughness and critical-strain energy release rates were found to increase with a tilt grain angle (0° associated with edge gluing and 90° with a butt joint). In some cases, a minimum resistance to fracture was found between 15 and 30°.
There was some evidence to suggest that resistance to failure was greatest for an intermediate glueline thickness. There appeared to be a slight trend toward larger toughness with thinner samples. It was also noted that the fracture toughness of edge-glued samples with polyvinylacetate was greater than corresponding solid wood samples.

## INTRODUCTION

The motivation for this research stemmed from a natural curiosity concerning the applicability of linear-elastic fracture mechanics (LEFM) to wood adhesive systems. After all, it is not intuitively obvious that the stress distribution near the tip of a crack, residing in a glueline bonding two orthotropic adherents, should be similar to the distribution near the tip of a crack in a homogeneous, isotropic material from which the concept of fracture toughness can be developed. Hence, should fracture toughness apply? On the other hand, the crack must concentrate stored energy at the tip, regardless of the microarchitecture of this region, and if, after a threshold loading has been exceeded, the crack extends releasing strained energy to the process of surface generation, is not this a basic tenet of the fracture theory? The characterization of crack-extension resistance of wood/adhesive systems using fracture mechanics would be useful technologically. It would add another dimension to the bond-strength literature, as well as providing a basis for load-bearing capacities given a knowledge of the size of inherent flaws.

Consequently, the objectives of this study were to: (1) verify whether fracture-mechanics theories could be applied to wood /adhesive systems and, if so, (2) obtain a variety of information relative to various species, adhesives, grain-orientation configurations and glueline thickness.

## MATERIALS AND METHODS

The seven wood species used in this study were: Softwoods - 1. Douglas-fir(*Pseudotsuga menziesii*); 2. spruce (*Picea sp.*); 3. southern pine (*Pinus sp.*);

Hardwoods (*diffuse porous*) - 4. yellow poplar (*Liriodendron tulipifera*); 5. sugar maple (*Acer saccharum*);

Hardwoods (*ring porous*) - 6. ash (*Fraxinus sp.*) ; 7. walnut (*Juglans nigra*).

Defect-free, flat-sawn boards were obtained from a local lumber yard (Roanoke, Virginia). Four commercial adhesives were used: 1. polyvinylacetate (PVA); 2. epoxy; 3. resorcinol; 4. casein.

The size, shape and configuration of the compact-tension specimen used in this study is shown in Fig. 1. In general, the orientation of the grain direction in the upper (u) or lower ($\ell$) halves of the sample relative to the crack propagation direction, $\vec{a}$ (in the crack plane and perpendicular to the crack front), can be specified with two angles, Fig. 2: (1) a twist angle $\psi$ and (2) a tilt angle $\theta$. In this study, the twist angles were not varied ($\psi_u = \psi_\ell = 0$). The tilt angles were kept symmetric $\theta_u = \theta_\ell = \theta$ and were varied in the interval $0 \leq \theta \leq \pi/2$.

The specimens were manufactured by randomly selecting grain orientations from the boards, microtoming the glue surfaces and conditioning the specimens to 9% equilibrium moisture content. Glue was spread at the nominal rate of 317 gm/m$^2$ (65 lb/MSF*) and 12 specimens (random grain angles) were placed in a device to hold the samples together under a pressure of 689 kPa (100 psi) while the adhesive cured at room temperature. The spread rate is fictitious, as the adhesive was squeezed out to a certain extent during manufacture. The desired crack length was insured by inserting a greased polyvinylchloride foil at the glueline. A set of samples were manufactured using shims to control the glueline thickness. The glueline thickness of most of the samples, however, was not controlled.

---

*MSF = 1,000 ft$^2$

A table model Instron testing machine was used to obtain force-deflection curves for each sample tested. A tensile or cleaving force was applied to the sample by means of loading pins inserted into the holes of the sample. A crosshead speed of 0.083 mm/sec. (0.20 in/min) was employed with the duration of the test lasting approximately 10 sec. The reader should consult Ruedy (1977) for more details concerning the test procedure.

## RESULTS AND DISCUSSION

### Apparent Fracture Toughness

Fracture toughness of a compact-tension specimen manufactured from an isotropic, elastic material can be determined from the equation:

$$K_{Ic} = \sigma_c \sqrt{\pi a} \; Y \qquad (1)$$

where $\sigma_c = Pc/bw$ and $P_c$ is a critical load taken from the load-displacement curve at the point where crack instability was initiated in the sample. The geometric correction factor Y for a compact-tension specimen is given in ASTM E399 (ASTM 1974) and is:

$$Y = 29.6 - 185.5\,\xi + 656\,\xi^2 - 1017\xi^3 + 6389\xi^4 \qquad (2)$$

with $\xi = a/w$. Equation (1) can be rearranged to obtain:

$$2 \log\left(\frac{K_{Ic}}{\sigma c Y}\right) = \log(\pi a) \qquad (3)$$

which indicates the dependence of the critical stress on the crack length provided $K_{Ic}$ is a material property and remains constant. Since $\sigma_c$ and a can be measured independently, equation (3) provides a means of evaluating whether a given system conforms to the theory of fracture.

To verify that the wood/adhesive system of Fig. 1 obeys the dictates of fracture mechanics, 280 yellow poplar/PVA samples were tested. Eight replicates were used for each combination of five crack lengths and seven tilt angles.

Three types of load-displacement curves were observed during testing. These are shown in Fig. 3. The recorded displacement is the crosshead movement of the testing machine which is assumed to be equivalent to the load-application-point displacement. Non-linear behavior was noted during the initial stages. This could have been due to increasing contact forces on the loading pins, resistance to rotation of the samples about the loading pins and/or increasing initial crack-opening stiffness at the crack tip.

Selection of the critical load for calculating fracture toughness of each type of failure mode was done as follows. For type I, the maximum load was used; i.e., the load at which catastrophic failure was initiated. For type II, the load at the first instability point was used, since the initial crack length was known at this point. It was not possible to measure the incremental crack growth after the first instability point was encountered. It was felt that the toughness calculated in this manner represented an absolute greatest lower bound of the samples with this type of failure mode. The maximum load was used for type III. It is obvious that a considerable amount of plastic/viscoelastic flow was encountered in the vicinity of the crack tip which in itself was not well defined. Type I curves accounted for 81% of the 280 samples, type II 5% and type III 14%.

Using the selected critical forces and original crack lengths, fracture toughness values were calculated (equation 1) for each sample and an average was determined for each tilt angle group. Using equation 3 with these average toughness values, the critical loads are compared to the crack lengths in Fig. 4. Plotted in this way, the experimental data should be clustered around the theoretical relationship which is a straight line through the origin having a unit slope. A regression line through the measured data has an intercept of -0.07 and a slope of 1.16. Thus, it would appear that fracture mechanics can be applied to this wood/adhesive system.

Average fracture toughness values for the yellow poplar/PVA samples are given in Table I. It appears that higher values of toughness are calculated for shorter crack lengths, at least with respect to the lower angles. Thus, the formula may need to be modified to account for anisotropy and dissimilar material property changes. The values are reasonably constant over crack length; however, thus, an "apparent" fracture toughness can be used to characterize the resistance to separation of the bonded wood adherents. For a given crack length, there appears to be a minimum toughness at a tilt angle between 0.26 and 0.52 radians (15° and 30°).

## Strain Energy Release Rate

The strain energy release rate, another parameter for characterizing resistance to failure, can be determined from an equation of the form:

$$G_{Ic} = \frac{1}{2b} P_c^2 \left(\frac{d\lambda}{da}\right) \qquad (4)$$

where λ is the sample compliance, a known function of the initial crack length. Generally, a sample is employed such that the functional dependence of the compliance on the crack length can be predicted theoretically. Mostovoy and Ripling (1966) employed a double-cantilever beam for evaluating epoxy/aluminum bond resistance, for instance. A tapered double-cantilever beam can be constructed such that the $d\lambda/da$ term is independent of crack length.

Since the load-displacement curves were measured for each of the 280 yellow poplar/PVA samples, a value for compliance could, in principle, be associated with each sample. The load-displacement curves were non-linear, hence, the maximum stiffness was extracted and its reciprocal used as the sample compliance. An empirical relationship was developed to express the dependence of the compliance as a function of crack length. It was found that an expression of the form:

$$\lambda = \lambda_0 e^{\alpha a + \beta a^2} \qquad (5)$$

where α, β and $\lambda_0$ are constants, seemed to fit the data reasonably well. It also has the property of being easily differentiated:

$$\left(\frac{d\lambda}{da}\right) = (\alpha + 2\beta a)\ \lambda_0 e^{\alpha a + \beta a^2} \qquad (6)$$

The resulting empirical constants of the curve-fitting analysis are given in Table 2 and a plot of compliance versus initial crack length is shown in Fig. 5.

The strain-energy release rates calculated from equations (4) and (6) are given in Table 3. As with fracture toughness, the strain-energy release rates appear to decrease slightly with crack length and increase with tilt angle. The butt joint, $\theta = 1.57$ (90°), has the greatest resistance to fracture.

A comparison of fracture toughness and strain-energy release rate is shown in Fig. 6. Both $K_{Ic}$ and $G_{Ic}$ versus tilt angle clearly indicate a minimum resistance to crack extension in the 0.26 to 0.52 radian (15 to 30 deg.) range. It is not clear, physically, why a minimum exists. The stress distributions near the crack tip are obviously different for each tilt angle. Glue penetration is also different. Whether the grain orientation concentrates more stored energy in vicinity of the crack tip, or whether the wood-glue interface configuration is simply inherently weaker at these intermediate tilt angles, configurations, or both, are possibilities that might explain these phenomena

It is interesting to note that fracture

toughness and strain-energy release rate appear to be reasonably correlated, Fig. 7. This is true despite the use of an inappropriate equation for $K_{Ic}$, the rather empirical nature of obtaining $G_{Ic}$ and the simplicity of the testing apparatus.

### Glueline Thickness

No attempt was made to control the glueline thickness during the manufacturing of the 280 yellow poplar/PVA specimens. Electron micrographs of the gluelines revealed, however, varying glueline thicknesses. To investigate the glueline thickness effects, maple/PVA samples were manufactured with shim stock serving as "stops" to control the bond thickness. The samples were edged glued; i.e., a tilt angle of 0.00 radians (0 deg.).

Fracture toughness as a function of glueline thickness is shown in Fig. 8. There is a maximum resistance around 250 μm (0.010 in) for this system. If this result is, in fact, a universal trait of wood/adhesive systems, it would be a useful technological design element for manufacturing wood products.

### Sample Thickness

Two groups of samples were manufactured with thicknesses other than 12.7 mm (0.50in.) One set had a thickness of 6.3 mm(0.25"); the other, 19.0 mm (0.75"). Fracture toughness is shown as a function of tilt angle for three different values of specimen thickness in Fig. 9. For each tilt angle less than 1.04 radians (60 deg.), there is a trend toward higher toughness with decreasing thickness. This conforms to the observations of Barrett (1976) who found that fracture toughness of Douglas-fir specimens decreased with specimen thickness. A minimum fracture toughness at intermediate tilt angles is also noted for these two additional sets of data.

### Fracture Surface

Three types of failure surfaces were observed for the 280 yellow poplar/PVA specimens (Fig. 10): (A) total adhesive failure; (B) mixed wood and adhesive failure; and (C) total wood failure. The frequency of samples whose surfaces have any wood failure (either type B or C, but not A) was found to decrease as the tilt angle increased in the manner of the box on this page.

At instability, the crack must "choose" the path of least resistance before it extends in a given direction. For sample configuration of this study, the "choice" was between extending in the glueline or fracturing along the grain, either in the lower half of the sample or the upper. Once the crack started "running", then a new, dynamic criterion was in effect to influence the further direction of crack propagation. For this reasons, the traditional wood failure measure of bond integrity is inappropriate for this test method. An attempt was made, however, to estimate wood failure in incremental regions near the crack tip. With the

| | | | | | | | |
|---|---|---|---|---|---|---|---|
| **Tilt angle θ, radians:** | 0.00 | 0.26 | 0.52 | 0.78 | 1.04 | 1.30 | 1.57 |
| **(degrees):** | 0 | 15 | 30 | 45 | 60 | 75 | 90 |
| **Frequency of samples with failure types B or C (not A), %** | 100 | 90 | 90 | 60 | 25 | 12 | 0 |

exception of the edge-glued samples (all wood failure) and butt joint samples (all adhesive failure), the general picture emerges of the crack starting at the crack tip with total adhesive failure and moving toward higher levels of wood failure as the crack progresses. In other words, having been initiated in the adhesive layer, the crack has an increasing probability of moving into the wood. This tendency is diminished, however, as the tilt angle increases.

### Species

Compact-tension specimens with a thickness of 12.7 mm (0.50 in.) manufactured from seven species of wood are shown in Fig. 11 as a function of tilt angle. With the exception of the yellow poplar specimens, eight replications were used with a crack length of 25.4 mm (1.00 in.).

Qualitatively the same trends were observed for these samples, although in some cases a definite minimum was not observed for intermediate tilt angles. The spruce/PVA samples showed the least resistance to fracture followed by the Douglas-fir/PVA specimens. That the resistance to failure of the bonded specimens was greater than the resistance of the wood itself is shown in Fig. 12, with ash being an exception.

### Adhesives

Yellow poplar and southern pine specimens were made with four adhesives. Their thickness was 12.7 mm (0.50 in.), the crack length was 25.4 mm (1.00 in.) and eight replicates were used (except yellow poplar). The fracture toughness of these specimens are shown in Fig. 13 as a function of tilt angle The distribution of samples having the three types of load-displacement curves are shown in Table 4.

The behavior of each adhesive was generally the same for the yellow poplar and southern pine specimens. PVA and resorcinol were more resistant to fracturing than epoxy or casein (the lowest). The resorcinol and casein acted in a brittle manner (no type III load-displacement curves), whereas the PVA and especially the epoxy exhibited a flow prior to crack extension.

Since there was a considerable amount of flow with the epoxy type III samples, it could be argued that linear-elastic fracture mechanics does not apply and a viscoelastic approach might be taken.

## CONCLUSIONS

1. Fracture mechanics can be applied to wood/adhesive systems with mismatched grain angles.

2. There appears to be a reasonably close correlation between fracture toughness and strain-energy release rate of yellow poplar /PVA specimens.

3. Fracture toughness of a yellow poplar /PVA specimen was found to be sensitive to glueline thickness.

4. Resistance to fracture was slightly higher for thinner specimens.

5. Fracture resistance of the species used in this study produced roughly the same trend with respect to tilt angle.

6. PVA and resorcinol specimens showed greater toughness than epoxy and casein samples. Epoxy and, to a lesser extent, PVA exhibited more viscoelastic flow prior to crack initiation.

## LITERATURE CITED

ASTM. 1974. Standard Method of Test for Plane-Strain Fracture Toughness of Metallic Materials (E 399-74). Annual Book of Standards, Part 10, Philadelphia, PA.

Mostovoy, S. and Ripling, G.J. 1964. Fracture Toughness of an Epoxy System. J Appl. Polymer Sci. 10:1351-1371.

Ruedy, T.C. 1977. The Effect of Grain Angle Orientation on the Fracture Toughness of Wood-Adhesive Systems. M.S. thesis, Va. Polytech. Inst. and State Univ., Blacksburg, VA.

Table 1. Apparent fracture toughness $K_{Ic}$ of yellow poplar/PVA samples as a function of crack length and tilt angle in units of $kPa\sqrt{m}$ ($psi\sqrt{in}$ in parentheses).*

| Tilt Angle $\theta$ rad. (deg.) | Crack length, $\underline{a}$ | | | | |
|---|---|---|---|---|---|
| | 12.7 mm (0.50 in) | 19.0 mm (0.75 in) | 25.4 mm (1.00 in) | 31.8 mm (1.25 in) | 38.1 mm (1.50 in) |
| 0.00<br>(0) | 728<br>(663) | 616<br>(561) | 644<br>(586) | 571<br>(520) | 581<br>(529) |
| 0.26<br>(15) | 621<br>(565) | 578<br>(526) | 505<br>(460) | 516<br>(470) | 468<br>(426) |
| 0.52<br>(30) | 621<br>(565) | 588<br>(535) | 538<br>(490) | 420<br>(382) | 531<br>(483) |
| 0.79<br>(45) | 670<br>(610) | 544<br>(495) | 690<br>(628) | 597<br>(543) | 481<br>(438) |
| 1.05<br>(60) | 725<br>(660) | 794<br>(723) | 699<br>(636) | 862<br>(785) | 842<br>(766) |
| 1.31<br>(75) | 983<br>(895) | 967<br>(880) | 945<br>(860) | 956<br>(870) | 927<br>(844) |
| 1.57<br>(90) | 1,025<br>(933) | 948<br>(863) | 1,269<br>(1,155) | 1,145<br>(1,042) | 1,297<br>(1,180) |

*Each $K_{Ic}$ is an average of eight samples.

Table 2. Empirical constants for the compliance of the yellow poplar/PVA compact-tension specimens.

| Tilt Angle $\theta$ rad. (deg.) | µm/N ($10^{-3}$ in/lb) | $mm^{-1}$ ($in^{-1}$) | $mm^{-2}$ ($in^{-2}$) |
|---|---|---|---|
| 0.00<br>(0) | 4.11<br>(0.72) | -0.0222<br>(-0.565) | 0.00200<br>(1.290) |
| 0.26<br>(15) | 2.74<br>(0.48) | 0.0126<br>(0.321) | 0.00152<br>(0.986) |
| 0.52<br>(30) | 3.37<br>(0.59) | 0.0119<br>(0.303) | 0.00162<br>(1.048) |
| 0.78<br>(45) | 3.83<br>(0.67) | -0.0150<br>(-0.380) | 0.00196<br>(1.262) |
| 1.04<br>(60) | 3.60<br>(0.63) | 0.0098<br>(-0.248) | 0.00168<br>(1.087) |
| 1.30<br>(75) | 2.11<br>(0.37) | 0.0333<br>(0.845) | 0.00071<br>(0.456) |
| 1.57<br>(90) | 2.45<br>(0.43) | 0.0231<br>(0.587) | 0.00078<br>(0.503) |

Table 3. Strain-energy release rates of the yellow poplar/PVA samples as a function of tilt angle in units of J/m$^2$ (in.-lb/in.$^2$ in parentheses).

| Tilt Angle $\theta$ rad. (deg.) | Crack Length | | | | |
|---|---|---|---|---|---|
| | 12.7 mm (0.50 in) | 19.0 mm (0.75 in) | 25.4 mm (1.00 in) | 31.7 mm (1.25 in) | 38.1 mm (1.50 in) |
| 0.00<br>(0) | 872<br>(4.98) | 930<br>(5.31) | 1,130<br>(6.45) | 844<br>(4.82) | 802<br>(4.58) |
| 0.26<br>(15) | 1,290<br>(7.37) | 1,200<br>(6.87) | 956<br>(5.46) | 800<br>(4.57) | 816<br>(4.66) |
| 0.52<br>(30) | 930<br>(5.31) | 1,050<br>(5.99) | 1,090<br>(6.25) | 511<br>(2.92) | 646<br>(3.69) |
| 0.78<br>(45) | 886<br>(5.06) | 893<br>(5.10) | 1,500<br>(8.56) | 1,140<br>(6.50) | 742<br>(4.24) |
| 1.04<br>(60) | 954<br>(5.45) | 1,440<br>(8.24) | 1,320<br>(7.54) | 1,450<br>(8.28) | 1,060<br>(6.06) |
| 1.30<br>(75) | 2,380<br>(13.59) | 2,230<br>(12.74) | 1,950<br>(11.15) | 1,280<br>(7.32) | 732<br>(4.18) |
| 1.57<br>(90) | 2,260<br>(12.92) | 1,940<br>(11.10) | 3,040<br>(17.36) | 1,610<br>(9.18) | 1,300<br>(7.46) |

Table 4. Distribution in percentage of load-displacement type (I, II, or III) curves for yellow poplar and southern pine compact-tension specimens bonded with four adhesives.

| | Yellow poplar | | | Southern pine | | |
|---|---|---|---|---|---|---|
| Adhesive | I | II | III | I | II | III |
| P.V.A. | 81 | 5 | 14 | 52 | 39 | 9 |
| Resorcinol | 48 | 52 | 0 | 48 | 52 | 0 |
| Epoxy | 23 | 30 | 47 | 45 | 23 | 32 |
| Casein | 77 | 23 | 0 | 86 | 14 | 0 |

$\theta$ = 0.00, 0.26, 0.52, 0.78, 1.04, 1.30, 1.57 rad
(0, 15, 30, 45, 60, 75, 90 deg)

a = 12.7, 19.0, 25.4, 31.7, 38.1 mm
(0.50, 0.75, 1.00, 1.25, 1.50 in.)

b = 6.3, 12.7, 19.0 mm
(0.25, 0.50, 0.75 in.)

e = 12.7 mm (0.50 in.)

h = 31.7 mm (1.25 in.)

w′= 50.8 mm (2.00 in.)

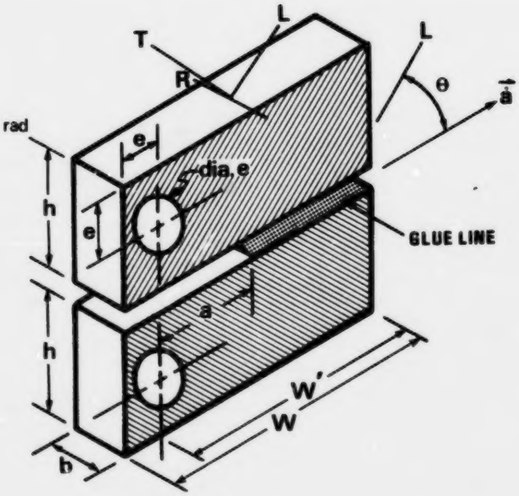
T
L
R
L
θ
$\vec{a}$
e
dia.e
h
e
GLUE LINE
a
h
W′
W
b

Figure 1 Details of the compact tension specimen used in this study.

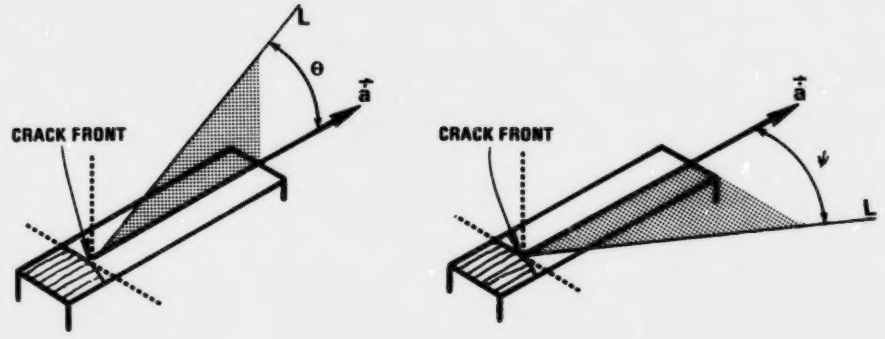
L
θ
$\vec{a}$
CRACK FRONT
$\vec{a}$
CRACK FRONT
ψ
L

TILT ANGLE $\theta$

TWIST ANGLE $\psi$

Figure 2 Angles needed to specify the orientation of the grain direction (L) with respect to the crack propagation direction ($\vec{a}$).

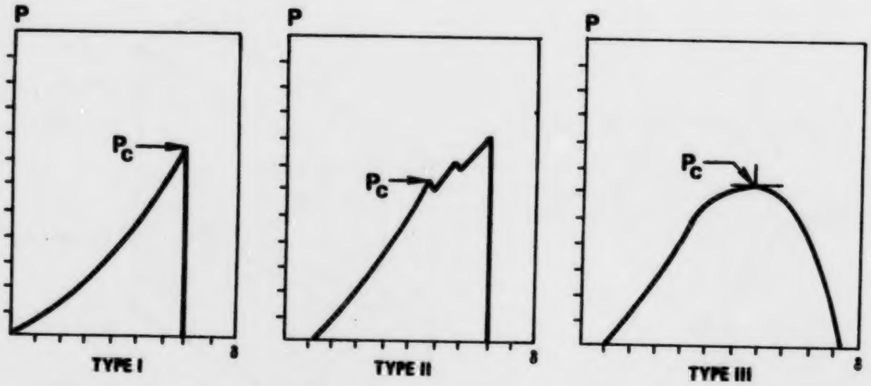

Figure 3 Three types of load-deflection curve observed for the yellow poplar/PVA samples.

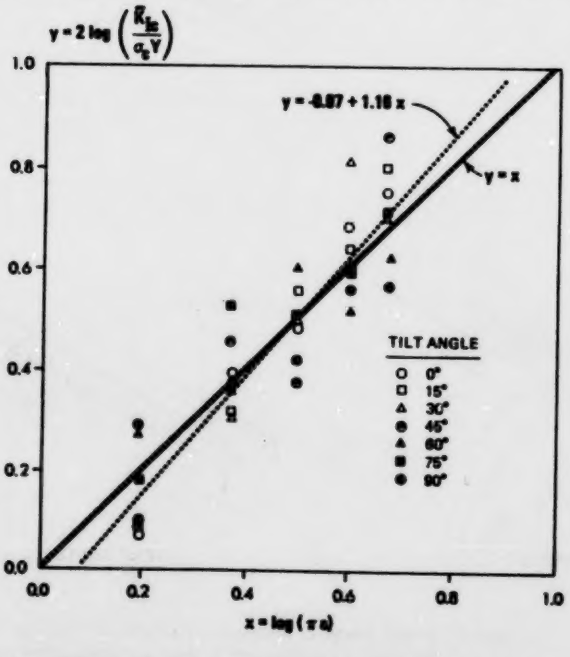

Figure 4 Critical stress versus crack length for the yellow poplar/PVA samples.

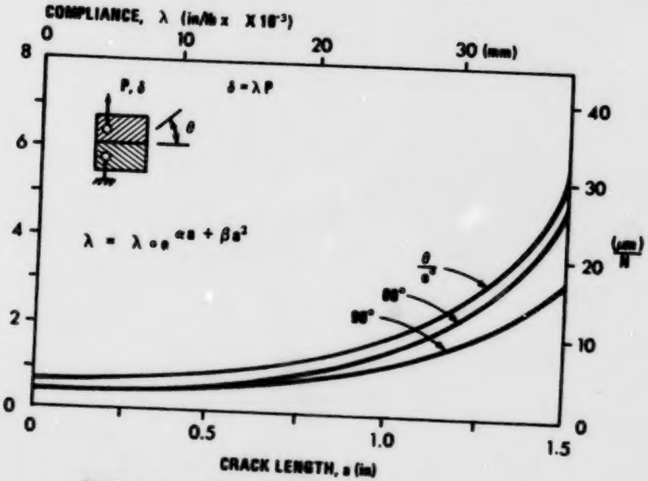

Figure 5 Compliance of compact tension specimens as a function of crack length.

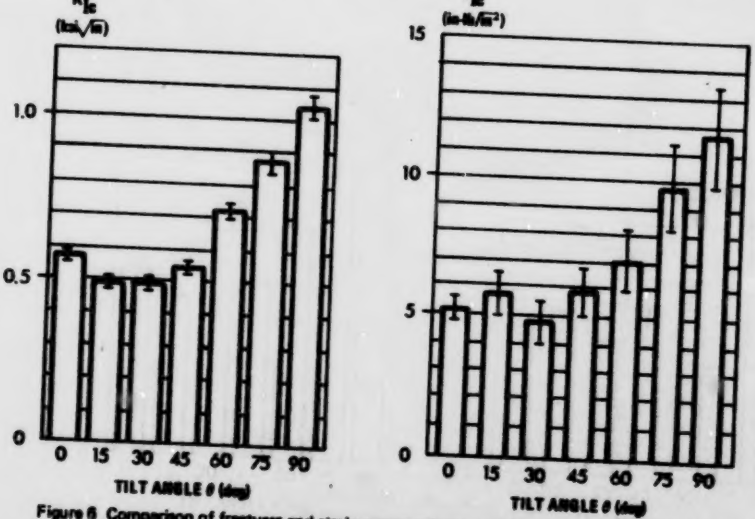

Figure 6 Comparison of fractures and strain energy release rate for yellow poplar/PVA samples.

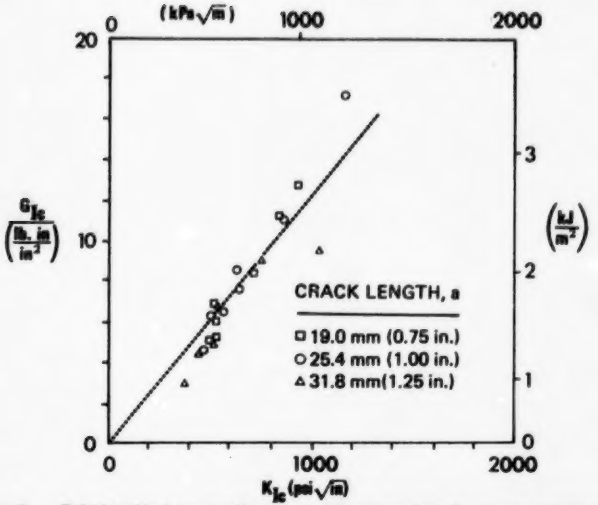

Figure 7 Relationship between fracture toughness and strain energy release rate.

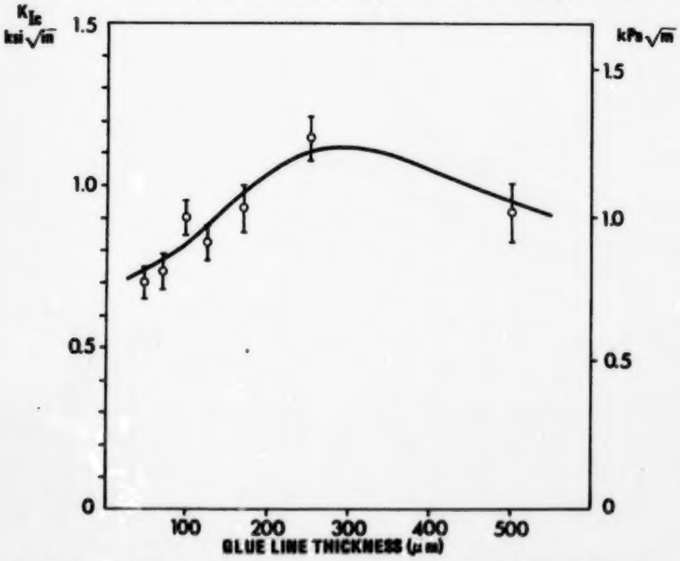

Figure 8 Fracture toughness of maple/PVA samples versus glue line thickness.

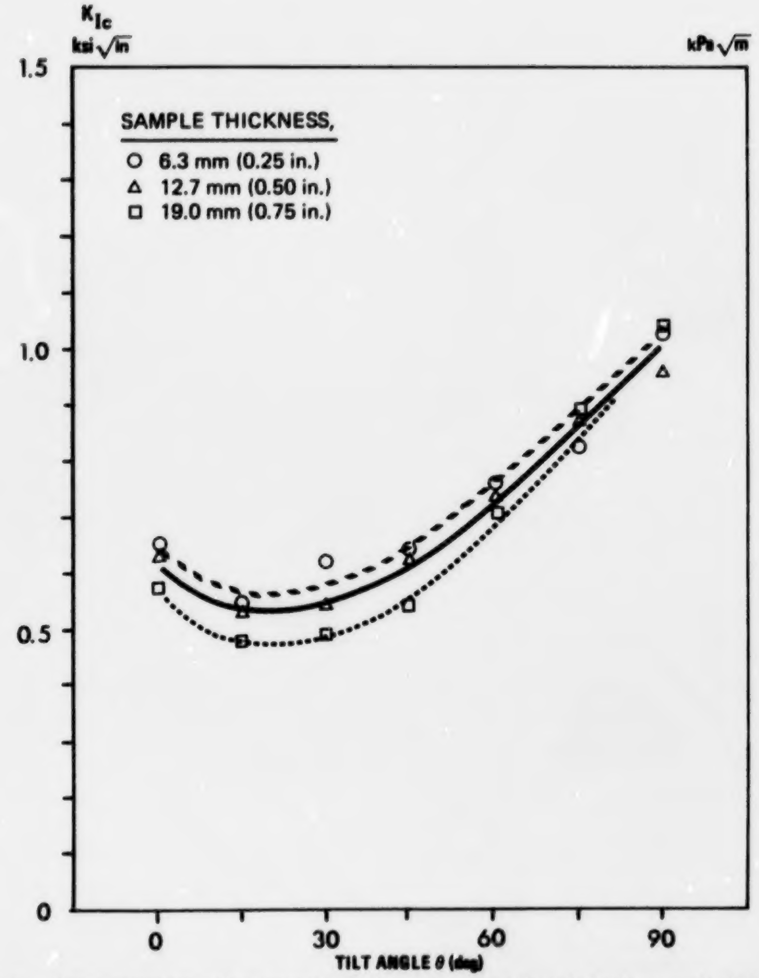

Figure 9 Fracture toughness of yellow poplar/PVA samples versus tilt angle for three sample thicknesses.

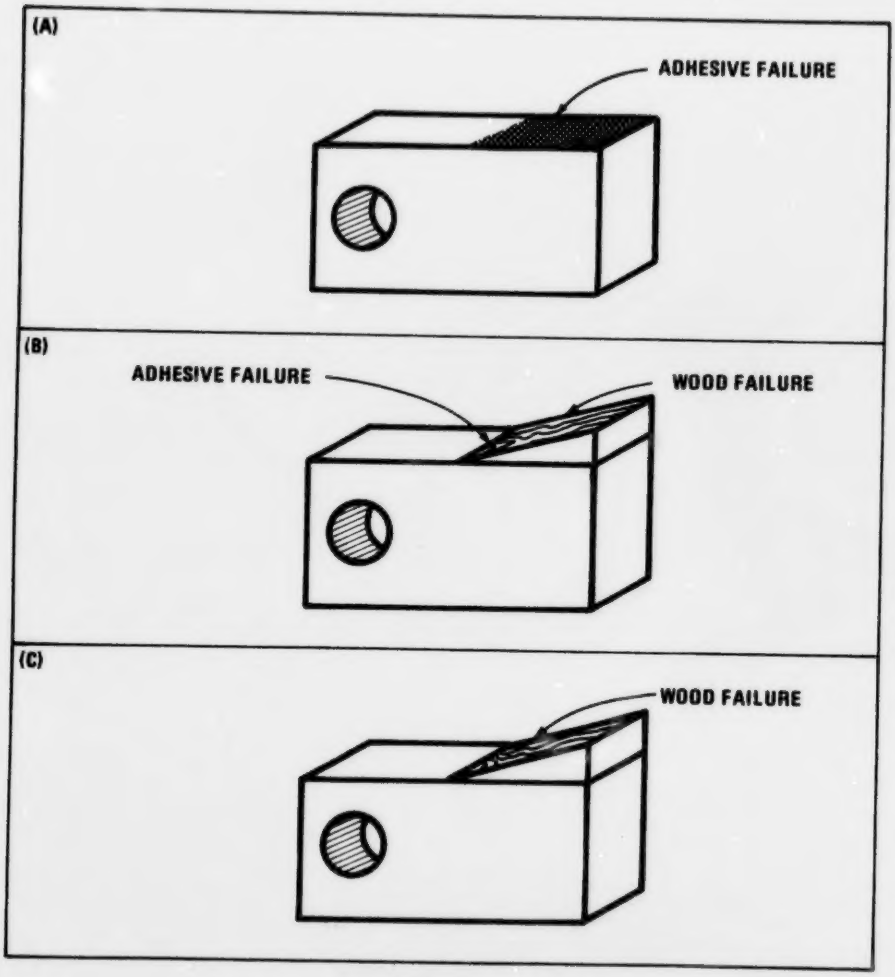
(A)
ADHESIVE FAILURE
(B)
ADHESIVE FAILURE
WOOD FAILURE
(C)
WOOD FAILURE

Figure 10 Three types of failure surfaces observed for yellow poplar/PVA compact tension specimens.

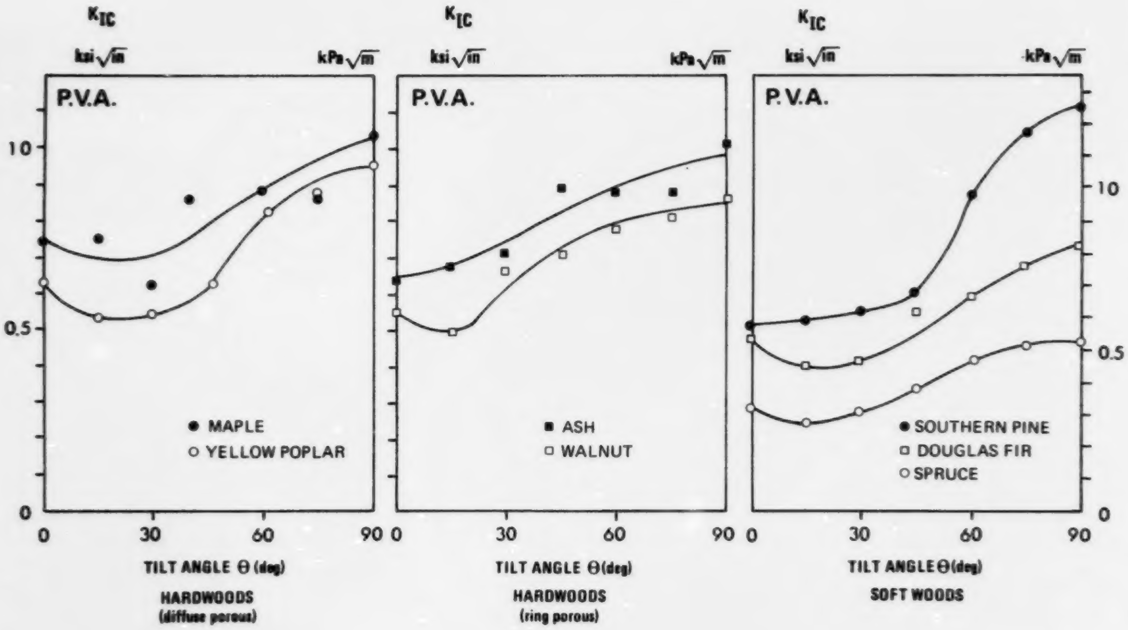

Figure 11 Fracture toughness of various wood species bonded with PVA.

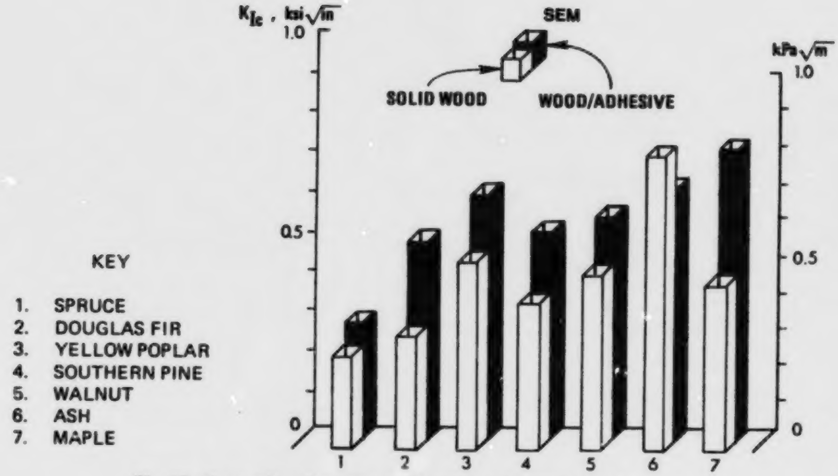

Fig. 12 Comparison between solid wood specimens (ITL) and edge glued specimens with PVA ($\theta$ = 0.00 rad).

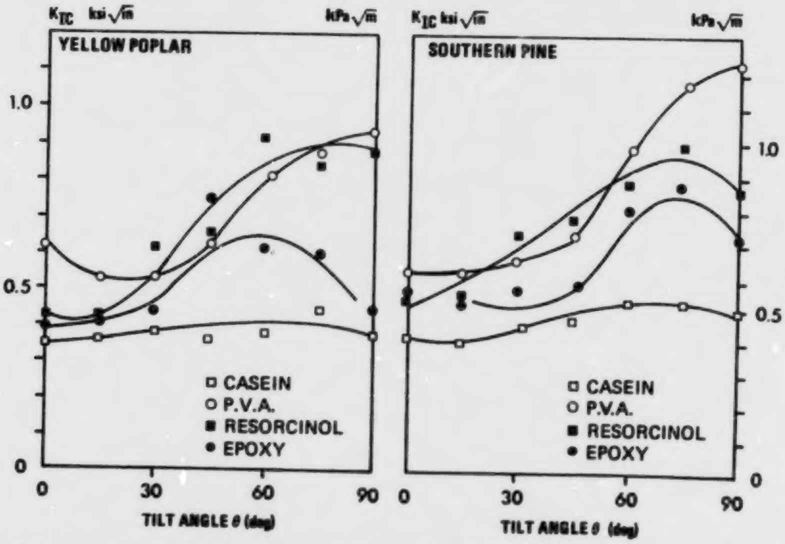

Fig. 13 Fracture toughness of yellow poplar and southern pine bonded with various adhesives.

# A SEVEN YEAR TALE: OR HOW BOARDS HAVE BREAKDOWNS FROM EVERYDAY PRESSURE

By

Arno P. Schniewind

---

University of California, Forest Products Laboratory, Richmond, CA.

## INTRODUCTION

The traditional concept of material strength as a limiting value of stress, expressed as P/A or load per unit area, is an appealingly simple one. However, it soon becomes apparent that this limiting value of stress is subject to variation caused by many factors. In wood such factors as moisture content and temperature must be recognized. Most materials are subject to a size factor, so that instead of the simple P/A more complex corrections must be used, depending on the volume of material under stress. It also turns out that for many materials, wood prominently among them, it is not stress alone that determines failure, but rather the stress history. For example, beams of wood or wood-based material, subjected to a constant load of about 45 to 60% of the load that would cause failure in a static test, will fail in approximately five years. At higher loads, failure will occur sooner and at lower loads later. This phenomenon has been referred to as "static fatigue" and is commonly known as the "duration-of-load factor". Another manifestation of the same phenomenon is the dependence of wood strength on rate of loading in static tests. Wood may be up to 50% stronger in rapid loading and 75% stronger on impact as compared with a static test of a few minutes duration.

The duration-of-load factor is of considerable practical importance. Present design rules, as used in the United States, provide for adjustment factors to published design stresses ranging from 0.9, when the duration exceeds 10 years, to 1.25 for a duration of seven days and up to 2.0 for impact loading. In recent years, details of these adjustments have come under re-examination. There is an active search for improved methods of accounting for the duration-of-load effect in the design of wood structural elements and systems.

## DURATION-OF-LOAD EFFECTS IN RELATION TO MATERIAL DEFORMATION AND FLOW

Early work on duration-of-load effects has been reviewed by Gerhards (1977a) and can be traced back to 1840. By the time of World War I, a duration-of-load factor of 9/16 was recommended for practical applications. According to Gerhards, the factor of 9/16 was derived from the ratio of the fiber stress at the proportional limit in static bending to the modulus of rupture. This indicates that at a very early stage duration-of-load effects where linked to deformation behavior.

The link to deformation was given more explicit expression when G. Ivanov (1938) formulated his concept of what he called the limit of plastic flow. This he defined as the stress at which a sharp increase in rate of deformation is observed in static loading. He proposed various types of experiments for determining the limit of plastic flow, one of which involved measuring time to failure of wood specimens subjected to various levels of constant stress. Assuming that flow would occur only at stresses above the limit of plastic flow, and that flow would eventually lead to failure, a curve of data from creep-rupture experiments would presumably suggest an asymptote equal to the limit of plastic flow. Since these particular experiments are time consuming and the interpretation of the data somewhat difficult, other methods were also suggested by Ivanov. These included plotting the first derivative of the stress-strain curve from static tests and then finding a proportional limit in the resulting plot, as well as more complex methods.

Sugiyama (1967) approached the problem somewhat more directly by defining a creep limit as, "The maximum value of sustained stress withstood by a specimen without causing failure". According to Sugiyama's review of Japanese work, the creep limit is about 40 to 50% of bending strength, about 50% of shear strength, and about 50 to 55% of compression strength.

Sugiyama considered that below the creep limit only instantaneously elastic and delayed elastic deformation took place. This would mean that at constant loads below the creep limit, deformations would tend to vanish if we assume classical models of delayed elastic deformation. The creep limit and the limit of plastic flow are thus seen to be one and the same. It also suggests that an alternate method for determining the creep limit would be to find the highest stress level which, when held constant, results in deformation rates that vanish with time. Precisely such an approach was taken by

Gillwald and Luthardt (1966) in determining the creep limit and, thus, the stress level at which loads can be sustained indefinately. They did this with experiments of six months duration or less. While the experimental advantages over other methods requiring years are obvious, there is also an element of doubt whether it can be determined with certainty over such a short time span that the deformation rate does in fact vanish.

Kalina (1971) found that he could predict the creep limit of composite beams and trusses from the deformation behavior of these elements loaded at the design load over a period of only 60 days. The ratio of load at the creep limit to ultimate load ranged from 40% for nailed beams and trusses to 61% for lumber I-beams and 60 to 65% for glued trusses. It is interesting to note that the various determinations of the creep limit yield values which are rarely much greater than the 9/16 (56.25%) mentioned earlier.

## CREEP-RUPTURE UNDER SUSTAINED LOADS AND RAMP LOADING TO FAILURE

A creep limit or limit of plastic flow, as discussed in the previous section, may or may not actually exist and there is no direct experiment that could ever settle this question. The other view that may be taken is that wood under load is subject to some process of degradation or breakdown in its ability to resist loads; that this process will occur at any stress with the rate depending on stress level. The objective of studies then changes from the determination of a limiting stress, at which loads can be resisted indefinitely, to the determination of a function relating stress level to time to failure, so that a safe stress level can be estimated for a given length of projected service life. Such a function, based mainly on sustained-load tests to failure of Douglas-fir specimens started in 1943, was published by Wood (1951). His curve was based on both sustained-load tests and ramp-loading tests, and was derived by plotting stress level vs. time to failure, regardless of the type of stress history. Wood chose to represent the data by a hyperbolic curve which actually had an asymptote at the 18.3% stress level (based on static tests of about 7-1/2 minutes as 100%). While this still suggested a lower limit of stress akin to the creep limit, it was too low to be of any practical significance. The curve developed by Wood forms the basis for duration-of-load adjustments in current engineering practice in the U.S., and in recent years has come to be known as the "Madison curve".

Pearson (1972) examined the available data from sustained-load and ramp-loading tests of wood in bending, and concluded that the results obtained by a number of different investigators were consistent with each other. The data did not show any evidence of what Pearson called a threshold-of-creep strength (creep limit), and he asserted that if such a threshold did in fact exist it would have to be at a stress level below 50%.

Ju. Ivanov (1976) proposed that the results of sustained-loading tests can be represented by a single curve, regardless of species, moisture content, and form of loading (bending, shear, etc.). However, this required certain adjustments of the data which did not appear to be explained in great detail. Gerhards (1977a) made a comprehensive analysis of data obtained from both sustained and ramp loading, including wood and wood-based materials and bending as well as other tests. He reported that sustained shear loads had a greater effect on time to failure than either compressive or bending loads. Some data obtained by Sugiyama (1967) in shear suggest the same effect. There is also evidence that tension-perpendicular-to-grain strength is more subject to duration-of-load effects than bending strength (Bach, 1975; Madsen, 1972c). One study of Strickler *et al.* (1976) dealt with tension parallel to grain. The authors incorporated proof loading and a special approach to estimate the 100% level instead of the more usual specimen matching. The results indicated that in tension parallel also the duration-of-load effect appeared to be somewhat more severe than in bending.

Tests with notched beams subjected to sustained loading indicated that, if the plane bisecting the notch was parallel to grain, the relationship between fracture toughness and time to failure followed essentially the Madison curve (Schniewind and Centeno, 1973; Schniewind, 1977). When the notch plane was perpendicular to grain, sustained-load tests could not be made, apparently because of stress distribution around the notch tip, but ramp-loading tests showed that in this configuration the fracture toughness increases with time (Schniewind, 1977). This is the only known situation where the normal duration-of-load trend is reversed.

When small beams subjected to sustained loading are also exposed to cyclic variations in moisture content, time to failure is greatly reduced, the reduction being proportional to the extent of the fluctuations in moisture content (Schniewind, 1967). Larger cross sections of the loaded beams resulted in less serious reductions in the time to failure, suggesting that under most circumstances structural lumber would not be significantly affected by daily and seasonal fluctuations in moisture content (Schniewind and Lyon, 1973).

The Madison curve as presented by Wood (1951) was based on both ramp-loading and sustained-loading tests, practical reasons dictating the use of ramp loading for short time scales (minutes or less) and sustained loading for longer time scales. As Gerhards (1977a) pointed out, given the same time to failure one would expect the failure stress to be higher for ramp loading than for sustained loading because, in ramp loading, the material experiences the highest stress for only a very short time. Available data were somewhat contradictory, but on the whole were in agreement with that expectation. Thus, strictly speaking, ramp-loading and sustained-loading data should not be compared directly or combined without suitable adjustments, but how such adjustments might be made is not readily apparent at this time.

## DURATION OF LOAD EFFECTS IN STRUCTURAL LUMBER

The discussion in the preceding section was largely based on work with small, clear specimens or wood-based materials. Recognizing that the behavior of clear wood in small specimens does not necessarily forecast the behavior of structural lumber, with its various imperfections, extensive testing has been done in Canada on full-size dimension lumber. Because of the random nature of growth and other defects in structural lumber, it is not possible to obtain piece-by-piece matching to establish 100% levels for sustained-load tests. Madsen (1971, 1972a, 1972b, 1972c) solved the problem of matching by going to ramp loading instead, approximated by a stepwise, regular addition of load increments. Loading rates varied, the slowest producing failure in about 2-1/2 months. Grouping the results according to time to failure, Madsen found that, in bending and in shear, the duration-of-load effect depended on failure-stress level. The upper percentiles within each group indicated a pattern like the Madison curve, while the lowest percentiles showed little or no influence of loading rate on the failure stress. This suggested that for structural lumber, where loads are based on stress levels appropriate to the weaker members of a given distribution (species and grade), duration-of-load effects need not be taken into account.

Additional work by Madsen and Barrett (1976) was done by matching distributions of lumber instead of the more usual pair matching. The conclusion again was that the Madison hypothesis was not valid for lumber in bending, and that there was a definite trend for a more pronounced duration-of-load effect at the higher stress levels. As a result of these and other recent studies, the concept and practice of duration-of-load adjustments has come under re-examination.

## MECHANISMS AND A WORKABLE FAILURE THEORY

With very few exceptions, the work to date on duration-of-load effects has involved either sustained or ramp loading. When both have been used, the problem arises as the how to reconcile the results. More significantly, in actual practice the load histories experienced by structures in service will seldom resemble the single-step input of sustained loading or ramp loading, as used in tests. Present practice is based on the concept that the effects of more than one loading period are cumulative, but to deal with intermittent loads they all have to be steps of equal stress level. What is needed, therefore, is a workable failure theory which can predict time to failure under a variety of continuous and intermittent loading histories. Ideally, such a theory should be based on an analysis of the failure mechanism involved. Thus it may be useful to examine some of the possible mechanisms that lead to the observed type of delayed failure.

Flow has been suggested as the controlling mechanism. However, there is no evidence that failure in wood is accompanied by significant flow. Thus, phenomena such as necking are not observed in wood. Detailed investigations of this question do not seem to have been made.

Bach (1973) proposed applying Reiner-Weissenberg's theory to time-dependent fracture in wood. According to this theory, fracture occurs when the stored delayed elastic potential reaches a critical value, regardless of the form of loading. First calculations appeared to be promising, but further confirmation is still lacking.

Another approach is to consider time-dependent fracture in terms of a rate process, where bond breaking takes place over a period of time until a critical weakening of the material has been achieved. On this basis, it is possible to predict the kind of semi-logarithmic relationship between stress level and time to failure in sustained load tests that is actually observed; i.e., a linear relationship between stress level and the logarithm of the time to failure. This approach has been used by Cousins (1974) to study strain-rate effects in tension perpendicular to grain and he found good agreement with the theory. It was based on the assumption that failure is governed by breaking of hydrogen bonds in the matrix (lignin and associated materials), which is plausible in the case of tension perpendicular to grain, but cannot so readily be accepted in the case of loading parallel to grain; e.g., tension where primary bonds must be assumed to play a major role.

Mindess *et al.* (1975, 1976) used a model of subcritical crack growth to deal with static fatigue in wood. According to the model, failure is governed by ever-present flaws or cracks. These will show slow growth at a rate, V, dependent on the stress-intensity factor, $K_I$. When $K_I$ reaches a critical value, failure occurs by rapid crack propagation. This model can be used to predict duration-of-load effects by obtaining and then integrating the $V$-$K_I$ plot for a material and loading situation. Potentially, the slow crack growth model would make it possible to predict the behavior over a time span of years on the basis of tests made in less than one day, but results so far show as yet irreconcilable differences between the results of short-term tests and the conventional long-term tests in the literature.

In contract to the model of Mindess *et al.* (1975), the cumulative-damage model of Gerhards (1977b) is empirical in the sense that it is not based on any particular failure mechanism. It presumes that the material has a characteristic lifetime at each stress level. Time spent at a particular stress level is accounted for in terms of fractional-life time. Failure occurs when the sum of all fractional-life times corresponding to the total stress history reaches unity. This model is still awaiting experimental verification.

## CONCLUSION

As may be evident from the foregoing discussion, we are still lacking insight into the subject of duration-of-loading effects in wood. Probably the most significant recent advance in this area is the realization that structural lumber does not necessarily behave the same as clear wood. In planning future work, it will therefore be important to consider whether the particular objectives can be achieved by use of small, clear specimens or whether full-size lumber must be used. Most of the work to date has been done in bending, and it has been assumed that the results can be applied to other forms of loading as well. Whether this assumption is justified is not at all clear and the question merits further study. Similarly, the quest for a suitable failure theory must be continued, preferably in conjunction with a search for discovery of failure mechanisms. Only in this way will a true understanding of the problem become possible.

## REFERENCES

Bach, L. 1973. Reiner-Weissenberg's theory applied to time-dependent fracture of wood subjected to various modes of mechanical loading. Wood Sci. 5(3): 161 - 171.

Bach, L. 1975. Failure perpendicular to the grain in wood subjected to sustained bending loads. Wood Sci. 7(4): 323 - 327.

Cousins, W.J. 1974. Effects of strain-rate on the transverse strength of *Pinus radiata* wood. Wood Sci. & Tech. 8(4): 307 - 321.

Gerhards, C.C. 1977a. Effect of duration and rate of loading on strength of wood and wood-based materials. USDA, Forest Serv., Res. Pap. FPL 283.

Gerhards, C.C. 1977b. Time-related effects of loads on strength of wood. Proc. Conf. Environmental Degradation of Engineering Mater., Coll. Engineering, Va. Polytech. Inst. Univ., Blacksburg, VA.

Gillwald, W. and H. Luthardt. 1966. Beitrag zur Dauerstandfestigkeit von Vollholz and Holzspanplatten. Holztechnologie 7(1): 25 - 29.

Ivanov, G.M. 1938. After-effect strain and the "limit of plastic flow" in wood. Comptes Rendu (Doklady), Acad. Sci. URSS 19(6/7): 549 - 552.

Ivanov, Ju.M. 1976. Ueber die einheitliche Gesetzmaessigkeit fuer die Dauerfestigkeit von Holz. Holztechnologie 17(1): 9 - 10.

Kalina, M. 1971. Zerstoerungsfreie Bestimmung der Dauerfestigkeit von Traegern aus dem rheologischen Verhalten unter Dauerlast. Holztechnologie 12(4): 239 - 243.

Madsen, B. 1971. Duration of load tests for dry lumber in bending. Univ. B.C., Dep. Civil Eng., Struct. Res. Ser. Rep. No. 3, Vancouver, B.C.

Madsen, B. 1972a. Duration of load tests for wet lumber in bending. Univ. B.C., Dep. Civil Eng., Struct. Res. Ser. Rep. No. 4, Vancouver, B.C.

Madsen, B. 1972b. Duration of load tests for dry lumber subjected to shear. Univ. B.C., Dep. Civil Eng., Struct. Res. Ser. Rep. No. 6, Vancouver, B.C.

Madsen, B. 1972c. Duration of load tests for wood in tension perpendicular to grain. Univ. B.C., Dep. Civil Eng., Struct. Res. Ser. Rep. No. 7, Vancouver, B.C.

Madsen, B. and J.D. Barrett. 1976. Time-strength relationship for lumber. Univ. B.C., Dep. Civil Eng., Struct. Res. Ser. Rep. No. 13, Vancouver, B.C.

Mindess, S., J.S. Nadeau, and J.D. Barrett. 1975. Slow crack growth in Douglas-fir. Wood Sci. 8(1): 389 - 396.

Mindess, S., J.S. Nadeau and J.D. Barrett. 1976. Effect of constant deformation rate on the strength perpendicular to grain of Douglas-fir. Wood Sci. 8(4): 262 - 266.

Pearson, R.G. 1972. The effect of duration of load on the bending strength of wood. Holzforschung 26(4): 153 - 158.

Schniewind, A.P. 1967. Creep-rupture life of Douglas-fir under cyclic environmental conditions. Wood Sci. & Technol. 1(4): 278 - 288.

Schniewind, A.P. 1977. Fracture toughness and duration of load factor II. Duration factor for cracks propagating perpendicular-to-grain. Wood & Fiber 9(3): 216 - 226.

Schniewind, A.P. and J.C. Centeno. 1973. Fracture toughness and duration of load factor I. Six principal systems of crack propagation and the duration factor for cracks propagating parallel to grain. Wood & Fiber 5(2): 152 - 159.

Schniewind, A.P. and D.E. Lyon. 1973. Further experiments on creep-rupture life under cyclic environmental conditions. Wood & Fiber 4(4): 334 - 341.

Strickler, M.D., R.F. Pellerin, and J.W. Martin. 1976. Duration of load characteristics of structural members in bending and tension. Wash. State Univ., Coll. Eng. Bull. 340, Pullman, WA.

Sugiyama, H. 1967. On the effect of the loading time on the strength properties of wood. Wood Sci. & Tech. 1(4): 289 - 303.

Wood, L.W. 1951. Relation of strength of wood to duration of load. USDA, Forest Serv., Forest Prod. Lab., Rep. 1916, Madison, WI.

# EFFECT OF PRE-LOADING ON FRACTURE TOUGHNESS OF WOOD

By

A.P. Schniewind , H.J. Bartels and B.W. Gammon

---

University of California, Forest Products Laboratory, Richmond, CA.

## INTRODUCTION

As interest has grown in applying the concepts of fracture mechanics to wood in relation to structural design, the question arises to what extent the necessary material parameters are subject to the duration-of-load factor. To examine this question, several investigators have used dead-load tests at various stress levels, as well as ramp-loading tests at various loading rates. Walsh (1971) examined three Australian species in the TL system (the first letter, T, denotes the normal to the crack plane and the second, L, the direction of crack propagation) using both ramp-loading and dead-load tests and concluded that the duration-of-load factor was about the same for the critical stress intensity factor, $K_{Ic}$, as it was for modulus of rupture. Similar tests on Douglas-fir, also in the TL system, led to the same conclusion (Schniewind and Centeno 1973). Dead-load tests of Douglas-fir in the TR system showed that $K_{Ic}$ in this system was somewhat less sensitive to duration-of-load effects, but qualitatively the same effect was observed (Schniewind 1978). The inference can then be made, on the basis of similarity in anatomic structure and the values of the critical stress intensity factors from static tests, that the TL, TR, RL, and RT systems show a duration-of-load effect which can be accounted for by what has come to be known as the "Madison curve" as originally proposed by Wood (1951).

When LT and LR systems have been examined, however, entirely different results have been obtained. Madsen (1972) tested some notched beams of Douglas-fir (system not specified, except that it was either LT or LR or both) at two rates of ramp loading. Dividing the total distribution into percentiles, the results indicated that the lower strength material decreased only slightly in strength when the time to failure was increased, while the higher strength material showed the opposite trend. Leicester (1974) reported on ramp-loading tests of an eucalyptus species (messmate stringybark), also notched beams in either LT or LR or both, made at loading rates to produce failure at times ranging from less than 1 to about 300 minutes. These data showed a maximum for $K_{Ic}$ at about 20 minutes for the time to failure. Finally, ramp-loading tests of messmate stringybark, using single-edge-notch tension specimens in the LR system and Douglas-fir using notched beams in the LT system, showed an increase in critical stress intensity factor when the loading rate was decreased, thus increasing the time to failure (Schniewind 1978). For the Douglas-fir tests, which include observations over approximately six decades of log time, the increase in $K_{Ic}$ was found to be statistically significant. These results, as well as observations made while unsuccessfully attempting to make constant-load creep-rupture tests in the LR and LT systems (Schniewind 1978) suggest that there is a redistribution of stresses taking place in the vicinity of the crack tip.

If slow loading facilitates redistribution of stresses, then a period of loading at loads high enough to cause significant stresses, but low enough to avoid failure or crack initiation, should result in an increase in the apparent critical stress intensity factor. In other words, certain loading regimes would be expected to lead to an increase in load-carrying capacity. The objective of the present report is to examine this question. The major part of the experiments was done with notched beams of Douglas-fir. Because of the effects of knots and knot holes on load-carrying capacity, some tests were made with specimens of white fir containing knots.

## MATERIAL AND METHODS

Douglas-fir (*Pseudotsuga menziesii* [Mirb.] Franco) specimen material was taken from 14 flat-sawn 1 x 12-inch boards ranging in specific gravity from 0.41 to 0.55 based on oven-dry weight and volume. White fir (*Abies concolor* [Gord. & Glend.] Lindl.) specimen material was obtained from 30 small boards from nine trees. The average specific gravity of the white fir was 0.38 based on oven-dry weight and volume, and individual specimens ranged from 0.31 to 0.49.

Tests to determine $K_{Ic}$ in the LT system were made using the specimen shown in Fig. 1, centrally loaded in bending over a span of 4 inches with the notch on the tension

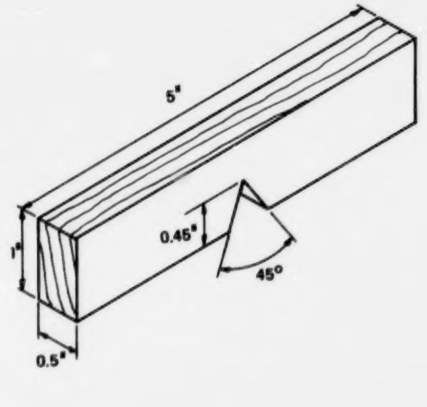

Fig. 1. Test specimen. Some specimens contained a knot in place of the notch.

side. Since in the LT system the crack does not propagate in the direction of the bisector of the notch, but rather follows the grain direction, $K_{Ic}$ calculations were based on load at first crack initiation. This was detected by two means. One was the load at the proportional limit in the plot of load versus crack opening displacement (COD). The other was the load at 50 counts of acoustic emissions (Schniewind and Centeno 1973; Schniewind 1978). Acoustic emission measurements were made using Dunegan/Endevco Series 3000 equipment with an S140B transducer. The total gain was 65 dB at a filter setting of 0.1 to 0.3 MHz. Total counts of acoustic emission were recorded as a function of load on an x-y recorder.

The testing scheme for notched Douglas-fir samples is shown in Fig. 2. First, static tests to failure were made on 10 specimens from each of 14 boards, which were used as controls for establishing 100% values for subsequent calculation of preload levels. Tests were made at a cross-head speed of 0.02"/min. Specimens were preloaded at 80% load level for 1 sec., and 1.5, 15, and 150 hrs. In addition, one group was preloaded at 60% load level for 15 hours. Load levels were calculated based on load at 50 counts in the control tests. These were computed separately for the material from each board, since there were large variations in specific gravity. There were three specimens per board for a total of 42 for each preloading treatment.

The preloading was done in dead-load test frames within a conditioning chamber held at 70°F and 65 percent relative humidity. Acoustic emissions were monitored during load application and for about 5 to 10 minutes thereafter. Specimens which gave more than 25 counts during this initial period were eliminated. One out of six specimens was monitored continuously during the entire preloading period. Except for one specimen among those monitored continuously, there were no cases of significant acoustic emission during the preloading period. In the one case where it did occur, the recorded signals were very intense over a very short period of time, suggesting that these were spurious signals. The 1-second preloading was done in the testing machine, by loading to the desired load level and immediately unloading again. The 1-second duration is thus nominal rather than actual preload time.

All specimens were allowed to recover for 10 minutes after removal of the preload and then tested to failure (crack initiation) in a testing machine.

White fir material included both notched samples (Fig. 1) and samples containing knots. The material with knots was divided into three groups: an entire small knot as close as possible to the edge (type A), half of one knot at the edge (type B), and half a knot hole at the edge (type C). Fig. 3 illustrates these groups, showing minimum, average, and maximum size in each group. Specimen groups were divided into two subgroups, matched as closely as possible on the basis of knot size and shape, to serve as controls and preload specimens.

Since the knot sizes varied considerably, samples with knots were preloaded at 60% load level. Only very small knots could be used with the specimen that had been adopted and, therefore, the available ma-

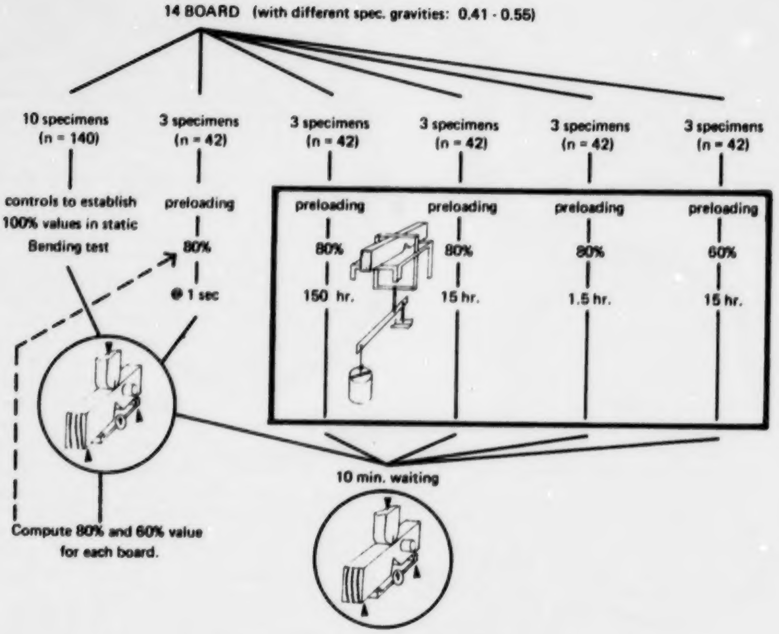
14 BOARD (with different spec. gravities: 0.41 - 0.55)
10 specimens (n = 140)
3 specimens (n = 42)
3 specimens (n = 42)
3 specimens (n = 42)
3 specimens (n = 42)
3 specimens (n = 42)
controls to establish 100% values in static Bending test
preloading
80%
@ 1 sec
preloading
80%
150 hr.
preloading
80%
15 hr.
preloading
80%
1.5 hr.
preloading
60%
15 hr.
10 min. waiting
Compute 80% and 60% value for each board.

Fig. 2. Testing scheme for Douglas-fir material.

terial was limited. The number of specimens varied from four to 11 depending on type and treatment. For the notched white fir material, 46 specimens were tested as controls. An equal number were used for preloading treatments, of which 21 were preloaded at 80% load level and 25 at 60% load level, both for a period of 20 hours. The measurements were made in the same way as with the notched Douglas-fir specimens.

## RESULTS AND DISCUSSION

The load at crack initiation was always determined by two methods, based on either acoustic emission (AE) or COD measurements. Fig. 4 shows a plot of all Douglas-fir data relating critical load at 50 counts AE to critical load at the proportional limit in the COD vs. load plot. The scales in Fig. 4 are somewhat odd because they are computer generated. Noteworthy is the high degree of correlation, with $r^2$=0.89. For perfect correspondence, the intercept should be zero and the slope unity; as shown on the figure, the intercept is at 5.02 lbs. and the slope constant equals 0.95. Thus in the lower range, the P(AE) values would tend to be somewhat higher than the P(COD) values, the opposite being true at loads in excess of about 100 lbs. Overall, however, the agreement can be considered a good one. Unless otherwise indicated, data and statistical analyses are based on AE measurements.

The results of tests of notched Douglas-fir specimens are summarized in Table 1. The mean value of $K_{Ic}$ of the control group (no preloading treatment) is lower than all the other means. At the 80% level of

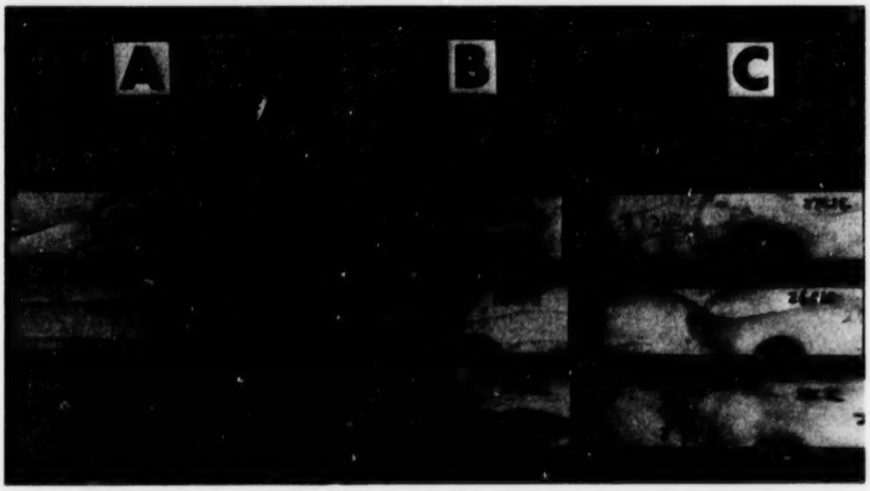

Fig. 3. White fir specimens containing knots instead of notches. Shown are Type A, entire knot, Type B, half knot, Type C, half knothole. For each type average, minimum, and maximum size are shown.

preloading, the mean is nearly equal to the control value at 1-second preloading time, but becomes larger as the length of the preloading period increases. The mean at 60% preload for 15 hours is about the same as the mean for 80% preload for 1.5 hours.

The above results are consistent with the hypothesis of time-dependent stress redistribution. At the 1-second preload, there is insufficient time for such redistribution to take place and there is virtually no change in fracture toughness. As the preloading time increases, redistribution becomes more extensive and the fracture toughness increases. At a lower stress level, the redistribution is less and at the same length of preloading period the increase in fracture toughness is less. Since there was a 10-minute period of recovery after preloading, a significant part of the delayed elastic deformation had the opportunity of being recovered. This suggests that the redistribution is largely due to irrecoverable or flow deformation.

A series of analyses of variance were made of the Douglas-fir data and the results are summarized in Table 2. First, all data were analyzed in a two-way analysis of variance, and both treatments and boards were found to be significant at the 1 percent level. Next some individual comparisons were made between pairs of data. This was done for two reasons: one to make specific comparisons, such as which treatments differed from the control group, and the other to be able to correct for bias resulting from the elimination of specimens with early counts of acoustic emission during preloading. Presumably, the specimens thus eliminated represent the weakest specimens in the group. Accordingly, when making comparisons between two groups, the control group was adjusted by eliminating the same percentage of the weakest specimens as had been lost in the treated group during preloading. This was done on a board-by-board basis. The adjustment had the effect of increasing the average fracture toughness value of the controls and, thus, made the statistical test stronger.

In making individual comparisons, boards were always significant on the 1 percent level. As expected, there is no difference between the controls and the 1-second preloading treatment, but for 1.5 hr. of preloading the increase in fracture toughness is significant at the 1 percent level. By extension, so are the longer times at the 80% load level. The only preloading treatment at 60% load level also shows a statistically significant increase in fracture toughness. In comparing load levels of 60 and 80% at the same preloading period of 15 hrs., the difference was not significant when using data based on AE, but was significant at the 1 percent level when COD was the basis. This was the only instance where the results of statistical analyses of Douglas-fir differed according to measurement basis.

The effect of preloading time at 80% load level on load at crack initiation is shown in Fig. 5. The data were first plotted and analyzed with the 1-second preload tests included. Since they did not fit very well, the analysis was repeated with the 1-second tests omitted. This omission can be justified because the 1-second designation is nominal and somewhat arbitrary, and because the model which has been proposed would require a leveling of the relationship at preloading times less than some value. If indeed flow is a major component of the observed effects, the amount of flow that could take place in, say, less than one hour would be very limited.

The coefficients of determination, $r^2$, are very small, which is a reflection of the large variability. This, of course, does not mean that preloading time is not a factor; it merely means that the percentage of the total variation which is explained by the regression is small. In fact, the regression is statistically significant, as shown in Table 3. Multiple regression analyses using specific gravity as an additional variable resulted in much larger values of $r^2$ and an increase in F-values as well (Table 3).

Fracture toughness values of white fir notched specimens preloaded at two load levels are shown in Table 4. The preload

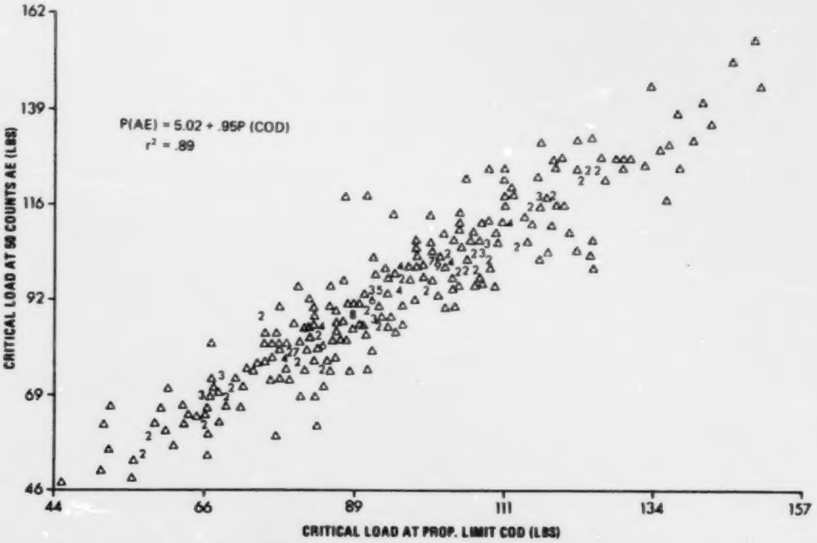

**Fig. 4.** Critical loads based on AE and COD measurements.

levels differ from the nominal values because of within-board matching. Thus, when preload specimens had to be eliminated because of early counts of acoustic emission, the corresponding controls were also taken out. This tended to increase the control average and thus lower the load level. Also, as may be seen from Table 4, values of $K_{Ic}$ differ according to measurement basis, AE based values being higher than those based on COD measurements. This would indicate that the level of emissions is species dependent. The criterion of 50 counts represents a calibration value appropriate for Douglas-fir, and it appears that either a lower count level or a higher dB setting would have been better for white fir.

At the (nominal) 60% preload level, the white fir shows lower $K_{Ic}$ values for the preloaded specimens than for the controls. Based on AE measurements, this difference was even statistically significant at the 5 percent level, as determined with a paired t-test (matched pairs from the same board). However, at the 80% level, the preloading treatment resulted in increased fracture toughness, just as had been observed in the case of Douglas-fir. The increase was statistically significant at the 5% level regardless of the measurement basis.

The results of tests of white fir containing knots are shown in Table 5. In this case the discrepancy between $K_{Ic}$ based on AE and COD measurements is even greater, AE measurements always giving the higher values. It might have been expected that the knots would become "noisy" before there was a measurable change in the deformation behavior, but the opposite effect has taken place.

The general level of values for knot samples is much higher than for notched samples of the same species. That was to be expected, especially in the case of knot holes, since their shape is much different from a sharp crack. Yet in calculating $K_{Ic}$ the pieces were assumed to have a sharp crack of a size equal to the depth of the knot itself or of the knot hole. Since the main purpose was to compare controls and preloaded specimens, more detailed modeling was not attempted.

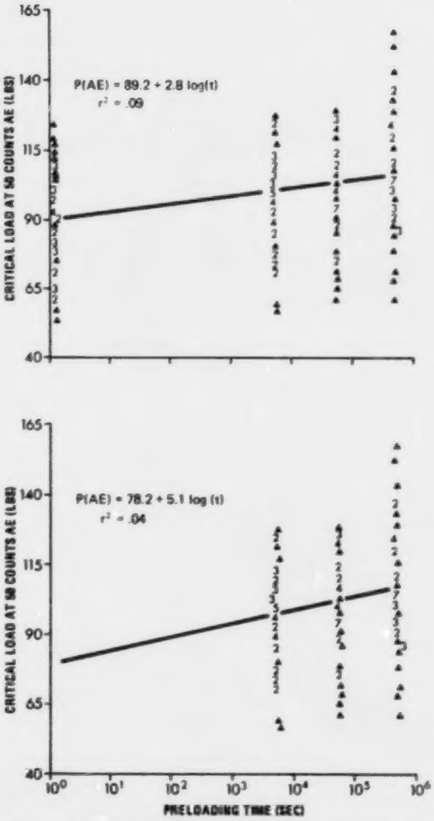

Fig. 5. Critical load as a function of preloading time, with (above) and without (below) specimens nominally preloaded for 1 sec.

The values of fracture toughness in groups B and C are about the same, in line with long experience that knots and knot holes of the same size and shape have about the same effect on strength. The group A values are higher, which is due to the fact that the knots seldom passed straight through the piece. Thus, on one face the knot might be tangent to the edge, while on the opposite face it would be somewhat away from the edge. The ligament of wood tissue that thereby remained at the edge no doubt had a strong strengthening influence.

In every group of knots, regardless of the measurement basis, the average fracture toughness value is higher for the preloaded specimens than for the controls. None of these differences were statistically different on the basis of t-tests. In view of the small sample numbers, this is not very surprising. The number of specimens had originally been 40 percent greater. Because of the large variability of the specimens with knots, many were lost due to early counts during preloading. To avoid bias, an equal number of the controls were eliminated, choosing those that had the lowest loads at crack initiation based on AE measurements. This was done on the basis that those same specimens would have been lost due to early counts, if they had been selected for preloading. An analysis of variance, using a two-way classification (knot type and preload treatment), similarly did not show statistically significant results. This does not necessarily mean that the observed increases are artifacts, but rather that the number of specimens was not sufficient. Thus the evidence is not as convincing as in the case of notches, but there is a strong indication that the fracture toughness of samples with knots is affected in the same general way.

Somewhat unexpected is the finding that the fracture toughness values for the notched white fir samples are about the same as the Douglas-fir samples. Also, the $K_{Ic}$ values for Douglas-fir are much lower than previously reported values (Schniewind and Centeno 1973). Specific gravity data were not reported by Schniewind and Centeno, but since the specimen material was still available, specific gravity was determined for a random sample of 18 specimens previously tested in the LT system. The average specific gravity was found to be 0.59 based on oven-dry weight and volume. Since this is much higher than the values of the present study, it is reasonable that the $K_{Ic}$ values should also differ. The present data for Douglas-fir controls, averaged by boards, and for white fir controls, averaged by tree of origin, are plotted in Fig. 6. In addition, a single point for the previously tested Douglas-fir, and a trend line which was hand fitted to some data published by Leicester (1974) for mixed Australian woods are shown in the figure.

The data assembled in Fig. 6 suggest that, while there is a relationship between fracture toughness values, this seems to hold true mainly for within-species variation. Thus virtually all of the difference between previous data and the present results for Douglas-fir can be explained on the basis of specific gravity differences. The Douglas-fir and white fir data seem to form distinct populations, and both regression lines differ from the trend line of Leicester's data. However, if the Douglas-fir and white fir species means are plotted together with Leicester's data for mixed species, no differences are apparent. In other words, there is considerable variation about the trend line and it represents the Douglas-fir and white fir data as well as the Australian species on which it is based.

## CONCLUSIONS

The data show that, as predicted from previous investigations, a period of preloading

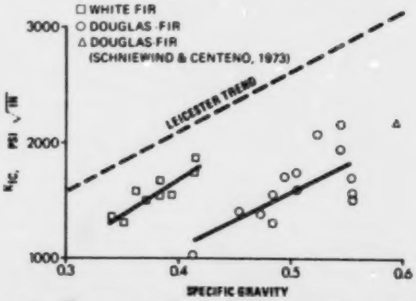

Fig. 6. $K_{Ic}$ as a function of specific gravity. Points for white fir are tree averages based on from one to 10 specimens (50 total); Douglas-fir data are board averages based on 10 specimens each.

of notches or cracks in the opening mode in the LT system (and presumably also in the LR system) results in an increase in the value of $K_{Ic}$. It is presumed that this is due to redistribution of stresses around the crack tip, which is a function of the magnitude of the preload and its duration. Limited tests on samples containing knots rather than notches indicate that they are subject to a similar effect.

While the results do not suggest a practical method of increasing the load-bearing capacity of wood structural members, they do show that, when designing on the basis of fracture mechanics concepts, $K_{Ic}$ values in the LR and LT systems need not be adjusted for duration-of-load effects, as is the case with other parameters used in wood structural design.

## REFERENCES

Leicester, R.H. 1974. Fracture strength of wood. First Aust. Conf. Eng. Mater., Univ. New South Wales, Sidney, Aust.

Madsen, B. 1972. Duration of load tests for wood in tension perpendicualr to grain. Dep. Civil Eng., Univ. B.C., Struct. Res.Ser. Rep. No. 7, Vancouver, B.C.

Schniewind, A.P. 1978. Fracture toughness and duration of load factor. II. Duration factor for cracks propagating perpendicular to grain. Wood Fiber (in press)

Schniewind, A.P., and J.C. Centeno. 1973. Fracture toughness and duration of load factor I. Six principal systems of crack propagation and the duration factor for cracks propagating parallel to grain. Wood Fiber 5(2):152-159.

Walsh, P.F. 1971. Cleavage fracture in timber. Aust. CSIRO, Div. Forest Prod. Technol., Pap. No. 65, Melbourne, Aust.

Wood, L.W. 1951. Relation of strength of wood to duration of load. U.S.D.A., Forest Prod. Lab. Rep. No. 1916, Madison, WI.

TABLE 1. $K_{Ic}$ values of notched Douglas-fir specimens

| Preload period | Preload level | | |
|---|---|---|---|
| | none ($\text{psi}\sqrt{\text{in}}$) | 60% ($\text{psi}\sqrt{\text{in}}$) | 80% ($\text{psi}\sqrt{\text{in}}$) |
| None | 1630 (362)* | | |
| 1 second | | | 1640 (343) |
| 1.5 hour | | | 1770 (313) |
| 15 hours | | 1780 (319) | 1860 (378) |
| 150 hours | | | 1950 (415) |

*Numbers in parentheses are standard deviations

TABLE 2. Analyses of variance of notched Douglas-fir data

| Classification | Source | d.f. | F value |
|---|---|---|---|
| 1. All treatments | Treatment | 5 | 26.6** |
| | Board | 13 | 69.5** |
| 2. Controls vs. 1 sec, 80% | Treatment | 1 | 0.001 n.s. |
| | Board | 13 | 27.7** |
| 3. Controls vs. 1.5 hr., 80% | Treatment | 1 | 15.5** |
| | Board | 13 | 27.4** |
| 4. Controls vs. 15 hr., 60% | Treatment | 1 | 18.2** |
| | Board | 13 | 25.9** |
| 5. 15 hr., 80% vs. 60% | Treatment | 1 | 2.7 n.s.[1] |
| | Board | 9[2] | 32.1** |

[1] Significant at the 1-percent level when using values based on COD.

[2] To avoid bias, boards where early counts caused specimen loss were omitted entirely from this particular comparison.

** Significant at the 1-percent level; n.s. not significant.

TABLE 3. Simple and multiple regression analyses at the 80% preloading level for critical load (AE), specific gravity, and preloading time

| Regression variables | N | Intercept (A) | Slope ($B_1$) | Slope ($B_2$) | $r^2$ | F-value |
|---|---|---|---|---|---|---|
| Critical load vs. preloading times | 168 | 89.23 | | 2.81 | .09 | 15.57** |
| Critical load vs. preloading times (without 1 sec. test) | 126 | 78.22 | | 5.07 | .04 | 5.15* |
| Critical load vs. spec. gr., preloading times | 168 | –67.31 | 311.77 | 2.81 | .47 | 72.46** |
| Critical load vs. spec. gr., preloading times (without 1-sec. test) | 126 | –81.19 | 317.45 | 5.08 | .44 | 48.98** |

*Significant at the 5% level

**Significant at the 1% level

TABLE 4. Fracture toughness of notched white fir specimens

| Measurement basis | Treatment | 51% (58%)[1] preload, N = 25<br>$K_{Ic}$ (psi$\sqrt{in}$) | <br>Paired t-test | 78% (90%)[1] preload, N = 21<br>$K_{Ic}$ (psi$\sqrt{in}$) | <br>Paired t-test |
|---|---|---|---|---|---|
| AE | Control | 1590 | −2.54* | 1620 | 2.16* |
|  | Preload | 1510 |  | 1700 |  |
| COD | Control | 1400 | −0.76 n.s. | 1350 | 2.26* |
|  | Preload | 1360 |  | 1500 |  |

[1] Actual values after adjustments, based on AE measurements. Values in parentheses are used on COD measurements.

* Significant at the 5-percent level; n.s. not significant

TABLE 5. $K_{Ic}$ values of white fir specimens with knots

| Measurement basis | Type of knot | $K_{Ic}$ values, psi$\sqrt{in}$<br>Control | <br>Preload |
|---|---|---|---|
| Acoustic | Type A, entire knot (N = 11) | 3680 | 4610 |
| Emissions | Type B, half knot (N = 10) | 2900 | 3480 |
|  | Type C, half knothole (N = 4) | 2790 | 3780 |
| Crack | Type A, entire knot (N = 11) | 2430 | 3020 |
| Opening | Type B, half knot (N = 10) | 1980 | 2010 |
| Displacement | Type C, half knothole (N = 4) | 2040 | 2170 |

# FRACTURE MECHANICS ANALYSIS OF BUTT JOINTS IN LAMINATED-WOOD BEAMS

By

F.W. Smith[1] and D.T. Penney[2]

---

[1] Professor, Department of Mechanical Engineering, Colorado State University, Fort Collins, Colorado

[2] Associate Engineer, IBM Corporation, Boulder, Colorado

## ABSTRACT

A theoretical and experimental study was conducted to determine the applicability of fracture-mechanics theory to predicting the failure of laminated-wood beams containing butt joints. Tests were conducted on laminated beams of Douglas-fir and southern pine, with the butt joints being subjected to loading states of pure bending, pure shear, and mixed states of bending and shear. In all cases, cracks were found to initiate from the butt joints and propagate in a direction parallel to the grain. Mode I fracture dominated the failures observed in most cases, indicating the importance of the radial-tension properties of the wood for predicting failure in these experiments. A small amount of experimentation was done with artificially induced cracks parallel to the grain which failed in pure Mode II.

Approximate fracture mechanics analyses of the cracks encountered were conducted and it was found that fracture-mechanics theory can predict failure as long as careful attention is given to the direction of crack growth.

## INTRODUCTION

Fracture mechanics is the area of solid mechanics devoted to the development of methods to predict the failure of cracked structures under the influence of applied loads. It is a relatively new science developed extensively since the 1950s primarily for the analysis of metallic structures. The theories of fracture mechanics provide the capability to predict the failure load of a cracked structure taking into account the crack size and shape, the structural geometry, the stress levels and the material properties.

The application of fracture mechanics to the design of wood structures has not received a great deal of attention. However, since wood appears to be a fairly brittle material and since failure phenomena in wood seem to involve cracking to a great degree, it seems reasonable that fracture mechanics might provide a powerful design tool, if properly developed and applied to problems of structural design in wood.

There has been recent interest in developing understanding of the effects of butt joints on the strength characteristics of wood glulam beams. This paper deals with a theoretical and experimental study of the effects of butt joints in glulam beams making use of fracture mechanics analysis to develop understanding of the failure behavior.

A butt joint in a laminated-wood beam may be thought of as a crack-like flaw in the beam, thus potentially lending itself to the application of the theories of fracture mechanics. In applying fracture mechanics to metals, it is normally assumed that there is a strain energy release rate associated with crack growth which, upon reaching a critical value, causes rapid unstable propagation of the crack. It is normally assumed that the crack extends in its own plane and this assumption leads to simple relationships between the strain energy release rate and the quantity known as the stress intensity factor.

The stress intensity factor is a quantity which may be calculated from the linear theory of elasticity and this quantity generally depends on the applied stress and the crack size and geometry. A large number of two-dimensional stress intensity factor solutions are available in the literature and many of these may be applicable to fracture analysis of cracks in wood, as long as the cracks invoved are found to extend in the initial plane of the crack. There are situations in wood structures where the propagation of cracks is the dominant mechanism in failure, but the crack propagation is not found to be in the plane of the initial crack. When this situation occurs, it is necessary to include the influence of crack propagation direction on the calculation of the stress intensity factors. If this is properly done, it is then possible to use fracture mechanics theory to predict unstable crack propagation, even for the cases where crack propagation is not in the direction of the original crack plane.

In the present study, a number of experiments in laminated-wood beams were conducted involving butt joints in the tension lamination and in the center or other laminations. In all cases, it was found that crack propagation took place parallel to the grain of the laminations at an angle approximating 90° to the original plane of the butt joint. Approximate analyses of the situations have been undertaken and these analyses have been used to analyze the results of a number of experiments using the theory of fracture mechanics in an attempt to develop a technique to predict the effects of butt joints in laminated-wood beams.

## EXPERIMENTS

A number of laminated-wood beams of Douglas-fir and southern pine were manufactured under the supervision of the American Institute of Timber Construction. The beams were made of clear wood with butt joints at prescribed locations. Clear wood was used to minimize the effects of knots and other discontinuities, so that the effects of the butt joints could be isolated. Otherwise, an effort was made to manufacture the beams as they normally would be made in production. The Douglas-fir beams were manufactured at the Weyerhaeuser Company's Cottage Grove plant in Oregon, and the southern pine beams were manufactured at Anthony Forest Product's plant in El Dorado, Arkansas. Figure 1 shows the cross-sectional dimensions of the beams as received.

### Edge Butt Joints

Six 6'-long laminated beams of each species, with butt joints in the tension lamination, were tested in four-point bending as shown in Figure 2. As the loading on the beams was increased, cracks slowly formed at the root of the butt joint and grew at right angles to the butt joint in the adjacent lamination until catastrophic failure occurred. The crack did not follow the glueline, but propagated in the RL system, as shown in Figure 3, in the adjacent lamination following the slope of grain. The failure proceeded in a way which caused the bottom lamination plus a small amount of the second lamination to peel away from the rest of the beam.

### Embedded Butt Joints, Pure Shear Loading

Three 10'-beams of each species were tested as shown in Figure 4. The loading arrangement provided a state of pure shear and zero moment at the location of the butt joint. The joint was located in the center lamination where it was subjected to maximum shear stress. Some subcritical crack growth was observed before failure, but more was observed in southern pine than in Douglas-fir. The cracks again grew at 90° to the butt joint in the adjacent lamination and failed in the opening mode, as shown in Figure 5, as opposed to the sliding mode of fracture. In these experiments, high loads were required to induce failure and some problems arose due to the failure of the wood in compression under the load points. This condition lead to early onset of buckling in the steel loading beam, making it difficult to achieve the load necessary to produce failure. This difficulty was alleviated by milling slots in the bearing plates, as recommended by Bodig (1), and this procedure increased the loading capacity of the apparatus allowing for completion of the experiments. Because of the loading problem described above, some of the butt joints in these experiments were extended by sawing to reduce the loads for failure and to assess the effects of defect length.

### Embedded Butt Joints, Mixed Mode Loading

Four 10' beams of each species were tested under mixed-mode loading conditions with both normal and shear stress present as shown in Figure 6. In each case, the shear stress was the same for a given load and the bending stress was changed to provide the differing ratios by using a butt joint in the same lamintion and changing the dimension d as shown in Figure 6. These beams failed similarly to the pure shear cases with the addition of some sliding noted in the failure as well as the presence of opening mode.

### Longitudinal Cracks, Pure Shear

As the result of noting that the pure shear butt joint tests were failing in the opening mode, as opposed to the sliding mode of failure, an attempt was made to develop a test in which the failure occurred entirely in the sliding mode. Cracks were artifically cut in the longitudinal direction in the center of two beams of each species without butt joints, as shown in Figure 7. The beams were loaded with the same loading arrangement as was used in the pure shear butt-joint tests. When loaded to failure, the crack propagated along the original plane in the RL system and a pure sliding-mode failure was noted with no opening mode present.

### Verification Experiments

In an effort to verify the analyses of the edge and embedded butt-joint experiments, a series of single edge notch bend tests were conducted using specimens cut from the cross section of the laminated beams, as shown in Figure 8. These beams were loaded in three-point bending and the crack propagated along its initial plane.

### Testing Procedures

In all of the experiments, the applied load and both the normal and shearing relative displacement between the faces of the butt joints were recorded. Displacements were measured on both sides of each beam to assess variations through the thickness of the beams. Figure 9 shows a load-displacement record taken for one of the edge butt-joint experiments conducted in Douglas-fir. The rapid increase in crack opening displacement with no increased load designates the point at which rapid crack propagation took place and is designated as the point at which the stress intensity factor equations are evaluated to estimate the fracture toughness of the material. In the case of the experiments conducted on butt joints in the tension laminations, this failure condition was accompanied by a small amount of noise and followed by a slow peeling of the tension lamination from the bottom of the remainder of the beam. In the case of the embedded butt joints subjected to pure shear or mixed mode loading, the failure indication on the load-deflection records were accompanied by a loud bang and an obvious total failure of the beam.

### Test Results

Tables 1 and 2 present the data which resulted from all of the experiments conducted. The data given are those which resulted directly from the tests before any fracture mechanics analysis was done. In the following sections of this paper, the fracture mechanics analysis will be discussed.

## THEORETICAL DEVELOPMENTS

Because of the fact that the cracks in these experiments did not grow in the original plane of the butt joint, it was necessary to develop stress intensity factor solutions which account for the 90° rotation of the crack. Problems of the type encountered here could be easily analyzed using the finite element method, which could account for the cracked geometries encountered as well as the anisotropic material behavior. While it would be desirable to obtain the needed stress intensity factor solutions in this way, it was decided instead to use an approximate approach.

Figure 10 shows the superposition process which was used to deal with the problem of a butt joint in a tension lamination. Figure 9C shows the problem to which a solution is desired. The right-hand end of the beam in Figure 9C is taken to be a plane of symmetry cut through the plane of the butt joint. In this case, the crack is shown emanating in a leftward direction from the root of the butt joint. The desired solution is obtained by superimposing the solutions of parts A and B of Figure 10. Part A shows the beam being split apart by equal and opposite moments $M_0$. For this case a stress intensity factor solution is given by Tada (2) as:

$$K_I = \frac{M_o}{\sqrt{2bI}} \qquad (1)$$

where:

$$\bar{I} = \frac{I_1 I_2}{I_1 + I_2} \qquad (2)$$

and $I_1$ and $I_2$ are as shown in Figure 10.

If the moment $M_o$ is taken to be the moment required to bend the bottom lamination up to the remainder of the beam, then $M_o$ is found to be given by

$$M_o = \frac{E\bar{I}}{\rho_2} \qquad (3)$$

where $\rho_2$ is the radius of curvature of the bottom lamination. If we take

$$M = \frac{E I_1}{\rho_1} \qquad (4)$$

and if we assume for small deformations that

$$\rho_1 = \rho_2 \qquad (5)$$

we find $M_o$ to be given by $M_o = \frac{\bar{I}}{I_1} M_2$ (6)

Substituting this result into equation 1 results in

$$K_I = \frac{M}{I_1} \sqrt{\frac{\bar{I}}{2b}} \qquad (7)$$

This expression for the stress intensity factor can be expressed in the form

$$K_I = \sigma \frac{n^2}{(n-1)^2} \quad \frac{(n-1)\,h}{6[(n-1)+1]}^{1/2} \qquad (8)$$

for a beam having n laminations with a lamination thickness of h, a width b and an outer fiber bending stress σ.

Figure 11 describes the situation analyzed for the embedded butt joints. The butt joint is shown to be at the right-hand end of the segment of the beam being analyzed and the crack is shown to be emanating from one end of the butt joint in a leftward direction. Penney (3) estimated the stress intensity factor for this situation by considering only the strain energy due to shear. He found that the stress intensity factor could be roughly approximated as

$$K_i = \frac{6\bar{A}}{5b} \frac{E_R}{G_{LR}}^{1/2} \frac{V_1}{A_1} - \frac{V_2}{A_2} \qquad (9)$$

$$\bar{A} = \frac{A_1 A_2}{A_1 + A_2}$$

This analysis neglects any effect of bending, it was necessary to assume the values for the ratio $E_R/G_{LR}$ and the ratio of the shear loads $V_1$ to $V_2$ were found by assuming an undistributed parabolic stress distribution over the cross section. Equation (9) should be considered only a very rough approximation.

The fracture mechanics analysis of the experiments of the type diagrammed in Figure 8 was conducted using the formulas for the isotropic case due to Brown and Srawley (4). For the longitudinal-crack shear stress it was assumed that the stress intensity factor is given by

$$K_{II} = \tau \sqrt{\pi C} \qquad (10)$$

because the crack is relatively small compared to the dimensions of the beam and the crack was found to grow in its own plane.

## RESULTS

The fracture-toughness results are summarized in Table 3 for all tests which produced pure Mode I failure. The values obtained for the edge notch butt joint tests are results of substitution into equation (8). The values obtained for the pure shear embedded butt joint test are the results of substitution into equation (9). The values for the verification experiment were obtained by substitution into the standard equations found in reference (4). Ideally, all of the calculations of fracture toughness should predict the same value independent of the crack geometry and loading condition as long as pure Mode I fracture dominates. In Table 3, a very good agreement between the edge notch butt joint experiments and the verification experiments is noted for both species. The verification experiment results are also found to agree well with $K_{IC}$ results of other investigators, as summarized by Mindness *et al.* (6). The Mode I fracture toughness was found to vary between 234 and 373 psi $\sqrt{in}$ for a wide variety of tests on Douglas-fir. The results for the embedded butt joint subjected to pure shear are somewhat low in comparison, but it must be remembered that the analysis for this case is very approximate.

The results of the mixed-mode experiments are summarized in Table 4. The $K_I$ values were calculated using equation (9). In these experiments there was some Mode II present at fracture. Penney (3) made some very rough estimates of the magnitude of the Mode II stress intensity factor based on the nominal bending stress at the location of the butt joint, and found the $K_{II}$ to be approximately 25% of those shown in Table 4. From a failure criterion proposed by Wu (5) for embedded cracks in orthotropic plates, it was found that for $K_{II}$ values in this range there was only6% change in the predicted failure load using Wu's failure criterion. From this analysis, it was concluded that $K_{II}$ was not an important parameter in the tests conducted here. However, more work is needed to accurately assess the influence of $K_{II}$ on butt joints subjected to high bending stresses.

The agreement of the mixed-mode results with the verification test was about the same as for the pure shear embedded butt joints. The average of the tests on Douglas-fir is 10% above the average of the verification tests and the average $K_{IC}$ for southern pine is 25% high. This agreement is not very good, but is considered to be fair in light of the highly approximate nature of the analysis.

Table 5 presents the results of the pure shear longitudinal-crack experiments. These experiments did produce an in-plane failure and would seem to indicate that the Mode II fracture toughness is approximately six times greater than the Mode I fracture toughness.

## CONCLUSION

A series of experiments was conducted to assess the fracture behavior of cracks emanating from butt joints in laminated-wood beams. It was found that the cracks tended to grow at right angles to the original plane of the butt joints and the failures were dominated by Mode I fracture. The Mode I fracture toughness of Douglas-fir was found in these experiments to be approximatey 270 psi $\sqrt{in}$ and the fracture toughness of southern pine was found to be approximately 430 psi $\sqrt{in}$. It was found that it is important to include the effect of cracked growth direction in the analysis and that by so doing it was possible to calculate Mode I fracture toughness values which are comparable to those found by other investigators for Douglas-fir.

## REFERENCES

1. Bodig, J. 1969. Improved Load-Carrying Capacity of Wood in Transverse Compression. Forest Prod. J. 19(12):39-44.
2. Tada, H., P.C. Paris and G.R. Irwin. 1973. *The Stress Analysis of Cracks Handbook.* Del Res. Corp., Hellertown, Pa.
3. Penney, D.T. 1977. Fracture Mechanics Analysis of Butt Joints in Laminated Wood Beams. Master's thesis, Colo. State Univ., Fort Collins, Colo.
4. Brown, W.F., Jr. and Srawley, J.E. 1967. *Plane Strain Crack Toughness Testing of High Strength Metallic Materials.* ASTM Spec. Tech. Publ. 410, Philadelphia, Pa.
5. Wu, E.M. 1967. Application of Fracture Mechanics to Anisotropic Plates. J. Appl. Mech. 34E (4):967-974
6. Mindness, S., J.S. Nadeau and J.D. Barrett. 1975. Slow Crack Growth in Douglas-fir. Wood Science 8(1):389-396.

TABLE 1. Unreduced data for Douglas-fir tests.

| | Douglas-fir | | | |
|---|---|---|---|---|
| TEST | $\sigma$ | $\tau$ | $P_{CR}$ | a |
| Edge butt joint | 2153 | 0 | 10,250 | 1.50 |
| | 2153 | 0 | 10,250 | 1.50 |
| | 2573 | 0 | 12,250 | 1.50 |
| | 1890 | 0 | 9,000 | 1.50 |
| | 2415 | 0 | 11,500 | 1.50 |
| | 2048 | 0 | 9,750 | 1.50 |
| Verification experiment | 200 | 0 | 260 | .50 |
| | 216 | 0 | 281 | .50 |
| | 213 | 0 | 277 | .50 |
| | 210 | 0 | 273 | .50 |
| Pure shear embedded butt joint | 0 | 368 | 24,500 | 1.50 |
| | 0 | 465 | 31,000 | 1.50 |
| | 0 | 353 | 23,500 | 2.63 |
| Mixed-mode embedded butt joint | 725 | 350 | 25,000 | 1.50 |
| | 440 | 385 | 27,500 | 1.50 |
| | 424 | 371 | 26,500 | 1.50 |
| | 248 | 385 | 27,500 | 1.50 |
| Pure-shear longitudinal | 0 | 533 | 35,500 | 6.00 |
| | 0 | 390 | 26,000 | 12.00 |

$\sigma$ = Nominal bending stress (psi)

$\tau$ = Nominal shear stress (psi)

$P_{CR}$ = Critical failure load (pounds)

a = Full crack length (inches)

TABLE 2. Unreduced data for southern pine tests.

| | Southern pine | | | |
|---|---|---|---|---|
| TEST | $\sigma$ | $\tau$ | $P_{CR}$ | a |
| Edge butt joint | 3220 | 0 | 11,500 | 1.30 |
| | 3360 | 0 | 12,000 | 1.30 |
| | 4270 | 0 | 15,250 | 1.30 |
| | 4760 | 0 | 17,000 | 1.30 |
| | 3500 | 0 | 12,500 | 1.30 |
| | 3500 | 0 | 12,500 | 1.30 |
| Verification experiment | 437 | 0 | 460 | .38 |
| | 413 | 0 | 435 | .38 |
| | 390 | 0 | 410 | .38 |
| | | 0 | - | - |
| Pure shear embedded butt joint | 0 | 748 | 44,000 | 1.30 |
| | 0 | 417 | 24,500 | 2.38 |
| | 0 | 459 | 27,000 | 3.00 |
| Mixed-mode embedded butt joint | 1428 | 714 | 42,000 | 1.30 |
| | 1170 | 731 | 29,250 | 1.30 |
| | 765 | 765 | 45,000 | 1.30 |
| | 723 | 723 | 42,500 | 1.30 |
| Pure shear longitudinal | 0 | 711 | 39,500 | 4.00 |
| | 0 | 756 | 42,000 | 4.00 |

$\sigma$ = Nominal bending stress (psi)

$\tau$ = Nominal shear stress (psi)

$P_{CR}$ = Critical failure load (pounds)

a = Full crack length (inches)

TABLE 3. $K_{IC}$ results.

| | | $K_{IC}$(psi$\sqrt{in}$) | |
|---|---|---|---|
| Test | Species | Douglas-fir | Southern pine |
| Edge butt joint | | 243 | 344 |
| | | 243 | 359 |
| | | 291 | 456 |
| | | 214 | 508 |
| | | 273 | 374 |
| | | 232 | 374 |
| | AVE | 249 | 403 |
| Pure shear embedded butt joint | | 142 | 282 |
| | | 180 | 294 |
| | | 245 | 412 |
| | AVE | 189 | 329 |
| Verification experiment | | 260 | |
| | | 281 | 454 |
| | | 277 | 430 |
| | | 273 | 405 |
| | AVE | 273 | 430 |

TABLE 4. Mixed-mode fracture results.

| | | Mixed-mode $K_{IC}$ | |
|---|---|---|---|
| $\sigma/\tau$ | Species | Douglas-fir | Southern pine |
| 2 | | 283 | 520 |
| 1.5 | | 311 | 547 |
| 1 | | 299 | 558 |
| 0.5 | | 311 | 527 |
| AVE | | 301 | 538 |

TABLE 5. $K_{IIC}$ results.

| | | $K_{IIC}$ | |
|---|---|---|---|
| Test | Species | Douglas-fir | Southern pine |
| Pure shear longitudinal crack | | 1614 | 2505 |
| | | 1720 | 2664 |
| | AVE | 1667 | 2585 |

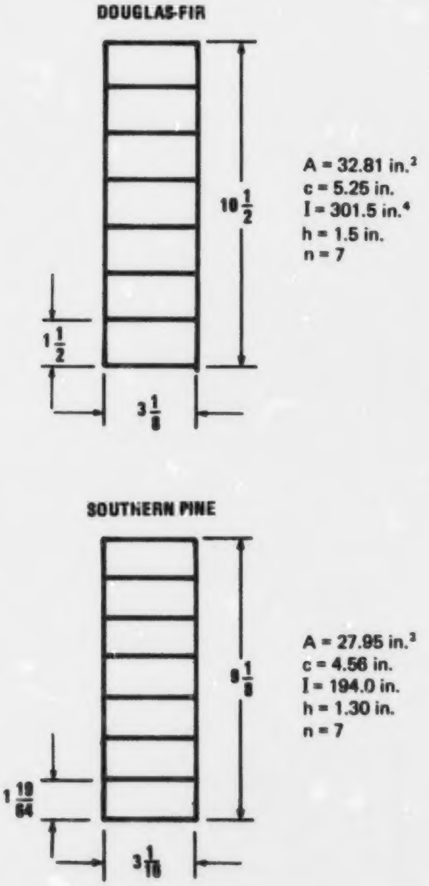
DOUGLAS-FIR
10 1/2
1 1/2
3 1/8
A = 32.81 in.$^2$
c = 5.25 in.
I = 301.5 in.$^4$
h = 1.5 in.
n = 7
SOUTHERN PINE
9 1/8
1 19/64
3 1/16
A = 27.95 in.$^3$
c = 4.56 in.
I = 194.0 in.
h = 1.30 in.
n = 7

Figure 1. Cross-sectional dimensions of test beams.

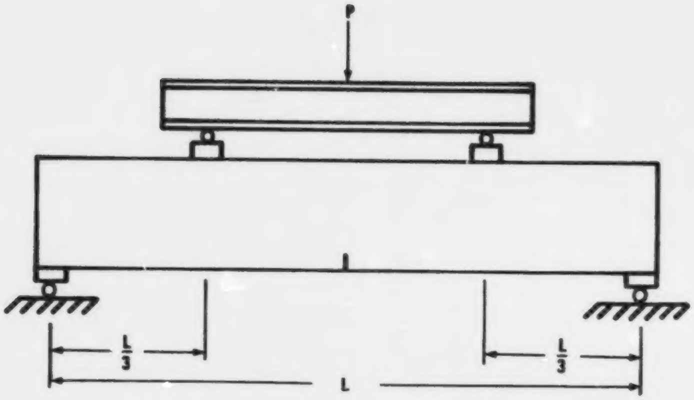

Figure 2. Edge notch butt joint test

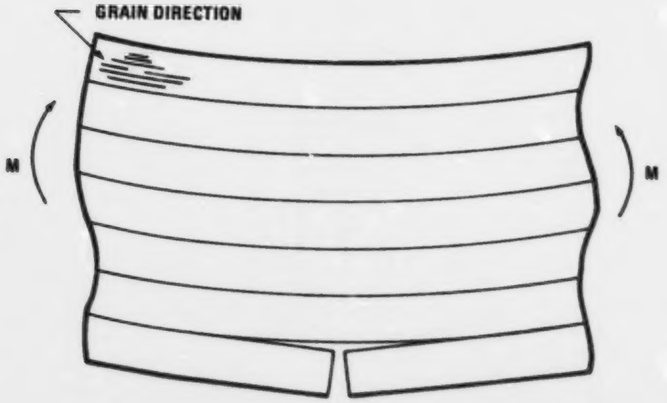
GRAIN DIRECTION
M
M

Figure 3. Edge butt joint failure as a "T" crack

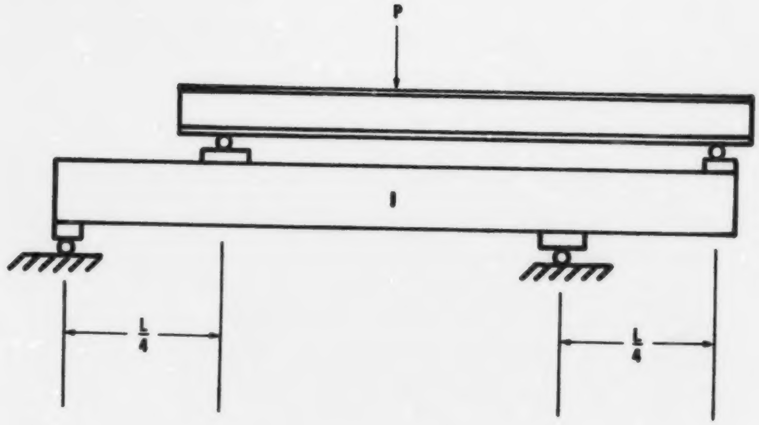

Figure 4. Pure shear embedded butt joint test

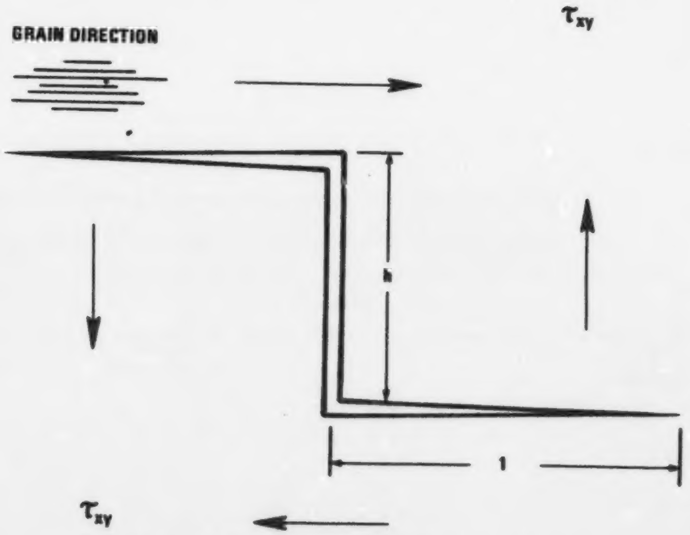
GRAIN DIRECTION
$\tau_{xy}$
h
1
$\tau_{xy}$

Figure 5. Pure shear embedded butt joint failure as a "z" crack

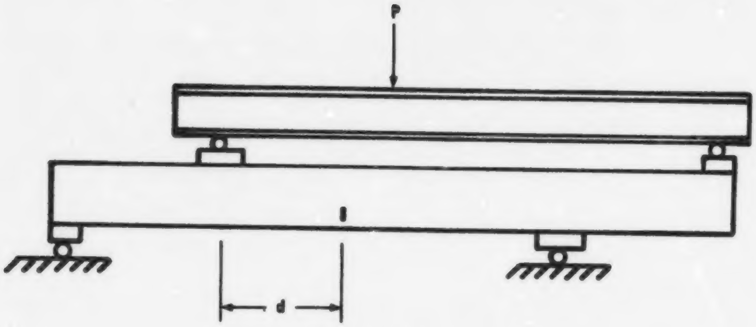

Figure 6. Mixed-mode embedded butt joint test

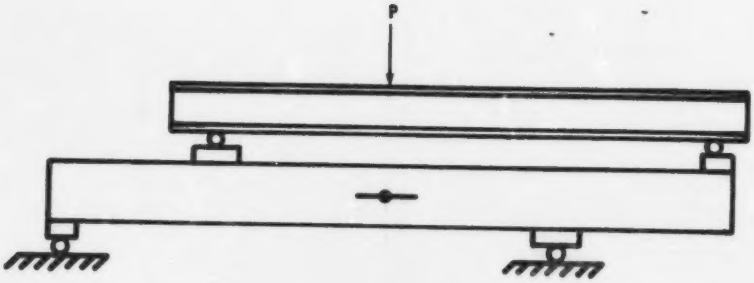

Figure 7. Pure shear longitudinal crack test

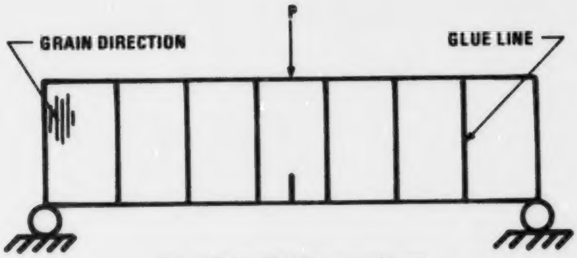
P
GRAIN DIRECTION
GLUE LINE

Figure 8. Verification experiment

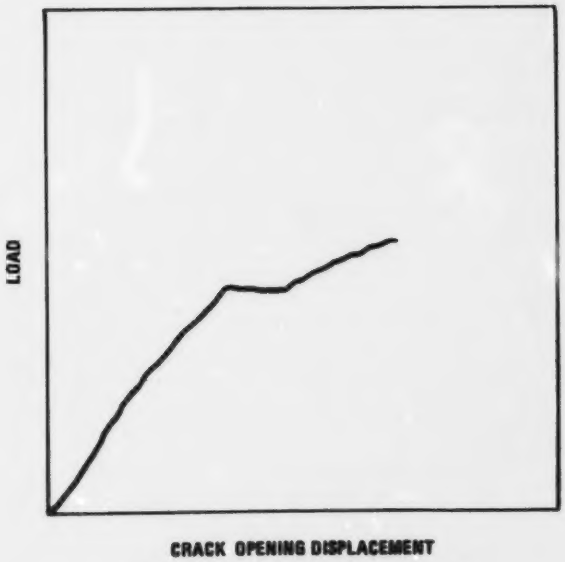

Figure 9. Typical load-displacement record

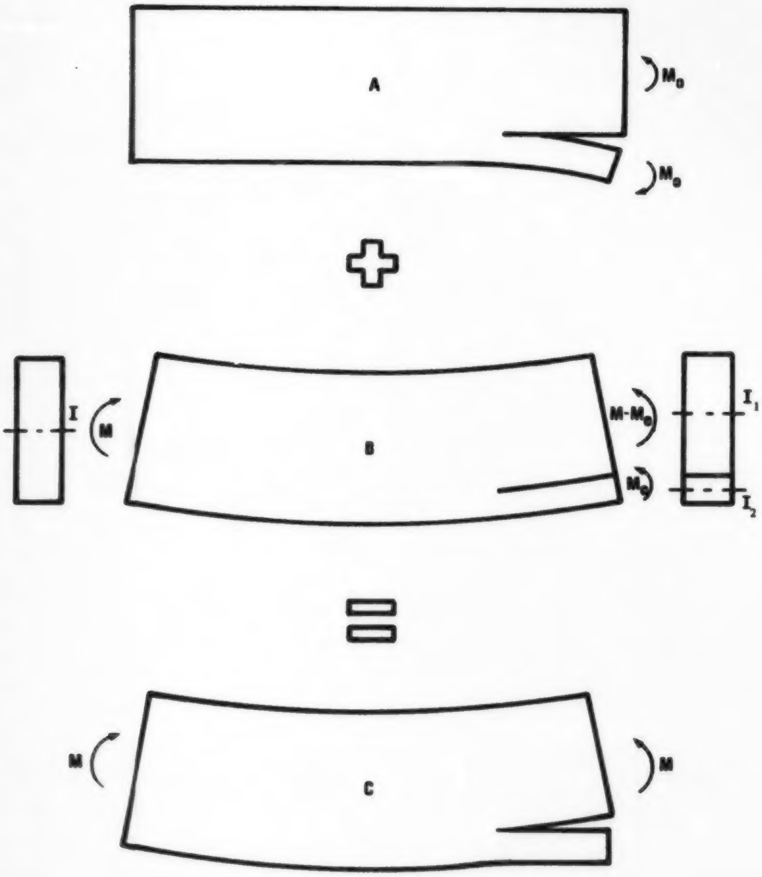
A
$M_o$
$M_o$
I
M
B
$M-M_o$
$M_o$
$I_1$
$I_2$
M
C
M

Figure 10. Edge-notch butt joint solution method

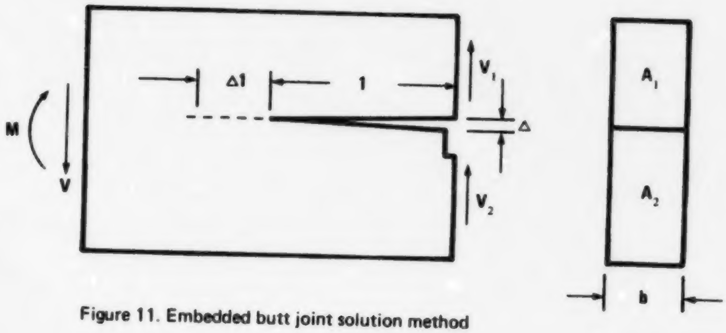
M
V
Δl
l
$V_1$
Δ
$V_2$
$A_1$
$A_2$
b

Figure 11. Embedded butt joint solution method

# RATE OF LOADING EFFECT IN BENDING FOR DOUGLAS-FIR LUMBER

By

Richard Spencer

---

Assistant Professor, University of British Columbia, Department of Civil Engineering, Vancouver, B.C., Canada. This work was supported by the Western Forest Products Laboratory and the University of British Columbia.

## INTRODUCTION

The effect of rate of loading and duration of load on the bending strength of wood has been studied by a number of investigators. Wood (1) in 1951 suggested a relationship for Douglas-fir which can be written:

$$SR = .180 + .731T^{-0.04635} \quad (1)$$

where: T = duration of stress in hours;

SR = stress at failure expressed as a ratio of the stress at failure when the duration of stress is 5 minutes.

Wood suggested that this relationship could be used for data from both short-term tests, in which the stress was increased continuously to failure (ramp-function loading), and long-term tests, in which the stress was applied at a predetermined level and then held constant (step-function loading). Pearson (2) in 1972 reviewed data from eight investigations, covering a number of species, moisture contents and loading arrangements, but in most cases using small specimens having a maximum cross section dimension of 2 inches and a span of 40 inches or less. Pearson suggested that the effective duration of stress for ramp-function loading could be taken as 20% of the duration of stress for step-function loading.

Using this assumption, the regression equation derived by Pearson for the data he considered can be written:

$$SR = .927 - .067 \log_{10} T_r \quad (2)$$

where: $T_r$ = time to failure for ramp loading in hours;

SR = stress ratio, as in equation (1).

Equation (1) can be used to obtain the multiplying factors for the effect of duration of load on allowable stress recommended in current codes (3,4) and equation (2) gives reasonably close agreement. These factors give allowable stresses for load duration of 1 second, which are twice those for a duration of 10 years and 1.6 times those for a duration of 1 week.

Barrett and Foschi (5) have developed two creep-rupture models which enable them to develop relations for the variation of the stress ratio SR with duration of stress for both ramp loading and step-function loading. The relationships suggested by Wood, Pearson and Barrett and Foschi for ramp loading are shown in Figure 1.

The tests described in this report were undertaken to provide more data on the effects of ramp loading at rapid rates, and to investigate the extent to which relationships similar to those mentioned above are applicable to commercially available in-grade lumber with times to failure of about 100 hours or less.

## MATERIAL TESTED

The material tested was commercially available Douglas-fir 2 in. by 6 in. boards 12 feet long, sold as Grade 2 and Better. It was obtained from three different suppliers, "A", "B" and "C". Half of the boards came from supplier A, one quarter each from suppliers B and C. All boards were supplied kiln dried and were subsequently allowed to dry further in the laboratory before testing. The mean moisture content of the boards as tested was 11.4%, with a standard deviation of 1.24%. The moisture content of 98% of the boards was between 9% and 16%, with 90% of the boards between 10% and 13%.

The boards were divided into eight groups, for testing at eight different rates of loading. In each group, the proportion of boards from each supplier was approximately the same as it was in the sample as a whole. The elastic modulus, E, as measured in a flexural test at low load was assumed to predict the strength of each board, and the boards from each supplier were assigned to groups, so as to make the distribution of E values approximately the same in each group. It was then assumed that, if each group had been tested at a standard rate of loading, a similar distribution of bending strengths would have been obtained for each group.

Each board was graded in the laboratory according to the NLGA 1970 grading rules (6). The composition of each group by supplier and grade is summarized in Table 1.

## TEST METHOD

All boards were tested in four-point bending with a clear span of 99 inches. Because of the large number of boards to be tested, four separate test rigs were used. All were of similar design, and each used an MTS servo-controlled hydraulic actuator to apply load at the third points through a spreader beam. Loads and support reactions were applied through 1/2" steel plates 1 1/2" wide and 4 inches long. A support plate at one end of the span was free to rotate, while the other three plates could both rotate and translate longitudinally as the board deflected. The board was restrained against lateral buckling at the supports and load points.

All tests were made with ramp loading applied at a constant rate until the board failed. At all loading rates except the highest, the load applied was measured with a load cell mounted between the actuator and the spreader beam. For the tests at the highest loading rate, a load cell was placed under one support, as the load cell attached to the actuator measured the force required to accelerate the spreader beam when the test began, which was not negligible at this rate.

Load and displacement (measured by a transducer in the actuator) were recorded continuously on an X-Y recorder during each test, except at the highest rate of loading. For this rate, the data was recorded on an FM analogue tape recorder, and the recording was then played back at 1/100 of the recording speed to produce the X-Y plot. Before tests began at this rate, an oscilloscope was used to check the variation of load versus time against the ramp function used for load control, and to check the data recording method. The results were satisfactory in both cases. The use of a single load cell under one support to measure load was also checked using corrected data from the load cell attached to the actuator.

## STRESSING RATES

Each of the eight groups of boards was loaded at a different rate as summarized in Table 2. Rates of stressing, calculated assuming a cross section of 1.5 inches by 5.5 inches, are also shown. Times to failure for each group are shown in Table 2, based on the mean strength and the 5th and 95th percentiles for strength for each group. Because of the length of time required to complete the tests at the slowest rate, only half of the selected group of boards, made up of those from suppliers B and C, was tested.

## RESULTS

The cumulative probability distribution for bending strengths for each group is shown in Figures 2 to 9 with a log normal curve fitted to each distribution. As noted above, only the boards from suppliers B and C in group 8 were tested. It was evident from the results for each of the other groups that the expected strength of boards from these two suppliers was generally higher than for the complete group (e.g. see Figure 10). For this reasons, the results for group 8 were adjusted for comparison with the results for the other seven groups. This was done by calculating the ratios of the mean strength and the percentiles for all boards to the mean strength and percentiles computed for boards from suppliers B and C only, for each of the groups 1 to 7. The mean and each percentile for group 8 was then multiplied by the average of the ratios found for the same quantity in groups 1 to 7, and the adjusted values were assumed to represent the results that would have been found if all boards in group 8 had been tested. The ratios are shown in Table 3 and means and percentiles for all groups are given in Table 4. Percentiles for bending strength for all boards in each group (with adjusted values for group 8) are plotted against the log of the rate stressing in Figure 11, with straight lines fitted by regression analysis for each percentile. Similar results for supplier A only, and for suppliers B and C only, are shown in Figures 12 and 13. The regression equations for each line:

$$S = A + B \log_{10} R \qquad (3)$$

where:

$S$ = stress at failure (psi)

$R$ = rate of stressing (psi/sec)

$A$ = constant from the regression analysis (psi)

$B$ = gradient from the regression analysis

are summarized in Table 5. In all cases percentiles are found by linear interpolation between adjacent points on the cumulative probability distribution for strength.

The time to failure for any percentile is given by the failure stress divided by the rate of stressing. A curve showing the rate of stressing required to fail boards of any strength in five minutes is shown on Figures 11, 12 and 13. It is assumed that the percentiles for the idealized strength distribution that would be obtained if each board in a group could be loaded to failure in 5 minutes are given by the intersection of this curve with the straight lines fitted to each set of percentiles. Stress ratios, SR, corresponding to each percentile, are then given for each rate of stressing by:

$$SR = \frac{\text{value of percentile for the given rate}}{\text{value of assumed percentile for a 5 minute test}}$$

Stress ratios for boards from supplier A alone, and for boards from all suppliers differentiated by grade, are derived from results excluding tests at the lowest rate of stressing of 0.022 psi/sec. Other stress ratios are found from results obtained at all rates of stressing.

Stress ratios for the 5th and 95th percentiles for all boards from all suppliers are shown in Figure 14, plotted against the log of the time to failure $T_r$, in hours, given by:

$$T_r = \frac{\text{value of percentile for a given rate of stressing}}{\text{rate of stressing (psi/hr)}}$$

It is assumed that straight lines can represent the relationship between stress ratio and log time to failure, as shown in Figure 14. Each line passes through two points found from the appropriate regression equation (equation 3), using stresses and times to failure corresponding to the fastest and slowest rates of stressing, and can be represented by:

$$SR = C + D \log T_r \qquad (4)$$

where $T_r$ has the same meaning as previously, and C and D are a constant and the gradient of the line, respectively. Equation (4) is directly comparable with equations (1) and (2), over the range of times to failure considered. Values of the gradient D were found for each percentile for all boards and for boards differeniated by grade, for all suppliers, for supplier A only, and for suppliers B and C. These values are shown in Figures 15, 16 and 17, plotted against the estimated 5-minute strength used to calculate the stress ratio SR.

## CONCLUSIONS

The percentiles for strength for boards from all suppliers, shown in Figure 11, suggest that the eight groups of boards were sufficiently similar to allow comparison of the results for different rates of stressing. It seems clear that the stronger boards show an increasing strength as the rate of stressing increases, but this effect becomes less pronounced for the weaker boards. Madsen and Barrett (7) observed similar trends for Hem-Fir. The regression equations (Table 5) confirm this trend and show that, for the 5th percentile, there is a loss of strength with increasing rate of stressing.

Similar trends can be seen in the results for boards from supplier A only and from suppliers B and C (Figures 12 and 13), although none of the percentiles for suppliers B and C show an actual loss of strength with increasing rate of stressing.

The values of the stress ratio gradient D from equation (4) plotted in Figures 15, 16 and 17 range from -0.071 to 0.043. The results for all boards for all suppliers (Figure 15) show a trend of increasing values of D with decreasing strength, with a maximum value of D of 0.033 for the line representing the stress ratios given by the 5th percentile values for each group. If this value of D was assumed to be a typical value for commercially available Douglas-fir sold as Grade 2 and Better, it would have important consequences for design. As mentioned earlier, current design specifications and codes allow increases in allowable stress for loads of short duration that are consistent with a gradient D of about -0.07. The positive values of D found suggest that such increases are not justified for lumber similar to that tested and loaded to failure in 100 hours or less. It is especially significant that the biggest positive values of D are found for the weakest boards.

The stress ratio gradients found, when the percentiles for Select Structural grade boards from all suppliers were analyzed, range from -0.028 to -0.051 (Figure 14), indicating that there was a gain in bending strength with increasing rate of stressing for boards of all strengths, although this gain was less than that assumed in the codes. However, the lowest percentile values for the Select Structural grade boards from supplier A had a positive gradient. Other percentiles for Select Structural boards for suppliers B and C gave negative gradients as small as -0.017. Since the sample sizes for these latter groups are quite small, the reliability of these values is somewhat uncertain. However they do suggest that it would be prudent to reduce or eliminate the increases in allowable stress permitted by codes as they apply to Select Structural grade Douglas-fir loaded to failure in 100 hours or less. More data is need to confirm the extent of the required reduction.

The gradients for boards from supplier A alone and for boards from suppliers B and C appear to show somewhat different trends. Had the testing been confined to the latter boards, it might have been concluded that a representative value of the gradient D would lie in the range from -0.02 for weaker boards to -0.04 for stronger boards. This conclusion would apply to neither the former boards nor to all boards from all suppliers combined. No reason is offered here for this difference, althoguh it should be noted that suppliers B and C are in similar regions, and both are some distance from supplier A.

The difference between the gradients reported here and those discussed in the introduction would appear to be due in large part to the fact that most earlier tests were on clear material, while these tests were made on commercially available material with normal defects. Both the increasingly negative gradients for the higher percentiles and the somewhat different trends seen for Select Structural boards suggest that the stress ratio gradients would tend to approach the range of -0.07 if material with fewer defects was tested. It is also significant that a higher proportion of splintering tension failures, which resulted in boards breaking into completely separate pieces, was observed at the highest rate of stressing. This also suggests that knots and other defects have an important influence on rate of stressing effects, and helps to explain the lower stress ratios SR found for the weaker boards at this rate.

## REFERENCES

1. Wood, L. 1951. Relation of Strength of Wood to Duration of Load. U.S. Forest Prod. Lab., Madison, WI , Rep. No. 1916

2. Pearson, R.G. 1972. The Effect of Duration of Load on Bending Stength of Wood. Holzforschung 26(4):153-158.

3. Code for the Engineering Design of Wood. 1976. Can. Standards Assoc. Standard 086-1976, Rexdale, Ont.

4. National Design Specification for Stress Grade Lumber and Fastenings. Nat. Lumber Manuf. Assoc., Washington, D.C.

5. Barrett, J.D., and Foschi, R.O. 1978. Duration of Load and Failure Probability in Wood. Part I: Modelling Creep Rupture. Can. J. Civil Eng. 5(4): 504-514.

6. Standard Grading Rules for Canadian Lumber. 1970. Nat. Lumber Grades Auth., Vancouver, B.C.

7. Madsen, B. and Barrett, J.D. 1976. Time-Strength Relationship for Lumber. Univ. B.C., Civil Eng. Dep., Struct. Res. Series No. 13, Vancouver, B.C.

## TABLE 1

Composition of Groups by Supplier and Grade

| | | Number of boards in group | | | | | | | | Total | |
|---|---|---|---|---|---|---|---|---|---|---|---|
| Supplier | Grade | 1 | 2 | 3 | 4 | 5 | 6 | 7 | 8 | No. | % |
| A | SS | 17 | 37 | 30 | 23 | 35 | 27 | 33 | Not | 202 | 42 |
| | 1 | 23 | 10 | 12 | 28 | 4 | 12 | 4 | tested | 93 | 20 |
| | 2 | 12 | 15 | 15 | 14 | 18 | 17 | 23 | " | 114 | 24 |
| | Other | 15 | 7 | 12 | 4 | 10 | 12 | 8 | " | 68 | 14 |
| | Total | 67 | 69 | 69 | 69 | 67 | 68 | 68 | | 477 | 100 |
| B | SS | 44 | 46 | 44 | 27 | 44 | 34 | 37 | 49 | 325 | 57 |
| and | 1 | 7 | 8 | 11 | 37 | 5 | 11 | 11 | 1 | 91 | 16 |
| C | 2 | 14 | 10 | 14 | 8 | 15 | 22 | 22 | 11 | 116 | 20 |
| | Other | 8 | 7 | 3 | 1 | 8 | 6 | 2 | 8 | 43 | 7 |
| | Total | 73 | 71 | 72 | 73 | 72 | 73 | 72 | 69 | 575 | 100 |
| All | SS | 61 | 83 | 74 | 50 | 79 | 61 | 70 | 49 | 527 | 50 |
| | 1 | 30 | 18 | 23 | 65 | 9 | 21 | 15 | 1 | 182 | 17 |
| | 2 | 26 | 25 | 29 | 22 | 33 | 41 | 45 | 11 | 232 | 22 |
| | Other | 23 | 14 | 15 | 4 | 18 | 18 | 10 | 8 | 111 | 11 |
| | Total | 140 | 140 | 141 | 142 | 139 | 141 | 140 | 69 | 1052 | 100 |

TABLE 2

Rates of Stressing and Times to Failure

| Group | Rate of Loading (lb/sec) | Rate of Stressing (psi/sec) | Time to Failure | | |
|---|---|---|---|---|---|
| | | | Mean Strength | 5th perc. | 95th perc. |
| 1 | 50,000 | 109,065 | .061 sec | .02 sec | .13 sec |
| 2 | 2,500 | 5,453 | 1.18 sec | .45 sec | 2.32 sec |
| 3 | 250 | 545 | 11.66 sec | 4.91 sec | 23.7 sec |
| 4 | 33.3 | 72.7 | 1.43 min | .58 min | 2.66 sec |
| 5 | 3.33 | 7.26 | 14.1 min | 6.47 min | 27.0 min |
| 6 | .555 | 1.21 | 1.33 hr | .57 hr | 2.45 hr |
| 7 | .0667 | .145 | 11.0 hr | 4.98 hr | 20.51 hr |
| 8 | .0101 | .022 | 71.2 hr | 32.9 hr | 130.1 hr |

## TABLE 3

### Adjustment of Data for Group 8

$$\text{RATIO} = \frac{\text{Strength for all suppliers}}{\text{Strength for suppliers B and C}}$$

|  |  |  |  | Group |  |  |  |  |
|---|---|---|---|---|---|---|---|---|
| Percentile | 1 | 2 | 3 | 4 | 5 | 6 | 7 | Average of ratios |
| 95th | .94 | .96 | .97 | .96 | .96 | .90 | .94 | .95 |
| 90th | .77 | .89 | .85 | .94 | .89 | .86 | .93 | .88 |
| 75th | .87 | .87 | .84 | .77 | .84 | .84 | .82 | .84 |
| 50th | .90 | .86 | .79 | .81 | .86 | .83 | .87 | .85 |
| 25th | .93 | .80 | .82 | .84 | .82 | .82 | .87 | .84 |
| 10th | .84 | .85 | .84 | .94 | 1.01 | .88 | .99 | .91 |
| 5th | .94 | .89 | .87 | 1.02 | .92 | .98 | 1.13 | .96 |
| Mean | .87 | .88 | .86 | .85 | .90 | .85 | .88 | .87 |

## TABLE 4

Bending Strength - Percentiles

and Means (psi)

| | Group | | | | | | | |
|---|---|---|---|---|---|---|---|---|
| Percentile | 1 | 2 | 3 | 4 | 5 | 6 | 7 | 8* |
| 95th | 13709 | 12646 | 12890 | 11601 | 11772 | 10676 | 10704 | 10300 |
| 90th | 11573 | 10632 | 10630 | 10817 | 10413 | 9152 | 9977 | 9142 |
| 75th | 8644 | 8060 | 8092 | 7994 | 7660 | 7172 | 7234 | 7040 |
| 50th | 5739 | 5865 | 5413 | 5665 | 5627 | 5372 | 5074 | 5284 |
| 25th | 4198 | 3945 | 3998 | 3776 | 4037 | 3811 | 3708 | 3602 |
| 10th | 2960 | 3120 | 2987 | 2918 | 3193 | 2755 | 3172 | 2859 |
| 5th | 2375 | 2440 | 2674 | 2520 | 2820 | 2500 | 2599 | 2606 |
| Mean | 6663 | 6433 | 6354 | 6218 | 6143 | 5789 | 5747 | 5640 |

*Adjusted using average ratios given in Table 3

## TABLE 5

Regression Equations for

Strength Percentiles (psi)

($S = A + B \log_{10} R$, Equation 3)

| All Suppliers | Percentile | | | | | | |
|---|---|---|---|---|---|---|---|
| | 95th | 90th | 75th | 50th | 25th | 10th | 5th |
| Constant A | 11036 | 9821 | 7390 | 5369 | 3778 | 2914 | 2611 |
| Gradient B | 508 | 318 | 235 | 92 | 72 | 32 | –30 |

| Supplier A | Percentile | | | | | | |
|---|---|---|---|---|---|---|---|
| | 95th | 90th | 75th | 50th | 25th | 10th | 5th |
| Constant A | 8254 | 7413 | 6083 | 4410 | 3504 | 2892 | 2606 |
| Gradient B | 314 | 279 | 172 | 120 | 6 | –16 | –106 |

| Suppliers B and C | Percentile | | | | | | |
|---|---|---|---|---|---|---|---|
| | 95th | 90th | 75th | 50th | 25th | 10th | 5th |
| Constant A | 11714 | 10973 | 8900 | 6374 | 4530 | 3184 | 2650 |
| Gradient B | 494 | 442 | 289 | 116 | 59 | 79 | 19 |

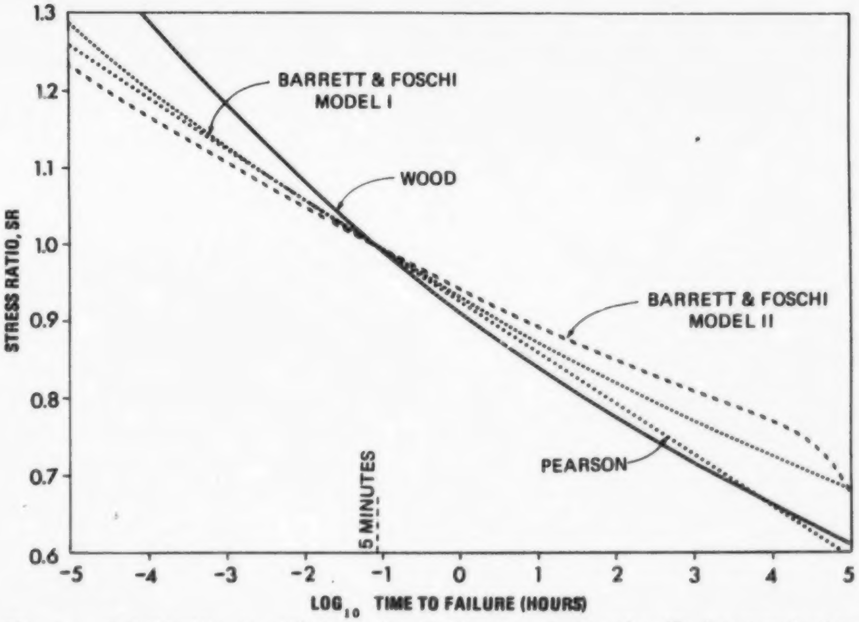

Fig. 1. Relationships for effect of time to failure on stress ratio, SR, for ramp loading.

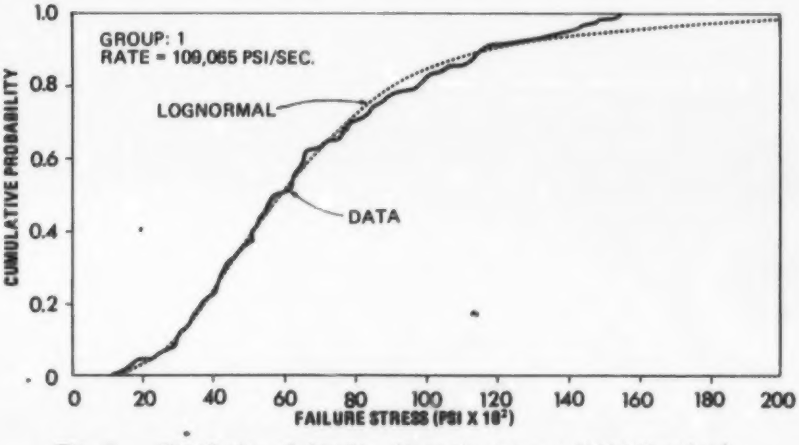

Fig. 2. Distribution of Bending Strengths, Group 1 (109,065 psi/sec)

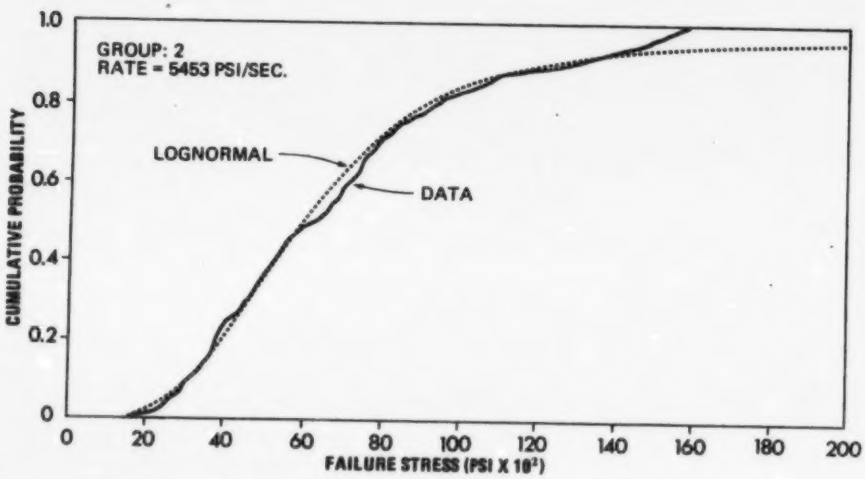

Fig. 3. Distribution of Bending Strengths, Group 2 (5,453 psi/sec)

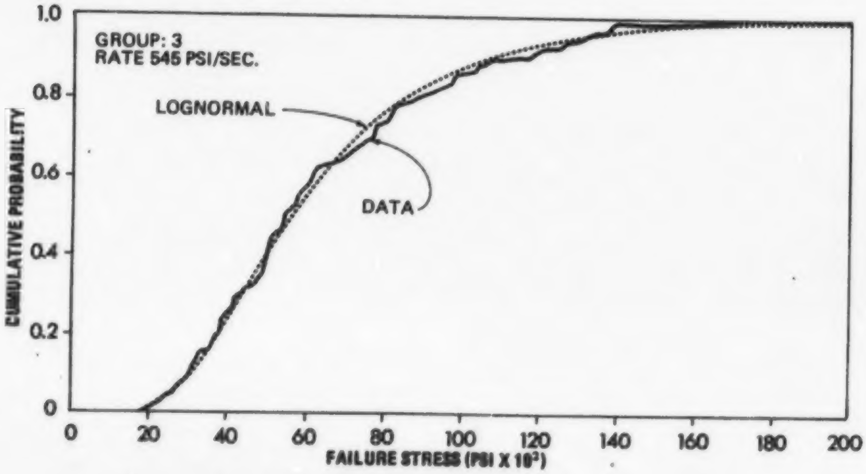

Fig. 4. Distribution of Bending Strengths, Group 3 (545 psi/sec)

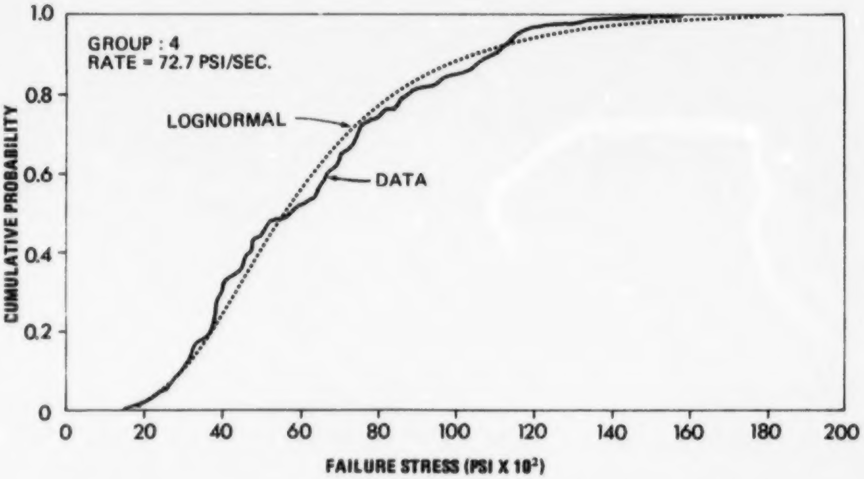

Fig. 5. Distribution of Bending Strengths, Group 4 (72.7 psi/sec)

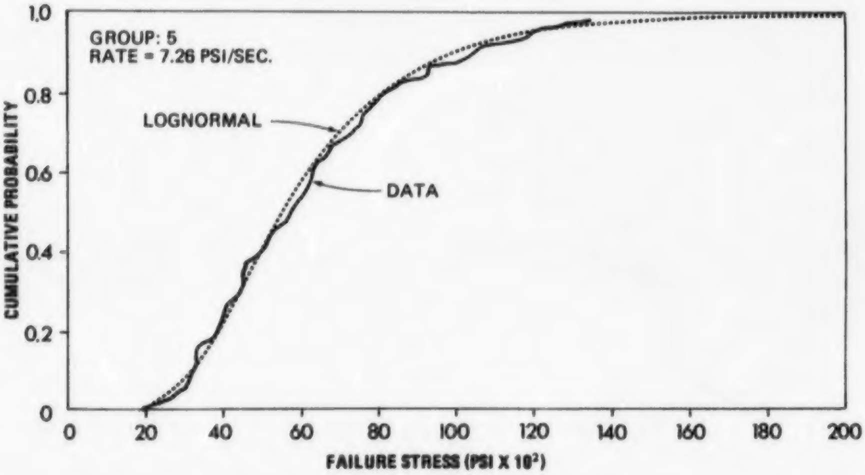

Fig. 6. Distribution of Bending Strengths, Group 5 (7.26 psi/sec)

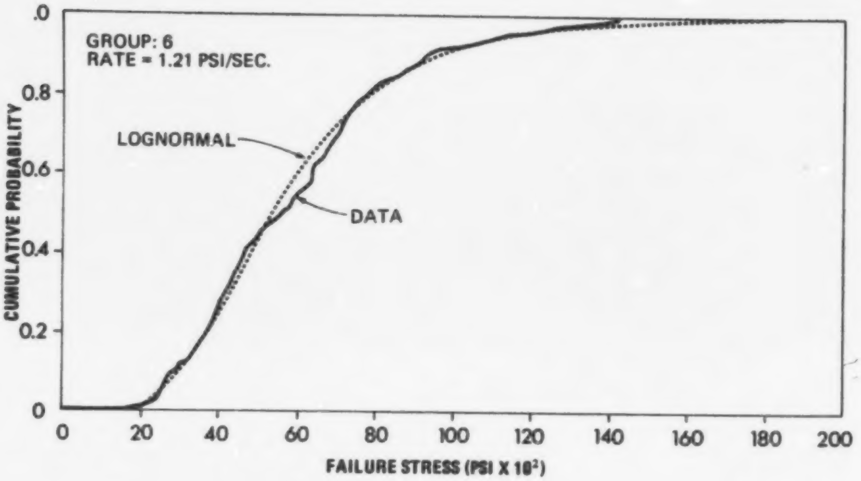

Fig. 7. Distribution of Bending Strengths, Group 6 (1.21 psi/sec)

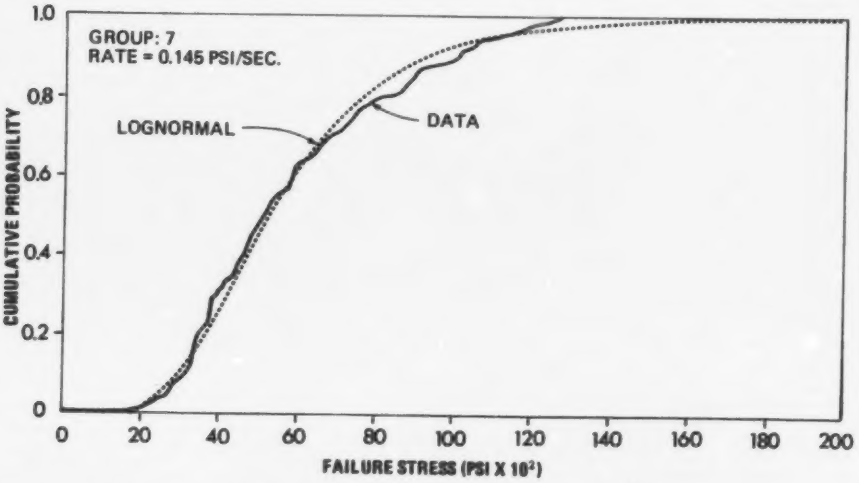

Fig. 8. Distribution of Bending Strengths, Group 7 (0.145 psi/sec)

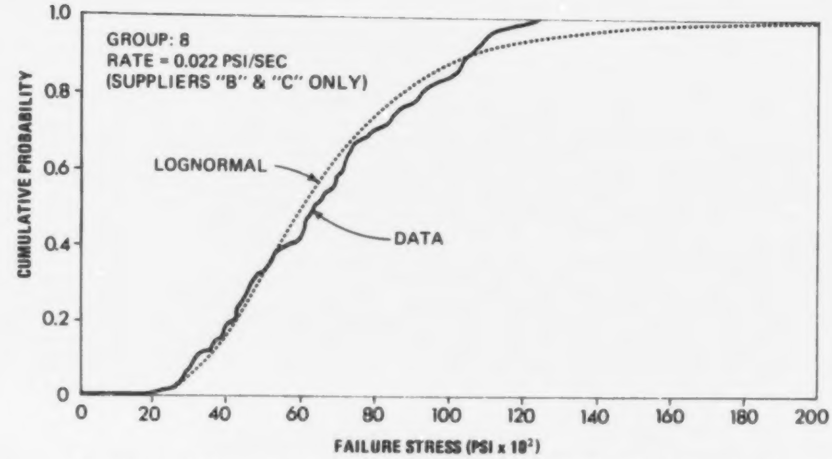

Fig. 9. Distribution of Bending Strengths, Group 8 (0.022 psi/sec) (Suppliers B and C only)

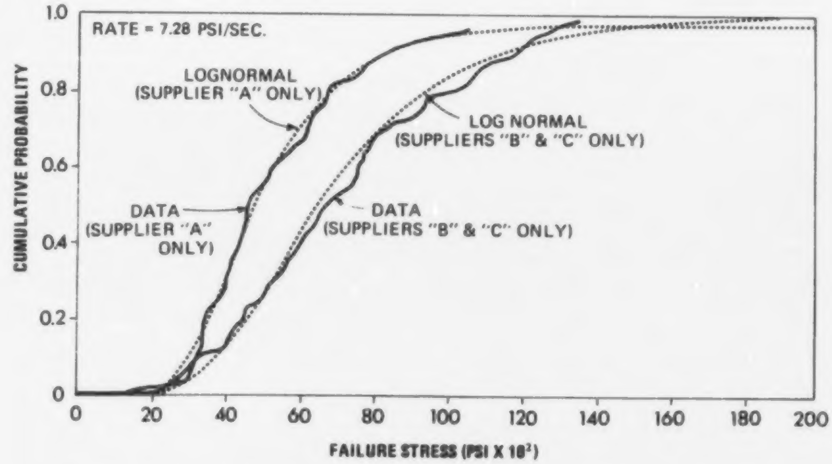

Fig. 10. Comparison of strength distributions for supplier A and suppliers B and C, Group 5 (7.28 psi/sec)

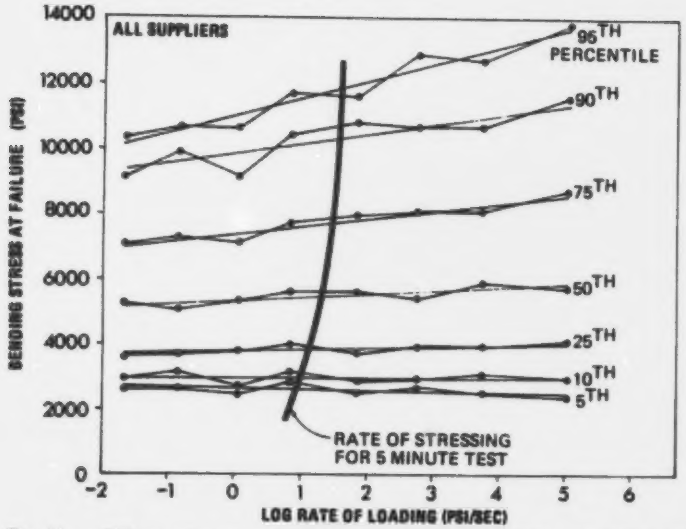

Fig. 11. Effect of rate of loading on bending strength, all grades and suppliers.

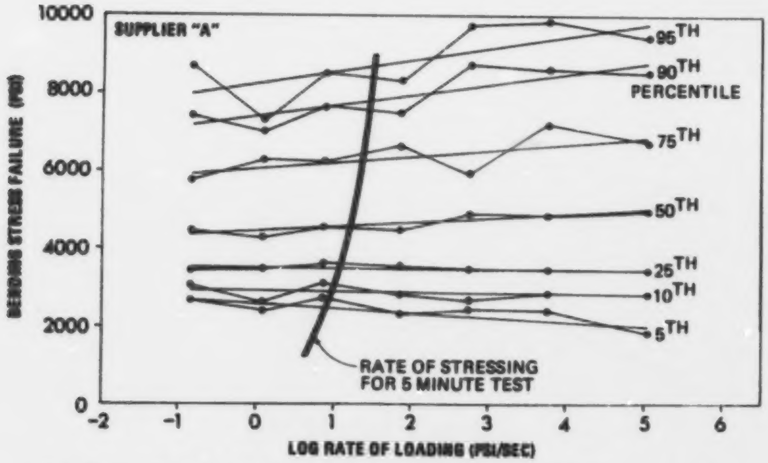

Fig. 12. Effect of rate of loading on bending strength, all grades, supplier A.

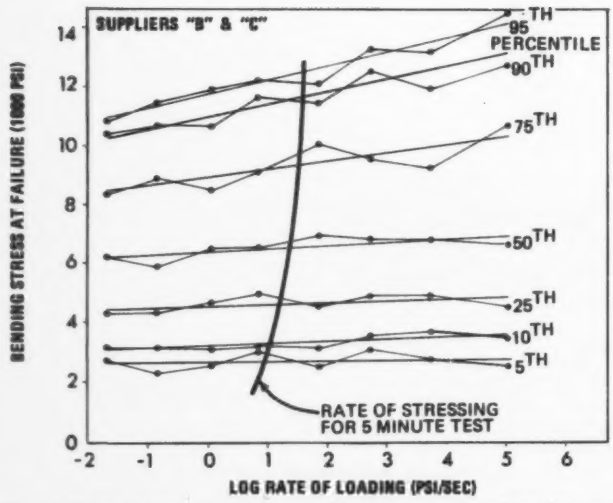

Fig. 13. Effect of rate of loading on bending strength, all grades, suppliers B and C only.

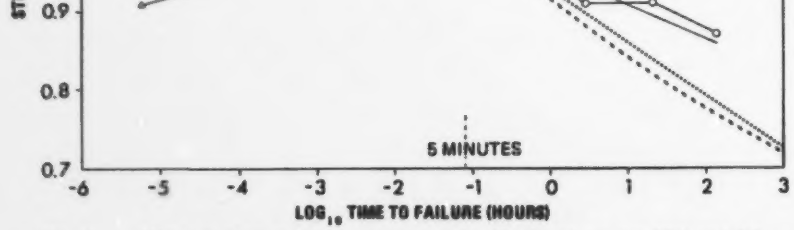

Fig. 14. Effect of time to failure on stress ratio, SR, found for the 95th and 5th percentiles for all boards for all suppliers.

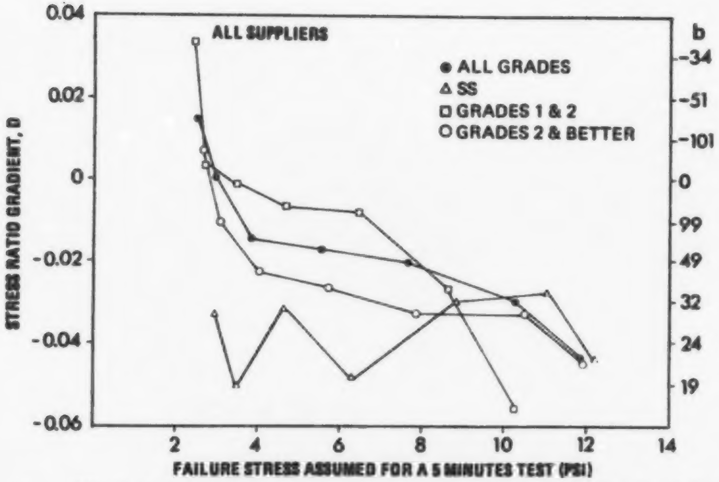

Fig. 15. Effect of estimated 5-minute strength on the gradient D of SR = C + D $\log_{10}T$ (Equation 4). Data for all suppliers.

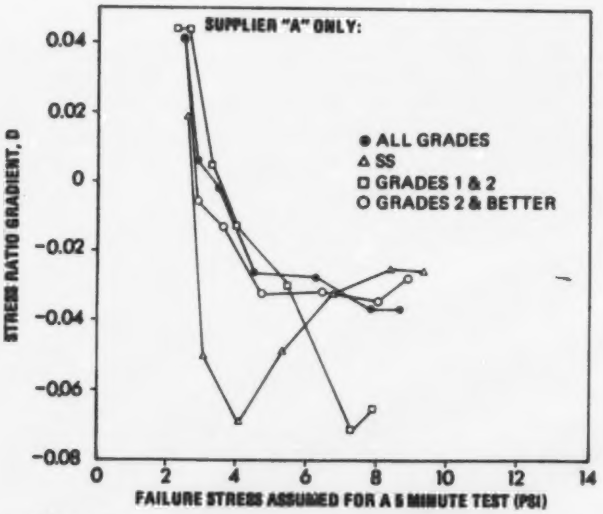

Fig. 16. Effect of estimated 5-minute strength on the gradient D of SR = C + D $\log_{10}T$ (Equation 4). Data for supplier A only.

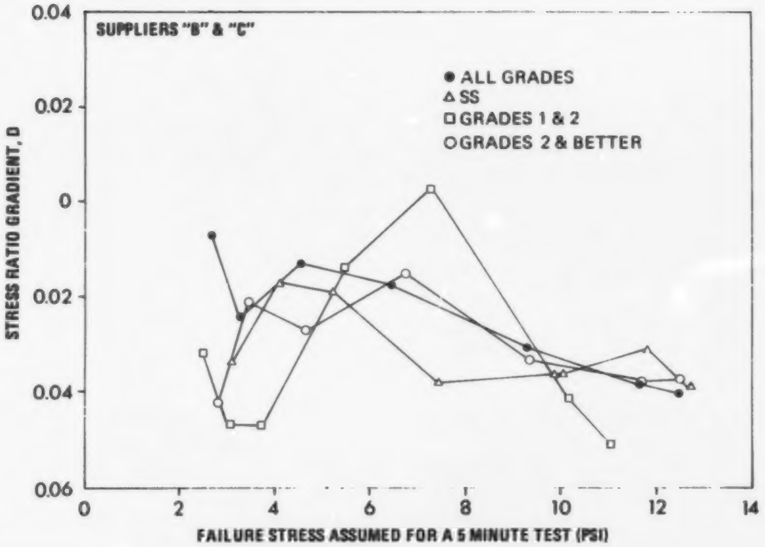

Fig. 17. Effect of estimated 5-minute strength on the gradient D of SR = C + D $\log_{10}T$ (Equation 4). Data for suppliers B and C.

# THEORETICAL ANALYSIS OF THE BEHAVIOR OF BENDING CREEP IN WOODEN BEAMS

By

**Hideo Sugiyama**

---

Professor, Department of Forest Products, Faculty of Agriculture, University of Tokyo, Japan.

## 1. Foreword

I have been considering, from the rheological point of view, that the creep of a beam subjected to bending should be regarded as "retarded elasticity", which is apparently different from plasticity, in the condition that the stresses of outermost fibers on the compression side over a cross section do not exceed the proportional limit stress for compression just after the application of sustained load. The critical limit pointed out above would be "creep limit" for bending to be considered to secure the safety of a beam permanently under long-time loading.

I think it is necessary to re-examine, from the above point of view, the present world-wide thinking of induction of the allowable unit stress for bending under long-time loading. This serious problem was already discussed in the author's paper, so here it is not discussed more.

I would like to discuss theoretically the behavior of bending creep of a beam having rectangular cross section subjected to a constant sustained load being less than the creep limit load about which has been explained in the beginning of this paper.

The contents of this paper were already reported in Japanese in 1969 [1]** and the similar discussion about a beam having cross section of box or I type in Japanese in 1970 [2].

## 2. Assumptions

The main assumptions are as follows:

(1) Young's modulus for simple compression is the same as that for simple tension;

(2) The stress of the outermost fiber on compression side of a beam does not reach the stress at proportional limit in compression just after a constant sustained load is applied to the beam;

(3) Creep strain under a constant tensile stress is negligible;

(4) Creep strain under a constant compressive stress below the stress at proportional limit is linearly proportional to the constant sustained compressive stress. According to this assumption the total compressive strain $\Sigma(t)$ under constant stress is written

$$\varepsilon(t) = \varepsilon_e + \varepsilon_c(t) = \varepsilon_e\{1 + \phi_c(t)\} \qquad (1)$$

$$\phi_c(t) = \varepsilon_c(t)/\varepsilon_e \qquad (2)$$

where

$\varepsilon_e$ = compressive initial (elastic) strain

$\varepsilon_c(t)$ = compressive creep strain

$\phi_c(t)$ = creep function in compression

(5) Total compressive strain under a constant sustained compressive stress changing with time is given by

$$\begin{aligned}\varepsilon_t(t) &= \frac{\sigma_c(0)}{E_c}\{1 + \phi_c(t)\} \\ &\quad + \frac{1}{E_c}\{\sigma_c(t) - \sigma_c(0)\}\{1 + \tfrac{1}{2}\phi_c(t)\} \\ &= \frac{\sigma_c(t)}{E_c} + \frac{1}{2E_c}\{\sigma_c(t) + \sigma_c(0)\}\phi_c(t) \qquad (3)\end{aligned}$$

where $\sigma c(0)$ and $\sigma c(t)$ denote the compressive stress at time t=0 and that at time t=t, respectively, and $E_c$ Young's modulus for compression. In eq. (3), the first and the second terms on the right side mean, respectively, the elastic strain due to $\sigma c(t)$ and the creep strain corresponding to the elapsed time t due to the mean stress of the stresses at time t=0 and t=t.

---

**The number of reference cited.

## 3. Bending Creep Behavior of a Beam

Assuming that the stress-strain relations for both tension and compression hold Hooke's law, stress and strain distributions over the cross section of a beam subjected to constant load at time t=0 and t=t are shown in Fig. 1(a) and (b), respectively.

The meaning of notations shown in Fig. 1 are as follows:

$\sigma_c(0), \sigma_c(t)$ - the stresses of the outermost fibers on the compression side at t=0 and t=t, respectively;

$\varepsilon_c(0), \varepsilon_c(t)$ - the strains of the outermost fibers on the compression side at t=0 and t=t, respectively;

$\sigma_t(0), \sigma_t(t)$ - the stresses of the outermost fibers on the tension side at t=0 and t=t, respectively;

$\varepsilon_t(0), \varepsilon_t(t)$ - the strains of the outermost fibers on the tension side at t=0 and t=t, respectively;

$\bar{\sigma}_c(0)$, $\bar{\sigma}_c(t)$, $\bar{\varepsilon}_c(0)$, $\bar{\varepsilon}_c(t)$ - the stresses or strains on the compression side at t=0 or t=t at the distance Z from neutral axis;

$\bar{\sigma}_t(0)$, $\bar{\sigma}_t(t)$, $\bar{\varepsilon}_t(0)$, $\bar{\varepsilon}_t(t)$ - the stresses or strains on the tension side at t=0 or t=t at the distance Z from neutral axis;

$\theta(0), \theta(t)$ - the rotation angles of cross section;

$\eta(t)$ - distance between neutral axes at t=0 and t=t;

$\lambda_0$ - distance between the outermost fiber and neutral axis at t=0;

$d$, $b$ - depth and width of cross section, respectively;

$E_c$, $E_t$ - Young's moduli for compression and tension.

Assuming $E_c \neq E_t$, the stresses and strains on the compression side at t=0 and t=t are writen as follows.

(1) Stresses at time t=0

$$\begin{aligned}\bar{\sigma}_c(0) &= \bar{\varepsilon}_c(0)E_c = \theta(0)E_c(Z+\eta)\\ \bar{\sigma}_t(0) &= \bar{\varepsilon}_t(0)E_t = \theta(0)E_t(Z+\eta)\end{aligned} \tag{4}$$

(2) Stresses and strains at time t=t for the region $C_1$ (see Fig. 1)

$$\begin{aligned}\bar{\varepsilon}_c(t) &= \frac{\bar{\sigma}_c(t)}{E_c} + \frac{1}{2E_c}\left\{\bar{\sigma}_c(t)+\bar{\sigma}_c(0)\right\}\phi_c(t)\\ &= \frac{\bar{\sigma}_c(t)}{E_c}\left\{1+\frac{1}{2}\phi_c(t)\right\} + \frac{1}{2E_c}\bar{\sigma}_c(0)\phi_c(t)\end{aligned} \tag{5}$$

$$\begin{aligned}\bar{\sigma}_c(t) &= \frac{1}{1+\frac{1}{2}\phi_c(t)}\left\{E_c\bar{\varepsilon}_c(t) - \frac{1}{2}\bar{\sigma}_c(0)\phi_c(t)\right\}\\ &= \frac{E_c}{1+\frac{1}{2}\phi_c(t)}\left\{\theta(t)Z - \frac{1}{2}\theta(0)(Z+\eta)\phi_c(t)\right\}\end{aligned} \tag{6}$$

(3) Stresses and strains at time t=t for the region $C_2$ (see Fig. 1)

$$\bar{\sigma}_c(t) = \frac{E_c\theta(t)Z}{1+\frac{1}{2}\phi_c(t)\frac{Z}{(-\eta)}} \tag{7}$$

Region $C_2$ is the zone between neutral axes at time t=0 and t=t and eq. (7) can be induced by the following process. At the neutral axis at time t=0, in other words, at $Z = -\eta(t)$ the stress starting from zero increases the value of compressive stress as time elapses and reach $\frac{\bar{\sigma}_c(t)}{2}$ at time t=t. Considering that the mean compressive stress acts as the constant sustained stress during elapsed time t, we obtain

$$\begin{aligned}\bar{\varepsilon}_c(t) &= \frac{\bar{\sigma}_c(t)}{E_c} + \frac{1}{2E_c}\bar{\sigma}_c(t)\phi_c(t)\\ \bar{\sigma}_c(t) &= \frac{-E_c\theta(t)\eta(t)}{1+\frac{1}{2}\phi_c(t)}\end{aligned} \tag{8}$$

Substituting $Z = -\eta(t)$ in eq. (6), it agrees with eq. (8). Assuming that, for the region $C_2$, the development of compressive creep strain has no relation to the prior history subjected to tensile stress and depends upon the elapsed time t' sustaining compressive stress, we obtain the creep function $\phi_c(t')$ at distance Z from the neutral axis at time t=t

$$\phi_c(t') = \phi_c(t)\frac{Z}{(-\eta)} \qquad (9)$$

Then, the compressive stress $\bar{\sigma}_c(t)$ at time t=t for the region $C_2$ is given by eq. (7). Substituting Z=0 and $Z=-\eta(t)$ into eq.(7), $\bar{\sigma}_c(t)=0$ and eq. (8) are obtained respectively, those satisfying the boundary conditions for the region $C_2$.

(4) Stresses at time t=t for the region T (see Fig. 1). The stresses on the tension side, in other words, for the region T are written by

$$\overline{\sigma_t}(t) = E_t\,\theta(t)Z \qquad (10)$$

**Equilibrium over the cross section at time t=0**

Considering the condition of equilibrium of longitudinal stresses over the cross section, we obtain

$$b\int_{-(h-\lambda_0+\eta)}^{\lambda_0-\eta}\overline{\sigma_c}(0)\,dZ = b\int_{-(h-\lambda_0+\eta)}^{-\eta}\theta(0)E_c(Z+\eta)\,dZ + b\int_{-\eta}^{\lambda_0-\eta}\theta(0)E_t(Z+\eta)\,dZ = 0 \qquad (11)$$

from which

$$E_c(h-\lambda_0)^2 = E_t\lambda_0^2 \qquad (12)$$

By using eq. (13), we obtain eq. (14)

$$\gamma^2 = E_t/E_c \qquad (13)$$

$$\frac{\lambda_0}{h} = \frac{1}{\gamma+1} \qquad (14)$$

The condition of equilibrium of moment over the cross section is given by

$$b\int_{-(h-\lambda_0+\eta)}^{-\eta}\theta(0)E_c(Z+\eta)Z\,dZ + b\int_{-\eta}^{\lambda_0-\eta}\theta(0)E_t(Z+\eta)Z\,dZ = M \qquad (15)$$

from which

$$\theta(0) = \frac{M}{\frac{bh^3}{3}\left(1-\frac{\lambda_0}{h}\right)^3E_c} \qquad (16)$$

when $E_c = E_t$, we can obtain the following famous equation from eq. (16)

$$\theta = \frac{M}{\frac{bh^3}{12}E} = \frac{M}{EI} \qquad (17)$$

where

$$I = \frac{bh^3}{12}$$

**Equilibrium over the cross section at time t=t**

The condition of equilibrium of longitudinal stresses over the cross section is

$$b\frac{E_c}{1+\frac{1}{2}\phi_c}\int_{-(h-\lambda_0+\eta)}^{-\eta}\left\{\theta(0)Z - \frac{1}{2}\theta(0)(Z+\eta)\phi_c\right\}dZ + bE_c\int_{-\eta}^{0}\frac{\theta(t)}{1+\frac{1}{2}\phi_c\frac{Z}{(-\eta)}}Z\,dZ + bE_t\int_{0}^{\lambda_0-\eta}\theta(t)Z\,dZ = 0 \qquad (18)$$

from which

$$\frac{1}{2}\delta\gamma^2\phi_c(1+\Theta) - \Theta\gamma(\gamma+1)\left\{1+\left(1+\frac{1}{2}\phi_c\right)\gamma\right\}N + \frac{4(1+\phi_c/2)}{\phi_c^3}\Theta(\gamma+1)^2\left\{\log\left(1+\frac{\phi_c}{2}\right) - \frac{\phi_c}{2} + \frac{1}{8}\delta^2\phi_c^2\right\}N^2 = 0 \qquad (19)$$

where

$$\Theta = \theta(t)/\theta(0), \quad N = \eta(t)/h \qquad (20)$$

When $E_c = E_t$, namely $\delta=1$ and $\lambda_0=h/2$, eq. (19) becomes to

$$\frac{1}{8}\phi_c(1+\Theta) - \Theta\left(1+\frac{\phi_c}{4}\right)N + 4\Theta\frac{1+\frac{1}{2}\phi_c}{\phi_c^3}\left\{\log\left(1+\frac{\phi_c}{2}\right) - \frac{\phi_c}{2} + \frac{\phi_c^2}{8}\right\}N^2 = 0 \qquad (21)$$

The third term on the left side of eq. (21) is negligible in comparison with the first and the second terms, because

1) $N^2$ is a small quantity of the second order

2) when $0 \leq \phi_c \leq 2$, we can develop the series in a form as shown in eq. (22), the value of the parenthesis of the third term of eq. (21) reducing approximately to zero

$$\log\left(1+\frac{\phi_c}{2}\right) \fallingdotseq \frac{\phi_c}{2} - \frac{\phi_c^2}{8} + \frac{\phi_c^3}{24} - \frac{\phi_c^4}{64} \qquad (22)$$

We, thus, arrive at

$$\frac{1}{12}\phi_c(1+\theta) - \theta\left(1+\frac{\phi_c}{4}\right)N = 0 \qquad (23)$$

The condition of equilibrium of moment over the cross section is

$$b\int_{-(h-\lambda_0+\xi)}^{\lambda_0-\xi} \bar{\sigma} z\,dA = b\int_{-(h-\lambda_0+\xi)}^{-\xi} \frac{E_c}{1+\frac{1}{2}\phi_c}\left\{\theta(t)z^2 - \frac{1}{\xi}\theta(0)(z^2+\xi z)\phi_c\right\}dz + b\int_{-\xi}^{0}\frac{E_c}{1+\frac{1}{2}\phi_c\left(\frac{z}{-\xi}\right)}\theta(t)z^2\,dz + b\int_{0}^{\lambda_0-\xi} E_t\,\theta(t)z^2\,dz = M \qquad (24)$$

from which

$$\frac{\gamma}{\gamma+1}\left[2\left(\theta-\frac{\phi_c}{2}\right)\left\{\left(\frac{\gamma}{\gamma+1}\right)^2+3\frac{\gamma}{\gamma+1}N+3N^2\right\}+\frac{3}{2}\phi_c N\left(\frac{\gamma}{\gamma+1}+2N\right)\right] + 2\theta\left(1+\frac{1}{2}\phi_c\right)\gamma^2\left(\frac{1-\gamma N-N}{\gamma+1}\right)^3 - 48\theta\frac{N^3}{\phi_c^3}\left(1+\frac{1}{2}\phi_c\right)\left\{\frac{\phi_c}{2}-\frac{\phi_c^2}{8}-\log\left(1+\frac{\phi_c}{2}\right)\right\} = \frac{M\left(1+\frac{\phi_c}{2}\right)}{\frac{bh^3}{6}\theta(0)E_c}$$

Taking into consideration that $N^3$ is the third order of N ($N < 1$) and that the relation of eq. (22) exists, the last term on the left side of above equation may be neglected in comparison with other terms. Then,

$$4\gamma(\gamma+1)(\theta-1) - 2\gamma(2\gamma-\theta+1)\phi_c - 3\gamma(\gamma+1)(1+2\theta)\phi_c N + 12(\gamma+1)^2\left(1+\gamma+\frac{1}{2}\gamma\phi_c\right)\theta N^2 = 0 \qquad (25)$$

When $E_c = E_t$, the above equation becomes

$$4\theta\left(1+\frac{1}{4}\phi_c\right) - 4\left(1+\frac{3}{4}\phi_c\right) - 3(1+2\theta)\phi_c N + 12\theta(4+\phi_c)N^2 = 0 \qquad (26)$$

From eq. (23)

$$\theta = \frac{\frac{1}{12}\phi_c}{N\left(1+\frac{1}{4}\phi_c\right)-\frac{1}{12}\phi_c} = \frac{\theta(t)}{\theta(0)} \qquad (27)$$

Substituting eq. (27) in eq. (26), the factor of $N^2$ becomes zero, and then we get

$$N = \frac{\frac{1}{4}\phi_c + \frac{1}{12}\phi_c^2}{1+\phi_c+\frac{5}{24}\phi_c^2} = \frac{\eta(t)}{h} \qquad (28)$$

## 4. Changes of stresses, strains and rotation angle over a cross section due to creep

The stresses, strains and rotation angle over a cross section change with time due to creep. Here, the changing rate of the above magnitudes are investigated under the assumption $E_c = E_t$. We define the rate of movement of neutral axis and the rate of change of rotation angle by eqs. (28) and (27), respectively. Furthermore, we define the changing rate of stresses and strains over the cross section as follows.

The changing rate of strain of the outermost fiber on the compression side:

$$\varepsilon_c' = \frac{\varepsilon_c(t)}{\varepsilon_c(0)} = \theta(1+2N) \qquad (29)$$

The changing rate of stress of the outermost fiber on the compression side:

$$\sigma_c' = \frac{\sigma_c(t)}{\sigma_c(0)} = \frac{1}{1+\frac{1}{2}\phi_c}\left\{\theta(1+2N) - \frac{1}{2}\phi_c\right\} \qquad (30)$$

The changing rate of strain of the outermost fiber on the tension side:

$$\varepsilon_t' = \frac{\varepsilon_t(t)}{\varepsilon_t(0)} = \theta(1-2N) \qquad (31)$$

The changing rate of stress of the outermost fiber on the tension side:

$$\sigma_t' = \frac{\sigma_t(t)}{\sigma_t(0)} = \theta(1-2N) \qquad (32)$$

We can find that the changing rate of each magnitude shown in eqs. (27) to (32) depends upon the creep function $\phi_c(t)$ for compression and is not influenced by the magnitude of the sustained load.

It can be said that the changing rate of deflection is approximately proportional to the changing rate of rotation angle. Then eq. (27), explaining that the changing rate of rotation angle has no relation to the magnitude of the sustained load coincides with the fact, which was pointed out by author's test result [3], that bending creep function (the ratio of creep deflection to the initial deflection) is almost constant without distinction of the magnitude of the sustained load when it is below the creep limit load for bending. This also indicates that the assumption that the creep strain for simple compression is linearly proportional to the sustained stress, when it is less than the proportional limit stress, is appropriate.

The relations between above mentioned changing rates and compression creep function $\phi_C(t)$, for the range $\phi_C(t)=0\sim 2$, are shown in Fig. 2. Here, it should be noted that the abscissa of Fig. 2 indicates the elapsed time t through the medium of $\phi_C(t)$ measured in the creep test for simple compression.

We can find the followings from Fig. 2. Although the rate of movement of neutral axis (N) shows a curve, it can be seen to be almost a straight line except the initial portion of the curve, this tendency indicating that the assumption in eq. (9), in other words, in eq. (7) is appropriate.

The magnitude of movement of neutral axis is about 8% of beam depth at $\phi_C(t) = 1$ and about 13% at $\phi_C(t) = 2$.

The changing rate of rotation angle increases linearly as $\phi_C(t)$ increases, it arriving at about 1.5 for $\phi_C(t) = 1$ and about 1.9 for $\phi_C(t) = 2$. The above tendency shows good agreement with the test results observed by many researchers [3,4,5]. That is, the total deflection under the sustained load below the creep limit load reaches 1.6 times to twice the initial deflection observed just after the application of the sustained load. The elapsed time corresponding to $\phi_C(t) = 2$ is so long that the bending creep deflection almost decreases, in other words, may reach the ultimate stage of creep.

Fig. 2 shows that $\sigma_t'$ (the increasing rate of the stress of the outermost fiber on the tension side) reaches about 1.4 at $\phi_C(t) = 2$; this suggesting the outermost fibers on the tension side do not reach the failure due to creep, because those do not arrive at the tensile stress at the proportional limit as far as those do not exceed the stress equivalent to the absolute value of the stress at the proportional limit for compression just when subjected to the sustained load. On the other hand, it is seen from Fig. 2 that the stress of the outermost fiber on the compression side decreases down to about 80% of the initial stress at $\phi_C(t) = 1$ and about 75% at $\phi_C(t) = 2$.

The strain of the outermost fiber on the compression side increases about 1.7 times the initial stress at $\phi_C(t) = 1$ and about 2.4 times at $\phi_C(t) = 2$; these showing that buckling may take place in the fibers at and near the extreme fibers.

## 5. Conclusions

The theory of bending creep mentioned in this paper can well explain the characteristics of the test results of bending creep observed by the author and others. In other words, for a beam subjected to the sustained load less than the creep limit load for bending, the following can be theoretically verified.

(1) The creep function for bending is constant and has no relation to the magnitude of the sustained load.

(2) Deflection of a beam subjected to bending creep reaches eventually about 1.5 to twice the initial elastic deflection caused by the application of the sustained load.

(3) The fiber stress of the outermost fiber on the tension side does not reach the proportional limit stress for tension, when subjected to sustained load.

It should be noted that "sustained load" explained above implies a sustained load less than the creep limit load for bending.

## References Cited

1. Sugiyama, Hideo. 1969. Theoretical analysis of the behavior of bending creep in wooden beam (Part 1). Transactions of Architectural Institute of Japan, No. 155.

2. Sugiyama, Hideo. 1970. Theoretical analysis of the behavior of bending creep in wooden beam (Part 2). Transactions of Architectural Institute of Japan, No. 170.

3. Sugiyama, Hideo. 1958. Experimental data on the prediction of the creep limit of wood in bending from creep and creep recovery tests. Research Reports of the Faculty of Engineering, Meiji University, No. 11.

4. Hisada, Toshihiko. 1950. The strength of wood under long-time load and the influence of notch on it. Research Reports of Architectural Institute of Japan, No. 9

5. Takeyama, Kenzaburo. 1944. Preliminary tests on the creep of wood and wooden joints. Transacions of Architectural Institute of Japan, No. 33

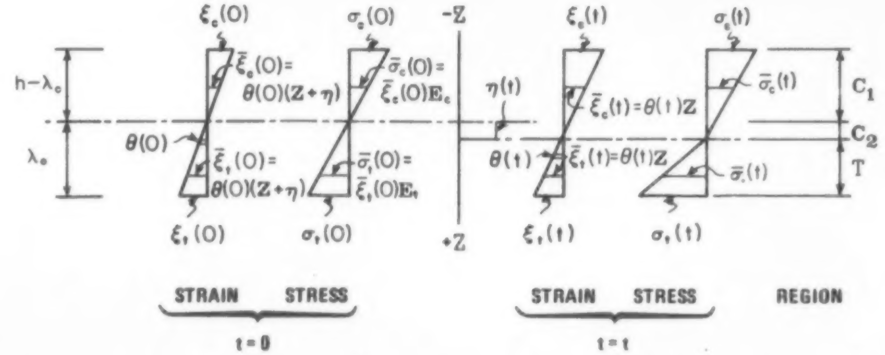

$\xi_c(0)$
$\sigma_c(0)$
$-Z$
$\xi_c(t)$
$\sigma_c(t)$
$h-\lambda_c$
$\lambda_c$
$\bar{\xi}_c(0)=\theta(0)(Z+\eta)$
$\bar{\sigma}_c(0)=\bar{\xi}_c(0)E_c$
$\eta(t)$
$\bar{\xi}_c(t)=\theta(t)Z$
$\bar{\sigma}_c(t)$
$C_1$
$C_2$
$T$
$\theta(0)$
$\bar{\xi}_t(0)=\theta(0)(Z+\eta)$
$\bar{\sigma}_t(0)=\bar{\xi}_t(0)E_t$
$\theta(t)$
$\bar{\xi}_t(t)=\theta(t)Z$
$\bar{\sigma}_t(t)$
$\xi_t(0)$
$\sigma_t(0)$
$+Z$
$\xi_t(t)$
$\sigma_t(t)$
STRAIN
STRESS
STRAIN
STRESS
REGION
t = 0
t = t

Figure 1. Strain and stress distribution over cross section of beam subjected to constant sustained load.

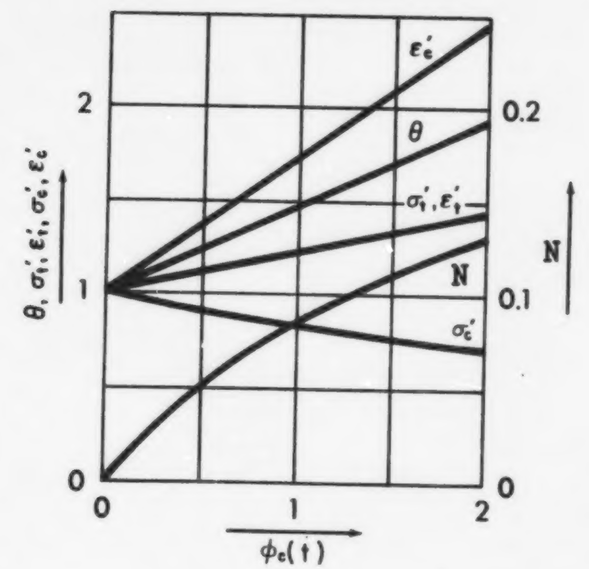

$\varepsilon_c'$
$\theta$
$\sigma_t', \varepsilon_t'$
N
$\sigma_c'$
$\theta, \sigma_t', \varepsilon_t', \sigma_c', \varepsilon_c'$
N
2
1
0
0.2
0.1
0
0
1
2
$\phi_c(t)$

Figure 2.

# ON COMPRESSION FAILURE IN WOOD MATERIALS:
# A MATHEMATICAL AND EXPERIMENTAL SIMULATION

James B. Wilson,[1]

Robert P. McEvoy Jr.[2]

and

Richard W. Perkins[3]

---

[1] Assistant Professor of Forest Products, School of Forestry, Oregon State Univ., Corvallis; [2] Graduate Research Assistant and [3] Professor, Department of Mechanical and Aerospace Engineering, Syracuse Univ., Syracuse, N.Y. The authors gratefully acknowledge the support of the U.S. National Science Foundation through Grant GK-3810. This is paper 1334 of the Forest Research Laboratory, OSU.

## INTRODUCTION

High uniaxial compression loading causes localized failure in woody materials. In other materials, such as metals (6), these compression failures are referred to as slip bands; we will use that term here. Slip bands occur as a result of a local material instability, so they should not be confused with structural instability or buckling. Thus, the formation of slip bands depends on the type of material.

Slip bands occur in the cell walls of wood fibers (2, 5) as in Figure 1, in gross samples of wood loaded in compression along the grain (4), and in wood composites such as linerboard (Fig. 2).

The development of kink bands in rock formations (3) outwardly resembles the development of slip bands in wood fibers. Although rock formations are many times larger than the wood cell wall, both are surprisingly similar when considered as layered composites.

The development of these slip bands is fundamentally related to the gross strength of the material. Furthermore, the development and growth of slip bands in the cell walls of individual wood fibers are believed to be closely related to the plastic behavior of solid wood when subjected to compressive axial loading (2).

We have investigated the inclination of slip bands that form in an anisotropic plate subjected to compression loading. The anisotropic plate could be used to model the cell wall of a fiber, gross wood, paper, or any similar anisotropic material. We used plastic plates reinforced with glass fiber in differing amounts to vary anisotropy.

To describe this phenomenon mathematically, we performed an analysis similar to that of Biot (1) who analytically studied slip bands as an internal instability of a nonlinear elastic medium. Biot approached the problem through the mechanics of incremental deformations, making a nonlinear problem linear by conisdering the incremental "tangent" moduli of a material as it changed with load. Mathematically the internal stability is attributed to the hyperbolic or mixed hyperbolic or mixed hyperbolic-elliptic nature of the equations for the incremental field beyond certain critical values of the initial stress. Thus, Biot was able to define a characteristic direction that represents a path along which a slip band would most likely occur. However, while determining the orientation of the slip band, we extended Biot's analyses to also predict the load at which the slip band begins.

To predict the critical compressive load and the angle of slip band formation when given the elastic constants of the plate, we analytically modeled an anisotropic plate loaded uniaxially in compression to failure.

## EXPERIMENTAL PROCEDURE

Plate specimens reinforced with glass fiber were prepared and tested to determine their strengths in the $x_1$ and $x_3$ directions, as well as the angle of inclination of the slip band. G-glass rovings were imbedded in one part of Bakelite epoxy ERL-2795 to four parts of Bakelite hardener 226-0814.

Unidirectionally reinforced plates 1/8" x 2" x 6" were fabricated by winding a glass roving on a metal form and applying epoxy resin in layers until reaching the desired fiber concentration. The plates were cured for four hours at 212°F, then cut to 1/8" x 2" x 3-1/2". After plexiglass tabs were bonded with epoxy to both ends to prevent elastic buckling and end crushing, the specimen width was reduced to eliminate end effects (Fig. 3).

When the plate was loaded in the $x_1$ direction, the slip band occured on the edge, the $x_1$, $x_2$ plane (Fig. 4), and its angle of inclination was measured optically from the $x_1$ axis. Loading specimens along ($x_1$) and perpendicular ($x_3$) to the direction of reinforcement at a head rate of 0.03 in./min. yielded critical strengths ($X_1$, $X_3$). Table 1 gives results for the various test specimens.

We measured the elastic properties of $E_{11}$, $E_{33}$, $\nu_{13}$, $\nu_{31}$ $\nu_{23}$, and $G_{12}$; however, we determined the other elastic parameters by considering the fiber-reinforced plate to be transversely isotropic in the $x_2$, $x_3$ plane. Thus, we have

$\nu_{13} = \nu_{12}$, $\nu_{31} = \nu_{21}$, $\nu_{23} = \nu_{32}$ and $E_{33} = E_{22}$. Table 2 gives the elastic properties for plates of different fiber concentrations.

## INCREMENTAL DEFORMATION ANALYSIS

Consider an incompressible, homogeneous, orthotropic plate with co-ordinate axes oriented along the directions of elastic symmetry. Let the $x_1$ direction represent the direction of reinforcement, the $x_2$ direction represent the thickness direction, and the $x_3$ direction represent the width of the plate. The slip instability is assumed to be a plane strain problem, since the surrounding elastic material restrains the material in the unstable region.

From Biot (1) we find that the plane-strain conditions of equilibrium for the two-dimensional stress field yield the equations:

$$\frac{\partial s_{11}}{\partial x_1} + \frac{\partial s_{12}}{\partial x_2} - 2S_{12}\frac{\partial \omega}{\partial x_1} + (S_{11} - S_{22})\frac{\partial \omega}{\partial x_2} = 0 \qquad (1a)$$

$$\frac{\partial s_{12}}{\partial x_1} + \frac{\partial s_{22}}{\partial x_2} + 2S_{12}\frac{\partial \omega}{\partial x_2} + (S_{11} - S_{22})\frac{\partial \omega}{\partial x_1} = 0 \qquad (1b)$$

where $s_{ij}$ are incremental stresses referred to a slightly rotated coordinate system (with $\omega$ the angle of rotation) and to unit areas in the deformed state, and where $S_{ij}$ are initial stresses applied in the direction of elastic symmetry (Fig. 5). According to Biot (1), the incremental stress-strain relations are given by:

$$s_{11} = C_{11}e_{11} + (C_{12} - S_{11})e_{22} \qquad (2a)$$

$$s_{22} = (C_{12} - S_{22})e_{11} + C_{22}e_{22} \qquad (2b)$$

$$s_{33} = (C_{31} - S_{33})e_{11} + (C_{23} - S_{33})e_{22} \qquad (2c)$$

$$s_{12} = 2(C_{66} + \frac{S_{11}}{2})e_{12} \qquad (2d)$$

Here, $C_{ij}$ are material properties related to small changes in stress and strain at some condition of the initial stresses, $S_{ij}$. Thus, they represent incremental tangent moduli. The strains and the rotations are given by:

$$e_{11} = \frac{\partial u_1}{\partial x_1} \qquad (3a)$$

$$e_{22} = \frac{\partial u_2}{\partial x_2} \qquad (3b)$$

$$e_{12} = \frac{1}{2}\left(\frac{\partial u_2}{\partial x_1} + \frac{\partial u_1}{\partial x_2}\right) \qquad (3c)$$

$$\omega = \frac{1}{2}\left(\frac{\partial u_2}{\partial x_1} - \frac{\partial u_1}{\partial x_2}\right) \qquad (3d)$$

where $u_i$ are the displacements.

If the load $S_{11}$ is applied in the $x_1$ direction and $S_{12} = S_{22} = S_{33} = 0$, substituting equations 2 and 3 into equation 1 and simplifying yields:

$$C_{11}\frac{\partial^2 u_1}{\partial x_1^2} + (C_{12} + C_{66})\frac{\partial^2 u_2}{\partial x_1 \partial x_2} + C_{66}\frac{\partial^2 u_1}{\partial x_2^2} = 0 \qquad (4a)$$

$$(C_{66} + S_{11})\frac{\partial^2 u_2}{\partial x_1^2} + (C_{12} + C_{66})\frac{\partial^2 u_1}{\partial x_1 \partial x_2} + C_{22}\frac{\partial^2 u_2}{\partial x_2^2} = 0 \qquad (4b)$$

For given boundary conditions, equation 4 yields a unique result when the initial stress, $S_{11}$, is zero. As $S_{11}$ increases from zero, the equations become elliptic and yield a unique solution; however, initial stress eventually becomes high enough that equation 4 no longer yields a unique solution. Then equation 4 no longer can be classified as elliptic. Biot (1) postulated that the mathematical condition for a nonunique solution to equation 4 also predicts the existence of a slip-band solution. Therefore, the slip band is considered to develop from a material instability.

Then the angle of the slip band is determined by the characteristic directions determined from the analysis of the partial differential displacement gradients:

$$d\left(\frac{\partial u_1}{\partial x_1}\right) = \frac{\partial^2 u_1}{\partial x_1^2}\,dx_1 + \frac{\partial^2 u_1}{\partial x_1 \partial x_2}\,dx_2 \qquad (5a)$$

$$d\left(\frac{\partial u_1}{\partial x_1}\right) = \frac{\partial^2 u_1}{\partial x_1 \partial x_2}\, dx_1 + \frac{\partial^2 u_1}{\partial x_2^2}\, dx_2 \quad \text{(5b)}$$

$$d\left(\frac{\partial u_2}{\partial x_1}\right) = \frac{\partial^2 u_2}{\partial x_1^2}\, dx_1 + \frac{\partial^2 u_2}{\partial x_1 \partial x_2}\, dx_2 \quad \text{(5c)}$$

$$d\left(\frac{\partial u_2}{\partial x_2}\right) = \frac{\partial^2 u_2}{\partial x_1 \partial x_2}\, dx_1 + \frac{\partial^2 u_2}{\partial x_2^2}\, dx_2 \quad \text{(5d)}$$

Equations 4 and 5 can be arranged in matrix form:

$$\begin{bmatrix} C_{11} & 0 & C_{66} & 0 & (C_{12}+C_{66}) & 0 \\ 0 & (C_{11}+C_{66}) & 0 & (C_{22}+S_{11}) & 0 & C_{22} \\ dx_1 & dx_2 & 0 & 0 & 0 & 0 \\ 0 & dx_1 & dx_2 & 0 & 0 & 0 \\ 0 & 0 & 0 & dx_1 & dx_2 & 0 \\ 0 & 0 & 0 & 0 & dx_1 & dx_2 \end{bmatrix} \bullet \begin{bmatrix} \frac{\partial^2 u_1}{\partial x_1^2} \\ \frac{\partial^2 u_1}{\partial x_1 \partial x_2} \\ \frac{\partial^2 u_1}{\partial x_2^2} \\ \frac{\partial^2 u_2}{\partial x_1^2} \\ \frac{\partial^2 u_2}{\partial x_1 \partial x_2} \\ \frac{\partial^2 u_2}{\partial^2 x_2} \end{bmatrix} = \begin{bmatrix} 0 \\ 0 \\ d\left(\frac{\partial u_1}{\partial x_1}\right) \\ d\left(\frac{\partial u_1}{\partial x_2}\right) \\ d\left(\frac{\partial u_2}{\partial x_1}\right) \\ d\left(\frac{\partial u_2}{\partial x_2}\right) \end{bmatrix} \quad \text{(6)}$$

A nontrivial solution can then be found by setting the determinant of the coefficient matrix equal to zero, which yields

$$\left(\frac{dx_2}{dx_1}\right)^4 + 2m \left(\frac{dx_2}{dx_1}\right)^2 + k^2 = 0 \quad \text{(7)}$$

where

$$m = \frac{C_{11}C_{22} + C_{12}^{\ 2} + 2\, C_{12}C_{66} + 2\, C_{66}^{\ 2} + C_{66}S_{11}}{2\, C_{11}\, (C_{66} + S_{11})}$$

$$k^2 = \frac{C_{22}C_{66}}{C_{11}\, (C_{66} + S_{11})}$$

The direction of the slip band, $dx_2/dx_1$, is given by

$$\left(\frac{dx_2}{dx_1}\right)_1 = \pm\, [-m + (m^2 - k^2)^{1/2}]^{1/2} \quad \text{(8a)}$$

$$\left(\frac{dx_2}{dx_1}\right)_2 = \pm\, [-m - (m^2 - k^2)^{1/2}]^{1/2} \quad \text{(8b)}$$

where $dx_2/dx_1$ will be real if $m > 0$ and $k^2 < 0$ (Case A), or $(dx_2/dx_1)_1$ and $(dx_2/dx_1)_2$ will both be real if $m < 0$ and $m^2 > k^2 > 0$ (Case B).

From equation 8, a positive and negative characteristic direction evidently exists if either Case A or B is satisfied, thus giving two equally potential planes at an angle $\theta$ from the $x_1$ axis. The angle of the slip band, $\theta$, is given by

$$\theta = \pm \tan^{-1} \left(\frac{dx_2}{dx_1}\right) \quad \text{(9)}$$

Let the critical strength $P_{cr}$ $(= -S_{11})$ be the applied stress at which the internal instability develops. For Case A, in which only $(dx_2/dx_1)_1$ is real, $P_{cr}$ is the applied stress for which $(dx_2/dx_1)_1$ equals zero and gives Biot's instability of the first kind. For Case B, in which both $(dx_2/dx_1)_1$ and $(dx_2/dx_1)_2$ are real, $P_{cr}$ is the applied stress for which $(dx_2/dx_1)_1$ equals $(dx_2/dx_1)_2$. Then a slip band will develop (Fig. 4), giving Biot's instability of the second kind.

Because no information is available on the incremental elastic moduli of a fiber-reinforced material, we must assume some general form. When the material is loaded in compression, the tangent modulus in the direction of loading initially remains constant; however, as the load continually increases, the tangent modulus decreases until it may only have a fraction of its initial value when instability begins. If the initial value of the tangent modulus is multiplied by the function $\exp(-P/k)$, where P is the load and k is the positive real number, then the incremental behavior of the tangent modulus will be similar to what is experimentally observed. For example, let

$$E_1 = (E_1)_i \exp(-P/k)$$

where $(E_1)_i$ is the initial value of the tangent modulus (Fig. 6). By varying the arbitrary constant k, $E_1$ can be made to decrease at a slower or faster rate. Likewise, the other tangent moduli ($E_2$, $E_3$, and $G_{12}$) could be assumed to vary similarly, although not necessarily at the same rate. Therefore, the incremental tangent moduli $E_1$, $E_2$, $E_3$, and $G_{12}$ are given as:

$$E_1 = (E_1)_i \exp(-P/x[1]) \qquad (10a)$$

$$E_2 = (E_2)_i \exp(-P/x[2]) \qquad (10b)$$

$$E_3 = (E_3)_i \exp(-P/x[3]) \qquad (10c)$$

$$G_{12} = (G_{12})_i \exp(-P/x[4]) \qquad (10d)$$

where x[1], x[2], x[3], and x[4] are constants. To satisfy the relations of orthotropic symmetry ($\nu_{ij}E_j = \nu_{ji}E_i$ for $i, j = 1, 2, 3$), we also must let $\nu_{12}$, $\nu_{13}$, and $\nu_{32}$ vary as some function of P. The simplest way is to let them vary linearly:

$$\nu_{12} = (\nu_{12})_i \ (1 + P/x[5]) \qquad (11a)$$

$$\nu_{13} = (\nu_{13})_i \ (1 + P/x[6]) \qquad (11b)$$

$$\nu_{32} = (\nu_{32})_i \ (1 + P/x[7]) \qquad (11c)$$

We do not claim that equations 10 and 11 are necessarily the exponential form for the actual experimental data. This function was selected only to provide a simple relation between the initial stress and the incremental tangent moduli. In our study, the form of these relations is unimportant. These aspects will be further reported in the future.

As the amount of fiber reinforcement was experimentally increased from 0 to 42 percent, the critical load increased from $2.0 \times 10^4$ psi to $4.3 \times 10^4$ psi (Fig. 7), and the angle of the slip plane increased from 55° to 70° (Fig. 8). Five levels of reinforcement were analytically increased from 0 to 10, 20, 30, and 40 percent. If the constants governing the incremental tangent moduli and Poisson's ratios are suitably chosen (Table 2), our analytical model is capable of consistently relating the corresponding values of the critical load and the angle of the slip plane (Figs. 7, 8). Apparently, the values of $P_{cr}$ and $\theta$ may be approximated by letting all the constants change by a certain percentage of their original value. However, more numerical analysis is needed to determine if this is indeed the case.

Note that the choice of constants is not at all arbitrary. For some choices, equation 7 will have only imaginary roots; for others, $(dx_2/dx_1)_1$ will not converge to zero, or $(dx_2/dx_1)_1$ and $(dx_2/dx_1)_2$ will not converge to the same value. In these cases, our model does not provide a solution — that is, no material instability exists. As yet, no general rules indicate how to choose these constants; they can only be chosen by observing what kind of results they predict. Despite this deficiency, we find that the critical load and inclination of the slip band can be predicted as a function of the anisotropy of the medium, thus concluding that the assumptions we made for our model are legitimate. Further study should clarify the correct relationship between the incremental tangent moduli and the initial compressive stress. Then the model could be used to study the compressive strength of materials that fail as a result of losing their internal material stability.

## Literature Cited

1. Biot, M.A. 1965. Mechanics of Incremental Deformations. John Wiley, New York.

2. Dinwoodie, J.M. 1968. Failure in timber. Part I. Microscopic changes in the cell wall structure associated with compression failure. J. Inst. Wood Sci. 21:37 - 53.

3. Donath, F.A. 1970. Some information squeezed out of rock. Am. Sci. 58(1):54 - 72.

4. Grossman, P.V.A., and M.B. Wold. 1971. Compression fracture of wood parallel to the grain. Wood Sci. Technol. 5:147-156.

5. Keith, C.T., and W.A. Cote Jr. 1968. Microscopic characterization of slip lines and compression failures in wood cell walls. Forest Prod. J. 18(3):67-74.

6. Nadai, A. 1950. Theory and Flow of Solids, Vol. I. McGraw-Hill, New York.

## Table 1

Linearized compressive strengths and slip band orientations[1] of anisotropic plates reinforced with glass fiber.

| Fiber content (percent) | Linearized strength (psi)<br>Perpendicular to fibers, $X_3$ | Linearized strength (psi)<br>Parallel to fibers, $X_1$ | Slip band orientation, $\theta$ (degrees) |
|---|---|---|---|
| 0 | 20,000 | 20,000 | 55.0 |
| 10.5 | 20,412 | 25,800 | 60.5 |
| 15.8 | 20,618 | 28,700 | 59.0 |
| 21.0 | 20,824 | 31,500 | 64.0 |
| 26.3 | 21,030 | 34,400 | 64.5 |
| 31.5 | 21,236 | 37,300 | 68.5 |
| 36.8 | 21,442 | 40,100 | 68.0 |
| 42.0 | 21,648 | 43,000 | 70.0 |

[1] Measured from the $x_1$ axis

## Table 2

Elastic properties of the plates used to predict the critical strength ($P_{cr}$) and the slip band orientation.

| | Fiber volume (%) of test plates<br>0 | 10 | 20 | 30 | 40 |
|---|---|---|---|---|---|
| $E_{11}$, psi x $10^6$ | 0.60 | 1.65 | 2.75 | 3.80 | 4.80 |
| $E_{22}$, psi x $10^6$ | 0.60 | 0.65 | 0.70 | 0.75 | 0.75 |
| $E_{33}$, psi x $10^6$ | 0.60 | 0.65 | 0.70 | 0.75 | 0.75 |
| $G_{12}$, psi x $10^6$ | 0.24 | 0.24 | 0.24 | 0.28 | 0.31 |
| $\nu_{21}$ | 0.25 | 0.20 | 0.17 | 0.15 | 0.14 |
| $\nu_{32}$ | 0.25 | 0.43 | 0.46 | 0.43 | 0.37 |
| $\nu_{12}$ | 0.25 | 0.51 | 0.67 | 0.76 | 0.90 |
| $\nu_{23}$ | 0.25 | 0.43 | 0.46 | 0.43 | 0.37 |
| $\nu_{13}$ | 0.25 | 0.51 | 0.67 | 0.76 | 0.90 |
| $\nu_{31}$ | 0.25 | 0.20 | 0.17 | 0.15 | 0.14 |
| x[1], psi x $10^3$ | 7.10 | 8.70 | 9.40 | 11.55 | 15.95 |
| x[2], psi x $10^3$ | 8.00 | 9.00 | 10.00 | 12.00 | 16.00 |
| x[3], psi x $10^3$ | 8.00 | 9.00 | 10.00 | 12.00 | 16.00 |
| x[4], psi x $10^3$ | 7.10 | 8.70 | 9.40 | 11.55 | 15.95 |
| x[5], psi x $10^3$ | 5.90 | 9.90 | 13.40 | 14.00 | 12.60 |
| x[6], psi x $10^3$ | 5.90 | 9.90 | 13.40 | 14.00 | 12.60 |
| x[7], psi x $10^3$ | 11.80 | 19.80 | 26.80 | 28.00 | 25.20 |

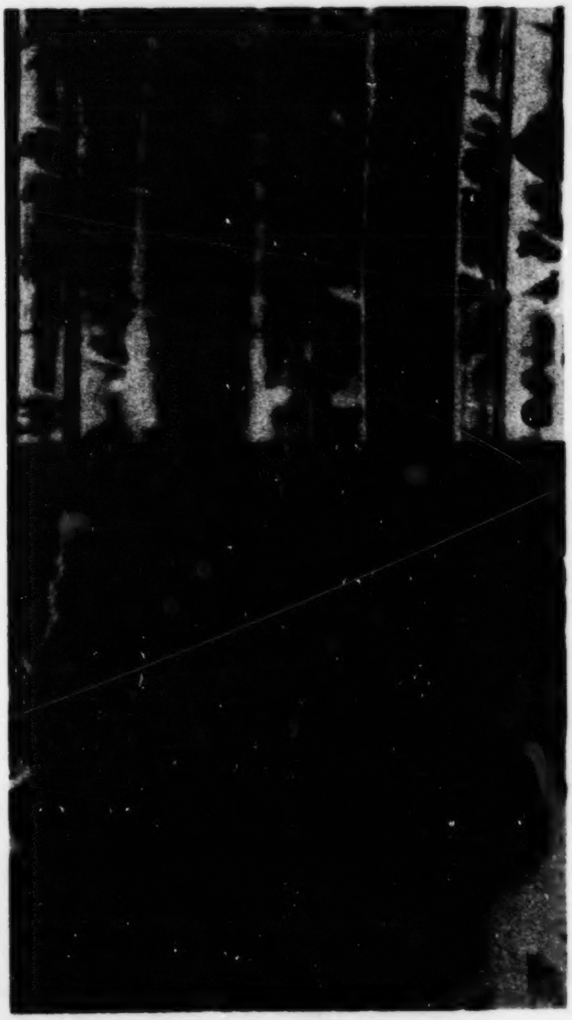

Figure 1. Slip bands in the cell wall of the wood fiber: (a) a light micrograph of a radial section of several fibers; (b) an electron micrograph of two slip bands on a radial section (5)

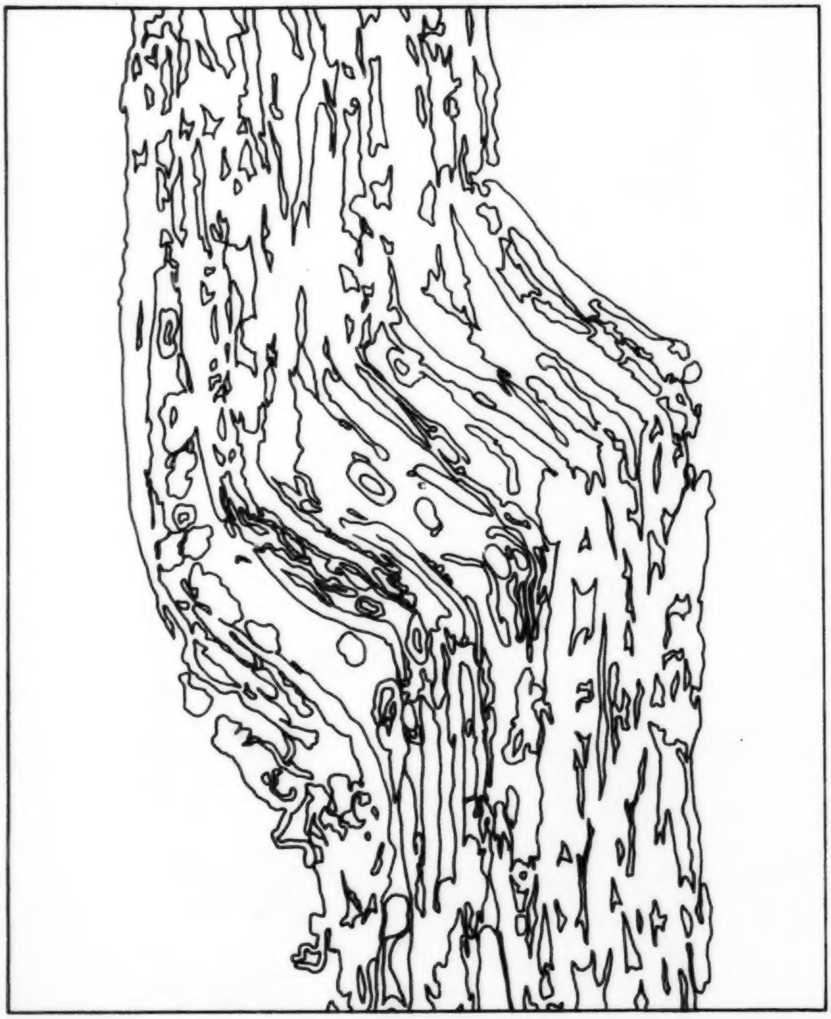

Figure 2. Schematic of slip band formed on the edge of a sheet of liner board loaded in compression in the plane of the sheet.

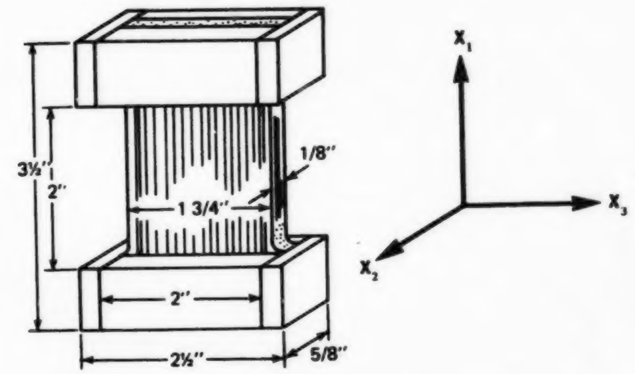
$X_1$
$X_3$
$X_2$
3½"
2"
1/8"
1 3/4"
2"
2½"
5/8"

Figure 3. Test configuration for compressing fiber-reinforced plate.

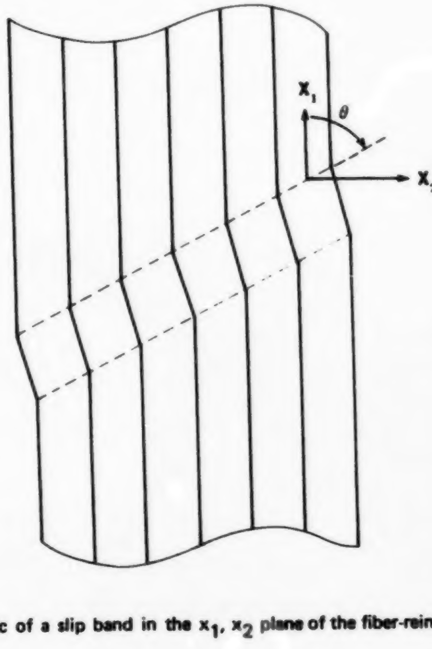

Figure 4. Schematic of a slip band in the $x_1$, $x_2$ plane of the fiber-reinforced plate.

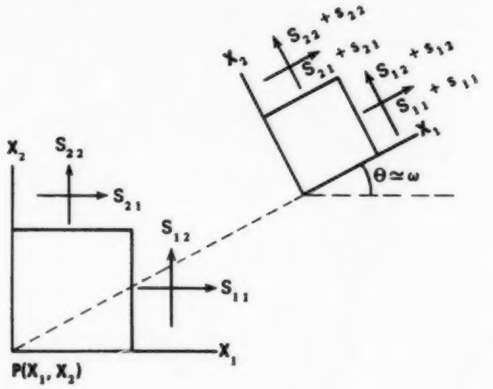
$S_{22} + s_{22}$
$X_2$
$S_{21} + s_{21}$
$S_{12} + s_{12}$
$S_{11} + s_{11}$
$X_1$
$X_2$
$S_{22}$
$S_{21}$
$\theta \simeq \omega$
$S_{12}$
$S_{11}$
$X_1$
$P(X_1, X_2)$

Figure 5. Representation of initial stresses, $S_{ij}$, and the incremental stresses, $s_{ij}$, in the rotated field.

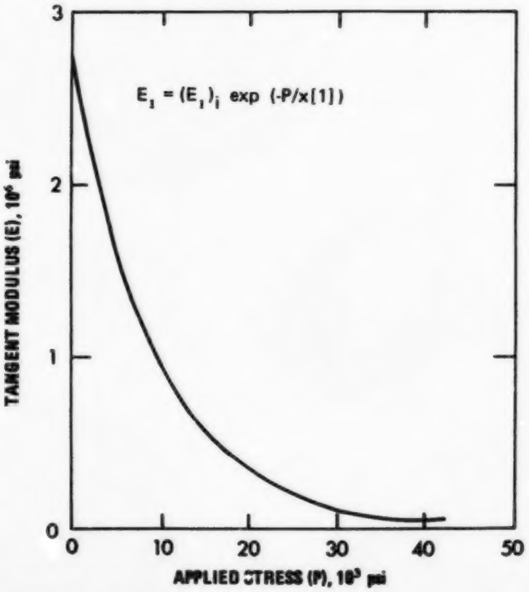

Figure 6. An assumed relationship of how the incremental tangent modulus, E, changes with applied stress, P.

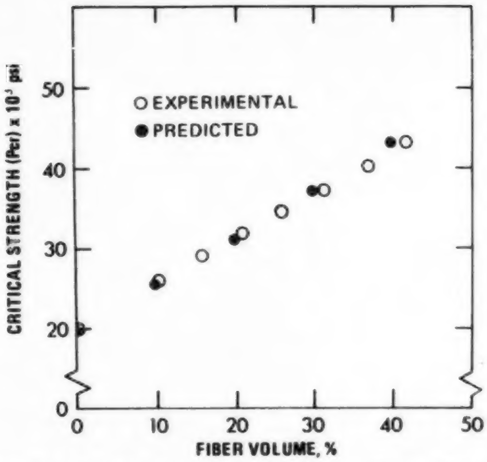

Figure 7. Critical strength at slip band formation as affected by varying anisotropy of the fiber-reinforced plate.

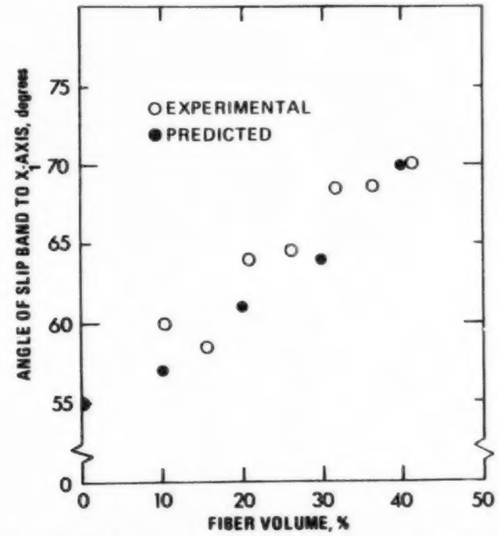

Figure 8. Slip-band orientation as affected by varying anisotropy (fiber volume) of the fiber-reinforeced plate.

## LIST OF PARTICIPANTS

| | |
|---|---|
| Aplin, E.N. | Eastern Forest Products Laboratory, Canada |
| Aune, P. | Norges Tekniske Hogskole, Norway |
| Bach, L. | MacMillan Bloedel Research Ltd., Canada |
| Barrett, J.D. | Western Forest Products Laboratory, Canada |
| Birkeland, R. | Norsk Treteknisk Institutt, Norway |
| Bovim, N.I. | Norsk Treteknisk Institutt, Norway |
| Brassell, T. | American Institute of Timber Construction, USA |
| Brundin, J. | Swedish Forest Products Laboratory, Sweden |
| Bryant, P. | Timber Research Unit, CSIRO, South Africa |
| Chow, C.L. | University of Hong Kong, Hong Kong |
| Crubile, P. | Centre Technique du Bâtiment, France |
| Darby, D. | Alberta Agriculture, Canada |
| Durrant, S.O. | Brigham Young University, USA |
| Edlund, B. | Chalmers University of Technology, Sweden |
| Egerup, A.R. | Technical University of Denmark, Denmark |
| Ehlbeck, J. | Technical University of Karlsruhe, West Germany |
| Foschi, R.O. | Western Forest Products Laboratory, Canada |
| Goodman, J.R. | Colorado State University, USA |
| Hagen, D. | University of Minnesota, USA |
| Hoffmeyer, P. | Technical University of Denmark, Denmark |
| Johnson, J.A. | Weyerhaeuser Company, USA |
| Kallsner, B. | Swedish Forest Products Laboratory, Sweden |
| Keenan, F.J. | University of Toronto, Canada |
| Kousholt, K. | Technical University of Denmark, Denmark |
| Koutsky, J.A. | University of Wisconsin, USA |

| | |
|---|---|
| Kufner, M. | Institut fur Holzforschung, West Germany |
| Kuipers, J. | University of Delft, The Netherlands |
| Kyanka, G. | State University of New York, USA |
| Larsen, H.J. | Aalborg University, Denmark |
| Lau, K. | Western Forest Products Laboratory, Canada |
| Lyon, D. | Mississippi State University, USA |
| Madsen, B. | University of British Columbia, Canada |
| Meyer, R.W. | Washington State University, USA |
| Mindess, S. | University of British Columbia, Canada |
| Murphy, J.F. | Forest Products Laboratory, USA |
| Nadeau, J. | University of British Columbia, Canada |
| Noren, B. | Swedish Forest Products Laboratory, Sweden |
| Pearson, R. | University of North Carolina, USA |
| Pellerin, R.F. | Washington State University, USA |
| Salinas, J. | Carleton University, Canada |
| Schniewind, A.P. | University of California, USA |
| Smith, F.W. | Colorado State University, USA |
| Spencer, R. | University of British Columbia, Canada |
| Stern, E.G. | Virginia Polytechnic Institute and State University, USA |
| Stluka, R. | Weyerhaeuser Company, USA |
| Sugiyama, H. | University of Tokyo, Japan |
| Sunley, J.G. | TRADA, United Kingdom |
| Ulrich, J.W. | Alberta Agriculture, Canada |
| Van Amstel, P. | TNO, The Netherlands |
| Vokey, H.P. | Canadian Wood Council, Canada |
| Williams, L. | Brigham Young University, USA |
| Wilson, J.B. | Oregon State University, USA |